DISSERTATION

SYNTHESIS OF BIOLOGICALLY RELEVANT MOLECULES

Submitted by

Margaret Braasch-Turi

Department of Chemistry

In partial fulfillment of the requirements

For the Degree of Doctor of Philosophy

Colorado State University

Fort Collins, Colorado

Spring 2023

Doctoral Committee:

Advisor: Debbie C. Crans

Andy McNally
Amy Prieto
Jessica Prenni

ABSTRACT

SYNTHESIS OF BIOLOGICALLY RELEVANT MOLECULES

Natural products total synthesis and bioorganic chemistry rely on organic synthesis to produce the compounds for biological study. Natural products and some biomolecules are naturally found in extremely low concentrations. Organic synthesis made it possible to acquire the amounts needed for biological studies. The research described herein discusses both areas. In the body of this document, the bioorganic work regarding lipoquinones, particularly ubiquinones and menaquinones, is described. Appendix IV described the natural products work. Chapter 1 provides a more detailed explanation as to the circumstances that led to two different areas of research.

Chapter 2 serves as the introduction to the bioorganic research. In this chapter, a review of the literature surrounding ubiquinones, plastoquinones, and menaquinones is complied with their properties at the forefront. Lipoquinones are incredibly hydrophobic molecules, and such properties are often ignored or misinterpreted in the literature. The review compares reported similarities and differences among the lipoquinones with respect to their headgroups, isoprene sidechain length, conformations, and location of lipoquinones in membrane environments. The review also highlights the need for and encourages more experimental studies to validate the computational work in the field.

Chapter 3 discusses the conformation and location of ubiquinone-2 in AOT reverse micelles. Previous work with menaquinone-2 determined the truncated lipoquinone derivative adopted a folded conformation in organic solvents and in AOT reverse micelles and suggest

menaquinone-2 is located near the lipid-water interface. We hypothesized ubiquinone-2 would also adopt a folded conformation in the membrane and be located near the lipid-water interface, but closer to the bulk water than menaquinone-2. We used 1D and 2D NMR spectroscopic methods to explore the solvent and membrane conformations and membrane location of ubiquinone 2. The conformations and locations of ubiquinone-2 were compared to menaquinone-2, and the location of ubiquinone-2 was found to be slightly closer to the interface than menaquinone-2.

Chapter 4 provides a review of the literature regarding the synthesis of naphthoquinone derivatives. There are five main synthetic approaches that have been used to synthesize naphthoquinone derivatives. The categories are (1) nucleophilic ring methods, (2) sidechain homologations and extensions, (3) metal-mediated and radical reactions, (4) electrophilic ring, and (5) pericyclic reactions. The advantages and disadvantages of each approach are discussed regarding selectivity, number of steps, yield, and overall safety. Some approaches are simpler to carry out for the non-expert and successfully yield product, although stereospecificity and yields of the reactions are less, whereas other routes are higher yielding.

Chapter 5 discusses the exploratory synthesis of menaquinone derivatives. The established Friedel-Crafts approach has poor regioselectivity, poor stereoretention of the first isoprene unit in the sidechain, and universally low yields. Using the knowledge gained in Chapter 4, a pericyclic approach using Diels-Alder adducts was used to exert regiocontrol of sidechain and maintain the stereochemistry of the sidechain. A convergent route was designed to provide access to a diverse library of sidechains to include E and Z isomers of the first isoprene unit and varying degrees of saturation along the sidechain.

Appendix IV discusses the progress towards the total synthesis of versiquinazoline A and versiquinazoline B, alkaloids with anti-cancer properties and a unique pyrazinoquinazolinedione

(6-6-6) and imidazoindolone (5-5-6) scaffold. Through this synthesis, the non-proteinogenic amino acid, 1-amino-1-cyclopropycarboxylic acid, was prepared to be used in the synthesis of versiquinazoline B. The synthesis of the 5-5-6 ring system explored the use of many peptide coupling conditions to afford a sterically hindered amide bond. After frequent unsuccessful trials, steps toward the total synthesis of versiquinazoline A were taken using alanine instead of 1-amino-1-cyclopropylcarboxylic acid. After successful amide coupling, the reoxidation of the aromatic sing system was explored using 2,3-dichloro-5,6-dicyanoquinone. This project ended prematurely due to the advent of COVID-19 and the passing of my advisor, Dr. Robert M. Williams.

ACKNOWLEDGEMENTS

So many people helped me get to this point in my life: family, friends, labmates, teachers, and even some students. Thank you for being there for me and going through this with me.

First, I would like to thank Dr. Robert M. Williams. Bob held a high standard of science, and I tried my best every day to reach that standard. Through him, I learned how to be an independent researcher and how to set goals for myself. Bob was an incredible organic chemist who could see synthetic connections in the most unique places, and I hope to see those connections too someday. Thank you, Bob, for challenging me to become the chemist I am today.

Thank you to Dr. Debbie C. Crans who accepted me into her research group with open arms and the unrelenting empowerment to pursue my interests. I came to her broken from the loss of Bob and frustrated by science. She showed me that I am capable and taught me to stop doubting my ideas and trust myself as a chemist. Through her encouragement, I have branched outside of my comfort zone and presented posters and given talks at three ACS conferences (regional and national), written three papers, and aided in submitting two NSF grants (one of which was recently funded!). Thank you, Debbie, for helping me realize I am capable of more and guiding me to where I am today. I look forward to learning more from you.

I have had so many mentors throughout the years that have helped me along the way. I cannot possibly name them all. Thank you, Margaret Smallbrock, Dr. Dan Heglund, Dr. Tsvetanka Filipova, Dr. David Boyles, Dr. Patty Somers, Dr. Anna Allen, Dr. Panduka Piyaratne, and Dr. Nancy Levinger for answering my questions and giving advice.

Thank you to my labmates in the Williams group: Jonathan Thielman, John Manganaro, Ryan Cerbone, Andrew Bates, Brooke Benson, Morgan McCauley, Taylor Ausec, Kimberly (Klas) Koehn, Christine Dunne, Nathan Bair, Anil Shelke, Subhadip De, Deepak Barange, and Siva Nagi Reddy Koti. I thoroughly enjoyed learning from all of you, sharing science, sharing stories, late night lab debates, "Would You Rathers?", and all the memories during the Ski Trips in Steamboat Springs. In particular, I want to thank Jonathan Thielman for being nosy and forcing me to talk about research: the good, the bad, and the awful. In the moment, it was really annoying, but it was always worth it in the end. I plan to have a similar approach with my own students.

Thank you to my labmates in the Crans group: Jordan Koehn, Andrew Bates, Skyler Markham, John Manganaro, Anny Galaeva, Cameron Van Cleave, Heide Murakami, Allison Haase, Kate Kostenkova, Zeyed Arhouma, and all the undergrads. I learned how to be a collaborator from all of you. Thanks for all the great science discussions and good laughs.

Thank you to the Lake Street Subway for being open late. Lab life is unpredictable, but Subway never is.

Thank you to all my friends who have helped me through all the tough times, celebrated with me during the good times, existed with me during the monotonous times: Lacey Beck, Mj Riches, Sylvia (Iverson) Johnson, Rashyll Leonard, Katie Wolff, Emily Kasper, Jackson, Bohlman, and Natalie Reed. Graduate school is not easy, but it was made easier through your love and support. In particular, I want to thank Lacey Beck, who lived with me during the three most difficult years of graduate school. Thanks for the trips to Target, annual autumnal Harry Potter Movie marathons, dinosaur chicken nuggets, and showing me there is more to life than chemistry. Thank you to Sylvia Iverson for taking me on hikes to I could see all the beautiful scenery in Colorado once in a while and thank you for tolerating how much I love chemistry. I love your

“chemistry face”. It was so wonderful to be able to escape to Denver and visit you. In this same thread, I want to thank all the important cats in my life: Fred (OG), Fred (2.0), and Winifred (Winnie). Thanks for the cuddles, lime time, and forcing me to take breaks.

Finally, I thank my parents for their never ending love and support. I would not have accomplished anything in my life if it were not for their encouragement and support of my dreams. Mom, thank you for answering all my questions when I call, helping me through the aftermath of Bob’s death, and encouraging me to do what I want to do. Dad, thank you for the hours and hours of talking on the phone about science and teaching, trying to understand what I am doing, and understand why I am doing it. I love it when you say “I love hearing your smile” when we talk on the phone. I could not have done any of this without both of you. Thank you.

“Wow! That’s a complicated endgame!”- Tohru Fukuyama after looking at my natural product.

You can say that again!

PREFACE

My mom was diagnosed with rheumatoid arthritis when I was in middle school. I watched her go through every standard prescribed treatment, and none of it worked. It was excruciating to see her in pain. Eventually, they landed on a "last resort": Rituxan, a monoclonal antibody treatment that essentially kills all her white blood cells in the hope that the new ones will not attack her joints. It costs an absurd amount of money per treatment that she is required to have twice a year. I remember thinking there has got to be a better way. All of this started before I had taken chemistry in high school, but the seeds of thought were there. Then when I was in organic chemistry I lab, we made phenytoin, an anti-epileptic drug. It was then I realized I could use organic chemistry to find a "better way". Then later, my uncle Timmy died of cancer. This only added to the list of ailments I wanted to "cure". I used this as motivation in graduate school to pick a natural product that either had anti-rheumatoid arthritis properties and/or anticancer properties. These seeds of thought bloomed into my total synthesis project (Appendix IV).

Since I started and ended the natural product project, three more significant people in my life have been diagnosed with cancer: Bob, Debbie, and my dad. As I have moved through my graduate career, I have broadened my interests to include both natural products total synthesis and bioorganic synthesis. As I move forward to my professional career, I want to pursue projects involving biologically active molecules. I am still interested in exploring the vast world of natural products to do my part in identifying the "better way". Whether that is by discovering the next best cancer drug or immunosuppressant or simply probing the fundamental biology of each system through bioorganic chemistry, I'm going to contribute to it.

DEDICATION

To my Mom and Dad

You are my first teachers.

GO SCIENCE!

Love,

Kakes

AMLATT

TABLE OF CONTENTS

Chapter 1: Introduction

1.1. Overview of Projects

Over the last six years, I have had the pleasure to work on three different projects as a member of two research groups. I spent the first four years of my graduate career as a member of Dr. Robert M. Williams research lab. During those years I embarked on the total synthesis of two alkaloids, versiquinazoline A and versiquinazoline B. This work did not result in a publication, and, as such, it is in the Appendix. Appendix IV describes the work done on the total synthesis of versiquinazoline V and B. Although this work did not result in a publication, it was important to me to detail the steps I took to solve the synthetic problems I faced. Additionally, it was also important for me to write up this work to honor the late Dr. Robert M. Williams and everything I learned as a member of his group. Bob passed away from a 2.5 year long battle with cancer in May of 2020. For this chapter, it is important to note the measurement of a reaction's success was rooted in percent yield. Reactions yielding less than 75% were deemed inadequate to continue for a robust total synthesis. In hindsight, this metric was very difficult to sustain, and it significantly influenced my decision making throughout the project.

I joined Dr. Debbie C. Crans' research group in July of 2020. As a member of the Crans group, I have participated in research that is taking a deep dive into the fundamental biology of the electron transport system of prokaryotes. On the surface, the electron transport system appears to be fully understood, but this is simply not true. The lipoquinone electron transport agents carry electrons and protons between protein complexes to ultimately form ATP, but there is still so much we do not know or understand about the location and conformation of lipoquinones in the membrane. The literature is unbalanced toward reports of ubiquinones, electron transporters in

eukaryotes, because it was discovered first. So much so, that mitochondria are often referred to as "the powerhouse of the cell" in mainstream science education. There is significantly less research about the location and conformation of menaquinones, the electron transport agents in prokaryotes. It is amazing to think about the work I have contributed to as a member of the Crans group is going to either support or completely challenge the status quo of lipoquinone location in biological membranes. There are so many factors to consider before anything becomes groundbreaking, but I am so grateful to have been a part of it.

During the last two years as a member of the Crans group, I used the skills I learned in the Williams group and applied them to exploring new avenues to synthesize menaquinone derivatives. Chapter 2 of my dissertation is a review of the chemistry of lipoquinones, particularly ubiquinones, plastoquinones, and menaquinones. Chapter 3 is the work done on comparing the conformation of ubiquinone-2 and menaquinone-2 in organic solvents and investigating the conformation and location of these two lipoquinones in AOT reverse micelles. Chapter 4 is a review of the current state of the literature regarding the synthesis of naphthoquinone derivatives. Finally, Chapter 5 describes my work on the exploratory use of a Diels-Alder adduct to synthesis of a diverse library of menaquinone derivatives in a convergent manner. It is important to note the work described in Chapter 5 did not result in a publication.

Chapter 2:
Chemistry of Lipoquinones: Properties, Synthesis, and Membrane Location of Ubiquinones, Plastoquinones, and Menaquinones

2.1. Introduction

Lipoquinones are molecules involved in a variety of biological processes. Their appearance may be simple, but their properties are deceptively complex. This class of lipids contains a redox active, polar 1,4-quinone headgroup and a hydrophobic sidechain consisting of several isoprenoid groups. Lipoquinones are components within the highly ordered lipid bilayer (Singharoy, Maffeo et al. 2020, Van Cleave, Koehn et al. 2021, Santis, Scoppola et al. 2022). One example of lipoquinone function is to act as the electron carriers responsible for transferring electrons between membrane-bound protein complexes within the electron transport chain, ultimately producing adenosine triphosphate (ATP). The structure of lipoquinones, such as headgroup structure and composition of the sidechain, varies between whether the biological system is bacterial, plant, or mammalian and their biological functions. This is not surprising because the structure of the quinone headgroup and isoprenoid sidechain has been used for taxonomic identification of prokaryotes and eukaryotes prior to the development of genetic classification (Dunphy and Brodie 1971, Kawamukai 2018).

With this in mind, it is not fully understood how the length and degree of unsaturation along the lipoquinone sidechain impacts both their chemical and biological properties other than the fact that lipoquinones are required for survival (Okada, Kainou et al. 1998, Hihi, Kebir et al. 2003, Kawamukai 2018). The relationship between structural diversity and chemical properties and the biological function of lipoquinones is a question that is often overlooked or ignored.

However, Hihi and coworkers explored the significance of the sidechain length through a UQ-derivative feeding study with *Caenorhabditis elegans clk-1* mutants (Hihi, Kebir et al. 2003). Therein, UQ-6 to UQ-9 were fed to UQ-8-depleted *C. elegans* to determine their effects on growth and behavior. They found the longer chain derivatives, like UQ-9 and UQ-8, restored the phenotypic behavior. The shorter chain derivatives, UQ-7 and UQ-6, sustained continuous growth in the mutants but halted certain UQ-dependent processes, such as fertility, and slowed development and behavior of *C. elegans* (Hihi, Kebir et al. 2003). This study suggests the sidechain length plays a significant role in the development of this model organism, but it does not address the properties of each UQ-derivative and how it could affect the results.

A study performed by Okada and coworkers used *Saccharomyces cerevisiae* as a model organism to assess the biological significance of the sidechain length of ubiquinone within the organism (Okada, Kainou et al. 1998). Different types of prenyl diphosphate synthases were expressed to produce UQ-5 to UQ-10, and the growth rate of each mutant was evaluated. UQ-6 is the preferred lipoquinone of *S. cerevisiae* showing the highest growth rate. The other UQ-derivatives did not affect the growth rate significantly which suggests the headgroup is more important than the sidechain. In their conclusion, they suggest the length of the sidechain may play an important role in adjusting the hydrophobicity of the UQ-derivative to the membrane environment (Okada, Kainou et al. 1998).Together these studies support the significance the length of the sidechain, but both clearly indicate the headgroup is the critical moiety for survival. In the present review, we describe the chemical properties of lipoquinones such as hydrophobicity, solubility, conformation, and redox potential organized according to the quinone headgroup type.

In this review, we will focus on three subclasses of lipoquinones: ubiquinone , plastoquinone, and menaquinone, which differ by headgroup structure. Ubiquinones (UQ) are comprised of a 1,4-benzoquinone headgroup with four substituents: two methoxy groups, isoprenyl sidechain, and one methyl group adjacent to the sidechain. Ubiquinones are found within the inner mitochondrial membrane, where they facilitate the electron transport chain of eukaryotes. Ubiquinone-10, also known as UQ-10 or coenzyme Q10, is the most well-known lipoquinone and UQ-derivative (Figure 2.1A). Plastoquinones (PQ) are also comprised of a 1,4-benzoquinone headgroup, but

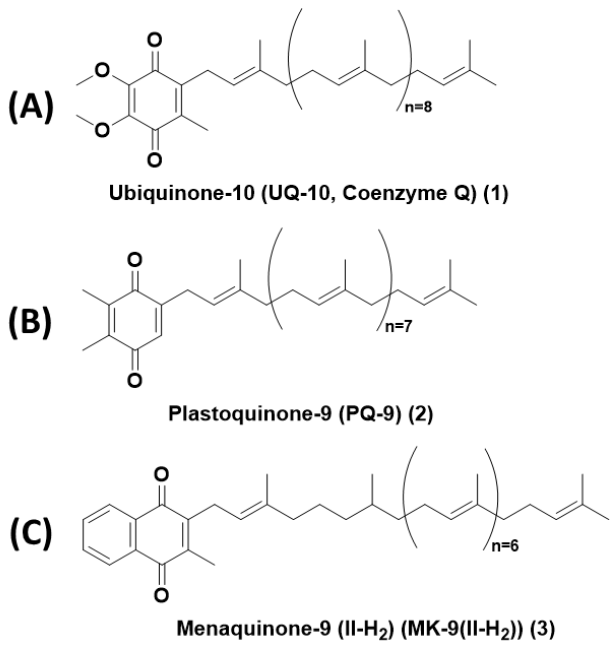

Figure 2.1. Structures of representative lipoquinones from each subclass. (A) Ubiquinone-10, also known as Coenzyme Q10 or UQ-10. (B) Plastoquinone-9 (PQ-9). (C) Menaquinone-9(II-H_2) (MK-9(II-H_2)).

differs from ubiquinones with two methyl group substituents, as seen in plastoquinone-9 (PQ-9, Figure 2.1B). Plastoquinones are found in the thylakoid membrane of chloroplasts and facilitate photophosphorylation. Menaquinones (MK) are comprised of a 1,4-naphthoquinone headgroup with a methyl group adjacent to the sidechain, as seen in menaquinone-9(II-H_2) (MK-9(II-H_2), §

2.1C). Menaquinones are found in the cytoplasmic membrane electron transport chain of prokaryotes.

For all three subclasses, the isoprenoid sidechains can vary in the length and degree of unsaturation. Some species have been found to have saturated isoprene units along the sidechain. The isoprenoid sidechains are biosynthesized from isopentyl diphosphate and dimethylallyl diphosphate via one of three pathways: mevalonate pathway, 2-C-methyl-D-erythritol 4-phosphate, and 1-deoxy-D-xylulose 5-phosphate pathway (Zhao, Wei-Chen et al. 2013). The origins of these pathways are hypothesized to have emerged from a common ancestor via the mevalonate pathway and diverged throughout evolution to the other two pathways (Lange, Rujan et al. 2000, Hoshino and Gaucher 2018).

The 1,4-quinone headgroup is responsible for the redox activity of lipoquinones. If all lipoquinones are capable of transferring electrons, it is curious that nature evolved such structural diversity in headgroups across lipoquinones to perform the same operations. The chemical redox properties of the headgroups vary and play a role in the setting the baseline reduction potentials required to transfer electrons between membrane-bound protein complexes. This trend appears true from an evolutionary perspective. Of the three lipoquinones discussed in this review, menaquinones evolved first within prokaryotes, which includes bacteria and archaea, which existed within a mostly anerobic environment and thus underwent anaerobic respiration. As time progressed, the environment became saturated with harsh UV light from the sun, which undoubtedly caused damage to cells. At some point, bacteria within the cyanobacteria phylum evolved plastoquinones to harvest energy from light to generate ATP via photophosphorylation that ultimately leads to the release of oxygen into the atmosphere. Interestingly, certain classes of cyanobacteria use both plastoquinone and menaquinone derivatives to facilitate photosynthesis.

PQ-9 is the electron transfer agent for photosystem II, and phylloquinone (MK-4 (II, III, IV-H_6) or vitamin K_1) is the electron transfer agent for photosystem I (Palace, Frankie et al. 1987, Nowicka and Kruk 2010). As more oxygen was introduced to the atmosphere, organisms needed to adapt lipoquinones that could withstand the oxidizing atmosphere. Eventually, organisms in the pseudomonadota (previously known as proteobacteria) phylum evolved ubiquinones. Ubiquinones are more resistant to oxidation than menaquinones (see the discussion in Section 2.2.3) (Schoepp-Cothenet, Lieutaud et al. 2009, Pelosi, Ducluzeau et al. 2016, Esposti 2017, Anand, Chen et al. 2019). This change in headgroup allowed for aerobic respiration to occur. Certain classes within the phylum, specifically α-, β-, and γ-proteobacteria, use both menaquinones and ubiquinones for electron transport. For example, *Escherichia coli*, a γ-proteobacterium, can switch between lipoquinones depending on specific growth conditions. Ubiquinone is best suited for aerobic growth conditions, and menaquinone is used in anaerobic growth conditions (Pelosi, Ducluzeau et al. 2016). The use of more than one type of lipoquinone by an organism supports the concept that the properties of lipoquinones are tailored to their redox activity.

Eukaryotic organisms primarily utilize ubiquinones for oxidative phosphorylation; however, all members of the plantae kingdom contain both ubiquinones and plastoquinones. The incorporation of each lipoquinone within this domain is hypothesized to have originated from the occurrence of two endosymbiotic relationships between a eukaryotic ancestor and organisms in both pseudomonadota and cyanobacteria phyla. Since all eukaryotes contain ubiquinone, the endosymbiosis of an α-, β-, or γ-proteobacterium must have occurred first. Over time, the endosymbiont became the mitochondria, an organelle that houses the electron transport chain in eukaryotes (Yang, Oyaizu et al. 1985, Stackebrandt, Murray et al. 1988, Keeling 2013, Zimorski, Ku et al. 2014). Similarly, the origin of chloroplast organelles is thought to have occurred via the

endosymbiosis of a cyanobacterium into a eukaryotic organism (Liu and Lu 2016). The incorporation of photosynthetic machinery into the cells allows these organisms to use plastoquinones to harness the energy from light for photosynthesis and use ubiquinones for oxidative phosphorylation within the mitochondria (Keeling 2013). The emergence of different lipoquinones with their intrinsic properties allowed for organisms to thrive in environments of varying levels of hostility.

The isoprenoid sidechain is thought to anchor the lipoquinone into the lipid bilayer. The sidechain is comprised of both single and double bonds that provide rigidity (double bond) and flexibility (single bonds) via multiple degrees of rotational freedom. The length and degree of unsaturation along the sidechain vary between species. For example, UQ-10 is the most common lipoquinone in humans, and UQ-9 is the prevalent species in rodents (Crane 2007). In prokaryotes, there is greater sidechain diversity of menaquinones between species. For example, *Halococcus morrhuae* contains MK-8(VIII-H_2), whereas *Mycolicibacterium smegmatis* (previously categorized as *Mycobacterium smegmatis)* and *Corynebacterium tuberculostearicum* contain MK-9 (II-H_2) and MK-9, respectively (Dunphy and Brodie 1971). The only difference between these two MK-derivatives is the presence of a saturated (reduction of a specific double bond) isoprene unit along the sidechain. In addition to the structure of the headgroup, electrochemical studies have shown the composition of the sidechain can affect the reduction potential of lipoquinones (Fujimoto, Kosaka et al. 2012). For example, the redox potentials of MK-4 and MK-8 have been found to be -20 to -30 mV and -80 mV, respectively. The variance in redox potentials shows the length of the sidechain impacts the reduction potential of the lipoquinone. Additionally, the reduction potential of MK-4 and phylloquinone (vitamin K_1 or MK-4 (II, II, IV- H_6)) are -20 to -30 mV and -500 to -700 mV, respectively. Even though MK-4 and phylloquinone contain the same

number of carbons in the sidechain, the presence of three saturated isoprene units significantly decreases the reduction potential (Fujimoto, Kosaka et al. 2012). Therefore, modifications to the sidechain are very likely to play a role in fine tuning the reduction potentials within their respective protein complexes.

In addition to lipoquinones role in the electron transport chain, they have antioxidant properties (Kawamukai 2018), which protects against lipid peroxidation and the damaging effects of reactive oxygen species throughout the membrane (Nowicka and Kruk 2010). Menaquinones are essential for human health as members of the vitamin K family of compounds: vitamin K_1 (phylloquinone), vitamin K_2 (MK-4), and vitamin K_3 (menadione, which lacks a sidechain). These vitamins are critical for mammalian metabolism and must be supplied through food or obtained from symbiotic bacteria living within the gut (Winckel, Bruyne et al. 2009). Vitamin K derivatives, especially vitamin K_1, are cofactors for blood clotting, (Vermeer and Schurgers 2000, Kaneki, Hosoi et al. 2006), components for modifications of proteins through post-translational processes (Winckel, Bruyne et al. 2009), and regulators of bone metabolism and growth (Kaneki, Hosoi et al. 2006). A review detailing recent advances in the roles of vitamin K has recently been reported (Popa, Bigman et al. 2021). UQ-10 has been found to behave as a redox sensor for the regulation of gene expression (Soballe and Poole 1999). PQ-9 serves as a redox sensor for the regulation of carotenoid biosynthesis (Mayer, Beyer et al. 1990, Norris, Barrette et al. 1995) and physiological responses to changes in the quality and intensity of light (Allen, Bennet et al. 1981).

Much of the lipoquinone literature has focused on their redox activity, interactions as cofactors, and contributions to healthy development of biological systems. However, little is known about their properties within the membrane when they are not associated with proteins. Diagrams depicting the electron transport chain generally show their location and function in the

membrane as an amorphous shape across the whole lipid bilayer and labeled simply "Q". This oversimplification perpetuates the disconnect between the location of lipoquinones and their properties. Early investigations into the location of lipoquinones began by considering their size compared to the size of the membrane. The extended length of UQ-10 is approximately 56Å, which could penetrate and span both leaflets of a typical phospholipid bilayer, including both hydrophilic and hydrophobic regions of the membrane (see Figure 2.2) (Trumpower 1981). Therefore, UQ-10 is too long to be accommodated within the membrane unless the isoprenoid chain is folded in some fashion or located parallel to the membrane surface at the midplane. A handful of studies have

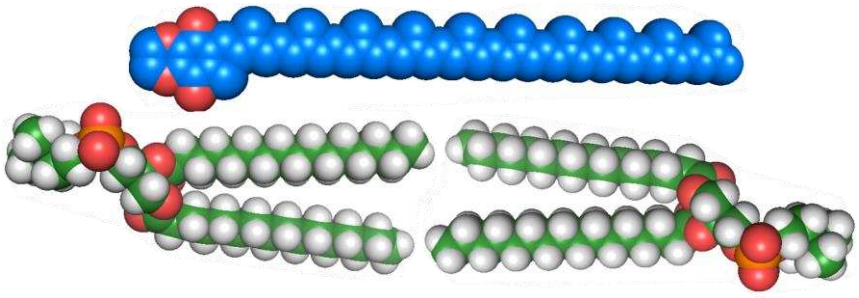

Figure 2.2. Space-filling model of UQ-10 ($C_{59}H_{90}O_4$) (top) and model bilayer of dipalmitoylphosphatidylcholine (DPPC) (16:0) (bottom). Illustration was inspired by a figure that appeared in Ref. (Trumpower 1981).

been performed to determine the location of the lipoquinone headgroup in the membrane; however, the topic remains controversial as no clear consensus has emerged. A summary of these studies' headgroup locations can be found in Table 2.1 (Kingsley and Feigenson 1981, Millner and Barber 1984, Stidham, McIntosh et al. 1984, Michaelis and Moore 1985, Ulrich, Girvin et al. 1985, Ondarroa and Quinn 1986, Cornell, Keniry et al. 1987, Chazotte, Wu et al. 1991, Joliot, Beal et al. 1992, Lenaz, Samori et al. 1992, Salgado, Villalain et al. 1993, Metz, Howard et al. 1995, Marchal, Boireau et al. 1998, Kirchoff, Horstmann et al. 2000, Soderhall and Laaksonen 2001, Afri, Ehrenberg et al. 2004, Hauss, Dante et al. 2005, Loll, Kern et al. 2007, Lambreva, Russo et al. 2014, Galassi and Arantes 2015, Jong, Liguori et al. 2015, van Eerden, de Jong et al. 2015, Gómez-

Murcia, Torrecillas et al. 2016, Kaurola, Sharma et al. 2016, Quirk, Lardner et al. 2016, Koehn, Magallanes et al. 2018, Teixeira and Arantes 2019, Van Cleave, Koehn et al. 2021, Braasch-Turi, Koehn et al. 2022)

Table 2.1. Summary of references regarding the membrane location of the quinone headgroup in lipoquinones. Experimental studies will be noted with superscripted "[E]", and computational studies will be denoted with superscripted "[C]".

Lipoquinone	Near Lipid Headgroups	Within Acyl Chains	Within Midplane
Ubiquinone	Kingsley and Feigenson [E] (Kingsley and Feigenson 1981) Stidham et al. [E] (Stidham, McIntosh et al. 1984) Lenaz et al.[E] (Lenaz, Samori et al. 1992) Galassi and Arantes [C] (Galassi and Arantes 2015) Gómez-Murcia et al.[E] (Gómez-Murcia, Torrecillas et al. 2016) Kaurola et al.[C] (Kaurola, Sharma et al. 2016) Quirk et al.[E] (Quirk, Lardner et al. 2016) Teixeira and Arantes[C] (Teixeira and Arantes 2019) Braasch-Turi et al.[E] (Braasch-Turi, Koehn et al. 2022)	Michaelis and Moore [E](Michaelis and Moore 1985) Cornell et al.[E] (Cornell, Keniry et al. 1987) Chazotte et al.[E] (Chazotte, Wu et al. 1991) Metz et al.[E] (Metz, Howard et al. 1995) Afri et al. [E] (Afri, Ehrenberg et al. 2004) Hauss et al. [E] (Hauss, Dante et al. 2005)	Ulrich et al. [E] (Ulrich, Girvin et al. 1985) Ondarroa and Quinn [E] (Ondarroa and Quinn 1986) Soderhall and Laaksonen [C] (Soderhall and Laaksonen 2001)
	Salgado et al. [E] (Salgado, Villalain et al. 1993)		
Plastoquinone	de Jong et al.[C] (Jong, Liguori et al. 2015) van Eerden et al.[C] (van Eerden, de Jong et al. 2015)		Millner and Barber (Millner and Barber 1984) Joliot et al.[E] (Joliot, Beal et al. 1992) Marchal et al.[E] (Marchal, Boireau et al. 1998) Kirchoff et al.[E] (Kirchoff, Horstmann et al. 2000) Loll et al.[C] (Loll, Kern et al. 2007) Lambreva et al.[C] (Lambreva, Russo et al. 2014)

Menaquinone	Koehn et al. [E] (Koehn, Magallanes et al. 2018) Van Cleave et al. [E & C] (Van Cleave, Koehn et al. 2021)		

The literature places the quinone headgroup in three locations across the bilayer: (1) near the phospholipid headgroup or the interface, (2) within the acyl chains, and (3) within the midplane (Figure 2.3). From these studies, ubiquinones were most often determined to be near the lipid headgroups, plastoquinones were most often determined to be within the bilayer midplane, , and menaquinones were most often determined to be at or near the interface (Figure 2.3). However,

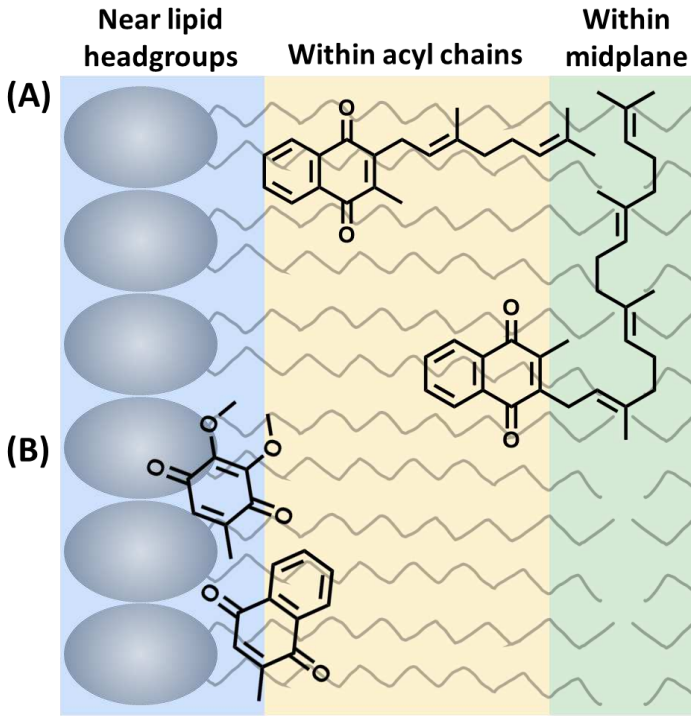

Figure 2.3: Three possible locations of the lipoquinone headgroup: (A) Example of the influence of sidechain on the location of the headgroup. UQ-2 and UQ-4 are both shown as illustrative examples within the acyl chains or within the midplane. (B) Example of the influence of headgroup polarity on the location of the quinone headgroup in the membrane (sidechains omitted for clarity). This figure was originally published in Ref. (Braasch-Turi, Koehn et al. 2022) to include UQ-derivatives in (A). It is licensed under CC-BY 4.0.

there were numerous studies favoring other locations. Although these results seem correlated to the polarity of the headgroup, analogous methods, such as chiral shift NMR, returned conflicting

results. A summary of the materials and methods used in each study can be found in Table 2.3 in Section 2.3.1. Undoubtedly, a more in-depth consideration of how the properties and structural diversity of lipoquinones would assist the interpretation of the results of experimental and computational studies.

In addition to the controversy surrounding the location of lipoquinones in the membrane, there is also considerable dispute over what influences the position of the quinone headgroup in the membrane (Figure 2.3). Many studies suggest the length of the isoprene sidechain determines the location of the headgroup where the longer derivatives are found closer to the midplane. For example, based on the trends observed for UQ-derivatives (Kingsley and Feigenson 1981, Stidham, McIntosh et al. 1984, Ulrich, Girvin et al. 1985, Lenaz, Samori et al. 1992), UQ-4 would be expected to be closer to the midplane than UQ-2 (Figure 2.3A). This is thought to be a result of the sidechain embedding deep into the midplane due to the hydrophobic effect. On the other hand, a few recent studies have shown the type of headgroup is the major influence on the position of lipoquinones in the membrane (Figure 2.3B)(Van Cleave, Koehn et al. 2021, Braasch-Turi, Koehn et al. 2022). For example, the ubiquinone headgroup is more polar than menaquinone; therefore, it would be expected that ubiquinone would be closer to the interface than menaquinone. The truth likely has several different cases depending on the biological system, and too few experimental studies have been reported to provide a consistent picture. In addition, some computational studies have shown the location of the lipoquinone headgroup is dependent on its proximity to proteins. In a recent computational study, the dominant species in lipid-rich environments was found to be the “swimming” quinone found near the interface, and “diving” quinones were the dominant species in protein-rich environments found near the midplane (Singharoy, Maffeo et al. 2020). However, it is likely that some of these quinones are moving within the membrane, making the

studies even more difficult. Therefore, it is important to consider what additional components are present in the membrane when interpreting the results of computational and experimental studies. For this review, we will primarily focus on the chemical and physical properties of lipoquinones, and in organic solvents and lipid environments. We will discuss how these properties (i.e., hydrophobicity, Section 2.2.1; solubility, Section 2.2.2; electrochemical properties, Section 2.2.3, location, Section 2.3; conformation of lipoquinones, Section 2.2.4; and the three lipoquinones Section 2.2.4) could impact the properties of the lipoquinone and be a cause of the inconsistent observations reported in experimental and computational studies (summarized in Section 2.3.1).

In the following review, we will describe the chemistry of lipoquinone with the objective to begin to consider: (*i*) how the properties of lipoquinones affect their shape, location, and redox activity, (*ii*) how their chemical environments impact the chemical and physical properties, and (*iii*) how their properties affect their biological functions within the membrane.

2.2. Properties of Lipoquinones

Lipoquinones are considered hydrophobic, but the consequences of this property are often not taken into consideration when approaching experiments and interpreting data. Herein we will discuss the hydrophobicity, solubility, electrochemistry, and conformational properties of lipoquinones.

2.2.1. Hydrophobicity

Although the presence of both polar and nonpolar regions of the molecules makes lipoquinones amphipathic, the molecules are overall described as hydrophobic. To allow for comparison of these molecules, we compiled reported logP values from the literature and PubChem and calculated logP values of the different lipoquinones with different headgroups, sidechain lengths and redox states in Table 2.2 (Rich and Harper 1990, Ishihara and Sakagami

2007, Tekin and Erkoc 2010, Fedor, Jones et al. 2017). The clogP values were calculated using programs such as Molinspiration and Chemicalize (Rich and Harper 1990, Ishihara and Sakagami 2007, Tekin and Erkoc 2010, Fedor, Jones et al. 2017). From the data in Table 2.2, it is clear the length of the sidechain influences logP and the value of logP increases as the length of the sidechain increases. For example, the logP values for UQ-0, UQ-2, and UQ-10 were found to be 0.8, 4.6, and 19.4, respectively (PubChem). The 20-fold change in logP demonstrates the significant effect an additional 40 carbons has on the hydrophobic properties of lipoquinones.

Table 2.2: LogP and clogP values of select lipoquinones from the literature.

LogP Values				
Lipoquinone	PubChem	Molinspiration	chemicalize	Experimental
UQ-0	0.8	0.22	0.608	0.78[a]
UQH_2-0	1	1.62	1.564	1.02[a]
UQ-1	2.8	2.69	2.219	>3[a]
UQH_2-1	3.2	3.63	3.293	>3[a]
UQ-2	4.6	4.53	3.878	
UQH_2-2	5.3	5.47	4.952	
UQ-4	8.3	8.2	7.198	8.3[b]
UQ-6	12	9.59	10.517	12[b]
UQ-8	15.7	10.15	13.837	15.7[b]
UQ-10	19.4	10.51	17.156	19.4[b], 14.72[c]
UQH_2-1	20.2	10.58	18.23	12.26[c]
PQ-0	1.2	1.31	1.82	
PQH_2-0	1.2	2.67	2.39	
PQ-1	3.4	3.09	3.43	>3[a]
PQH_2-1	3.3	4.24	4.12	>3[a]
PQ-2	5.2	4.94	5.086	
PQH_2-2		6.09	5.781	
PQ-9	18.2	10.38	16.704	
PQH_2-9	18.1	10.48	17.399	
MK-0	2.2	2.04	1.89	2.1[a]
MKH_2-0	2.8	2.99	2.869	
MK-1	3.4	3.83	3.501	3.474[d]

MKH_2-1	4.8	4.77	4.598	1.36[a]
MK-2	5.2	5.67	5.16	4.952[d]
MKH_2-2	6.6	6.62	6.257	
MK-3	7.1	7.52	6.82	6.43[d]
MK-4	8.9	8.86	8.48	7.909[d]
MK-5	10.8	9.44	10.139	9.387[d]
MK-6	12.6	9.8	11.799	10.866[d]
MK-7	14.5	10.7	13.459	12.344[d]
MK-8	16.4	10.28	15.119	
MK-9	18.2	10.45	16.778	
MKH_2-9	19.6	10.53	17.875	

Experimental logP values from Rich and Harper, 1990[a], Fedor et al., 2017 [b], Tekin and Erkoc, 2010[c], Ishihara and Sakagami, 2007[d].

Although the headgroup is the polar part of the lipoquinone, it also contributes to the hydrophobicity. The logP values for UQ-0, PQ-0, and MK-0 were found to be 0.8, 1.2, and 2.2, respectively (PubChem). The fact that the headgroup is hydrophobic is often overlooked even though the numeric changes are less dramatic than obtained from sidechains lengths. Recognizing that the headgroup is hydrophobic is particularly important when interpreting results.

It is logical that UQ-0 has the lowest logP value (0.8) because it is the most polar headgroup, and it has two additional polar C-O bonds. PQ-0 (1.2) and MK-0 (2.2) are more nonpolar, but the addition of the extra ring in the naphthoquinone headgroup plays a significant role in increasing the logP of MK-0. Another important trend to note is how the reduced forms, the corresponding quinols, affect the logP values. Surprisingly, nearly all the lipoquinols have a slightly higher logP value than their respective quinones (ChemAxon , Molinspiration , PubChem). For example, MK-9 and MKH_2-9 were found to have logP values of 18.2 and 19.6, respectively (PubChem). The increase in logP seems contradictory when considering the formation of the hydroxy groups, which allows for the introduction of two additional hydrogen bonds, thus enabling the quinols to interact with other polar molecules. This, however, is not the case, which suggests

that hydrogen bonds are not very significant. The increase in logP of the quinols could be due to the formation of the aromatic ring upon reduction; therefore, increasing the electron density on the aromatic ring. The two hydroxy groups on the aromatic ring are more likely to donate their electron density to the ring and thus not available for hydrogen bonding. In addition, the aromatic ring allows for additional noncovalent interactions, like π- π stacking, with the double bonds in the sidechain and the headgroups of other lipoquinones.

It is also important to note the variability in the calculated logP values of the same lipoquinone derivatives across Table 2.2. For example, UQ-10 was found to have a logP value of 19.4, 10.51, and 17.156 from PubChem, Molinspiration, and Chemicalize, respectively. Although all three values suggest these molecules are sufficiently hydrophobic, the differences in the numbers calculated by the different programs are significant. The discrepancies between sources could have major implications on how computational studies are performed and how the results are interpreted. For example, if a researcher used the PubChem value for UQ-10 (19.4) and another used the Molinspiration value (10.51) in the same experiments, such studies could result in conflicting conclusions for the same system.

The hydrophobicity of lipoquinones also plays a role in conformational structure. In terms of noncovalent interactions, how lipoquinones interact with their surrounding environment will be severely influenced by the hydrophobic effect. This feature led to their physical appearance to be described as “fat globs” which implies they do not adopt any specific conformations. However, polyisoprenoid molecules have been known to adopt specific conformations. For example, squalene epoxide was used in the biomimetic synthesis of cholesterol by Woodward and Bloch in 1953 (Woodward and Bloch 1953). Out of the 256 (2^8) possible isomers, only one stereochemical outcome was achieved, consistent with squalene epoxide adopting a preorganized conformation

prior to cyclization, and this preference for a single conformation affected the molecule's properties and reactivity. Such conformational preferences are likely governed by the hydrophobic effect and intramolecular π- π stacking interactions and suggests that the conformational preferences of lipoquinones are likely to exist.

2.2.2. Solubility

Lipoquinones are found naturally in cell membranes as anticipated since they share amphipathic characteristics with the lipids in the bilayer. However, hydrophobic molecules are likely to exhibit solubility issues when added to aqueous solutions, and this limitation must be taken into consideration when designing experiments or analyses. For example, standard laboratory practices can affect the experimental outcome, such as use of plastic Eppendorf tubes, aa common container in biological studies. Since these opaque vessels obscure the contents, researchers are prevented from observing if a solute has completely dissolved. Therefore, it is entirely possible the researchers did not check to make sure the LQ-derivatives had completely dissolved.

Another example involves measurements of the electrochemical properties of lipoquinones because the results are dependent on whether the compounds are dissolved in organic, aqueous, or mixed organic-aqueous solutions/suspensions. When determining or using reduction potentials of biologically relevant molecules, such as lipoquinones, the insolubility in aqueous solution affects the reduction potentials that are measured in organic solvents. The corresponding reduction potentials in life sciences are extrapolated to aqueous-biological systems.

Surfactants or dimethyl sulfoxide are often used to solubilize hydrophobic compounds in aqueous media, but it comes at the risk of introducing contaminants or additives that are difficult to purify or cause changes in molecular properties of the target compounds in such complex

mixtures. Solubility can therefore impact results obtained in biological assays, particularly with compounds such as lipoquinones. For example, MK-1 through MK-7 were investigated for their anticancer properties (Ishihara and Sakagami 2007). MK-1, MK-2, and MK-3 were found to exhibit cytotoxic activities, and the others, MK-4, MK-5, MK-6, and MK-7, did not (Ishihara and Sakagami 2007). The authors' conclusion was that the longer chain derivatives were not cytotoxic and therefore inadequate candidates for further consideration in their study. An alternative interpretation of these results and explanation of the absence of cytotoxic activity for the longer derivatives is simply aqueous insolubility. Thus, the correlations and proposed patterns of the measured activities may not be based on the true cytotoxicity of these compounds, but was a consequence of their physical properties, which in this case was the poor water solubility of the hydrophobic MK-derivatives with sidechains longer than four isoprenoid groups.

In another study, the substrate affinity of MK-1, UQ-1, MK-4, and MK-9 for MenJ was investigated based on an enzyme assay using surfactant to solubilize the substrates tested (Upadhyay, Kumar et al. 2018). In this study MenJ activity was observed when MK-1 and UQ-1 were used as substrates. However, as described above MK-4 and MK-9 are significantly less soluble, and the fact that no activity was observed in the enzyme assay with these two molecules (with one expected as the natural substrate) was attributed to the lack of solubility of MK-4 and MK-9. The lack of observed enzyme activity was because MK-4 and MK-9 are not soluble under the reported assay conditions (Upadhyay, Kumar et al. 2018).

Recently, truncated lipoquinones have been used to overcome solubility issues. These derivatives contain the same headgroups as the long-chain counterparts but with shorter sidechains (1-4 isoprene units). For example, MK-2 and UQ-2 have been used as truncated representatives of MK-9 and UQ-10, respectively. Although these short-chain derivatives are still hydrophobic, they

are more soluble in organic and aqueous solutions making them attractive alternatives for analysis in aqueous assays containing MK-derivatives. The truncated MK-derivatives are small enough to fit within a typical phospholipid bilayer. One of the first examples of using truncated lipoquinones occurred when Kishi and coworkers measured the reduction potentials of truncated lipoquinone and lipoquinol derivatives in dimethylformamide and calculated their potentials in water (Kishi, Saito et al. 2017). In our recent study, we synthesized MK-1 and MK-1(H_2) for conformational analysis using 1D and 2D NMR techniques (See Section 2.2.4 for additional details) (Koehn, Beuning et al. 2019). Therein we observed the chemical shifts of the aromatic protons shifted slightly between polar and non-polar solvents. As shown in Figure 2.4, the aromatic protons Ha/Hb and Hc/Hd shift closer together in polar solvents and spread further apart in nonpolar solvents.

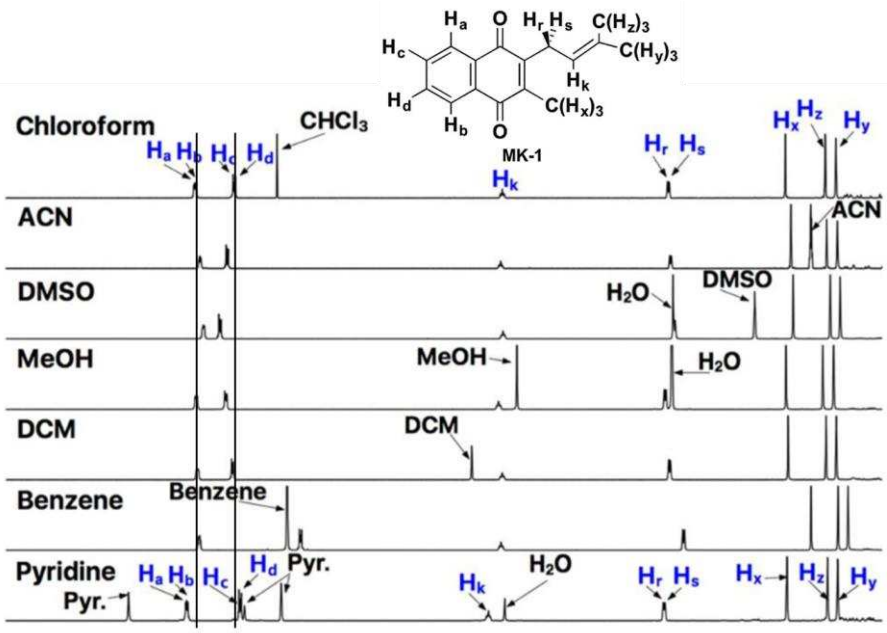

Figure 2.4: 1D NMR spectra of MK-1 in polar and nonpolar solvents. Lines through the aromatic protons, Ha/Hb and Hc/Hd, are provided to highlight the changes in chemical shift. Reprinted with permission from *Biochemistry* 2019, 58, 1596-1615. Copyright 2022 American Chemical Society.

Similar studies were reported using MK-2(Koehn, Magallanes et al. 2018) and UQ-2 (Braasch-Turi, Koehn et al. 2022). This was supported further through 2D NOESY and ROESY NMR

studies (See Section 2.2.4.1 and 2.2.4.3) Through the use the truncated derivatives, we were able to investigate the conformations of the lipoquinones not only in organic solvents but also in a model membrane system. Similar studies would not have been possible if the long chain derivatives were used for the NMR study; both because of the complications relating to the assignment of protons on the long sidechain and the fact that the model membrane system has a monolayer and the MKs with longer sidechains would span and then extend past the monolayer of the reverse micellar model system.

Since lipoquinones are sensitive to their environment regarding their structure and their properties, their hydrophobicities suggest that at sufficient concentration these compounds may aggregate and form micelles in aqueous solutions. In our above mentioned studies regarding the conformation of truncated menaquinones (MK-1and MK-2) and ubiquinone (UQ-2) in several organic solvents, we have not seen evidence for aggregation at the lower concentrations we have been examining these systems (Koehn, Magallanes et al. 2018, Koehn, Beuning et al. 2019). However, formation of micelles would be anticipated in aqueous solutions. When these molecules are in polar and non-polar organic solvents, we observed that both UQ and MKs fold over when the side chain is long enough. Since the interactions between the headgroup and one double bond is less than what is anticipated between two molecules of MK-derivatives (the most hydrophobic lipoquinone in this review), we would expect aggregation to take place when the concentration of the MK-derivative is sufficient in a solvent when the solubility is low, even though neither we nor others have direct evidence for such interactions at this time.

2.2.3. Electrochemical Properties

The quinone headgroup gives lipoquinones their redox activity as electron donors and acceptors in membranes as shown with a UQ-derivative in Figure 2.5 and an MK-derivative in Figure 2.6 (Peover 1962, Turner and Elving 1965, Crane 1966, Eggins 1969, Jaworski, Leniewska et al. 1979, Batanero, Saez et al. 2009, Guin, Das et al. 2011, Beuning Jan. 2020). Using "Q" as a general identifier for the redox state of the headgroup, the 1,4-quinone (**Q**) is reduced to the 1,4-quinol (**Q(H$_2$)**).The first addition of an electron forms the radical anion, referred to as a semiquinone radical anion (**Q1**$^{\cdot-}$). The second addition of an electron generates the dianion catecholate (**Q2**$^{-}$) that ultimately abstracts two protons to form the product, 1,4-quinol (**Q(H$_2$)**). The reaction is reversible to allow lipoquinones to traverse between different protein complexes to serve their function as electron transfer agents.

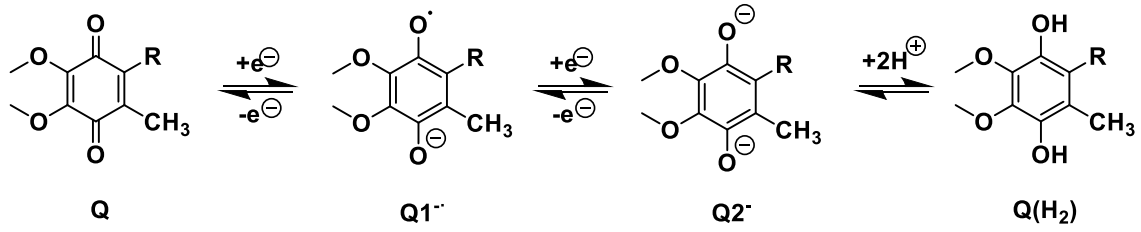

Figure 2.5. Illustration using a UQ-derivative as an example of a one electron reduction of the quinone (**Q**) to the semiquinone radical anion (**Ql**$^{\cdot-}$) and the second one electron reduction to the dianion (**Q2**$^{-}$). Abstraction of two protons results in **Q(H$_2$)**.

In organic solvents, the number of intermediates (**Q1**$^{\cdot-}$ and/or **Q2**$^{-}$) is dependent upon the proticity of the solvent (Peover 1962, Turner and Elving 1965, Crane 1966, Eggins 1969, Jaworski, Leniewska et al. 1979, Batanero, Saez et al. 2009, Guin, Das et al. 2011). For example, both intermediates are observed in aprotic solvents where there are no acidic protons available. The reduction of the quinone in anhydrous aprotic media such as acetonitrile (MeCN), dimethyl sulfoxide (DMSO), or pyridine hence follows a different path than in aqueous solution where protons are available. In protic solvents, including water, only one intermediate is observed. This is due to the radical anion and dianions rapidly abstracting the available protons and cause the two

intermediates to be observed as one (Figure 2.6 A and 2.6C). This difference is clearly observed in electrochemical studies by the location of the potentials in the cyclic voltammograms (CV). In

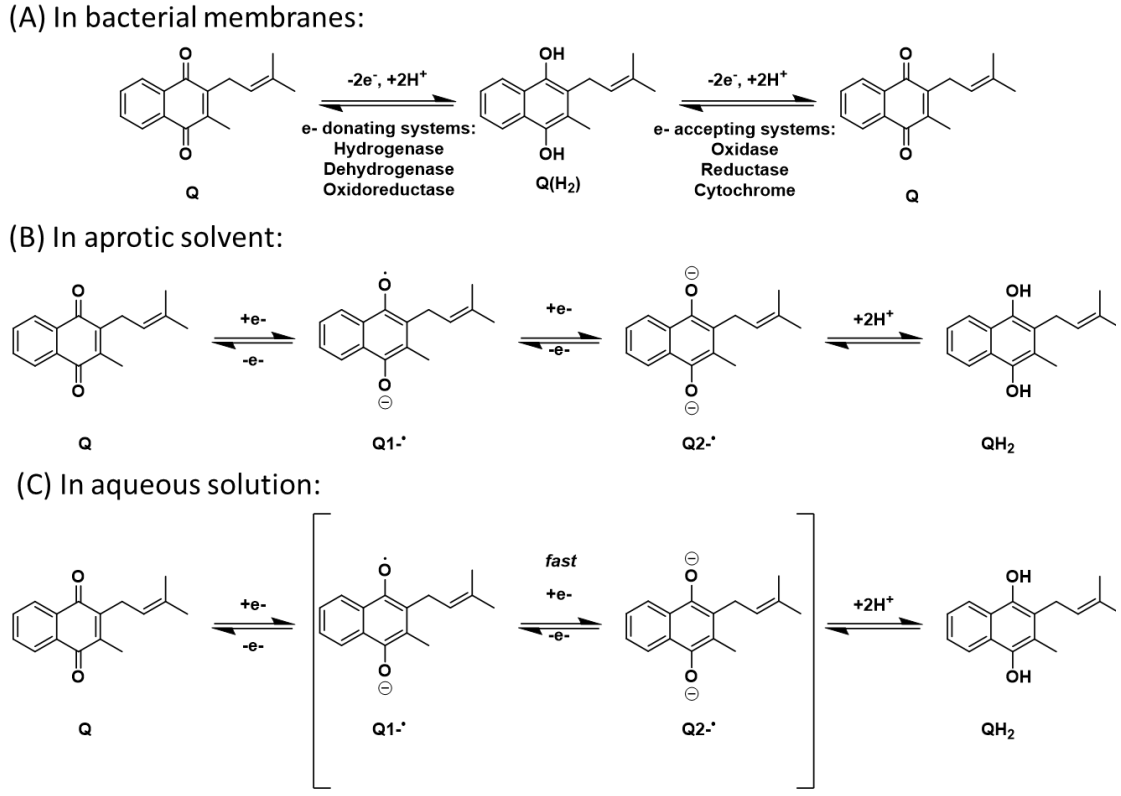

Figure 2.6. Electron transport mechanisms envisioned for (A) bacterial membranes, (B) aprotic solvents, and (C) aqueous solution.

biological systems, this reaction occurs in the hydrophobic membrane bilayer. Under these conditions the two different intermediates have finite lifetimes and can be observed; therefore, the bilayer behaves as an aprotic environment (Figure 2.6B). Quinone redox chemistry is generally investigated in aprotic solvents, where any differences in redox potentials can be measured reproducibly. We note that these aprotic organic solvents better reflect the hydrophobic regions of the lipid bilayer where lipoquinones are more likely to reside and allow for comparison in hydrophobic environments.

The half wave potentials can be calculated using equation (1) where E_{pc} and E_{pa} are the cathodic and anodic peak potentials, respectively. The i_{pc} and i_{pa} were measured from the CVs to determine if the reactions are reversible and all ratios equal 1. The number of electrons in each process can be determined using equation (2) and (3), where ΔE_p is the difference between cathodic and anodic peak potentials, which differ by 0.058V for one electron in in non-aqueous solvents.

$$E_{\frac{1}{2}} = \frac{E_{pc} + E_{pa}}{2} \quad (1)$$

$$\Delta E_p = E_{pc} - E_{pa} \quad (2)$$

$$n = x * \frac{0.059\ V}{\Delta E_p} \quad (3)$$

Although all three lipoquinones are capable of this redox activity, some undergo reduction and oxidation easier than others because of the nature of the headgroup and sidechain structure. For example, menaquinones are the most difficult to reduce, meaning the corresponding quinols are more easily oxidized (Figure 2.7). On the other hand, ubiquinones are easiest to reduce, and therefore ubiquinol is more difficult to oxidize. As mentioned in the introduction, the Great Oxidation Event brought on by the increased levels of atmospheric oxygen gave rise to ubiquinones that could withstand the oxidizing environment (Anand, Chen et al. 2019). According to the reduction potentials of plastoquinones, they would be found in between ubiquinone and menaquinone activity, which is schematically illustrated in Figure 2.7.

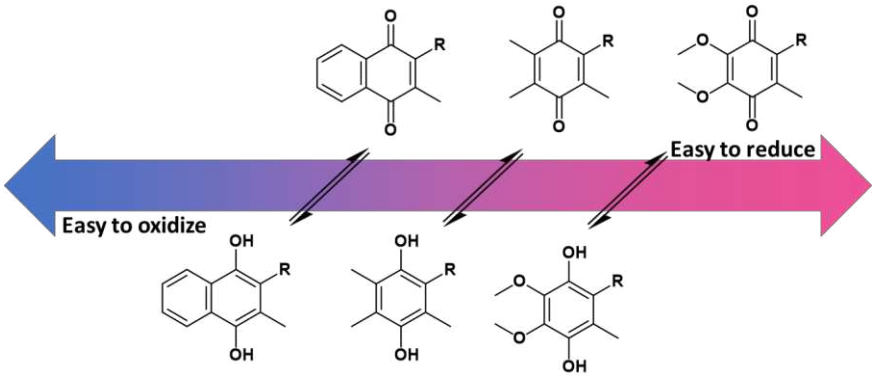

Figure 2.7. The redox potential of ubiquinone, plastoquinone, and menaquinone are shown relative to one another based on known reduction potential values (Becker, Elling et al. 2018). Overall, menaquinones are the most difficult to reduce to the quinol form. Therefore, the menaquinol form is the easiest to oxidize back to the quinone. Ubiquinone is the easiest to reduce, and therefore ubiquinol is the most difficult to oxidize. Details of the extrapolations from the experimental data to the redox potential relevant to biological conditions are described elsewhere in detail. The conversion between quinone to quinol is represented with equilibrium arrows, but it is important to note that equilibrium is condition dependent.

The chemical environment affects the redox reaction, and the hydrophobicity of lipoquinones affects their solubility. Therefore, the chemical environment could impact the number of intermediates observed in the redox reaction. Specifically, whether proton donors are available will determine if the intermediate semiquinone radical anion and dianion are sufficiently long lived and can be observed. In other words, the reaction is observed as one step with no observable intermediate, or as two steps with an observable semiquinone radical anion, respectively. The details of how the experimental data is obtained when the reaction is taking place are therefore paramount. Oftentimes values found in tables for reduction potentials in aqueous media have been extrapolated from measurements carried out in organic solvents because the compounds are not soluble in water. It is important to recognize that electrochemical studies are usually measured in the presence of sufficient ions (electrolytes) to measure electron transfer to and from organic molecules and hence the reaction conditions are probably not as close to those actually observed in the biological system where the environment in the membrane is likely to be more hydrophobic. These studies probing the redox reaction are therefore generally done in the

absence of water but at high enough substrate concentrations and electrolytes that the redox potentials can be measured. Unfortunately, the experimental limitations are often not discussed and appreciated. If limited details of the measurements, nor the extrapolations are mentioned, then comparison of the relevant redox potentials is more circumspect, and, in worst case scenarios, lead to an erroneous conclusion.

While the function of menaquinone derivatives is well established, the role of regiospecific partial saturation in the isoprenyl sidechain on menaquinone's redox potential remains unclear. The effects of structural differences on the redox potentials and diffusion coefficients of various MK-derivatives in three aprotic solvents (MeCN, DMSO, and pyridine) has been reported in a Ph.D. dissertation by Cheryle Beuning at Colorado State University (Beuning Jan. 2020). This Ph.D. dissertation investigates the partially saturated MK-2(II-H_2) and MK-3(II-H_2) derivatives, and these were found to be easier to reduce (more positive potentials), than the fully unsaturated and the fully saturated MK-derivatives, the latter being among the hardest MK-derivatives to reduce (more negative potentials). Most unsaturated MK-derivatives were in the mid-range of potentials measured. These results are in line with the interpretation that the composition of the sidechain plays a role in the reduction potential of the compound. In addition, there are examples of stable semiquinone species having biological activity with receptor sites in QH_2-reductases; however, the most common reduced form in biological systems is the quinol (Ohnishi, Salerno et al. 1982, Swallow 1982, De Vries, Berden et al. 1992). Undoubtedly, these patterns provide insight into these interesting molecules.

2.2.4. Conformation of Lipoquinones

As mentioned above, polyisoprenoid molecules have been known to adopt specific conformations in solution. In a study by Murgolo and coworkers, they determined dolichol-19, a

polyisoprenyl alcohol with 19 isoprene units, adopts a central coiled conformation flanked by two arms (Murgolo, Patel et al. 1989). In lipoquinones, the polyisoprenoid sidechain allows for multiple degrees of freedom to adopt a myriad of conformations. The sidechain's ability to rotate suggests the sidechain could associate with itself and/or the headgroup of the MK-derivative. To discuss the conformations, we will begin by describing the relationship between the headgroup and the sidechain using approximate dihedral angles about the bond connecting the headgroup to the sidechain (Figure 2.8). A folded conformation refers to a dihedral angle of ~90° where the sidechain is orthogonal to the headgroup (Figure 2.8A). A flat conformation refers to a dihedral

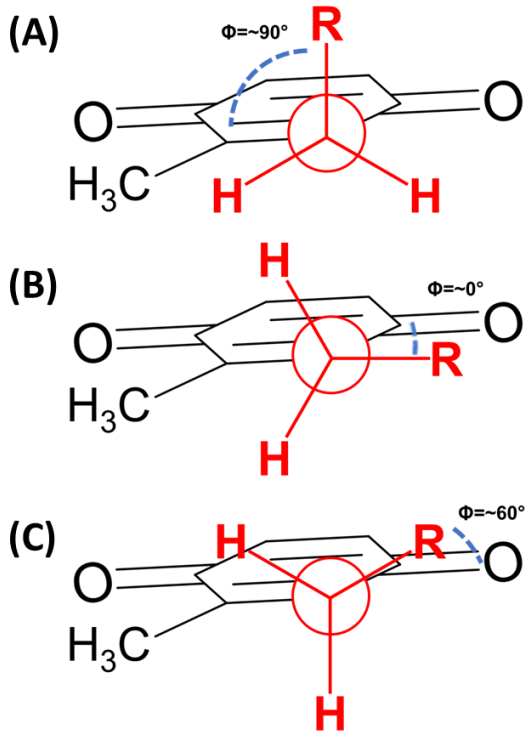

Figure 2.8: Newman projections of folded and flat conformations. (A) Folded conformation with a dihedral angle of approximately 90°. (B) Flat conformation with a dihedral angle of approximately 0°. (C) Gauche conformation with a representative dihedral angle of ~60°.

angle of ~0° where the sidechain is in plane with the headgroup (Figure 2.8B). A gauche conformation will refer to any dihedral angles in between, shown with a dihedral angle of 60° in Figure 2.8C.

The isoprene units along the sidechain have many degrees of freedom to allow for multiple points of rotation that could lead to countless conformations. For simplicity, we will focus on the overall direction the end of the sidechain points relative to the headgroup (Figure 2.9). When the sidechain extends straight from the headgroup to sidechain bond, this will be referred to a "extended", as shown in Figure 2.9A and 2.9B. When the end of the sidechain is positioned over

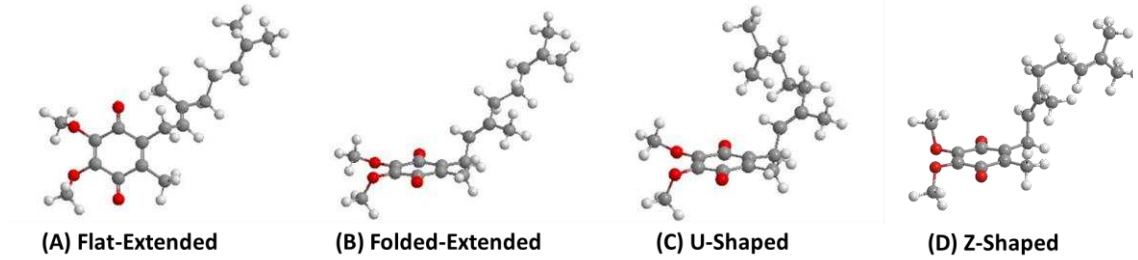

Figure 2.9. Four different possible conformations, using UQ-2 as an example, describing the relationship between the headgroup and the end of sidechain observed in computational studies. (A) Flat-extended conformation, (B) Folded-Extended, (C) U-Shaped. These images were reported in our recent paper regarding the conformations of UQ-2 (Braasch-Turi, Koehn et al. 2022) and licensed under CC BY 4.0. (D) Z-shaped, generated using calculations in Chem3D.

the headgroup and is referred to as a U-shaped conformation (Figure 2.9C). When the sidechain is pointed away from the headgroup, it will be referred to as "Z-shaped" (Figure 2.9D). Throughout the literature, ubiquinones, plastoquinones, and menaquinones have been shown to adopt some variation of a folded conformation in computational studies (Himo, Babcock et al. 1999, Nilsson, Eriksson et al. 2001, Nilsson, Lyubartsev et al. 2001, Ceccarelli, Procacci et al. 2003, Galassi and Arantes 2015, Jong, Liguori et al. 2015), but very few experimental studies have been able to support these findings until recently (Koehn, Magallanes et al. 2018, Koehn, Beuning et al. 2019, Eddine, Biaso et al. 2020, Braasch-Turi, Koehn et al. 2022)

2.2.4.1. Ubiquinones

Several computational studies have investigated the conformation of the headgroup relative to the sidechain by rotating about the bond attaching the sidechain to the headgroup and calculating the energy. Nilsson and coworkers determined the dihedral angle of UQ-et, an ethyl substituted

UQ-derivative, to be ~90 °at a global energy minimum (Nilsson, Lyubartsev et al. 2001). Ceccarelli and coworkers found similar results in their study using UQ-1, which showed two local minima: ~90°and ~270°, both orthogonal relationships (Ceccarelli, Procacci et al. 2003). Both studies support a folded conformation of the UQ-derivatives regardless of the type of sidechain. In contrast, Galassi and Arantes found the dihedral angle of UQ-1 to be ~180°, supporting a flat-extended conformation. Since all three studies were computational, it is difficult for the non-expert to determine if the differences between the studies were due to variations in parameters used or if the energy barriers are actually that low to rotate between flat and folded conformations (Galassi and Arantes 2015). In addition, other studies only investigating the location of lipoquinones in membrane environments reported figures that showed folded conformations, and whether or not this reflected in detailed conformational data is unknown (Joela, Kasa et al. 1997, Bernardo, Fato et al. 1998, Lenaz, Fato et al. 1999, Tekin and Erkoc 2010, Kaurola, Sharma et al. 2016). Experimental studies are then necessary to validate the computational findings.

In our recent study, we determined the conformation of UQ-2 in organic solvents using 2D ^{1}H-^{1}H NOESY and ROESY NMR spectroscopy (Braasch-Turi, Koehn et al. 2022). For example, the presence of a cross peak between the headgroup methyl protons and the protons along the sidechain suggest they must be within ~5Å to cause magnetization transfer between these two protons. Investigating conformations in polar and nonpolar organic solvents, such as DMSO, acetonitrile, and pyridine, we observed cross peaks that suggest UQ-2 adopted more of a U-shaped conformation in polar solvents. A clear indication of a U-shape verses the other possible conformations is a cross peak between the methyl group of the headgroup and the geminal dimethyl groups at the end of the sidechain, which will be referred to as the terminal methyl groups. To better visualize the differences between UQ-2 in acetonitrile and DMSO, we calculated the

distances between the atoms using the 2D NOESY and ROESY data (for additional details see (Braasch-Turi, Koehn et al. 2022)) to build the conformations, and the resulting conformations were superimposed and are shown in green and purple respectively in Figure 2.10. With the headgroups aligned, there is a slight change in dihedral angle along the bond connecting the headgroup to the sidechain. As the sidechain extends, this change in dihedral angle has

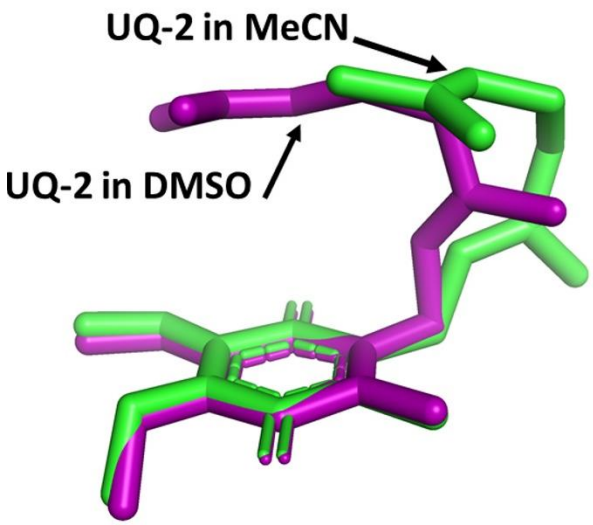

Figure 2.10. Superimposed 3D conformations of UQ-2 based on the 2D NMR data in d3-acetonitrile (MeCN, green) and d6-DMSO (purple). This figure was originally published in Ref. (Braasch-Turi, Koehn et al. 2022) and is licensed under CC-BY 4.0. The original figure was modified to include only the depicted image.

considerable influence on the position of the terminal methyl groups. In DMSO, the terminal methyl groups are located above the headgroup, almost parallel, leading to a U-shaped conformation. In acetonitrile, the terminal methyl groups are angled away from the headgroup leading to a more gauche conformation of the sidechain. In nonpolar solvents, such as benzene and pyridine, cross peaks between the headgroup methyl and the vinyl protons along the sidechain suggest UQ-2 adopts a folded conformation as well, but there were no cross peaks between the headgroup methyl and the terminal methyl groups. This indicates UQ-2 adopts a folded

conformation in nonpolar solvents, but the sidechain is extended or positioned as more of an open U-shaped conformation.

In our recent study, we also determined the conformation of UQ-2 in a model membrane system bis(2-ethylhexyl)sulfosuccinate sodium reverse micelles (abbreviated AOT RMs) using 2D ^{1}H-^{1}H NOESY and ROESY NMR spectroscopy (Braasch-Turi, Koehn et al. 2022). When UQ-2 was added to AOT RMs, cross peaks between the headgroup methyl group and the terminal methyl groups were observed, suggesting a U-shaped conformation. It would make sense that the UQ-2, when incorporated in a membrane, would adopt a more compact structure akin to the structure observed in d_6-DMSO. The full details on this study can be found in our publication (Braasch-Turi, Koehn et al. 2022).

2.2.4.2. Plastoquinones

Computational studies have shown plastoquinones adopting folded conformations in membrane (Jong, Liguori et al. 2015, Eddine, Biaso et al. 2020) and solvent environments (Himo, Babcock et al. 1999, Nilsson, Eriksson et al. 2001). A study by de Jong and coworkers determined the dihedral angle of plastoquinones were 100° and 250° in a membrane environment, supporting a folded conformation. Himo and coworkers investigated the conformation of PQ-et, UQ-et, and MK-et to understand how the C2 methyl group on the headgroup impacts rotational freedom of the sidechain in solvent environments (Himo, Babcock et al. 1999). In the presence of the methyl group, the dihedral angle of menaquinone and ubiquinones was found to be ~100° within a clear energy minimum along the indicated bond. This is consistent with a folded conformation. However, in the case of PQ-et, the local energy minimum was preceded by a low energy plateau from 0-100°. Nilsson and coworkers came to a similar conclusion (Nilsson, Eriksson et al. 2001). Although the energy minimum at 100° suggests the folded conformation is preferred, the plateau

implies the sidechain of PQ-et can rotate freely between flat and folded conformations without energy penalties. Considering the structure of each headgroup, plastoquinones do not contain the C2 methyl group; therefore, the C2 methyl group must behave as a rotational barrier to influence their conformations.

In addition to the conformation of the headgroup relative to the sidechain, de Jong and coworkers also investigated the preferred conformations of the sidechains within a simulated lipid bilayer using two different computational approached: United Atom (UA) and Coarse Grain (CG) (Jong, Liguori et al. 2015). Within both datasets, the sidechains were observed in three distinct conformations that they called U, L, and I conformations. In the U conformation, the sidechain extends into the midplane and then curves back towards the headgroup, intercalating the end of the sidechain into the acyl tails. The L conformation placed the end of the isoprenoid sidechain within the bilayer midplane, forming an approximate right angle. The I conformation extends the sidechain through the midplane into the opposite leaflet. In their simulations, they observed different populations of each conformation for the same lipoquinones. For example, the sidechain of PQ-9 was found to adopt L:I:U ratios of 53:16:13 and 46:18:13 for UA and CG studies, respectively. Overall, both computational approaches showed the L conformation was the most popular conformation, followed by I, and then U. The preference for the L conformation suggests the sidechain is embedded in the midplane to minimize interactions with polar environments.

2.2.4.3. Menaquinone

Of the three lipoquinones we examine in this review, the properties of menaquinones have received the least attention in the literature. In our recent publication, we reported an analogous study to the UQ-2 study described in Section 2.2.4.1 with truncated, MK-derivatives, MK-2, MK-1, and MK-1(H_2), in organic solvents using 1D and 2D NMR spectroscopy (Koehn, Magallanes et

al. 2018, Koehn, Beuning et al. 2019). Like UQ-2, MK-2 adopts a folded, U-shaped conformation in polar solvents, such as DMSO and acetonitrile. MK-2 was found to adopt a folded-extended or a more open U-shaped conformation in nonpolar solvents, such as benzene or pyridine. The details regarding the conformational determination of MK-2 in organic solvents can be found in our publication (Koehn, Crick et al. 2018).

The conformation of MK-2 in AOT RMs was similarly determined by the cross peaks between the headgroup and the terminal methyl protons suggest that the end of the sidechain is positioned over the headgroup, overall suggesting MK-2 adopts a folded, U-shaped conformation in AOT RMs. The conformations of MK-1 and MK-1(H_2) were also investigated using analogous NMR studies (Koehn, Beuning et al. 2019). Both derivatives were found to adopt folded-extended conformations in organic solvents and AOT RMs. This designation was attributed to the shorter sidechain that is not long enough to extend over the headgroup to achieve a U-shaped conformation.

In a recent study by Sitkowski and coworkers, MK-7 derivatives found in dietary supplements were characterized using multidimensional NMR analysis (Sitkowski, Bocian et al. 2018). The researchers also investigated the conformations of each isomer using DFT modeling studies. The resulting conformations show each MK-7 isomer is folded, showing an approximate 90° dihedral angle about the bond connecting the headgroup to the sidechain. The position of the sidechain seems to be dependent upon the geometry of the double bonds. By the definitions established at the beginning of this section, the sidechain of (E6,ω)-MK-7 adopts a folded-extended conformation. Interestingly, the sidechain of the (Z6,ω)-MK-7 isomer adopts a helical conformation that is extended away from the quinone headgroup. The authors note the similarities between the helix observed in the sidechain and the observed coiled conformations of dolichol

(Murgolo, Patel et al. 1989). Finally, the (E, Z3,ω)-MK-7 isomer adopts a less defined conformation along the sidechain. Overall, the derivative is folded, and the sidechain extends away from the headgroup for 2-3 isoprene units, adopting part of a helix at the Z3-isoprene unit. From there, the sidechain appears to extend further after the turn of the helix. This study suggests the conformation of the sidechain is dependent upon the geometries of the double bonds within the sidechain.

2.2.5. Comparison of Lipoquinone Conformations

The C2 methyl group adjacent to the sidechain impacts the conformation of lipoquinones. In a recent study by Eddine and coworkers, combined the results of DFT modeling and EPR spectroscopy, specifically ^{1,2}H hyperfine coupling constants, were used to evaluate the steric effects of the headgroup methyl group of long chain UQ-, MK-, and PQ-derivatives (Eddine, Biaso et al. 2020). Their results corroborate the findings of Himo and Nilsson and support the hypothesis that the headgroup methyl group behaves as a rotational barrier to cause lipoquinones to favor a folded conformation. Each energy diagram of UQ- and MK-derivatives have a distinct energy minimum around 90°. However, as described in Section 2.2.4.2, PQ-derivatives, showed an energy minimum around 100° with a low energy plateau leading up to it (Himo, Babcock et al. 1999). These differences are consistent with the notion that implies the headgroup structures were selected to afford specific conformations and that those differences could have implications in their functions.

These different results demonstrate that the conformations of lipoquinones are dependent on the chemical environment. As described in the previous sections, MK-2 and UQ-2 are sensitive to their solvent environment, adopting increasingly folded conformations in polar solvents and more open, folded conformations in nonpolar solvents (Koehn, Magallanes et al. 2018, Braasch-

Turi, Koehn et al. 2022). To compare the conformations, we superimposed the conformations of UQ-2 and MK-2 in DMSO to clearly show how the headgroup affects the conformation in the same solvent (shown in pink (UQ-2) and blue (MK-2) in Figure 2.11). With the headgroups aligned, the sidechains nearly overlap completely until just after the first isoprene unit. The

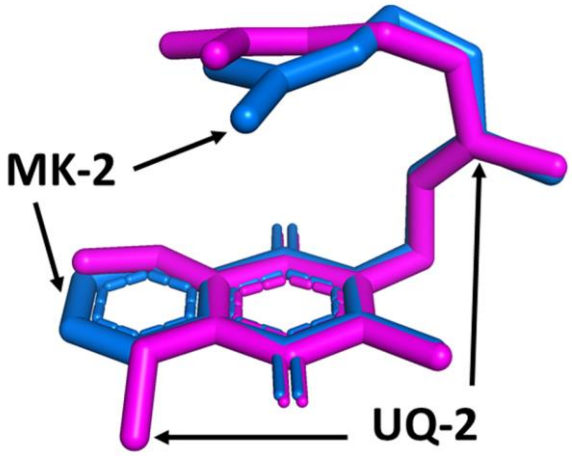

Figure 2.11. Superimposed 3D conformations of UQ-2 (pink) and MK-2 (blue) based on the 2D NMR data in DMSO. This figure was originally published in Ref. (Braasch-Turi, Koehn et al. 2022) and is licensed under CC-BY 4.0. The original figure was modified to include only the depicted image.

adoption of these folded conformations is likely due to the hydrophobic effect as well as noncovalent interactions such as π- π stacking, where the π bonds in the headgroup are interacting with the π bonds of the sidechain. These results suggest ubiquinones and menaquinones will adopt similar conformations when the chemical environments are similar. Considering a membrane, the hydrophobic effect could greatly influence the conformation of UQ-2 and MK-2 in the more polar region of the membrane. If the lipoquinones were located closer to the bilayer midplane, the nonpolar environment may influence the conformations to adopt more open folded or even flat conformations in line with the observed trend in the model studies.

2.2.6. Conformations of Lipoquinones in Protein Active Sites

Although the conformations of lipoquinones in organic solvents and membrane environments are very different than lipoquinone conformations associated with proteins and protein active sites, the function of lipoquinones involve proteins and their associations with lipids. Even in the cases of protein-associated lipoquinones, the conformations about the bond connecting the headgroup to the sidechain appears to be specific to the biological system at hand. For plastoquinone, the conformation of the headgroup relative to the sidechain of PQ_A within Q_A binding site of photosystem II depends on the species of bacteria. The dihedral angle was found to be -10°in *Thermosynechococcus elongatus* (Zhang, Bommer et al. 2017), 88-89° in *Pisum sativum* (Su, Ma et al. 2017), and ranging from 32-70° in *Thermosynechococcus vulcanus* (Tanaka, Fukushima et al. 2017). This variation suggests the conformations are influenced by the active site and consequently its specific function, perhaps tailoring the reduction potential of the plastoquinone to the target protein and individual species. This complementarity has also been observed in the lipoquinones cofactor binding sites. For example, MK-7 is an electron carrier in many species of bacteria. Within the reported crystal structure of polysulfide reductase active site of *Thermus thermophilis HB27* (Protein Data Bank (PDB) ID: 2VPW), the MK-7 ligand was simplified to show only part of the first isoprene unit deposited in the PBD crystal structure, which is shown in Figure 2.12A and 2.12B (Jormakka, Yokoyama et al. 2008). From this crystal structure, MK-7 appears to adopt a flat conformation, but it is impossible to determine the position of the sidechain from the simplified representation. Within the active site of the menaquinol oxidase of *Bacillus subtilis* (PDB ID: 6KOB), MK-7 was found to adopt a folded conformation with the sidechain pointed away from the headgroup, resulting in a Z shape (Figure 2.12C and 2.12D) (Xu, Z et al. 2020). Clearly, the active site is stabilizing the sidechain to adopt a Z-shaped conformation, which is observed less frequently in the membrane. Together these two examples of protein-

lipoquinone complexes show that for protein-associated lipoquinones there is a greater variety in lipoquinone conformations than when the lipoquinone is in the membrane. This also sheds light

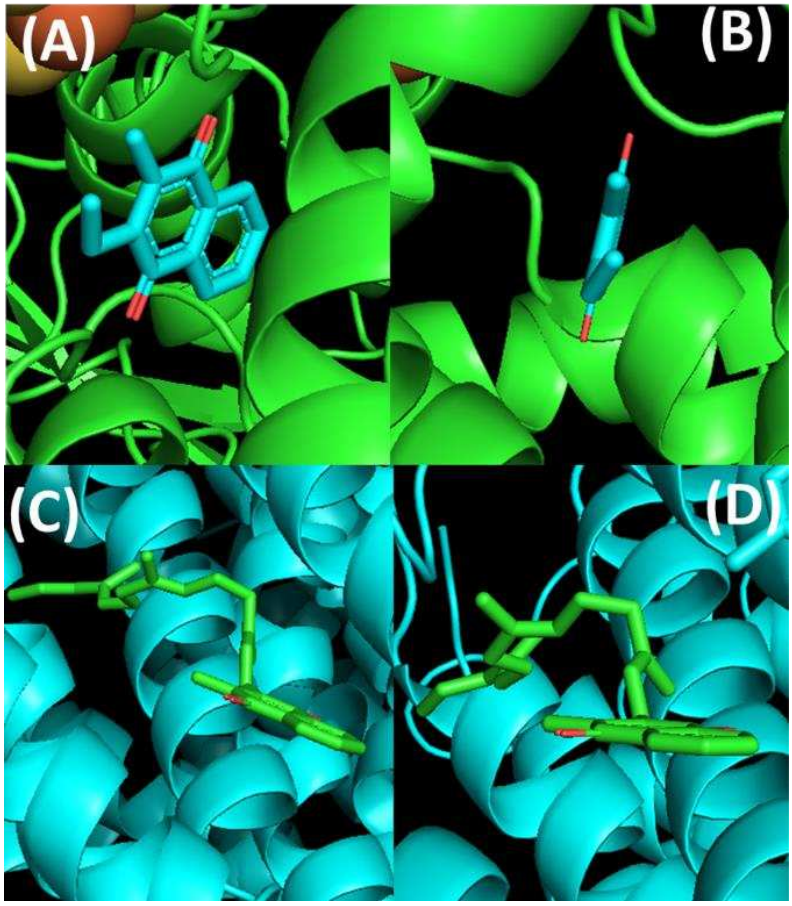

Figure 2.12. Conformations of MK-7 within the active sites of two different enzymes: Top: *Thermus thermophilis HB27* (PDB ID: 2VPW), and Bottom: *Bacillus subtilis* (PDB ID: 6KOB). (A) MK-7 (shown in cyan) full view. (B) MK-7 side view showing the plausible flat conformational relationship between the headgroup and the sidechain. (C) MK-7 (shown in green) full view highlighting the Z conformation. (D) MK-7 side view to highlight the folded conformation along the bond connecting the headgroup to the sidechain.

on how much information may be missing by omitting the full lengths of the sidechain when interpreting active site associations. Furthermore, it is possible that lipoquinones possess a baseline reduction potential which can be manipulated by their surroundings to tailor the reduction potentials required to transfer the electrons from the respective proteins.

In addition to the conformation of the sidechain, ubiquinones contain two additional functional groups, methyl ethers, which can be manipulated by its surroundings. For example, ubiquinones have been shown to adopt slightly different orientations between quinone binding sites, Q_A and Q_B, along the electron transport chain of eukaryotes (Nonella, Mathias et al. 2003). The differences in dihedral angle have been calculated for each binding site throughout the literature. Nonella and coworkers found a difference of <30° for the out-of-plane methoxy group between Q_A and Q_B in *Rhodobacter sphaeroides* (Nonella, Mathias et al. 2003). Later, Wraight and coworkers determined the dihedral angles of the Q_B C2 and C3 methoxy groups to be -90 ± 9°and 88 ± 20°, respectively, in the same bacterium (Wraight, Vakkasoglu et al. 2008). Taguchi and coworkers determined the C2 methoxy group of Q_B is 20-25° more out of the plane of the headgroup than Q_A, which places it approximate 50 or 155° relative to the headgroup.(Taguchi, O'Malley et al. 2013). These conformational changes were found to affect the reduction potentials within the active site, which further suggests conformational changes finetune the reduction potentials of the lipoquinone to the active site.

2.3. Location of Lipoquinones in Membranes

The different structures of the three lipoquinones seem to provide an opportunity to compare the effects of the headgroup on its position within lipid bilayers. However, since lipoquinones have been investigated with a range of different liposome compositions and analytical methods, a direct comparison is somewhat difficult. Furthermore, many experimental and computational studies have been performed with ubiquinones, followed by plastoquinones, but far fewer studies have been done to determine the location of menaquinones in lipid bilayer.

2.3.1. Ubiquinones

The location of ubiquinones in the membrane has been of interest to researchers for many years. It has been studied using a variety of experimental and computational techniques that are summarized in Table 2.3 (next page). Although determining the location has caught the attention of researchers, there has not been a consensus regarding its exact position. As a result, the benzoquinone headgroup has been found to be in all three sections of the bilayer. Unfortunately, experiments using similar methods have been reported to produce conflicting results. To highlight a few examples, two studies reported using chiral shift NMR spectroscopy. Specifically, Kinglsey and Feigenson used a deuterated model membrane system and Dy^{3+} and Tm^{3+} chiral shift reagents to investigate the location of UQ-10 (Kingsley and Feigenson 1981). They observed the chemical shifts of the methoxy groups were influenced by the presence of the chiral shift reagent. This led to the conclusion that the headgroup must be close enough to the interface to interact with the chiral shift reagent in the aqueous environment. On the other hand, Michaelis and Moore used Pr^{3+} & Eu^{3+} chiral shift reagents and found the chemical shifts were not affected by the chiral shift reagents. This led to the conclusion that the headgroup must be far away from the interface, at least past the C2 carbon of the acyl chains within the lipid tails (Michaelis and Moore 1985). Although these studies used the same analytical method, it is important to note they used different model membrane systems: Kingsley and Feigenson used dimyristoylphosphatidylcholine-*d*72 (DMPC-*d*72) and Michaelis and Moore used egg phosphatidylcholine (EPC). Furthermore, the two studies used different chiral shift reagents. It is possible the contradicting data could be a result of the model membranes or chiral shift reagents used.

Overall, many of the discrepancies between the studies can be attributed to the methods used and the varying detections limits between methods. Primarily, it is critical to consider the

hydrophobicity of lipoquinones when approaching the formation of lipid vesicles. It is also important to acknowledge the solubility of the analytes used in each study, the complexity of these systems, and the purity of the lipids used in the study. Most of the experimental studies listed in Table 2.3 formed the lipid vesicles using a similar procedure. The analyte was dissolved in a polar solvent, like chloroform, and the lipids were added to the mixture. The solvent was removed and then rehydrated with D_2O. It is important to note the variability in the concentration of lipoquinone and the ratio of lipids present in each study. The final membrane structure (lipids + lipoquinones) is a property of the mixture; therefore, the molar fraction of the lipoquinone and the composition.

Table 2.3. Summary of the location of the ubiquinone headgroup.

Author(s)	Compound(s)	Method(s)	Type of Membrane	Location of Quinone Headgroup	Location of Sidechain
Kingsley and Feigenson, 1981*	UQ-1-10 & $UQ(H_2)$-1-10	^1H NMR with chiral shift (Dy^{3+} & Tm^{3+})	DMPC-*d*72	Polar headgroups of lipids	Increase number of isoprenes, further into acyl tails
Stidham et al., 1984*	UQ-10	^{13}C NMR, light microscopy, & XRD	DMPC, DPPC, & EPC	Polar headgroups of lipids	Increase number of isoprenes, further into acyl tails
Ulrich et al., 1985*	UQ-2, 3, & 10	UV-Vis & NMR. Measured the rate of reduction of UQ with $NaBH_4$ & dithionite	DMPC & DPPC	Deep enough in acyl tails to not to be reduced by $NaBH_4$	UQ-2 and 3, close to interface, UQ-10 deep in membrane
Michaelis and Moore, 1985*	UQ-10	^1H NMR with chiral shift (Pr^{3+} & Eu^{3+}) & Electron microscopy	EPC	Acyl chains at least beyond C2	
Ondarroa and Quinn, 1986*	UQ-10	^1H NMR with chiral shift (Dy^{3+}) & ^{31}P NMR	DPPC & EPC	Midplane	
Cornell et al., 1987*	UQ-10 & various deuterated derivatives	^1H NMR, solid state ^2H NMR with deuterated lipids, & enzyme assays	dispersed in *E. Coli* plasma membranes & inner membranes of beet root mitochondria, DMPC & EPC	Acyl chains to midplane	

Lenaz et al., 1992*	UQ-3 & UQ-10	fluorescence quenching & linear dichroism	phospholipid purified from asolectin	UQ-3 is found throughout, UQ-10 was found to be parallel to acyl chains, headgroup near interface	
Chazotte et al., 1991†	NBDHA-Q (Fluorescent UQ-Derivative)	Fluorescence recovery after photobleaching & fluorescence spectroscopy	DMPC with & without cholesterol	Acyl chains to midplane. "Cholesterol region"	Isoprene tail by interface likely due to the fluorescent linker
Salgado et al., 1993*	UQ-10 & UQ-10(H_2)	magic angle ^{13}C NMR with Gd^{3+} chiral shift	Egg yolk phosphatidylcholine	Quinol perturbs membrane surface more than quinone- suggesting quinone is closer to the tails.	
Metz et al., 1995*	^{13}C-UQ-10	^{13}C NMR with Gd^{3+} chiral shift	DMPC & DHPC	headgroup buried in the lipid bilayer or in the midplane. Headgroup preferentially parallel to lipid chains	
Soderhall and Laaksonen, 2001‡	UQ-et & UQ-10	nanosecond MD calculations	DPPC bilayer	UQ-et between C4-C10 of palmitic tails, UQ-10, 2 positions: one close to lipid headgroup other close to midplane	UQ-10 able to move with headgroup and aligned parallel to palmitic tails
Afri et al., 2004*	UQ-10 & UQ-10(H_2)	NMR chemical shift-polarity correlation, 1D H and C, 2D COSY, HMQC, HMBC, and NOESY, measured rate of reduction of substrates with vitamin C	DMPC vesicle	Deep enough in acyl tails not to be reduced by vitamin C	Embedded in "slab"
Hauss et al., 2005*	UQ-10	neutron diffraction	deuterated DMPC doped with deuterated DMP-serine	Midplane	In midplane, may not be extended, could be "curled"
Galassi and Arantes, 2015‡	UQ-0,1,2 & 6 UQ(H_2)-0,1,2 & 6	MD calculations	POPC	Water-bilayer interface near glycerol groups, perpendicular to midplane, does not change significantly with length of tail	In acyl tails, moves with headgroup
Gómez-Murcia et al., 2016†	idebenone & idebenol	differential scanning calorimetry, X-ray diffractions, and ^2H NMR and NOESY MAS	DPPC, POPC, and deuterated DPPC	Close to lipid-water interface by NOESY	
Kaurola et al., 2016‡	UQ & UQ(H_2) 1,6,8,9,10	atomistic MD calcs	DLPC, DLPE, CL	Acyl groups right under headgroup region, stabilizes in midplane	

Quirk et al., 2016*	UQ-10	Surface-enhanced infrared adsorption spectroscopy & neutron reflectometry	deuterated DMPC	IR vibrations suggest headgroup is in both polar and nonpolar environments	Likely in midplane and has freedom to move with headgroup
Teixeira and Arantes, 2019‡	UQ-2,10 & UQ(H_2)-1,10, MK-9	MD calculations	POPC, DLPE, DLPC	Polar headgroups of lipids	
Murai M et al. 2014, Tsui et al 2019, & Allan et al. 2015	UQ-derivatives (Coq10 and Coq11)	Genetic and biochemical studies including photoaffinity labeling	*Saccharomyces cerevisiae*	Associated with Coq10 in the hydrophobic channel	Associated with Coq10 in the hydrophobic channel
Tsui et al 2019, Hernandez -Camacho 2018, Murai M et al.,	UQ-derivatives	Cellular studies (including genetics, and animal studies), X-ray and docking calculations	Human mitochondrial membrane	Associated with Coq10 in the hydrophobic channel	Associated with Coq10 in the hydrophobic channel

*Samples prepared using similar procedures: dissolve analyte and lipids in polar solvent, remove solvent, and rehydrate in D_2O. †Modified ubiquinone analyte. ‡Computational study.

Type of membrane abbreviations definitions: dimyristoylphosphatidylcholine (DMPC), dipalmitoylphosphatidylchol-ine (DPPC), egg phosphatidylcholine (EPC), diheptanoylphosphatidylcholine (DHPC), palmitoyl-oleoylphosphatidylcholine (POPC), dilinoleoylphosphatidylcholine (DLPC), dilauroylphosphoethanolamine (DLPE), and cardiolipin (CL).

2.3.2. Plastoquinones

Plastoquinones are located within the thylakoid membrane of chloroplasts. The exterior stroma and interior lumen of the thylakoid membrane are comprised of aqueous media, so the consensus seems to be that the hydrophobic plastoquinones molecules form a pool, freely diffusing throughout the bilayer midplane (Guskov, Kern et al. 2009, Zobnina, Lambreva et al. 2017, Havaux 2020). However, some computational studies have shown the plastoquinone pool is not one large pool throughout the midplane but rather a number of small pools throughout. Computational studies have shown higher concentrations near proteins (Joliot, Beal et al. 1992, Kirchoff, Horstmann et al. 2000, Van Eerden, Melo et al. 2016). On the other hand, recent computational studies have shown plastoquinone located near the polar lipid headgroups. That is, van Eerden and coworkers characterized the interactions of cofactors found in photosystem II in

different lipid systems present in thylakoid membranes, such as phosphatidylglycerol, digalactosyldiacylglycerol, monogalactosyldiaceylglycerol, and sulfoquinovosyldiacylglycerol (van Eerden, de Jong et al. 2015). Through their efforts, plastoquinone was found near the glycerol section of the polar lipid headgroups with the sidechain pointing towards the midplane (van Eerden, de Jong et al. 2015). Additionally, de Jong and coworkers performed a simulation of PQ-9 and other lipoquinones in a DPPC lipid bilayer. Therein they determined the headgroup of PQ-9 was located at or near the lipid headgroup (Jong, Liguori et al. 2015). These computational studies came to the same conclusion; however, there is currently not yet experimental evidence to support their findings.

2.3.3. Menaquinones

Recently, our group used truncated MK-derivative, MK-2, to shed light on the membrane location using AOT reverse micelles as a model membrane system using 2D ^{1}H-^{1}H NOESY and ROESY NMR spectroscopy (Koehn, Magallanes et al. 2018). Cross peaks were observed between aromatic headgroup protons of MK-2 and protons near the polar headgroup of AOT. Together these results suggest the menaquinone headgroup is located near the lipid-water interface of the AOT RMs (Koehn, Magallanes et al. 2018). Protons along the sidechain of MK-2 formed cross peaks with protons along the alkyl chains near the polar headgroup of AOT, which further support the location near the polar headgroup of AOT. In an analogous study, we determined MK-1 and MK-1(H_2) were also found near the interface of AOT reverse micelles (Koehn, Beuning et al. 2019). The location of MK-1 through MK-4 was determined using Langmuir monolayer studies and in computational study performed by our collaborators, Arantes and coworkers. Using dipalmitoylphosphatidycholine (DPPC) and dipalmitoylphosphorylethanolamine (DPPE) phospholipids, all the truncated MK-derivatives were found to migrate from the air-water interface

into the acyl tails at physiological surface pressure, showing the MK-derivatives do associate, but do not disrupt, the phospholipid packing (Van Cleave, Koehn et al. 2021). This contrasts with the results found for UQ-derivatives in a similar experimental study (Katsikas and Quinn 1982, Roche, Peretti et al. 2006, Roche, Peretti et al. 2006). In the accompanying computational study, Arantes and coworkers used palmitoyloleoylphosphatidylcholine (POPC) model membrane to determine the location of MK-1 through MK-4. They found that all four headgroups were localized near the polar lipid headgroups of POPC with only slight variations in position as highlighted in Figure 2.13 (Van Cleave, Koehn et al. 2021). Together these experimental and computational experiments suggest the lipoquinone headgroup has greater influence over the position of the molecule in the

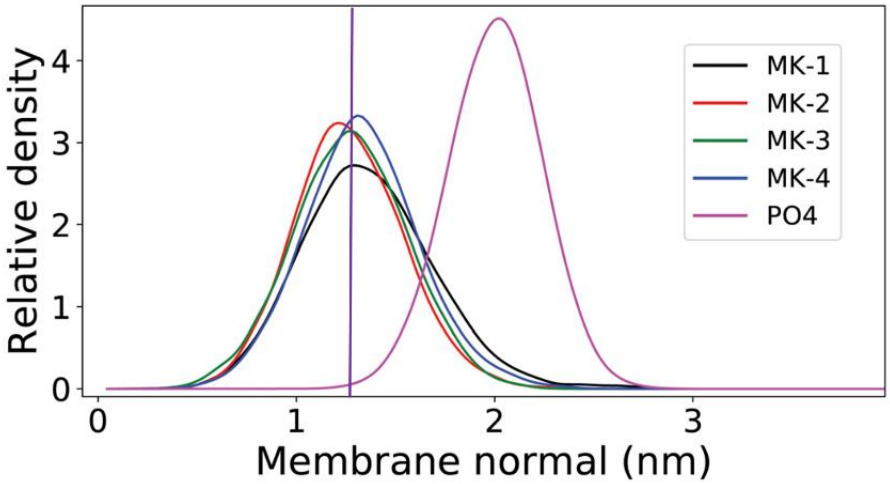

Figure 2.13. Relative mass density of the menaquinone headgroup along the membrane normal for MK-1 (black), MK-2 (red), MK-3 (green), and MK-4 (blue). The phosphate group of POPC (PO_4) is shown in magenta. The normal zero corresponds to the center of the bilayer. This figure was originally published in Ref. (Van Cleave, Koehn et al. 2021) and is licensed under CC-BY 4.0. The original figure was modified to include the purple, vertical line.

membrane than the length of the sidechain and challenges the "Dog vs Tail" metaphors that have been used to explain the influence of the headgroup versus the influence of the sidechain that was first described by Joela and coworkers (Joela, Kasa et al. 1997). The prevailing theory that the sidechain has the major influence over the position of the headgroup has been described to behave

like a tail wagging the dog, where the tail is stationary and the headgroup moves around. The opposite would be the dog wagging its tail, where the headgroup remains in a constant position, and the tail is mobile. The studies by Arantes show the headgroup structure is important in determining the location of the headgroup, and the sidechain is only influential in positioning the terminus of the sidechain. Combined, these works support the notion that the dog is wagging the tail and not the reverse; the headgroup does not change location with changes in sidechain length, whereas the sidechain will change location with sidechain length. Sidechain length will only determine the position of the sidechain, not the headgroup.

2.3.4. Comparison of Lipoquinone Headgroup Locations

The prevailing opinion in the literature is that the length of the isoprenoid sidechain has the major influence over the location of the quinone headgroup within a membrane bilayer. Although popular, this conclusion is rooted in computational studies supported by some experimental studies and series of data which leaves open the possibility that the headgroup may also be important for location in the membrane. The influence of headgroup types on location has only recently gained popularity fueled by computational studies. To validate the location of the lipoquinone headgroup in membrane environments, more experimental data is needed to support the computational findings and hence challenge the predominant theory that the length of the sidechain has the most influence.

In addition to the menaquinone study mentioned in Section 2.3.3, Arantes and coworkers have investigated the location of other lipoquinones in the membrane using similar computational methods (Galassi and Arantes 2015, Teixeira and Arantes 2019). Using lipoquinones of different headgroup types, redox state, and sidechain length, they calculated the distance of the phosphate groups, headgroups and sidechain from the membrane center (Figure 2.14). When comparing the

polar phosphate and quinone/quinol headgroups of the mixed bilayer of dilinoleoylphosphatidylcholine (DLPC) and dilauroylphosphoethanolamine (DPLE), the positions

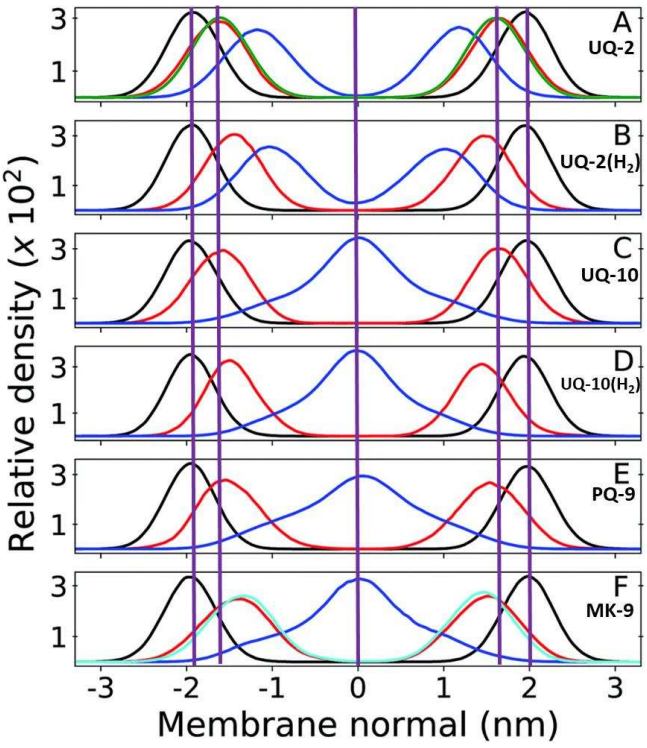

Figure 2.14. Relative mass density of multi-component bilayers with different lipoquinone derivatives (different lengths, degrees of unsaturation, and headgroups). The phosphate groups of DPLC and DLPE are shown in black, quinone headgroup in red, and sidechain in blue. Vertical purple lines are shown to emphasize the changes in position of the headgroup and the end of the sidechain relative to UQ-2 and the membrane center line. (A) UQ-2. Green curve shows the density of the DPLC and DPLE glycerol group; (B) ubiquinol-2 (UQH_2-2); (C) UQ-10. (D) ubiquinol-10 (UQH_2-10).;(E) PQ-9; and (F) MK-9. The cyan line shows the first 6 carbons of the naphthoquinone ring. The red line is the full ring system. The purple zero line corresponds to the center of the bilayer. Reproduced with permission from Teixeira and coworkers, "Effects of lipid composition on membrane distribution and permeability of natural quinones"; (Ref. (Teixeira and Arantes 2019)) published by Royal Society of Chemistry, 2016 (Teixeira and Arantes 2019). The figure was modified to include the purple, vertical lines and lipoquinone derivative labels.

of the quinone and quinol sidechains do change when the length of the chains change (as illustrated by the center purple line in Figure 2.14). When comparing UQ-2 and UQ-10 (Figure 2.14A & 2.14C) the position of the phosphate groups in the headgroup do not seem to be significantly affected by the increased sidechain length and only slightly when the redox state of the lipoquinone changes. The redox state of the lipoquinone headgroup does seem to affect the position of the

headgroup slightly. For example, the UQH_2-2 quinol headgroup is slightly closer to the membrane central plane than UQ-2, but both are still near the phospholipid headgroups (Figure 2.14A and 2.14B). In the case of the headgroups (Figure 2.14C and 2.14D), the position of the UQ-10 headgroup is in nearly the same position as the headgroup in UQ-2, but a change in redox state does seem to affect its position slightly. As discussed in 2.2.1, lipoquinols are more hydrophobic than lipoquinones and could explain why the quinol headgroup is found slightly closer to the midplane of the membrane. Between UQ-10, PQ-9, and MK-9, the headgroup seems to be slightly closer to the midplane as the polarity of the headgroup decreases, respectively (Figure 2.14C, 2.14E, and 2.14F). Although this computational study does not include the respective quinols of PQ-9 and MK-9, one could expect them to be slightly closer to the membrane center according to the trend observed with the ubiquinones and the ubiquinols. Together these computational results suggest the nature of the headgroup influences its position in the membrane slightly, but the length of the sidechain does not affect the location of the headgroup or the phosphate group. The location of the sidechain is dramatically influenced by the length of the sidechain and not by the headgroup or the phosphate group. The prevalent theory that the length of the sidechain has the most influence is therefore only valid for the location of the sidechain and not for the locations of the headgroup or phosphate groups.

In a recent study by our group, truncated UQ-derivative, UQ-2, was found to be closer to the bulk water of the AOT reverse micelle model system than MK-2 using 2D ^{1}H-^{1}H NOESY and ROESY NMR spectroscopic methods (Braasch-Turi, Koehn et al. 2022). The resulting intermolecular cross peaks between the lipoquinone and AOT led us to determine the location of each compound in RMs. Both lipoquinone derivatives were found near the interface; however, UQ-2 was slightly closer to the bulk water than MK-2 (Figure 2.15). This was determined by

evaluating the cross peaks between the protons on the headgroups and the protons of AOT. Cross peaks between the methoxy protons of UQ-2 and H1-H4 of AOT (labeled in Figure 2.15) where

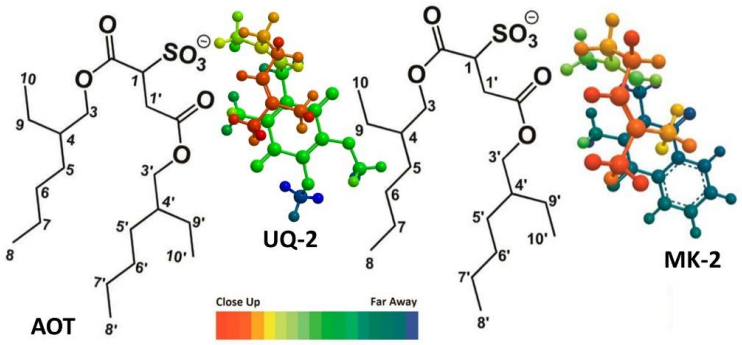

Figure 2.15. Comparison of the location of UQ-2 and MK-2 in AOT reverse micelles. AOT protons labeled provided. The color spectrum indicated relative depth when viewed from above. This figure was originally published in Ref. (Braasch-Turi, Koehn et al. 2022) (Frontiers in Chemistry 2022) and is licensed under CC-BY 4.0.

absent from the MK-2 spectrum suggesting the UQ-2 headgroup is closer to the interface than MK-2 (Koehn, Magallanes et al. 2018). The deeper penetration of MK-2 in the interface could be attributed to the relative polarity of each headgroup, and the trend suggests PQ-2 could be found somewhere in between UQ-2 and MK-2, but closer to MK-2. This experimental study supports the computational work by Arantes and workers described above (Van Cleave, Koehn et al. 2021), and together strengthens the argument that the type of quinone headgroup has more influence on the location of the quinone and quinol groups in the membrane.

2.4 Synthesis of Lipoquinones

Given the diversity in structure, only the most common lipoquinone derivatives are commercially available, and many of them must be prepared by the research group or synthetic collaborators or acquired through custom synthesis. Here we will describe an overview of the common approaches currently available (Figure 2.16) to make lipoquinone derivatives in reasonable amounts that can be used for biological studies. Some of the synthetic methods

describes are feasible to the non-expert, so we provide a section here summarizing the available synthetic approaches.

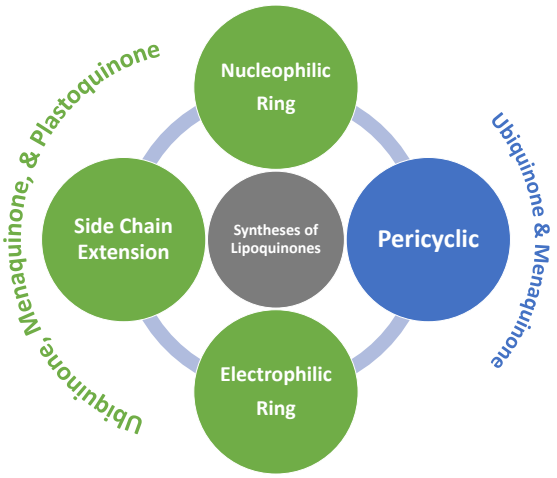

Figure 2.16. Synthetic methods used to synthesize lipoquinones.

The synthesis of all three lipoquinones have been achieved using nucleophilic ring methods, sidechain extensions, and electrophilic ring methods. Ubiquinones and menaquinones have also been synthesized using pericyclic methods. The number of steps, level selectivity, and technical skills required varies from method to method; however, each method yields product suitable for biological studies.

2.4.1. Nucleophilic Ring

Friedel-Crafts alkylation is one of the most common methods used to synthesize UQ-, MK-, and PQ-derivatives (Figure 2.17). These methods are attractive for their 2-3 step reaction sequences. Each synthesis begins with the reduction of the quinone rings **4-6** to the corresponding quinol **7-9** in the presence of a reducing agent, such as sodium dithionite (Figure 2.17A). The resulting quinol then undergoes Friedel-Crafts alkylation in the presence of a Lewis acid. For example, $ZnCl_2$ was used in the conversion of ubiquinol **13** to UQ-10(H_2) (not pictured), which was then further oxidized in the presence of $FeCl_3$ to form **1** (Figure 2.17B) (Upare, Pawar et al. 2007). BF_3-OEt_2 is the most popular Lewis acid for this purpose, which is conveniently used under

inert atmosphere conditions. For example, it was used to synthesize MK-2 (**15**), a truncated derivative of MK-9, by Koehn and coworkers (Figure 2.17C). First, menadione **5** was reduced

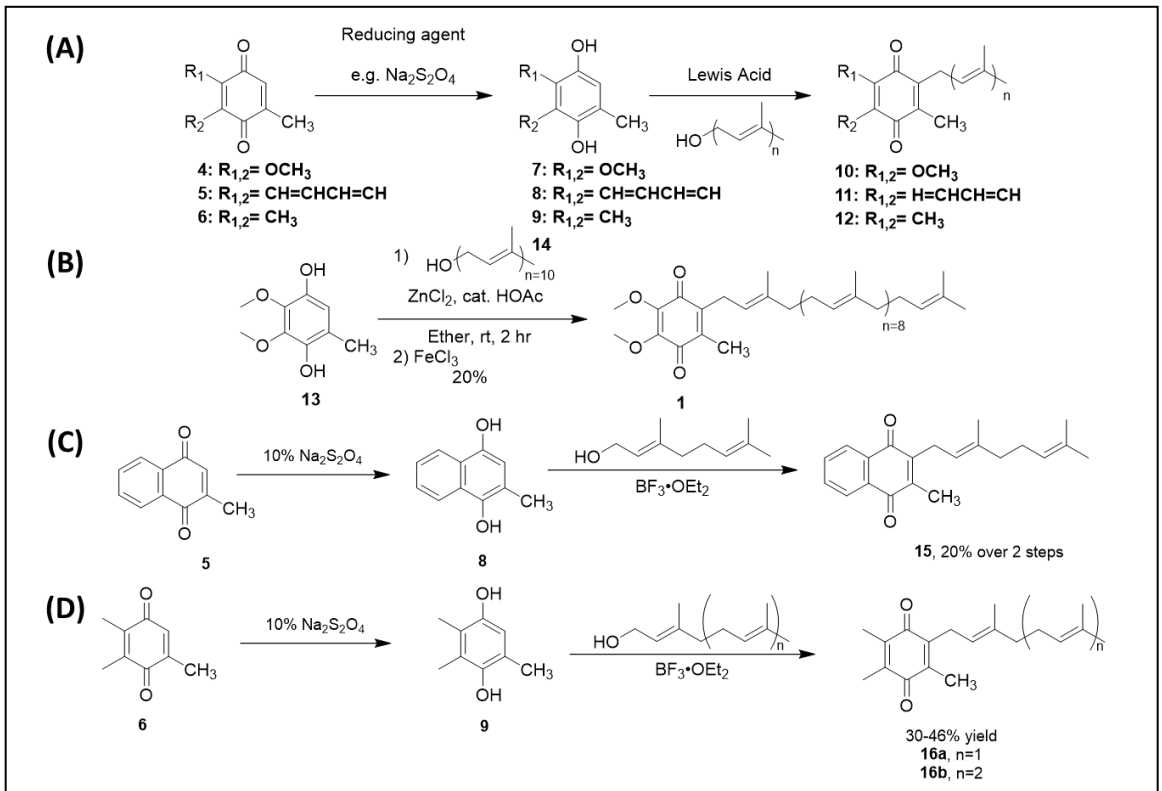

Figure 2.17. Examples of Friedel-Crafts reactions used to synthesize lipoquinones. (A). General reaction scheme for each lipoquinone. (B). Synthesize of UQ-10 (Upare, Pawar et al. 2007). (C). Synthesis of MK-2 (Suhara, Wada et al. 2010, Koehn, Magallanes et al. 2018). (D). Synthesis of PQ-2 and PQ-3 (Yoshimura, Hirota et al. 2020).

form the quinol **8**. The Friedel-Crafts reaction was performed in the presence of BF_3-OEt_2, which was first reported by Suhara and coworkers (Suhara, Wada et al. 2010), and commercially available geraniol to form **15** in 20% yield over two steps (Figure 2.17A)(Suhara, Wada et al. 2010, Koehn, Magallanes et al. 2018). It is important to note this route is impacted by the E/Z isomerism of the first isoprene unit leading to a loss of yield. The reported characterization of MK-2 by Suhara and coworkers is also not very thorough or even absent, making verification of the product difficult. Proper separation and characterization of each isomer is important when moving forward with biological studies. Both PQ-2 (**16a**) and PQ-3(**16b**) were synthesized using the same conditions (Figure 2.17D) (Yoshimura, Hirota et al. 2020). Although the yields are generally

considered low, this synthesis is short, yield milligram quantities, and is attractive to prepare lipoquinones for chemical biology studies. The Friedel-Crafts approach is most often utilized by medicinal chemists and biologists because it is convenient and produces adequate amounts of product for biological study.

2.4.2. Sidechain Extensions

Sidechain extension methods are another common strategy to synthesize long-chain lipoquinone derivatives, such as UQ-10. The syntheses begin with the installation of a carbon via homologation of the headgroup or installation of a single prenyl group. From here, the sidechain is functionalized further to add the remaining length in segments or all at once (Figure 2.18). For example, Lipshutz and coworkers utilized Negishi carboalumination to stereoselectively install the sidechain. Beginning with a polyprenyl terminal alkyne **17** (Figure 2.18A), the sidechain is then installed to a chloromethylated quinone ring **18** in the presence of a nickel catalyst, like Ni^0 or $NiCl_2(PPh_3)$ (Lipshutz, Kim et al. 1998, Lipshutz, Bulow et al. 1999, Lipshutz, Lower et al. 2005). Next, the elongation of the sidechain can also be achieved via the functionalization of the prenyl group. For example, Ravada and coworkers synthesized UQ-10 by reverse prenylation of **8** using Friedel-Crafts conditions to form quinol **20** (Ravada, Emani et al. 2009). One of the geminal dimethyl groups is transformed into an allyl bromide **21** via a four step sequence (Figure 2.18B). The bromo group then undergoes substitution with sodium p-toluenesulfonate to form the tolyl sulfone **22**. The carbon alpha to the sulfone is easily deprotonated to form a nucleophile to undergo substitution with the electrophilic polyprenyl bromide. Removal of the sulfone occurs in the presence of dissolved sodium metal, resulting in the desired product **1**.

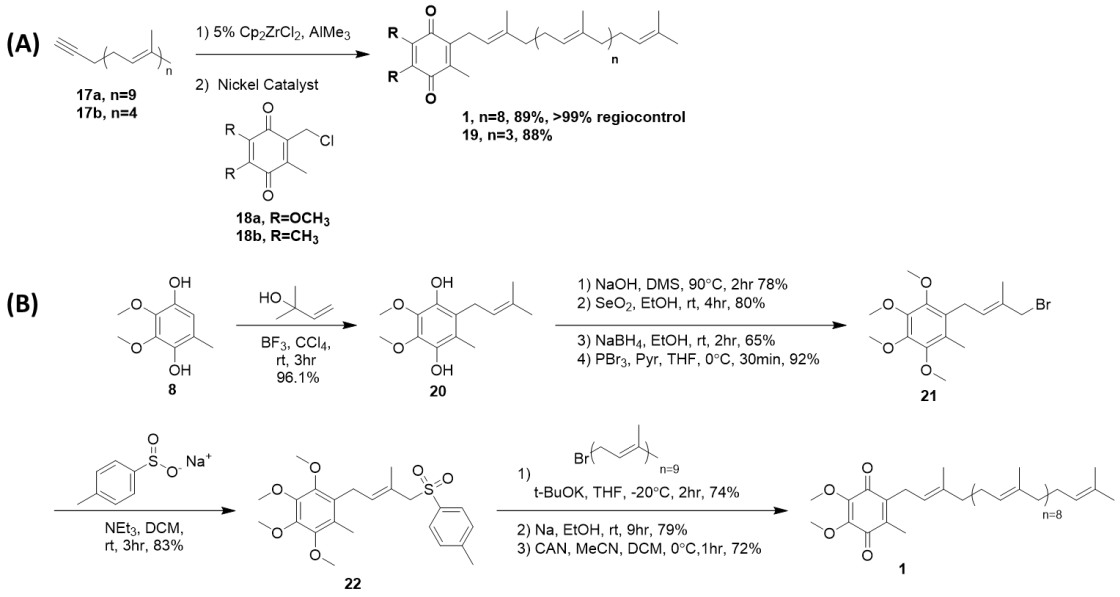

Figure 2.18. Examples of sidechain extension methods used to synthesize lipoquinones. (A) Synthesis of UQ-10 and PQ-5 through the elongation of the sidechain using Negishi carboalumination (Lipshutz, Bulow et al. 1999, Lipshutz 2007). (B) Synthesis of UQ-10 using the sulfonation of the prenyl group and nucleophilic attack of the polyprenyl halide (Ravada, Emani et al. 2009).

The literature shows no preference for using one method over the other, but it is important to note that both routes utilize very reactive reagents, such as organoaluminum and dissolved sodium metal, which requires significant technical skills to handle safely. However, Lipshutz and coworkers achieved coupling the headgroup to the sidechain in a convergent 2 step synthesis with excellent stereoselectivity and high yields (Lipshutz, Kim et al. 1998, Lipshutz, Bulow et al. 1999, Lipshutz, Lower et al. 2005, Ravada, Emani et al. 2009).

2.4.3. Electrophilic Ring

UQ-, MK-, and PQ-derivatives have been synthesized in one step using organostannane reagents, specifically, UQ-10 (**1**), MK-2 (**15**), and PQ-2 (**16a**) (Figure 2.19). Naruta and coworkers synthesized two geometric isomers of MK-2: MK-2 (with an *E* (or trans) alkene within the first isoprene unit) and MK-2(z1) (with a *Z* (or cis) alkene within the first isoprene unit). The stereochemistry of each MK-derivative was achieved using geranyl and neryl stannanes,

respectively. To their surprise, they observed complete stereoretention of the stereochemistry at the alpha isoprene unit for each derivative. (Maruyama and Naruta 1978, Naruta 1980, Naruta

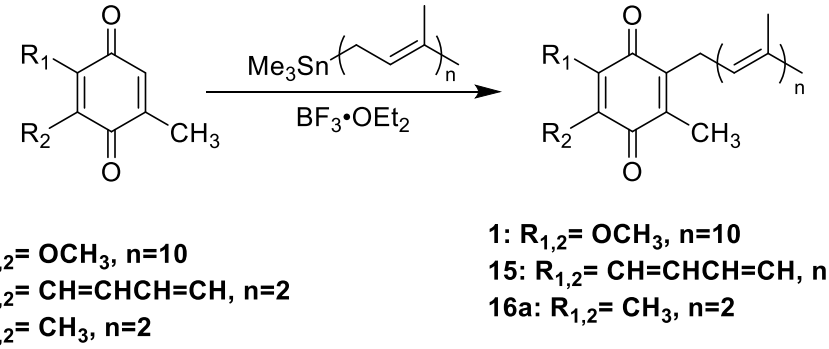

4: $R_{1,2}$= OCH_3, n=10
5: $R_{1,2}$= CH=CHCH=CH, n=2
6: $R_{1,2}$= CH_3, n=2

1: $R_{1,2}$= OCH_3, n=10
15: $R_{1,2}$= CH=CHCH=CH, n=2
16a: $R_{1,2}$= CH_3, n=2

Figure 2.19. Examples of electrophilic ring methods used to synthesize lipoquinones using organostannane nucleophiles resulting in 1,2- and 1,4-additons to the ring Refs. (Maruyama and Naruta 1978, Naruta 1980).

1980). Therefore, the use of organostannane reagents could be one way to ensure the retention of stereochemistry at the racemizable double bond. Although their affinity for stereoretention of alkenes is attractive, the organostannane reagents have been observed to add via both 1,2- and 1,4-additions to the quinone, resulting in a mixture of products and requiring elaborate purification procedures to obtain product of sufficient purity for use in biological studies.

2.4.4. Pericyclic

Diels-Alder reactions have been used to synthesize various menaquinone and ubiquinone derivatives (Figure 2.20) (Büchi and Rüttimann 1986, Rüttimann 1986, Lu and Chen 2004). Application of the Diels-Alder reaction for preparation of lipoquinones is unquestionably the most elegant method. This regioselective approach takes advantage of the adduct formed between the quinone headgroup and cyclopentadiene, which results in a sp^3 hybridized C2 and C3 carbons alpha to the carbonyls. In general, the C3 alpha proton is susceptible to deprotonation with a strong base to form the corresponding enolate. Alkylation can then occur with the respective prenyl halide

to form the alkylated adduct. The alkylated adduct is unstable leading it to undergo spontaneous retro Diels-Alder reactions, but this is often facilitated through reflux.

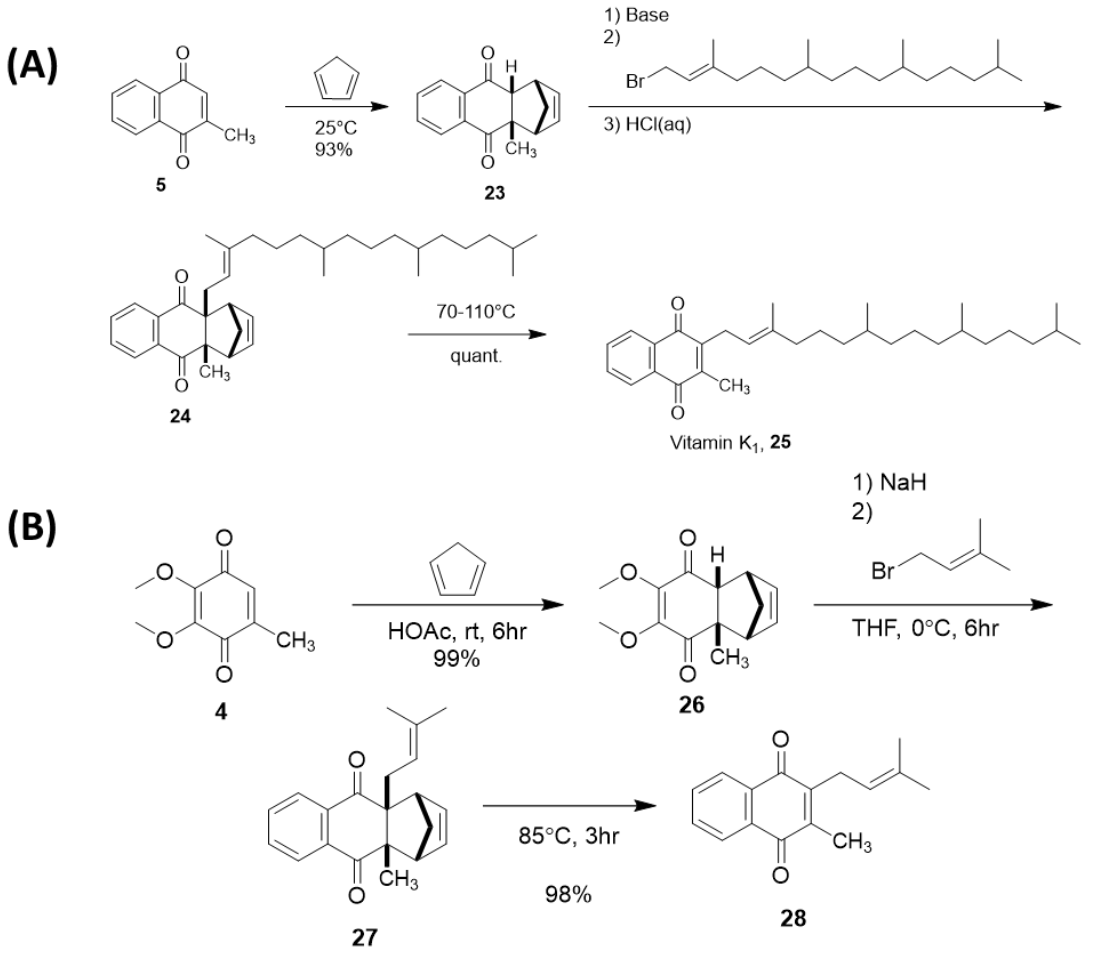

Figure 2.20. Examples of Diels-Alder reactions being used to control the regioselectivity of the sidechain installation. (A) Synthesis of vitamin K1 (Büchi and Rüttimann 1986, Rüttimann 1986). (B) Synthesis of UQ-1 (Lu and Chen 2004).

This method gained popularity through the patented syntheses of vitamin K_1 **25** on the gram scale (Figure 2.20A) (Büchi and Rüttimann 1986, Rüttimann 1986). The cycloadduct **23** is formed between menadione **5** and cyclopentadiene. Enolate alkylation with phytyl bromide forms the functionalized adduct **24**. Vitamin K_1, **25**, is formed via the subsequent retro-Diels-Alder reaction, removing the auxiliary cyclopentadiene group. A truncated derivative of ubiquinone, UQ-1 (**28**), has also been synthesized using the same approach via the cycloadduct **26** and

alkylated-adduct **27** (Figure 2.20B) (Lu and Chen 2004). Although conceptionally attractive, this approach has been carefully optimized for the reported syntheses, structure, and scale. This method introduces considerable competition between the enolate alkylation of the sidechain to the headgroup and an elimination reaction between the base and the prenyl halide. Therefore, more technical skill is required to achieve high selectivity. Therefore, it may not be as generally adoptable as desired to modified lipoquinone systems.

2.5. Summary and Future Outlook

Lipoquinone are hydrophobic molecules for which a major function is transport of electrons between membrane-bound proteins in the electron transport chain in cellular membranes. Understanding the location of lipoquinones in the membrane will have great impacts on experiments related to the use of such compounds in the fields of chemistry, biology, biochemistry, and medicine. Studies of more complex, protein-containing systems with established baseline locations of lipoquinones in such membrane environments would allow observation of how their locations change in the presence of proteins. This would have implications in the emerging "swimming" vs "diving" arguments for lipoquinone location, which are largely supported by computational studies. However, the understanding of the cellular environment has changed, and these environments are more crowded and consequently less polar than previously believed, thus supporting the conclusions regarding the existence of concentrations of "swimming" vs "diving" lipoquinones. A baseline location would also help clarify the behavior and function of the lipoquinone pool, which is thought to be within the midplane between membrane-bound protein complexes of the electron transport chain and surface of the membrane; however, as we show above, that depends on the length of the sidechain. The location of lipoquinones remains important since the lipoquinone pool serves as a reservoir to replenish the quinone electron potential.

The location of the lipoquinone in the membrane will also define their local chemical environments with more polar or nonpolar regions. The chemical environment alters the conformation of the lipoquinones and changes the electrochemical properties of these compounds' location, is a useful parameter when considering the electrochemical properties of the lipoquinone in specific environments. The analysis and general findings could potentially be extended to other isoprenoid and olefinic biomolecules, although the specific details will depend on the structure, location, environment, and specific function of the molecule.

Although simple in construction, lipoquinones are deceptively complex molecules. Their physical properties are often ignored or misinterpreted, leading to conflicting conclusions about their behavior and function in the literature. Their roles as electron transport agents in association with proteins in the electron transport chain have been widely studied, but little is known regarding their behavior within the membrane. For example, studies looking into the location of the quinone headgroup are riddled with contradictory reports. Often studies have been performed with a variety of different experimental and computational approaches, model membrane systems, and analytical methods, which make it difficult to directly compare the results. When discussing such studies, it is important to remember these molecules are very hydrophobic and hence it is difficult to ensure compound dissolution in aqueous-containing environments. To overcome this, many researchers have turned to computational methods to investigate the location and conformation of lipoquinones in solvent and membrane environments, which does not require consideration of solubility. Similarly, the redox potentials of lipoquinones are sensitive to local environments, and therefore their function is likely to be closely tied to their location, although at this point, limited information is available on this topic. Many studies are limited because the programs, datasets, and parameters

used to describe the properties are not uniform; therefore, the resulting interpretations and conclusions may vary significantly from study to study.

An attempt to overcome some of these limitations has recently been introduced in an experimental approach using truncated lipoquinone derivatives overriding solubility problems. Although still hydrophobic, short-chain lipoquinones derivatives, such as UQ-2 and MK-2, are more soluble in both organic and aqueous media, making them perfect candidates for comparison studies. Our group has demonstrated their usefulness and evaluated the locations of short chain UQ and MK in AOT reverse micelles using 1D and 2D NMR spectroscopy and in Langmuir monolayers trough studies. Our results support the importance of the headgroup on lipoquinone location within the membrane, and this conclusion was supported by Arantes computational work with similar derivatives with varying sidechain lengths. As such we have clarified the ongoing controversy on the location of the menaquinones in the membrane.

In order to carry out any studies, the compounds must be available, and hence we summarize several approaches reported to make these molecules when they are not commercially available. Reported methods will assist the experimentalist interested in using modified or isotopically labeled lipoquinone derivatives and can facilitate investigations of biological function. Lipoquinone derivatives are accessible, and structural modifications could assist future studies into exploring the fundamental properties of the biological systems or potential applications of systems requiring lipoquinones.

We emphasize the importance for researchers in the future to bridge the gap between experimental and computational methods and incorporate properties-focused, experimental studies to support computational findings. As the field moves forward, considerations of more realistic biomimetic membranes (including lipids, cholesterols, and proteins) will be paramount to

understanding the true behavior of lipoquinones in the membrane, particularly if the location and conformation of lipoquinones in the membrane and possible interactions with Coq10 chaperone protein are important to the questions being addressed.

References

Afri, M., B. Ehrenberg, Y. Talmon, J. Schmidt, Y. Cohen and A. A. Frimer (2004). "Active oxygen chemistry within the liposomal bilayer Part III: Locating vitamin E, ubiquinol and ubiquinone, and their derivatives in the lipid bilayer." Chem. Phys. Lipids **131**(1): 107-121.

Allan, C., A. Awad, J. JOhnson, D. Shrasaki, C. Wang, C. Blaby-Haas, S. Merchent, J. Loo and C. Clarke (2015). "Identification of Coq11, a New Cosynzyme Q Biosynthetic Protein in the CoQ-Synthone in Saccharomyces Cerevisiae." J. Biol. Chem. **290**(12): 7517-7534.

Allen, J., J. Bennet, K. Steinbeck and C. Arntzen (1981). "Chloroplasts protein phosphorylation couples plastoquinone redox state to distribution of excitation energy between photosystems." Nature **291**: 25-29.

Anand, A., K. Chen, L. Yang, A. V. Sastry, C. A. Olsen, S. Poudel, Y. Seif, Y. Hefner, P. V. Phaneuf, S. Xu, R. Szubin, A. M. Feist and B. O. Palsson (2019). "Adaptive evolution reveals a tradeoff between growth rate and oxidative stress during naphthoquinone-based aerobic respiration." PNAS **116**(50): 25287-25292.

Batanero, B., R. Saez and F. Barba (2009). "Electroreduction of Quinones Under Aprotic Conditions." Electrochim. Acta **54**(21): 4872-4879.

Becker, K. W., F. J. Elling, J. M. Scroder, J. S. Lipp, T. Goldhammer, M. Zabel, M. Elvert, J. Overmann and K.-U. Hinrichs (2018). "Isoprenoid quinones resolve the stratification of redox processes in a biogeochemical continuum from the photic zone to deep anoxic sediments of the black sea." Appl. Environ. Microbiol. **84**(10): e02736-02717.

Bernardo, S. D., R. Fato, R. Casadio, P. Fariselli and G. Lenaz (1998). "A high diffusion coefficient for coenzyme Q10 might be related to a folded structure." FEBS Lett. **426**: 77-80.

Beuning, C. (Jan. 2020). Analytical Spectroscopy Method Development to Study Mechanisms of Alzheimer's and Tuberculosis Diseases. Ph.D., Colorado State University.

Braasch-Turi, M., J. T. Koehn, K. Kostenkova, C. Van Cleave, J. W. Ives, H. A. Murakami, D. C. Crick and D. C. Crans (2022). "Electron Transport Lipids Fold Within Membrane-Like Interfaces." Front. Chem. **10**: 827530.

Büchi, G. and A. Rüttimann (1986). Process For The Manufacture of Quinone Derivatives. United States of America, Hoffmann-La Roche, Inc.

Ceccarelli, M., P. Procacci and M. Marchi (2003). "An Ab Initio Force Field for the Cofactors of Bacterial Photosynthesis." J. Comput. Chem. **24**: 129-142.

Chazotte, B., E.-S. Wu and C. R. Hackenbrock (1991). "The mobility of a fluorescent ubiquinone in model lipid mebranes. Relevance to mitochondrial electron transport." Biochim. Biophys. Acta Bioenerg. **1058**: 400-409.

ChemAxon. from https://chemicalize.com/.

Cornell, B. A., M. A. Keniry, A. Post, R. N. Robertson, L. E. Weir and P. W. Westerman (1987). "Location and activity of ubiquinone-10 and ubiquinone analogues in Model and Biological Membranes." Biochemistry **26**(24): 7702-7707.

Crane, F. L. (1966). "Quinones in Energy-Coupling Systems." Physiol. Rev **46**(4): 662-695.

Crane, F. L. (2007). "Discovery of ubiquinone (coenzyme Q) and an overview of functoin." Mitochondrion **7**: 2-7.

De Vries, S., J. A. Berden and E. C. Slater (1992). 6-Function and Properties of a Semiquinone Anion Located in the QH2: Cytochrome c Oxidoreductase Segmant of the Respiratory Chain. Function of Quinones in Energy Conserving Systems. B. L. Trumpower, Academic Press**:** 235-246.

Dunphy, P. J. and A. F. Brodie (1971). [233] The structure and function of quinones in respiratory metabolism. Methods Enzymol., Elsevier. **18:** 407-461.

Eddine, M. S., F. Biaso, J. Rendon, E. Pilet, B. Guigliarelli, A. Magalon and S. Grimaldi (2020). "1,2H hyperfine spectroscopy ad DFT modeling unveil the demethylmenasemiquinone binding mode to E. coli nitrate reductase A (NarGHI)." Biochim Biophys Acta- Bioenerg. **1861**: 148203.

Eggins, B. R. (1969). "Interpretation of Electrochemical Reduction and Oxidation Waves of Quinone-Hydroquinone System in Acetonitrile." J. Chem. Soc. D **1969**(21): 1267-1268.

Esposti, M. D. (2017). "A journey across genomes uncovers the origin of ubiquinone in cyanobacteria." Genome Biol. Evol. **9**(11): 3039-3053.

Fedor, J. G., A. J. Y. Jones, A. D. Luca, V. R. I. Kaila and J. Hirst (2017). "Correlating kinetic and structural data on ubiquinone binding and reduction by respiratory complex I." PNAS **114**(48): 12737-12742.

Fujimoto, N., T. Kosaka and M. Yamada (2012). Menaquinone as Well as Ubiquinone as a Crucual Component in the Escherichia coli Respiratory Chain. Chemical Biology. D. Ekinci, IntechOpen**:** 187-208.

Galassi, V. V. and G. M. Arantes (2015). "Partition, orientation and mobility of ubiquinones in a lipid bilayer." Biochim. Biophys. Acta **1847**: 1560-1573.

Gómez-Murcia, V., A. Torrecillas, A. M. de Godos, S. Corbalán-García and J. C. Gómez-Fernández (2016). "Both idebenone and idebenol are localized near the lipid–water interface of the membrane and increase its fluidity." Biochim. Biophys. Acta, Biomembr. **1858**(6): 1071-1081.

Guin, P. S., S. Das and P. C. Mandal (2011). "Electrochemical Reduction of Quinones in Different Media: A Review." Int. J. Electrochem. **2011**: 1-22.

Guskov, A., J. Kern, A. Gabdulkhakov, M. Broser, A. Zouni and W. Saenger (2009). "Cyanobacterial photosystem II at 2.9-A resolution and the role of quinones, lipids, channels, and chloride." Nat. Struct. Mol. Biol. **16**(3): 334-342.

Hauss, T., S. Dante, T. H. Haines and N. A. Dencher (2005). "Localization of coenzyme Q10 in the center of a deuterated lipid mebrane by neutron diffraction." Biochim Biophys Acta **1710**: 57-62.

Havaux, M. (2020). "Plastoquinone In and Beyond Photosynthesis." Trends Plant Sci. **25**(12): 1252.

Hernandez-Camacho, J. D., M. Bernier, G. Lopez-LLuch and P. Navas (2018). "Coenzyme Q10 Supplementatoin in Aging and Disease." Front. Physiol. **9**(44): 1-11.

Hihi, A. K., H. Kebir and S. Hekimi (2003). "Snesitivity of Caenorhabditis elegans clk-1 Mutant to Ubiquinone Side-Chain Length Reveals Multiple Ubiquinone-dependent Processes." J. Biol. Chem. **278**(42): 41013-41018.

Himo, F., G. Babcock and L. Eriksson (1999). "Conformational Analysis of Quinone Anion Radicals in Photosystem II and Photosynthetic Bacteria." J. Phys. Chem. A **103**: 3745-3749.

Hoshino, Y. and E. A. Gaucher (2018). "On the Origins of Isoprenoid Biosynthesis." Mol. Biol. Evol. **35**(9): 2185-2197.

Ishihara, M. and H. Sakagami (2007). "QSAR of Molecular Structure and Cytotoxic Activity of Vitamin K2 Derivatives with Concept of Absolute Hardness." Anticancer Res. **27**: 4059-4064.

Jaworski, J. S., E. Leniewska and M. K. Kalinowski (1979). "Solvent Effect on the Redox Potential of Quinone-Semiquinone Systems." J. Electroanal. Chem. Interfacial Electrochem **105**(2): 329-334.

Joela, H., S. Kasa, P. Lehtovuori and M. Bech (1997). "EPR, ENDOR, and TRIPLE Resonance and MO Studies on Ubiquinones (Q-n): Comparison of Radical Anions and Cations of Coenzymes Q-10 and Q-6 with the Model Compounds Q-2 and Q-0." Acta Chem. Scand. **51**: 233-241.

Joliot, P., L. Beal and D. Beal (1992). "Plastoquinone compartmentation in chloroplasts. I. Evidence for domains with different rates of photo-reduction." Biochim Biophys Acta **1101**: 1-12.

Jong, D. H. d., N. Liguori, T. v. d. Berg, C. Arnarez, X. Periole and S. J. Marrink (2015). "Atomistic and Coarse Grain Topologies for the Cofactors Associated with the Photosystem II Core Complex." J. Phys. Chem. B **119**: 7791-7803.

Jormakka, M., K. Yokoyama, T. Yano, M. Tamakoshi, S. Akimoto, T. Shimamura, P. Curmi and S. Iwata (2008). "Molecular mechanism of energy conservtation in polysulfide respiration." Nat. Struct. Mol. Biol. **15**: 730.

Kaneki, M., T. Hosoi, Y. Ouchi and H. Orimo (2006). "Pleiotropic actions of vitamin K: protector of bone health and beyond?" Nutrition **22**: 845-852.

Katsikas, H. and P. J. Quinn (1982). "The polyisoprenoid chain length influences the interaction of ubiquinones with phospholipid bilayers." Biochim Biophys Acta **689**: 363-369.

Kaurola, P., V. Sharma, A. Vonk, I. Vattulainen and T. Rog (2016). "Distribution and dynamics of quinones in the lipid bilayer mimicking the inner membrane of mitochondria." Biochim. Biophys. Acta **1858**(9): 2116-2122.

Kawamukai, M. (2018). "Biosynthesis and applications of prenylquinones." Biosci. Biotechnol. Biochem. **82**(6): 963-977.

Keeling, P. J. (2013). "The number, speed, and impact of plastid endosymbioses in eukaryotic evolution." Annu. Rev. Plant Biol. **64**: 583-607.

Kingsley, P. B. and G. W. Feigenson (1981). "1H-NMR Study of the Location and motion of ubiquinone in predeuterated phosphatidylcholine bilayers." Biochem. Biophys. Acta **635**: 602-618.

Kirchoff, H., S. Horstmann and E. Weis (2000). "Control of the photosynthetic electron transport by PQ diffusion microdomains in thylakoids of higher plants." Biochim Biophys Acta **1459**: 148-168.

Kishi, S., K. Saito, Y. Kato and H. Ishikita (2017). "Redox potentials of ubiquinones, menaquinone, phylloquinone, and plastoquinone in aqueous solution." Photosynth. Res. **134**: 193-200.

Koehn, J. T., C. N. Beuning, B. J. Peters, S. K. Dellinger, C. Van Cleave, D. C. Crick and D. C. Crans (2019). "Investigating Substrate Analogues for Mycobacterial MenJ: Truncated and Partially Saturated Menaquinones." Biochemistry **58**(12): 1596-1615.

Koehn, J. T., D. C. Crick and D. C. Crans (2018). "Synthesis and Characterization of Partially and Fully Saturated Menaquinone Derivatives." ACS Omega **3**(11): 14889-14901.

Koehn, J. T., E. S. Magallanes, B. J. Peters, C. N. Beuning, A. A. Haase, M. J. Zhu, C. D. Rithner, D. C. Crick and D. C. Crans (2018). "A Synthetic Isoprenoid Lipoquinone, Menaquinone-2, Adopts a Folded Conformation in Solution and at a Model Membrane Interface." J. Org. Chem. **83**(1): 275-288.

Lambreva, M., D. Russo, F. Polticelli, V. Scognamiglio, A. Antonacci, V. Zobnina, G. Campi and G. Rea (2014). "Structure/Functin/Dynamics of Photosystem II Plastoquinone Binding Sites." Curr. Protein Pept. Sci **15**: 285-295.

Lange, B. M., T. Rujan, W. Martin and R. Croteau (2000). "Isoprenoid biosynthesis: The evolution of two ancient and distinct pathways across genomes." PNAS **97**(24): 13172-13177.

Lenaz, G., R. Fato, S. D. Bernardo, D. Jarreta, A. Costa, M. L. Genova and G. P. Castelli (1999). "Localization and mobility of coenzyme Q in lipid bilayers and membranes." BioFactors **9**: 87-93.

Lenaz, G., B. Samori, R. Fato, M. Battino, G. P. Castelli and I. Domini (1992). "Localization and preferred orientations of ubiquinone homologs in model bilayers." Biochim. Cell. Biol. **70**(504-514).

Lipshutz, B., G. Bulow, F. Fernandez-Lazaro, S.-K. Kim, R. Lowe, P. Mollard and K. Stevens (1999). "A Convergent Approach to Coenzyme Q." J. Am. Chem. Soc. **121**: 11664-11673.

Lipshutz, B., A. Lower, V. Berl, K. Schein and F. Wetterich (2005). "An improved synthesis of the "Miracle Nutrient" Coenzyme Q10." Org. Lett. **7**(19): 4095-4097.

Lipshutz, B. H. (2007). New Ubiquinone Analogs and Methods of Use.

Lipshutz, B. H., S.-k. Kim and P. Mollard (1998). "An Expeditious Route to COQn, Vitamins K1 and K2, and Related Allylated para-Quinones Utilizing Ni(0) Catalysis." Tetrahedron **54**: 1241-1253.

Liu, M. and S. Lu (2016). "Plastoquinone and Ubiquinone in Plants: Biosynthesis, Phsyiological Function, and Metabolic Engineering." Front. Plant. Sci. **7**: 1898.

Loll, B., J. Kern, W. Saenger, A. Zouni and J. Biesiadka (2007). "Lipids in photosystems II: Interactions with protein and cofactors." Biochim Biophys Acta **1767**: 509-519.

Lu, L. and F. Chen (2004). "A Novel and Convenient Synthesis of Coenzyme Q1." Syn. Commun. **34**(22): 4049-4053.

Marchal, D., W. Boireau, J. Laval, J. Moiroux and C. Bourdillon (1998). "Electrochemical Measurement of Lateral Diffusion Coefficient of Ubiquinones and PLastoquinones of Various Isoprenoid Chain Length Incorporated in Model Bilayers." Biophys. J. **74**: 1937-1948.

Maruyama, K. and Y. Naruta (1978). "Synthesis of naturally occurring quinones. Part 3. Allylation of quinones with allyltin reagents. New synthesis of coenzyme Q1 and plastoquinone-1." J. Org. Chem. **43**(19): 3796-3798.

Mayer, M., P. Beyer and H. Kleinig (1990). "Quinone compounds are able to replace molecular oxygen as terminal electron acceptor in phytoene desaturation in chloroplasts of Narcissus pseudomarcissus L." Eur. J. Biochem. **191**: 359-363.

Metz, G., K. P. Howard, W. B. S. v. Liemt, J. H. Prestegard, J. Lugtenburg and S. O. Smith (1995). "NMR Studies of ubiquinone locationin oriented model membranes: evidence for a single motionally-averaged population." J. Am. Chem. Soc. **117**: 564-565.

Michaelis, L. and M. J. Moore (1985). "Location of ubiquinone-10 (CoQ-10) in phospholipid vesicles." Biochim Biophys Acta **821**(121-129).

Millner, P. and J. Barber (1984). "Plastoquinones as a mobile redox carrier in the photosynthetic membrane." FEBS **169**(1): 1341.

Molinspiration. "Molinspiration Cheminformatics free web services." from https://www.molinspiration.com.

Murai, M., K. Matsunobu, S. Kudo, K. Ifuku, M. Kawamukai and H. Miyoshi (2014). "Identification of the binding site of the quinone-headgroup in mitochondrial Coq10 by photoaffinity labeling." Biochemistry **53**(24): 3995-4003.

Murgolo, N. J., A. Patel, S. S. Stivala and T. K. Wong (1989). "The Conformation of Dolichol." Biochem. **28**(253-260).

Naruta, Y. (1980). "Allylation of quinones with allyltin reagents." J. Am. Chem. Soc. **102**(11): 3774-3783.

Naruta, Y. (1980). "Regio- and stereoselective synthesis of coenzymes Qn (n = 2-10), vitamin K, and related polyprenylquinones." J. Org. Chem. **45**(21): 4097-4104.

Nilsson, J. A., L. A. Eriksson and A. Laaksonen (2001). "Molecular dynamics simulations of plastoquinone in solution." Mol. Phys. **99**(3): 247-253.

Nilsson, J. A., A. Lyubartsev, L. A. Eriksson and A. Laaksonen (2001). "Molecular dynamics simulations of ubiquinone; a survey over torsional potentials and hydrogen bonds." Mol. Phys **99**(21): 1795-1804.

Nonella, M., G. Mathias, M. Eichinger and P. Tawan (2003). "Structures and vibrational frequencies of the Quinones in Rb. sphaeroides derived by a combined density functional/molecular mechanics approach." J. Phys. Chem. B **107**: 316-322.

Norris, S., T. Barrette and D. DellaPenna (1995). "Genetic dissection of carotenoid synthesis in Arabidopsis defines plastoquinone as an essential component of phytoene desaturation." Plant Cell **7**: 2139-2149.

Nowicka, B. and J. Kruk (2010). "Occurrence, biosynthesis and function of isoprenoid quinones." Biochim Biophys Acta **1797**(9): 1587-1605.

Ohnishi, T., J. C. Salerno and H. Blum (1982). 7-Ubisemiquinones in Electron-Transfer Systems of Mitochondria. Function of Quinones in Energy Conserving Systems. B. L. Trumpower, Academic Press**:** 247-261.

Okada, K., T. Kainou, H. Matsuda and M. Kawamukai (1998). "Biological significance of the side chain length of ubiquinone in Saccharomyces cerevisiae." FEBS Lett. **431**: 241-244.

Ondarroa, M. and P. J. Quinn (1986). "Proton magnetic resonance spectroscopic studies of the interaction of ubiquinone-10 with phospholipid model membranes." FEBS **155**(2): 353-361.

Palace, G. P., J. E. Frankie and J. T. Warden (1987). "Is phylloquinone an obligate electron carrier in photosystem I?" FEBS Lett. **215**(1): 58-62.

Pelosi, L., A.-L. Ducluzeau, L. Loiseu, F. Barras, D. Schneider, I. Junier and F. Pierrel (2016). "Evolution of Ubiquinone Biosynthesis: Multiple Proteobacterial Enzymes with Various Regioselectivities to Catalyze Three Contiguous Aromatic Hydroxylation Reactions." mSystems **1**(4): 1-16.

Peover, M. E. (1962). "A Polarographic Investigation into the Redox Behaviour of Quinones: the Roles of Electron Affinity ans Solvent." J. Chem. Soc. **0**: 4540-4549.

Popa, D.-S., G. Bigman and M. E. Rusu (2021). "The Role of Vitamin K in Humans: Implications in Againg and Age-Associated Diseases." Antioxidants **10**: 556.

PubChem PubChem. Bethesda, MD, National Library of Medicine.

Quirk, A., M. J. Lardner, Z. Tun and I. J. Burgess (2016). "Surface Enhanved Infrared Spectroscopy and Neutron Reflectivity Studies of Ubiquinone in Hybrid Bulayer Membranes under Potential Control." Langmuir **32**: 2225-2235.

Ravada, S., L. Emani, M. Garaga, B. Meka and T. Golakota (2009). "Synthesis of Coenzyme Q10." Am. J. Infect. Dis. **5**(2): 83-89.

Rich, P. R. and R. Harper (1990). "Partition coefficients of quinones and hydroquinones and their relation to biochemical reactivity." FEBS Letters **269**(1): 139-144.

Roche, Y., P. Peretti and S. Bernard (2006). "DSC and Raman studies of the side chain length effect of ubiquinones on the thermotropic phase behavior of liposomes." Thermochim. Acta **447**(1): 81-88.

Roche, Y., P. Peretti and S. Bernard (2006). "Influence of the chain length on their interaction with DPPC mixed monolayers." Biochim. Biophys. Acta **1758**(4): 468-478.

Rüttimann, A. (1986). "Recent Advances in the Synthesis of K-Vitamins." Chimia **40**(9): 290-306.

Salgado, J., J. Villalain and J. C. Gomez-Fernandez (1993). "Magic angle spinning 13C-NMR spin-lattice relaxation study of the location and effects of a-tocopherol, ubiquinone-10, and ubiquinol-10 in unsonicated model membranes." Eur. Biophys. J. **22**: 151-155.

Santis, A. d., E. Scoppola, M. F. Ottaviani, A. Koutsioubas, L. C. Barnsley, L. Paduano, G. D'Errico and I. R. Krauss (2022). "Order vs Disorder: Cholesterol and Omega-3 Phospholipids Determine Biomembrane Organization." Int. J. Mol. Sci **23**: 5322.

Schoepp-Cothenet, B., C. Lieutaud, F. Baymann, A. Vermeglio, T. Friedrich, D. M. Kramer and W. Nitschke (2009). "Menaquinone as pool quinone in a purple bacterium." PNAS **106**(21): 8549-8554.

Singharoy, A., C. Maffeo, K. H. Delgado-Magnero, E. Tajkhorshid, A. Aksimentiev and K. Schulten (2020). "Atoms to Phenotypes: Molecular Design Principles of Cellular Energy Metabolism." Cell **179**: 1098-1111.

Sitkowski, J., W. Bocian and A. Szterk (2018). "The application of multidimensional NMR analysis to cis/trans isomers study of menaquinone-7 (vitamine K2MK-7), identification of the (E,Z3, E2,ω)-menaquinone-7 isomer in dietary supplements." J. Mol. Struct. **1171**: 449-457.

Soballe, B. and R. Poole (1999). "Microbial ubiquinones: multiple roles in respiration, gene regulation, and oxidative stress management." Microbiology **145**: 1817-1830.

Soderhall, J. A. and A. Laaksonen (2001). "Molceular dynamics simulations of ubiquinone inside a lipid bilayer." J. Phys. Chem. B **105**: 9308-9315.

Stackebrandt, E., R. Murray and H. Truper (1988). "Proteobacteria classis nov., a name for the phylogenic taxon that includes the "purple bacteria and their relatives"." Int. J. Syst. Bacteriol. **38**(231-325).

Stidham, M. A., T. J. McIntosh and J. N. Siedow (1984). "On the locatization of ubiquinones in phosphatidylcholine bilayers." Biochim Biophys Acta **767**: 423-431.

Su, X., J. Ma, X. Wei, P. Cao, D. Zhu, W. Chang, Z. Liu, X. Zhang and M. Li (2017). "Structure and assembly mechanism of plant C2S2M2-type PSII-LHCII supercomplex." Science **357**: 815-820.

Suhara, Y., A. Wada, Y. Tachibana, M. Watanabe, K. Nakamura, K. Nakagawa and T. Okano (2010). "Structure–activity relationships in the conversion of vitamin K analogues into menaquinone-4. Substrates essential to the synthesis of menaquinone-4 in cultured human cell lines." Bioorg. Med. Chem. **18**(9): 3116-3124.

Swallow, A. (1982). 3- Physical Chemistry of Semiquinones. Function of Quinones in Energy Conserving Systems. B. L. Trumpower, Academic Press**:** 59-72.

Taguchi, A. T., P. J. O'Malley, C. A. Wraight and S. A. Dikanov (2013). "Conformational Differences between the Methoxy Groups of QA and QB Site Ubisemiquinones in Bacterial Reaction Centers: A Key Role for Methoxy Group Orientation in Modulating Ubiquinone Redox Potential." Biochemistry **52**: 4648-4655.

Tanaka, A., Y. Fukushima and N. Kamiya (2017). "Two different structures of the oxygen-evolving complex in the same polypeptide frameworks of photosystem II." J. Am. Chem. Soc. **139**: 1718-1721.

Teixeira, M. H. and G. M. Arantes (2019). "Effect of lipid composition on membrane distribution and permeability of natural quinones." RSC Adv. **9**: 16892.

Tekin, E. D. and S. Erkoc (2010). "Structural and electronic features of the ubiquinone and ubiquinol molecules: molecular dynamics and quantum chemical treatments." Molecular Simulation **36**(10): 763-771.

Trumpower, B. L. (1981). "New Concepts on the Role of Ubiquinone in the Mitochondrial Respiratory Chain." J. Bioenerg. Biomem. **13**(1/2): 1-24.

Tsui, H. S., N. V. B. Pham, B. R. Amer, M. C. BRadley, J. E. Gosschalk, M. Gallagher-Jones, H. Ibarra, R. T. Clubb, C. E. Blaby-Hass and C. F. Clarke (2019). "Human COQ10A and COQ10B are distinct lipid-binding START domain proteins required for coenzyme Q function." J. Lipid Res. **60**(7): 1293-1310.

Turner, W. R. and P. J. Elving (1965). "Electrochemical Behavior of the Quinone-Hydroquinone System in Pyridine." J. Electrochem. Soc. **112**(12): 1215-1217.

Ulrich, E. L., M. E. Girvin, W. A. Cramer and J. L. Markley (1985). "Location and mobility of ubiquinones of different chain lengths in artificial membrane vesicles." Biochemistry **24**(10): 2501-2508.

Upadhyay, A., S. Kumar, S. A. Rooker, J. T. Koehn, D. C. Crans, M. R. McNeil, J. S. Lott and D. C. Crick (2018). "Mycobacterial MenJ: An Oxidoreductase Involved in Menaquinone Biosynthesis." ACS Chem. Biol. **13**(9): 2498-2507.

Upare, A., N. Pawar, G. Wagh, A. Chavan, M. Roy and H. Sivaramakrishnan (2007). Novel Intermediates Useful for the Preparation of Coenzymes, Process for the Preparation of Novel Intermediates and an Improved Process for the Preparation of Cozymes. N. P. I. Limited.

Van Cleave, C., J. T. Koehn, C. S. Pereira, A. A. Haase, B. J. Peters, S. W. Croslow, K. G. McLaughlin, K. R. Wrest, A. L. Goach, D. C. Crick, G. M. Arantes and D. C. Crans (2021). "Interactions of truncated menaquinones in lipid monolayers and bilayers." Int. J. Mol. Sci **22**: 1-22.

van Eerden, F., D. de Jong, A. de Vries, T. Wassenaar and S. Marrink (2015). "Characterization of thylakoid lipid membranes from cyanobacteria and higher plants by molecular dynamics." Biochim Biophys Acta **1848**: 1319-1330.

Van Eerden, F., M. Melo, P. Frederix, X. Periole and S. Marrink (2016). "Exchange pathways of plastoquinone and plastoquinol in the photosystem II complex." Nat. Commun. .

Vermeer, C. and L. Schurgers (2000). "A comprehensive review of vitamin K and the vitamin K antagonists." Hematol. Oncol. Clin. N. Am. **14**: 339-353.

Winckel, M. V., R. D. Bruyne, S. V. D. Velde and S. V. Biervliet (2009). "Vitamin K, and update for the paediatrician." Eur. J. Pediatr. **168**: 127-134.

Woodward, R. B. and K. Bloch (1953). "The Cyclization of Squalene in Cholesterol Synthesis." J. Am. Chem. Soc. **75**(8): 2023-2024.

Wraight, C. A., A. S. Vakkasoglu, Y. Poluektov, A. J. Mattis, D. Nihan and B. H. Lipshutz (2008). "The 2-methoxy group of ubiquinone is essential for function of the acceptor quinones in reaction centers from Rba. sphaeroides." Biochim Biophys Acta **1777**: 631-636.

Xu, J., D. Z, B. Liu, S. Yi, J.-H. Li, Z. Zhang, Y. Liu, J.-H. Li, L. Liu, A. Zhou, R. Gennis and J. Zhu (2020). "Structure of the cytochromeaa3-600 heme-copper menaquinol oxidase bound to inhibitor HQNO shows TM0 is part of the quinol binding site." Proc Natl Acad Sci U S A **117**: 872-876.

Yang, D., H. Oyaizu, G. Olsen and C. Woese (1985). "Mitochondrial origins." Proc. Natl. Acad. Sci. U. S. A. **82**: 4443-4447.

Yoshimura, H., Y. Hirota, S. Soda, M. Okazeri, Y. Takagi, A. Takeuchi, C. Tode, M. Kamao, N. Osakabe and Y. Suhura (2020). "Study on structure-activity relationship of vitamin K derivatives: Conversin of the naphthoquinone part into another aromatic ring and evaluation of their neuronal differentiation-inducing activity." Bioorg. Med. Chem. Lett. **30**: 127059.

Zhang, M., M. Bommer, R. Chatterjee, R. Hussein, J. Yano, H. Dau, J. Kern, H. Dobbek and A. Zouni (2017). "Structural insights into the light-driven auto-assembly process of the water-oxidizing Mn4CaO5-cluster in photosystem II." Elife **6**.

Zhao, L., Wei-Cchen, W. Chang, Y. Xiao, H.-w. Liu and P. Liu (2013). "Methylerythritol Phosphate Pathway of Isoprenoid Biosynthesis." Annu. Rev. Biochem. **82**: 497-530.

Zimorski, V., C. Ku, W. F. Martin and S. B. Gould (2014). "Endosymbiotic theory for organelle orgins." Curr. Opin. Microbiol. **22**: 38-48.

Zobnina, V., M. Lambreva, G. Rea, G. Campi, A. Antonacci, V. Scognamiglio, M. Giardi and F. Polticelli (2017). "The plasoquinol-plasotquinone exchange mechanism in photosystem II: insight from molecular dynamics simulations." Photosynth. Res. **131**: 15-30.

Chapter 3:
Electron Transport Lipids Fold in Membrane-Like Environments

3.1. Introduction

Molecular conformations are paramount to the physical and chemical properties that dictate recognition and function of molecules within biological systems. The location and conformation of lipoquinones within biological membranes is not well understood and highly debated (Kingsley and Feigenson 1981, Michaelis and Moore 1985, Ulrich, Girvin et al. 1985, Salgado, Villalain et al. 1993, Soderhall and Laaksonen 2001, Afri, Ehrenberg et al. 2004, Galassi and Arantes 2015, Quirk, Lardner et al. 2016, Koehn, Magallanes et al. 2018, Koehn, Beuning et al. 2019). Lipoquinones are hydrophobic membrane-bound molecules consisting of a redox-active quinone headgroup and an isoprenyl side chain. There are three major structural subgroups of lipoquinones which differ only in the structure of the headgroup. Ubiquinones (UQ), such as Ubiquinone-10 (UQ-10, Figure 3.1A), comprise of a benzoquinone ring with two methoxy substituents, plastoquinones (PQ) with a dimethylbenzoquinone such as plastoquinone-9 (PQ-9), and menaquinones (MK), such as menaquinone-9 (MK-9, Figure 3.1B), contain a methylnaphthoquinone ring. Lipoquinones function as essential components of the respiratory electron transport system (ETS), where they shuttle electrons and protons between membrane-bound protein complexes, ultimately ending in the production of ATP (Nowicka and Kruk 2010, Kawamukai 2018). UQ and MK are involved in the ETS of oxidative phosphorylation in mammalian and bacterial cells, but PQ is involved in photosynthetic ETS in plants and photosynthetic bacteria (Kawamukai 2018). For the purpose of this study, we will focus on UQ

and MK. Even though the ETS is vital for life through the production of ATP, the role of lipoquinones is commonly distilled to an abbreviation within a diagram, such as "Q" for Coenzyme

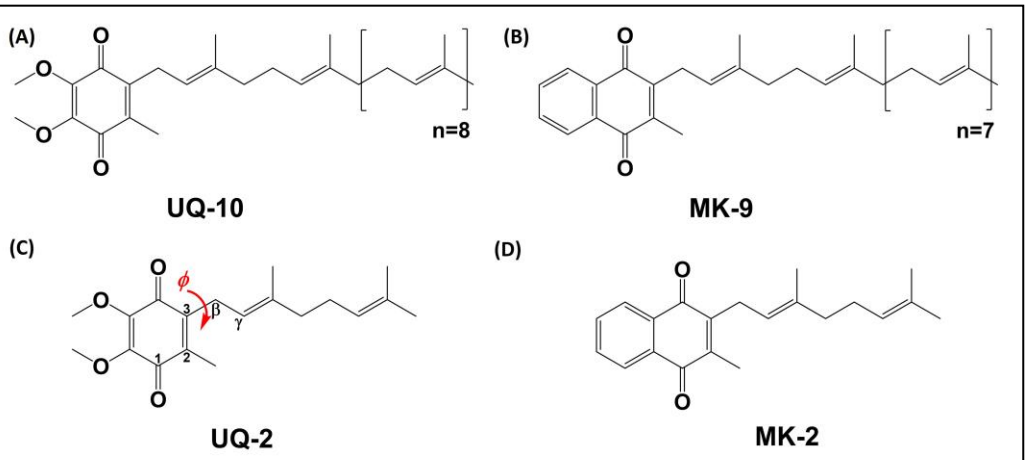

Figure 3.1. Schematic structures of native lipoquinones: (**A**) Ubiquinone-10 (UQ-10), and (**B**) Menaquinone-9 (MK-9). Schematic structures of truncated lipoquinone analogs: (**C**) Ubiquinone-2 (UQ-2) with the C2C3CβCγ bond indicated in red with dihedral angle, φ , and (**D**) Menaquinone-2 (MK-2).

Q (UQ-10), the major electron transport agent in eukaryotes (Trumpower 1981, Kawamukai 2018), ignoring the conformation and location of these molecules as a whole. Similar to lipoquinones, polyprenyl compounds have been known to adopt preorganized, folded conformations due to hydrophobic effect and π-π interactions (Woodward and Bloch 1953, Murgolo, Patel et al. 1989). The synthesis of cholesterol relies on the preorganized conformation of squalene epoxide to produce a single stereochemical outcome out of 256 (2^8) possible conformations (Woodward and Bloch 1953). Moreover, dolichol-19 adopts a coiled conformation (Murgolo, Patel et al. 1989). A handful of computational studies have investigated the dihedral angle (φ) about the C2C3CβCγ bond (as shown in red in Figure 3.1C) in UQs (Nilsson, Lyubartsev et al. 2001, Ceccarelli, Procacci et al. 2003, Galassi and Arantes 2015, Eddine, Biaso et al. 2020), MKs (Eddine, Biaso et al. 2020), and plastoquinones (Nilsson, Eriksson et al. 2001, Jong, Liguori et al. 2015, Eddine, Biaso et al. 2020), which determined φ was ~90°, 100°, and 90°, respectively. In this study we determined the location, orientation, and conformation of UQ-2 (Figure 3.1C), a truncated, representative analog

for native UQ-10, using 1D and 2D NMR spectroscopic methods in organic solvents and in biological model membrane systems comprised of AOT reverse micelles (RM) (Van Horn, Ogilvie et al. 2008). This analysis will allow us to compare the location and conformation of UQ-2 with MK-2 (Figure 3.1D) (Koehn, Magallanes et al. 2018) in membrane-like environments to shed light on the controversies regarding the location and conformation of lipoquinones in cellular membranes.

The location of UQ-10 within the membrane has been widely studied using experimental and computational methods, but it continues to be controversial. Briefly, there is no consensus regarding the location of UQ-10 with its locations spanning the entire width of the membrane bilayer leaflet. Out of these studies, three schools of thought have emerged; the quinone headgroup is located: (**i**) at or near the lipid headgroups (Kingsley and Feigenson 1981, Stidham, McIntosh et al. 1984, Lenaz, Samori et al. 1992, Salgado, Villalain et al. 1993, Galassi and Arantes 2015, Gómez-Murcia, Torrecillas et al. 2016, Kaurola, Sharma et al. 2016, Quirk, Lardner et al. 2016, Teixeira and Arantes 2019), (**ii**) within the acyl chains(Michaelis and Moore 1985, Cornell, Keniry et al. 1987, Chazotte, Wu et al. 1991, Salgado, Villalain et al. 1993, Metz, Howard et al. 1995, Afri, Ehrenberg et al. 2004, Hauss, Dante et al. 2005), or (**iii**) within the bilayer midplane (Ulrich, Girvin et al. 1985, Ondarroa and Quinn 1986, Soderhall and Laaksonen 2001) (Figure 3.2). Even though the location of the headgroup is controversial, the field does seem to agree that at least part of the isoprenyl side chain is embedded within the bilayer midplane, and the headgroup is thought to extend into one of the membrane leaflets. This bend (~90° turn) in the isoprenyl side chain allows UQ-10 to be accommodated within the bilayer, which addresses the fact that UQ-10 is

roughly the same length as a typical phospholipid bilayer if UQ-10 were in fully-extended conformation (Trumpower 1981).

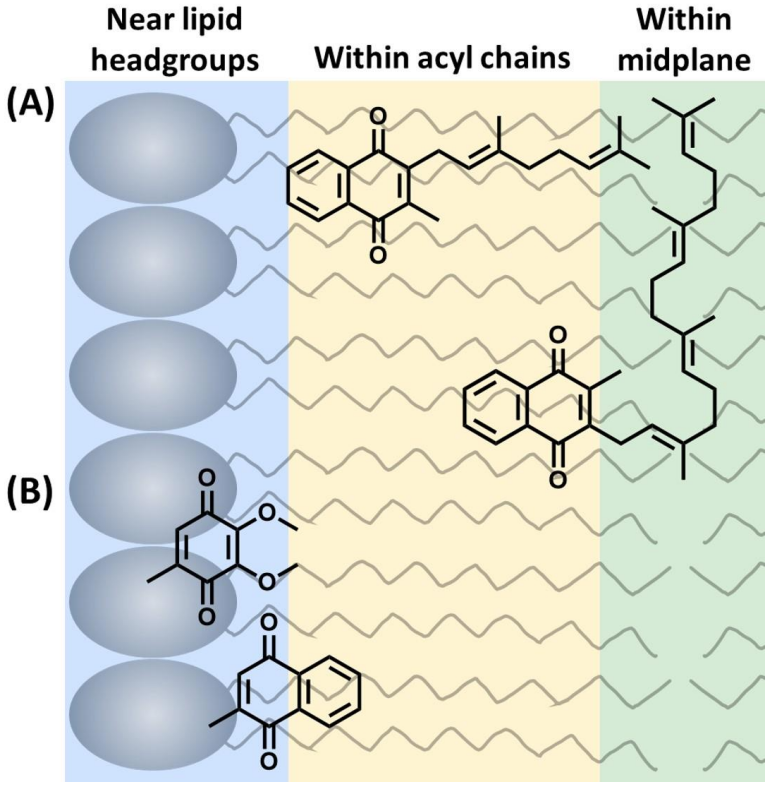

Figure 3.2. Three possible locations of lipoquinone headgroup: (**A**) Example of the influence of the isoprenyl side chain length on location of the quinone headgroup. MK-2 and MK-4 are shown as a 2D schematics. MK-2 has been determined to fold in membrane-like interfaces (Koehn, Magallanes et al. 2018). (**B**) Relative placement based on headgroup polarity (side chain omitted for clarity) (Van Cleave, Murakami et al. 2020, Van Cleave, Koehn et al. 2021).

Two hypotheses have been reported to explain the headgroup position within the membrane. First, the length of the isoprenyl side chain was reported to affect the position of the quinone headgroup by pulling the headgroup closer to the midplane as the side chain length increases. For example, the quinone headgroup of MK-4 would be found closer to the midplane than MK-2 (Figure 3.2A). On the other hand, the polarity of the headgroup is also thought to anchor its location within the membrane. Recent computational studies by Arantes and coworkers determined UQ associates with the lipid headgroups (Galassi and Arantes 2015, Teixeira and

Arantes 2019). Together, we recently showed for the series of MK-1, MK-2, MK-3, and MK-4 that the location of the headgroup remained constant as the side chain length increased using both experimental and computational techniques (Van Cleave, Murakami et al. 2020, Van Cleave, Koehn et al. 2021). As a consequence of the latter, one would anticipate a difference in the location of the more polar UQ headgroup compared to the more hydrophobic MK headgroup as illustrated in Figure 3.2B (Van Cleave, Murakami et al. 2020). Lipoquinone headgroup is also linked to diffusive motion. "Swimming" lipoquinones are associated with the phospholipid headgroups, and "diving" are found near the midplane. A few computational and experimental studies determined UQ and various analogs are stabilized in the swimming position (Soderhall and Laaksonen 2001, Van Cleave, Murakami et al. 2020). A recent computation study determined the lipoquinone position depends on the local protein content of the membrane (Singharoy, Maffeo et al. 2020). If the region is lipid-rich, swimming lipoquinone is the dominant species, and diving lipoquinones are the most common in the vicinity of protein complexes (Gupta, Khaniya et al. 2020, Singharoy, Maffeo et al. 2020).

Although lipoquinone conformation is likely to be critical for function and recognition, the topic of conformation of the UQ and MK headgroup relative to the isoprenyl side chain is curiously ignored in the literature aside from a handful of computational studies (Joela, Kasa et al. 1997, Bernardo, Fato et al. 1998, Lenaz, Fato et al. 1999, Nilsson, Eriksson et al. 2001, Nilsson, Lyubartsev et al. 2001, Soderhall and Laaksonen 2001, Ceccarelli, Procacci et al. 2003, Tekin and Erkoc 2010, Galassi and Arantes 2015, Jong, Liguori et al. 2015, Ismail, Leroux et al. 2016, Kaurola, Sharma et al. 2016, Eddine, Biaso et al. 2020, Feng, Wang et al. 2021). Additionally, a few of the computational studies investigating the location of lipoquinones in the membrane contained figures suggesting φ was $\sim 90°$ (Joela, Kasa et al. 1997, Bernardo, Fato et al. 1998,

Lenaz, Fato et al. 1999, Soderhall and Laaksonen 2001, Tekin and Erkoc 2010, Ismail, Leroux et al. 2016, Kaurola, Sharma et al. 2016, Feng, Wang et al. 2021), leading to the expectation of a folded conformation. However, there was no discussion regarding the conformation of the headgroup relative to the isoprenyl side chain prior to our work in 2018 (Koehn, Magallanes et al. 2018). The implications of conformation on lipoquinone locomotion were hypothesized by Joela and coworkers (Joela, Kasa et al. 1997). Therein, they speculated the quinone headgroup is located close to the enzyme active site and moves between membrane and enzyme binding pocket by rotating about the C2C3CβCγ bond. They describe this limited movement with a stationary side chain and a mobile headgroup as if the "tail is wagging the dog." The isoprenyl chain would serve to the anchor the quinone headgroup location. Since we previously found that the side chain did not dictate the headgroup location for MK-1 through MK-4, we hypothesized that the anchoring of the headgroup drives the extension of the side chain, and that the more polar UQ-2 headgroup will be closer to the interface than the more hydrophobic headgroup of MK-2. Hence, we carried out studies in which the location and conformation of UQ-2 were elucidated in environments that allow direct comparison to previously reported MK-2, which folds within model membrane interfaces (Koehn, Magallanes et al. 2018). This study will illuminate how headgroup structure changes the position, orientation, and conformation, which are critical to recognition and function, of prominent lipoquinones within membrane-like environments.

3.2. Results & Discussion

3.2.1. Synthesis of UQ-2

UQ-2 **8** was prepared using a 6-step synthesis (Figure 3.3) starting from commercially available 3,4,5-trimethoxytoluene **1**. The synthetic route has been reported in literature (Naruta 1980, Lu and Chen 2004); however, we scaled up the reactions and used modified procedures and conditions to overcome synthetic challenges encountered. The aldehyde **2** was prepared efficiently and was practically pure upon workup using a Rieche formylation reaction with $TiCl_4$, which is

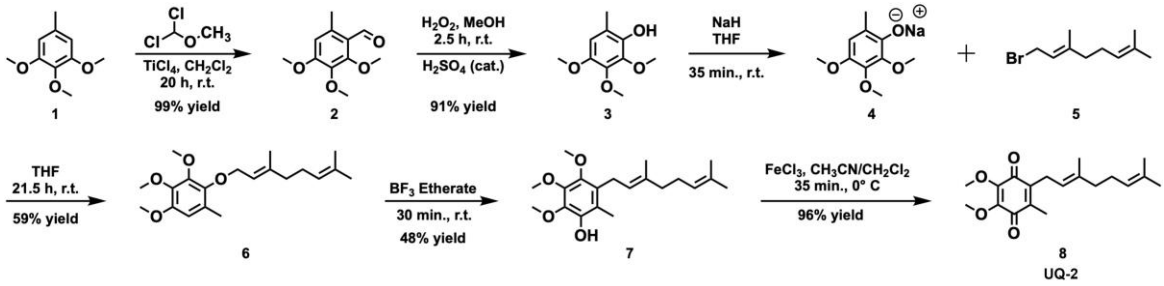

Figure 3.3. Synthetic scheme for the six-step synthesis to obtain UQ-2 **8** from 3,4,5-trimethoxytoluene **1** using modified protocols as reported (Matsumoto, Kobayashi et al. 1984, Lu and Chen 2004, Bovicelli, Borioni et al. 2008).

the traditional Lewis acid catalyst for this reaction. Efforts to achieve this reaction using $AlCl_3$ as the Lewis acid catalyst were low yielding and resulted in impure compound in our hands. An acid-catalyzed Dakin oxidation reaction was used to afford phenol **3** in excellent yield even after chromatographic purification (Rüttimann 1986). The geranyl ether **6** was prepared via an S_N2 reaction between phenolate **4** and geranyl bromide **5** in a modest yield. Efforts to achieve the allylic rearrangement to yield compound **7** close to yields reported in literature (Dötz 1984) was met with limited success. A 48% yield was the highest yield we obtained compared to 73% in literature (Dötz, Pruskil et al. 1982). Attempts to improve this yield failed, and reactions times longer than 30 minutes decreased the yield and appeared to increase the amount of unknown side products. While compound **7** was efficiently oxidized to **8** using $FeCl_3 \cdot 6H_2O$ in a mixture of dichloromethane and acetonitrile at 0 °C, attempts to follow a published procedure (Tso and Chen

1995) using $FeCl_3$ in a mixture of ethanol and H_2O at ambient temperature yielded only starting material. (Matsumoto, Kaobayashi et al. 1984, Lu and Chen 2004, Bovicelli, Borioni et al. 2008).

3.2.2. 1D ^{1}H NMR Spectroscopic Studies of UQ-2 in Organic Solvents

To establish that UQ conformation is sensitive to its surrounding environment, UQ-2 was first characterized using 1D ^{1}H NMR spectroscopy. Figure 3.4 shows the 1D ^{1}H NMR spectra of UQ-2 in isooctane (2,2,4-trimethylpentane), d_6-benzene, d_5-pyridine, d_6-DMSO, d_3-acetonitrile,

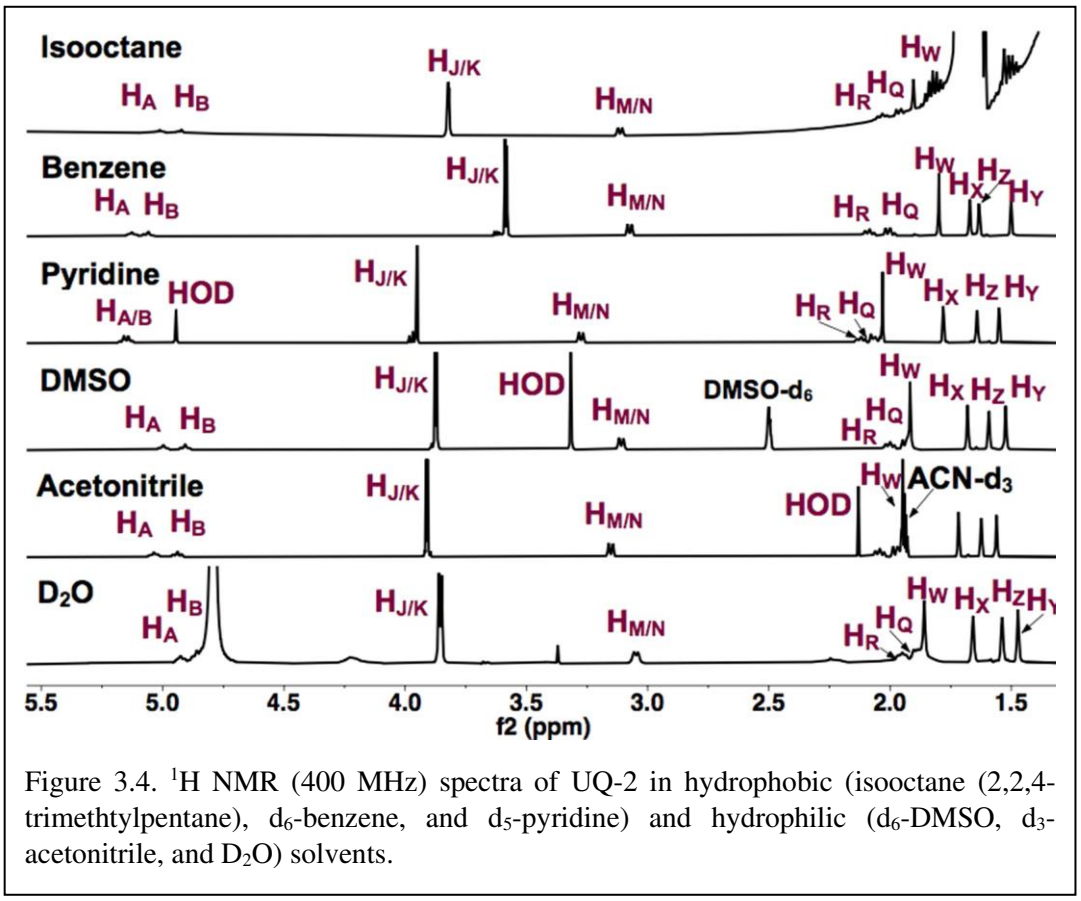

Figure 3.4. ^{1}H NMR (400 MHz) spectra of UQ-2 in hydrophobic (isooctane (2,2,4-trimethtylpentane), d_6-benzene, and d_5-pyridine) and hydrophilic (d_6-DMSO, d_3-acetonitrile, and D_2O) solvents.

and D_2O. The observed chemical shifts of UQ-2 vary dramatically in the different solvents shown. Different spectroscopic trends are observed in the hydrophobic (isooctane, d_5-pyridine, and d_6-benzene) and the hydrophilic (d_3-acetonitrile, d_6-DMSO, and H_2O/D_2O) solvent environments. For example, the isoprenyl protons H_M/H_N and methoxy protons H_J/H_K are observed at significantly different chemical shifts between the two different classes of solvents. The observations could be

described by conformational changes of UQ-2 in the various solvent environments investigated, alterations of the electronic state due to interaction with the solvent, or most likely, a combination of both. There were similarities and differences among the investigated solvents. For the hydrophobic solvents, protons H_M/H_N have similar chemical shifts in isooctane and benzene, but they appear more downfield in pyridine, whereas they appear in similar chemical shifts in the hydrophilic solvents. The chemical shifts for H_J and H_K are in significantly different locations in each solvent, which suggests the methoxy groups are changing environments in the different solvents (Nilsson, Lyubartsev et al. 2001). The chemical shifts of the vinyl protons H_A and H_B are increasingly more downfield as the polarity of the hydrophobic solvents increases. In the hydrophilic solvents, H_A and H_B are found in similar chemical shifts aside from D_2O where they appear slightly upfield and obscured by the HOD peak.

3.2.3. ^{1}H-^{1}H 2D NOESY and ^{1}H-^{1}H 2D ROESY NMR Spectroscopic Studies of UQ-2 in d_6-DMSO, d_3-acetonitrile, d_6-benzene, and d_5-pyridine

To determine the conformation of UQ-2 in organic solvents, we utilized two complementary 2D NMR methods, ^{1}H-^{1}H 2D NOESY and ^{1}H-^{1}H 2D ROESY (Jones, Butts et al. 2011). We chose to highlight the NOESY and ROESY spectra of UQ-2 in d_6-DMSO for direct comparison to our previous work with MK-2 (Koehn, Magallanes et al. 2018). The corresponding spectra for d_3-acetonitrile, d_6-benzene, and d_5-pyridine can be found in Figures 3.S15-S23 in the Appendix I. Looking at the structure of UQ-2, a folded conformation, which is defined by a ~90° dihedral angle about the C2C3CβCγ bond, would be indicated by cross peaks between the headgroup and particular protons on the isoprenyl side chain such as the methyl protons H_W and protons further down the side chain, such as H_A, H_Y, and H_Z. In the full NOESY spectrum in d_6-DMSO, there is a cross peak observed between H_W and vinyl protons, H_A and H_B (Figure 3.5 and proton labeling scheme is shown in Figure 3.6A). The proton H_B is close enough to H_W have NOE

interactions; however, H_A would be too far away to have NOE interactions unless the molecule is in a folded conformation. In addition, there are cross peaks that confirm the 1D ^{1}H NMR spectra

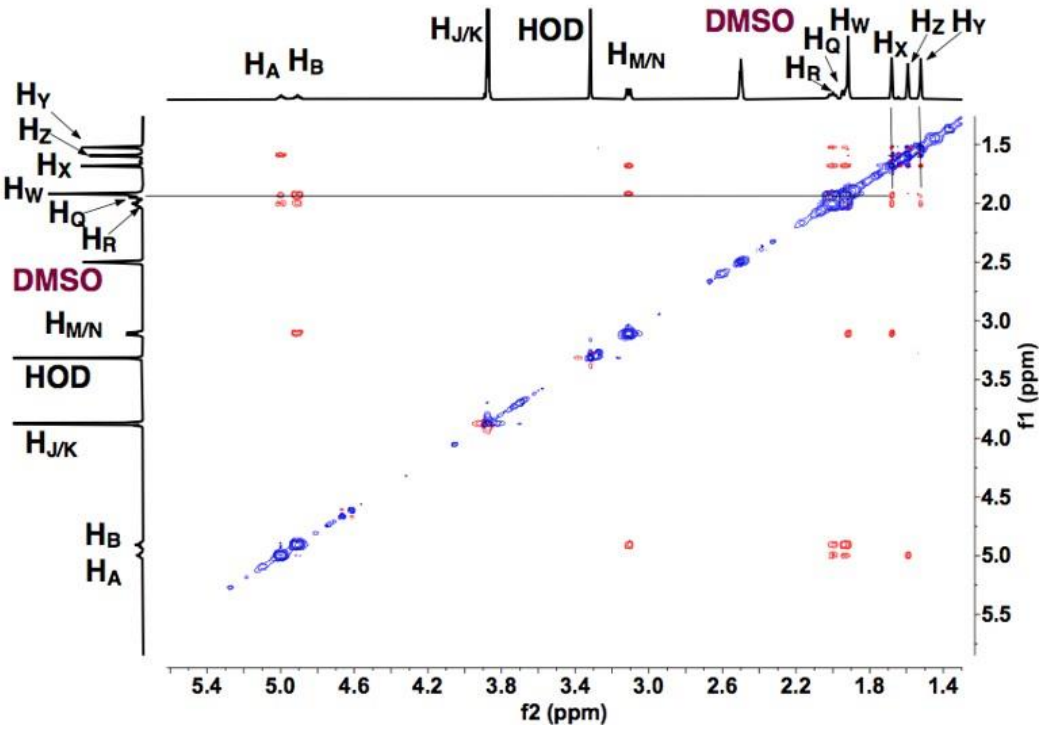

Figure 3.5. Full ^{1}H-^{1}H 2D NOESY spectrum of UQ-2 in DMSO.(Koehn, Magallanes et al. 2018)

assignments along the isoprenyl tail, such as H_W and allylic protons H_M and H_N and between H_A/H_B and methyl protons H_X, H_Y, and H_Z. The folded conformation is also suggested by the cross peaks observed between methyl protons H_W and methyl protons, H_X, H_Y and H_Z (Figure 3.6B). These cross peaks are also observed in the ROESY spectrum (Figure 3.6C and 3.6D). Enlarged full ROESY spectrum is also shown in the Appendix I: Figure 3.S13). These cross peaks are indicative of a U-shaped conformation (example shown in Figure 3.7), placing the terminal methyl groups over the quinone headgroup for UQ-2 in d_6-DMSO.

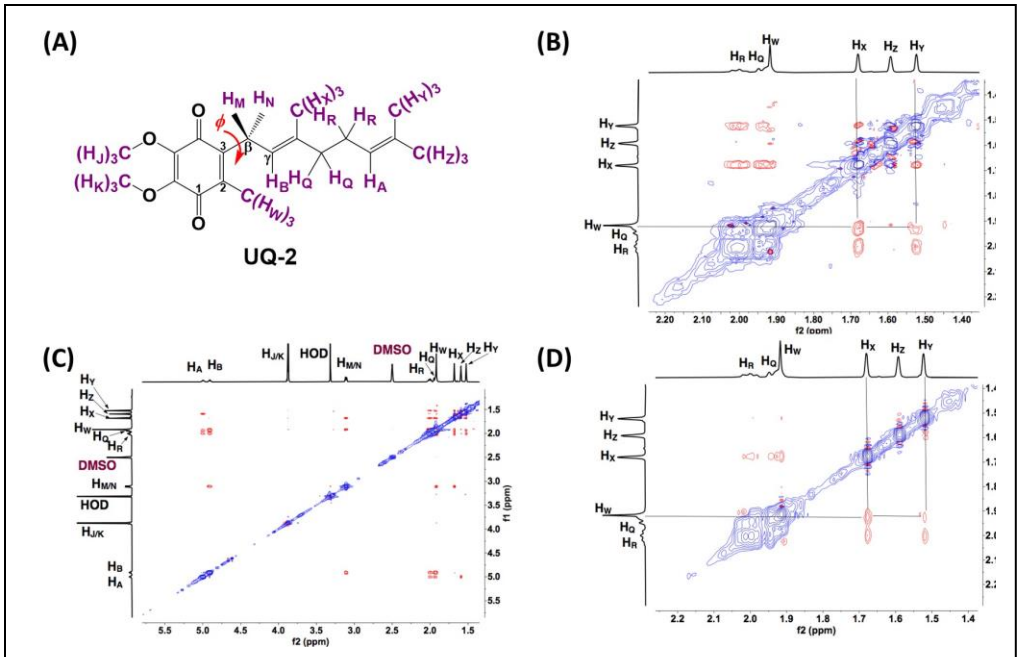

Figure 3.6. (**A**) Proton labeling scheme for UQ-2. (**B**) Partial ^{1}H-^{1}H 2D NOESY spectrum of UQ-2 in DMSO. (**C**) Full ^{1}H-^{1}H 2D ROESY spectrum of UQ-2 in DMSO. Full ROESY spectrum can also be found in Appendix I, Figure 3.S13. (**D**) Partial ^{1}H-^{1}H 2D ROESY spectrum of UQ-2 in DMSO. Full ROESY spectrum can be found in the Appendix I, Figure 3.S13. (Koehn, Magallanes et al. 2018, Koehn, Beuning et al. 2019)

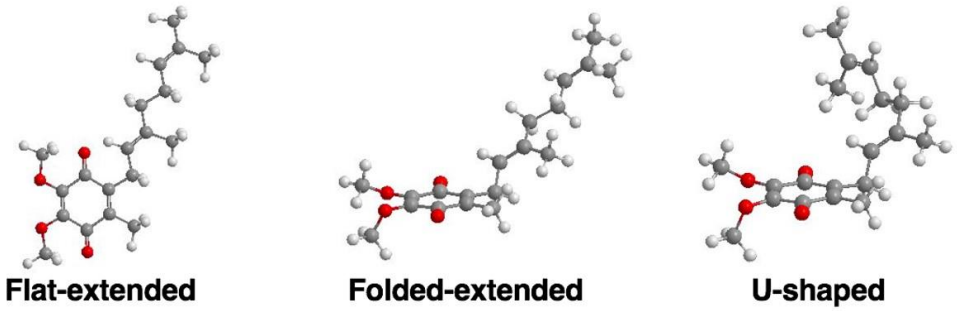

Figure 3.7: Examples of three possible classes of UQ-2 conformations: Flat-extended, Folded-extended, and U-shaped.

In the case of the 2D NOESY and ROESY spectra of UQ-2 in d_3-acetonitrile (Figures 3.S16 and 3.S17), there are cross peaks observed between H_W and vinyl protons, H_A and H_B, and methyl protons, H_X, H_Y, and H_Z, similar to d_6-DMSO. Together these suggest a folded, U-shaped conformation, but the results are somewhat inconclusive. The reference peak for d_3-acetonitrile,

1.93 ppm, is close to H_W (1.94 ppm) and almost overlapping. Therefore, it is hard to conclude if the cross peaks observed are a result of intramolecular NOE interactions or interactions with the solvent. For 2D NOESY and ROESY spectra of UQ-2 in d_6-benzene (Figures 3.S19 and 3.S20), there are cross peaks observed between H_W and H_B, H_X, and H_M/H_N. In both the flat-extended and folded-extended conformations (example shown in Figure 3.7), H_B, H_X, and H_M/H_N are all within the 5 Å NOE range of H_W. To distinguish between the two, we looked for cross peaks between H_W and the terminal methyl protons, H_Y and H_Z. In the flat-extended conformation, the average distance between H_W and H_Y is approximately 5.1 Å, which is just outside the observable NOE range. In the ROESY spectrum, there are cross peaks present between H_W and H_Y and H_Z (Figure 3.S20); however, they are not present in the corresponding NOESY (Figure 3.S19). Therefore, the absence of a cross peak between H_W and H_Y in the NOESY (Figure 3.S19) suggests H_Y is outside the NOE range and therefore indicates a folded-extended conformation in d_6-benzene. Similar observations were found for 2D NOESY and ROESY spectra for UQ-2 in d_5-pyridine (Figures S22 and S23). There are cross peaks observed between H_W and H_A/H_B, H_X, and H_M/H_N, and there is not a cross peak observed between H_W and H_Y. Similar to benzene, artifact cross peaks between H_W and H_Y and H_Z are seen in the ROESY of UQ-2 in d_5-pyridine, but they are not present in the NOESY. At minimum, this together suggests UQ-2 adopts a folded-extended conformation in d_5-pyridine.

3.2.4. Illustrating UQ-2 Conformations determined by NMR using Molecular Mechanics

UQ-2 has a short repeating isoprenyl chain (C_{10}) but enough carbons with numerous degrees of rotational freedom; therefore, even the truncated version of UQ, UQ-2, can assume many different specific conformations and still be considered folded by our definition. We created 3D conformations (Figure 3.8) of UQ-2 for visualization using Molecular Mechanics where intramolecular distances between specific protons obtained from 2D NOESY/ROESY NMR spectra (Table 3.S1) were used as geometric constraints. While the exact position of the isoprenyl side chain varies slightly from solvent to solvent, UQ-2 adopts a folded conformation in all four solvents examined in the 2D NMR studies, where the dihedral angle about the C2C3CβCγ bond (Figure 3.1C) is ~90°.

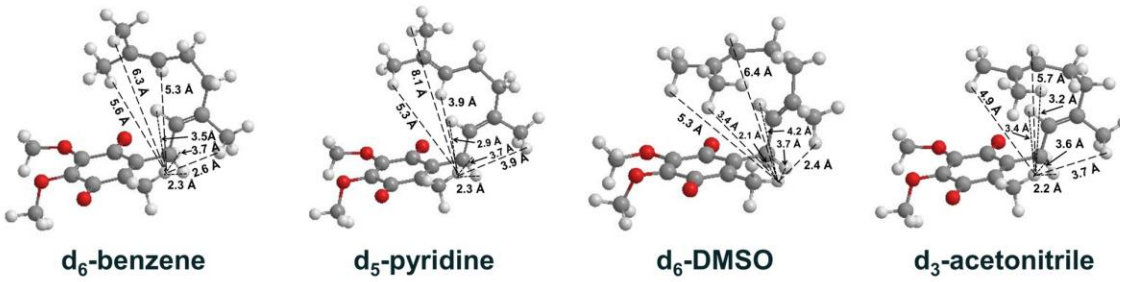

Figure 3.8. UQ-2 conformations generated using 2D NMR data distance constraints and MMFF94 calculations to illustrate the conformations elucidated in d_6-benzene, d_5-pyridine, d_6-DMSO, and d_3-acetonitrile. Intramolecular distances (Å) between H_W and select protons on the side chain are shown (dashed lines).

To understand the differences between the conformations of UQ-2 and MK-2, we first had to determine the distances between the protons on the isoprenyl side chain and the headgroup methyl proton H_W. We used the volume integrals from the 2D NOESY spectra and correlated them to intramolecular distances. The volume integral of the H_W and H_M/H_N cross peak, which has a known intramolecular distance of ~3.5 Å, was set to 1, and each volume integral was standardized against it. From here, the values obtained were used to determine if the cross peaks were strong (>1.5), medium (0.6-1.5), or weak (<0.6). These intensities were translated to distance in

Ångstroms accordingly: (**i**) strong (<3 Å), (**ii**) medium (3-4 Å), and (**iii**) weak (> 4 Å). The intramolecular distances were then used to construct the conformations, and MMFF94 minimization calculations were performed to correct bond lengths. The distances in Table 3.S1 reflect the intramolecular distances post minimization.

DMSO and pyridine were chosen due to the distinctly different 1D ^{1}H NMR spectra to better illustrate the differences in conformation (Koehn, Magallanes et al. 2018). Since NOESY and ROESY spectra are products of an average conformation, the intramolecular distances generated are representative of the most abundant conformation. As described previously, the interactions between headgroup methyl protons H_W and protons along the isoprenyl side chain, such as vinyl protons H_A and methyl protons H_X, H_Y, and H_Z, are critical to evaluate UQ-2 conformation in organic solvents. The distances between H_W and H_A, H_X, H_Y, and H_Z imply there is a folded conformation about the C2C3βCγ bond, and the position of the terminal methyl protons H_Y and H_Z relative to H_W suggest differences in the position of the end of the isoprenyl side chain: U-shaped or folded-extended conformation.

For UQ-2 in d_5-pyridine, the intramolecular distance between H_W and H_X is shown to be 3.9 Å, which is slightly out of range for NOE interactions. However, the distance between H_W and vinyl proton, H_A, 3.9 Å, supports a folded conformation. The intramolecular distances between H_W and H_Y and H_Z were found to be 8.1 Å and 5.3A, respectively. Although these values are outside the range of NOE influence, cross peaks were observed in the 2D NOESY and ROESY spectra (Figures 3.5 and 3.6C, respectively). Therefore, we cannot preclude the possibility that UQ-2 adopts both a folded-extended or a more open U-shaped conformation in d_5-pyridine. These results are in line with MK-2 in d_5-pyridine, which was previously found to adopt a folded-extended conformation (Koehn, Magallanes et al. 2018).

We superimposed the conformations of UQ-2 in d_3-acetonitile and d_6-DMSO to better visualize the minute differences observed between conformations (Figure 3.9). The superimposed conformations of UQ-2 in d_6-benzene and d_5-pyridine are found in the Appendix I (Figures 3.S25). In Figure 3.9A, UQ-2 in d_3-acetonitrile and d_6-DMSO are shown in purple and green, respectively. With the headgroups aligned, there is a slight variation in the dihedral angle along the C2C3CβCγ

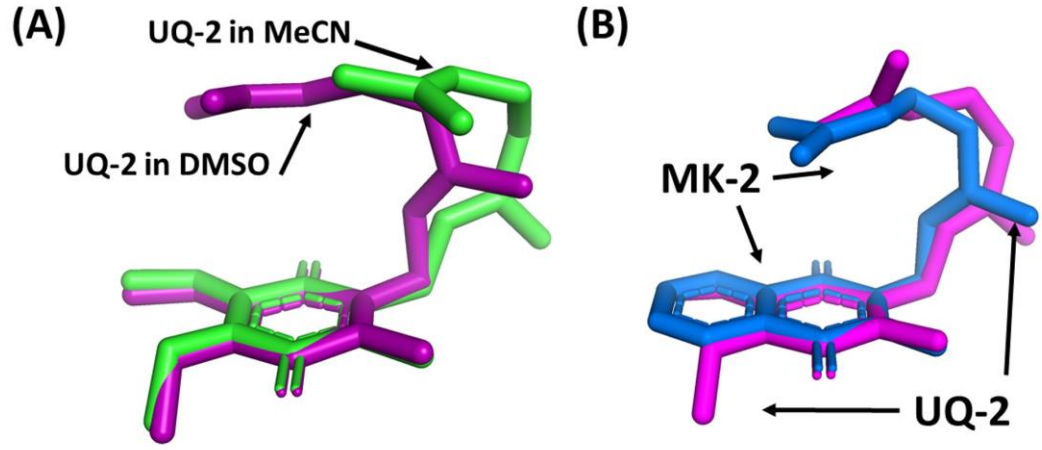

Figure 3.9. Superimposed 3D conformations of (**A**) UQ-2 based on the 2D NMR data in d_3-acetonitrile (purple) and d_6-DMSO (green) and (**B**) UQ-2 (pink) and MK-2 (blue) based on the 2D NMR data in d_6-DMSO.

bond, and the trend continues along the sidechain through the second isoprene unit. This accounts for the differences observed in intramolecular distances toward the end of the isoprenyl side chain. The terminal methyl groups of UQ-2 in d_6-DMSO appear directly above the headgroup leading to a U-shaped conformation. The same methyl groups in d_3-acetonitrile appear to be above but not centered over the headgroup, which is consistent with possibility of U-shaped or folded-extended conformation. In Figure 3.9B, the conformation of UQ-2 and MK-2 in d_6-DMSO are superimposed to visualize how the headgroup structure affects the conformation. The C2C3CβCγ bond in both UQ-2 and MK-2 are nearly identical to one another, but the conformation along the side chain

starts to deviate at the first alkene. Taking into consideration the many degrees of freedom about the isoprenyl side chain, it is not unexpected to see deviations in conformation along the side chain.

The folded conformations observed for UQ-2 are likely a result of non-covalent interactions. Firstly, UQ-2 is folding upon itself to minimize interactions with the solvent due to the hydrophobic effect. This is especially apparent in the U-shaped conformations of UQ-2 in the hydrophilic solvents, DMSO and acetonitrile, whereas the hydrophobic solvents, pyridine and benzene, afford an open U-shaped or folded-extended conformation. Additionally, the folded conformation is likely reinforced by π-π interactions between the π bonds in the quinone headgroup and the isoprenyl side chain. This idea is supported by the work done on farnesol, where farnesol does not adopt a folded conformation, regardless of the increased number of degrees of freedom along the molecule (Zahn, Eilers et al. 2000). Therefore, the presence of the quinone headgroup plays a significant role in the ability of the lipoquinone to adopt a folded conformation, but we only saw modest differences between the folded UQ-2 and MK-2 conformations. In addition to the presence of the lipoquinone headgroup, a study suggests the methyl proton, H_W, on the quinone also plays an important role in influencing a folded conformation (Eddine, Biaso et al. 2020). The quinone methyl group serves as a rotational barrier by preventing the side chain from freely rotating between folded and flat conformations.

3.2.5. 1D ^{1}H NMR Spectroscopic Studies of UQ-2 in RMs

Our ultimate objective was to determine how UQ-2 behaved with respect to membrane-like interfaces. We used a system comprised of nanosized water droplets encased in AOT surfactant to create reverse micelles (RMs) inside an isooctane (hydrophobic) solvent. This simple model system will provide useful information regarding location, orientation, and conformation of UQ-2 at an interface using NMR spectroscopy with minimal overlap between surfactant proton

peaks and key UQ-2 proton peaks. 1D ^{1}H NMR spectra of varying RM sizes were collected in D_2O (w_0: 4, 8, 12, 16, 20, where $w_0 = [D_2O]/[AOT]$), shown in Figure 3.10. The placement of the UQ-2 molecules inside the membrane system was determined via the chemical shifts that UQ-2

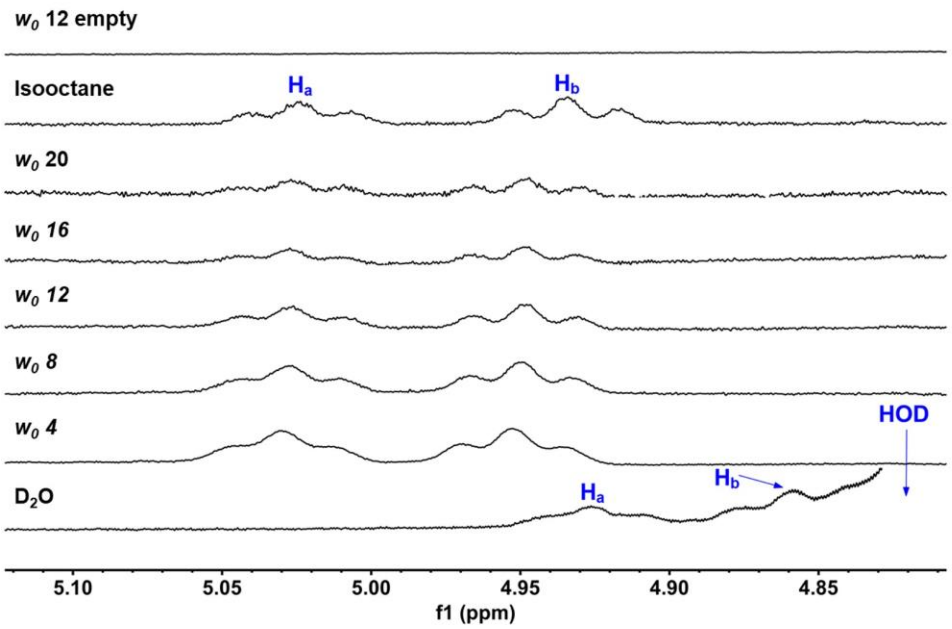

Figure 3.10. 1D ^{1}H NMR (400 MHz) spectra of UQ-2's alkene protons, H_A and H_B, in D_2O, isooctane, and different sized RMs. An empty RM lacking UQ-2 is also shown for comparison. Peak labelling corresponds to the proton labelling scheme key in Figure 3.6A.

protons undergo as the RM size changes. Typically, aromatic protons often offer ideal peaks to compare and analyze shifts, as they lie far from any AOT peaks. However, as there are no aromatic protons to observe in UQ-2, we instead observed the vinyl protons peaks (H_A/H_B), which are both triplet peaks that are easily discernable from the AOT peaks. The peak locations for H_A and H_B respectively are 5.02 ppm and 4.93 ppm for isooctane, 5.03 ppm and 4.95 ppm for w_0 20, 5.03 ppm and 4.95 ppm for w_0 16, 5.03 ppm and 4.95 ppm for w_0 12, 5.03 ppm and 4.95 ppm for w_0 8, 5.03 ppm and 4.95 ppm for w_0 4, 4.93 ppm and 4.86 ppm for D_2O. The chemical shifts of these peaks do not change significantly enough as the RM changes in size to reliably indicate where in the RM interface the UQ-2 resides. However, the large shift between the D_2O sample and the RM samples

(-0.10 ppm for H_A and -0.09 ppm for H_B from w_0 4 to D_2O) compared to the much smaller shift between the isooctane sample and the RM samples (0.01 ppm for H_a and 0.02 ppm for H_b from isooctane to w_0 20) would indicate that the UQ-2 does not reside within the bulk water or in the isooctane of the RM system, and thus UQ-2 must reside somewhere in the RM interface. However, 2D NMR studies will enable the exact location, orientation, and conformation of UQ-2 in RMs to be identified.

Dynamic Light Scattering (DLS) was used to determine the hydrodynamic radius of RMs containing UQ-2 and verify that RMs formed in the samples used and that the properties and stability of the samples were consistent with previous studies (see Section V of the Appendix I). DLS samples were prepared following the sample preparation method used for NMR spectroscopic studies except that DDI H_2O was used instead of D_2O. The results showed that RMs formed and that the sizes of the RMs made were in excellent agreement with that of the literature (Maitra 1984). These results indicate that the introduction of UQ-2 into the RM system does not significantly affect the size or stability of the RMs.

3.2.6. ^{1}H-^{1}H 2D NOESY NMR Spectroscopic Studies of UQ-2 in a RM Model Membrane System.

To determine the exact location, orientation, and conformation of UQ-2 within RMs, we obtained an ^{1}H-^{1}H 2D NOESY NMR of UQ-2 in a w_0 12 RM (Figure 3.11). Figure 3.11A shows a full NOESY spectrum. To elucidate the location and orientation of UQ-2 within the RM, we looked for the interactions of UQ-2 with AOT (Figure 3.11C). Methoxy protons H_J and H_K and benzoquinone methyl protons H_W are shown to have cross peaks with AOT between H1', H4, AOT-CH_2, and AOT-CH_3. Additionally, H_W shows cross peaks with H1 and H3 of AOT. Vinyl protons H_A/H_B were found to have cross peaks with H1, H3, and H3'. Allylic protons H_M/ H_N were

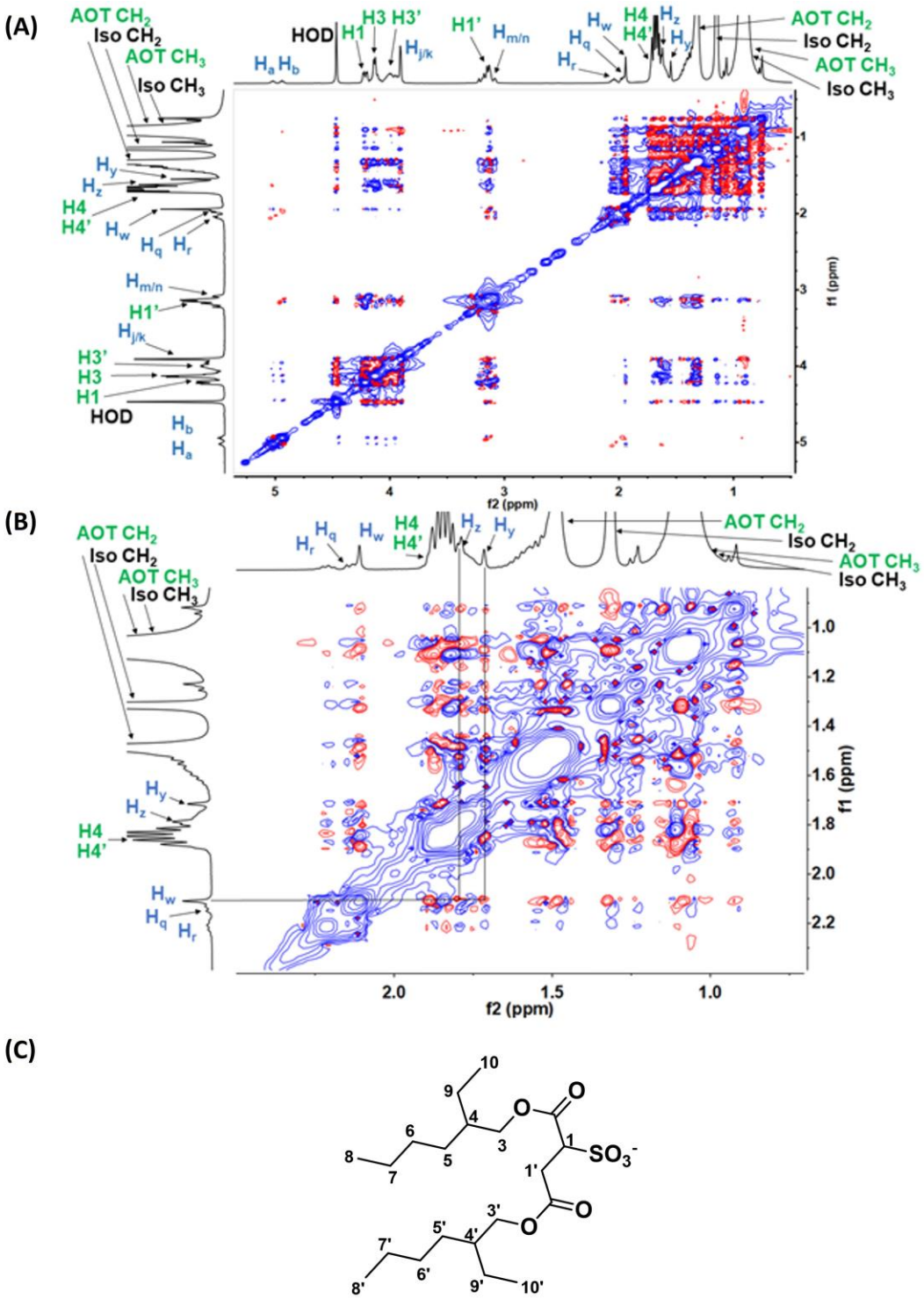

Figure 3.11. 1H-1H 2D NOESY NMR spectra of UQ-2 in w_0 12 AOT-RM: (**A**) full spectrum, (**B**) partial spectrum. (**C**) Labeled structure of AOT. Blue text labels correspond to UQ-2 protons and green text labels to AOT protons.

found to have interactions with H1, H3, H3' and AOT-CH_2, and H_Q/H_R were found to have interactions with H1'. Although UQ-2 is less hydrophobic than MK-2, it is still shown to penetrate the AOT-water interface. The 2D NOESY cross peaks illustrate that UQ-2 is positioned near the interface of AOT with the methoxy groups of the headgroup oriented towards the alkyl chains of AOT (Figure 3.12). This orientation is similar to that of MK-2 (Koehn, Magallanes et al. 2018), however the interactions between H_W and H_J/H_K with H4 indicate the molecule is positioned closer

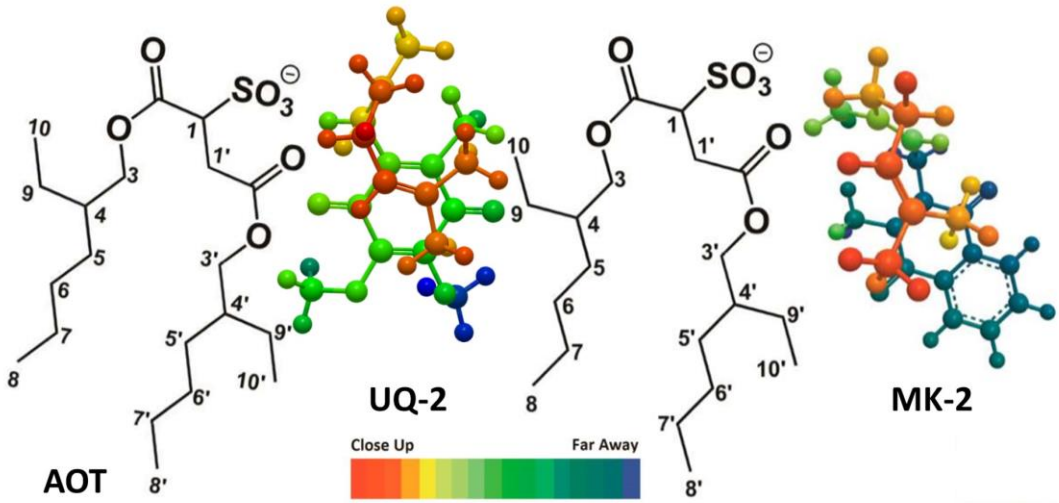

Figure 3.12. Illustration of UQ-2 and MK-2's proposed folded, U-shaped conformations and placement within the RM interface. The arrangements are consistent with ^{1}H-^{1}H 2D NOESY and ROESY NMR spectral data obtained in a w_0 12 RM. Color depth gradient shows dark red as closer in distance and the dark blue as farther in distance from the reader. AOT proton labeling scheme key is shown.

to the interface than MK-2, which is in agreement with our previous work showing the UQ headgroup is closer to the water pool than MK-2 in phospholipid bilayers (Koehn, Magallanes et al. 2018, Van Cleave, Murakami et al. 2020, Van Cleave, Koehn et al. 2021). The cross peaks observed between H_W and H_Y/H_Z and H_A/H_B indicate UQ-2 is in a folded conformation, specifically a U-shaped conformation. This conformation would not be possible unless the isoprenyl side chain was positioned over the headgroup (Figure 3.11B). Using methods described above in Section 3.2.4, the interproton distances of UQ-2 in a w_0 12 AOT-RM system were

determined between H_W and protons along the sidechain (Table 3.S2). The intramolecular distance between H_W and H_X is shown to be 2.4 Å. Additionally, the distances between H_W and H_Y and H_Z were found to be 3.4 Å and 5.3 Å, respectively. Although the distance for H_Z is slightly outside of the NOE range, cross peaks were observed in the 2D NOESY (Figure 3.11B). Together this supports a U-shaped conformation for UQ-2 in AOT-RMs. As a confirmatory measure, 1D NOE experiments were performed to confirm the interactions of H_A/H_B with H_W, H_Z and H1' within the w_0 12 AOT-RM system (Figure 3.S24). Additionally, the 2D NOESY NMR experiment in AOT-RMs was repeated multiple times, and the same conclusions were made regarding location, orientation, and conformation of UQ-2 in the interface of the AOT-RM system.

3.2.7. Interaction of UQ-2 with Langmuir Phospholipid Monolayers.

3.2.7.1. Compression Isotherms of Pure and Mixed Monolayers

Finally, we wanted to understand how UQ-2 interacted with the interface of a phospholipid-based membrane monolayer and compare these results to the RM system. UQ-2 was found to have a collapse pressure of 21 mN/m in this study (Figure 3.13). Our value was obtained by taking the second derivative of area per molecule with respect to surface pressure, with the lowest point representing the collapse pressure. Reported literature values varied widely, with some as high as 35 mN/m and others reporting that UQ-2 dissolved into the subphase (Rüttimann 1986, Liebeskind and Foster 1990, Coman, Parvulescu et al. 2010). These discrepancies may be

due to the slightly soluble nature of UQ-2, differences in the composition of the subphase, and even stirring of the subphase.

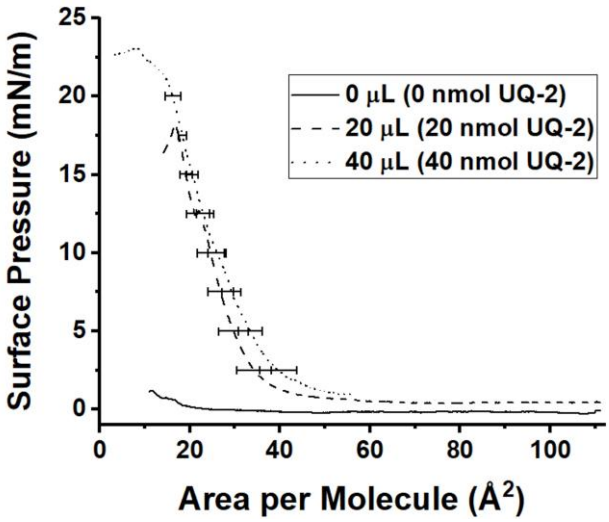

Figure 3.13. Compression isotherms of different amounts of 1 mM UQ-2. The solid black curve represents pure phosphate buffer with no UQ-2 present, the dashed curve represents an injection of 20 µL of UQ-2, and the dotted curve represents an injection of 40 µL of UQ-2. Curves are the average of at least three measurements. Standard deviations of the area were calculated for every 5 mN/m of surface pressure.

Pure films of DPPC and DPPE were in line with the literature (Raynolds, Manning et al. 1977, Chenard, Manning et al. 1980), with DPPC exhibiting its signature gas-liquid transition between 0-5 mN/m and its liquid-liquid condensed transition from 5-10 mN/m of surface pressure. The gas-liquid transition disappears upon the addition of UQ-2. The normalized 75:25 DPPC:UQ-2 curve does not overlap with the control curve. However, the variability in our measurements makes it impossible to draw a solid conclusion on whether UQ-2 is compressed out of the DPPC monolayer. Regardless, compression modulus analysis showed that increasing amounts of UQ-2 caused the DPPC monolayer to become more elastic (Figure 3.S26).

Compression isotherms with DPPE did not exhibit a significant difference in collapse pressure, as seen in Figure 3.14. The 25:75 and 50:50 DPPE:UQ-2 monolayers exhibited a liquid

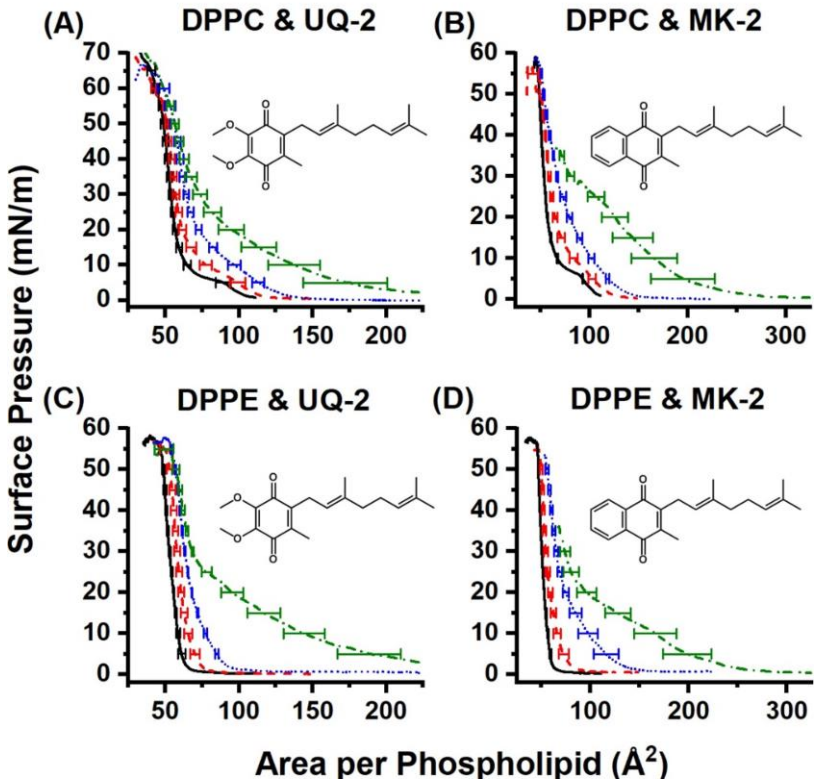

Figure 3.14. Normalized compression isotherms of mixed monolayers of UQ-2 (**A** and **C**) or MK-2 (**B** and **D**) and either DPPC (**A** and **B**) or DPPE (**C** and **D**). Solid black curves represent pure phospholipid monolayers, red dashed curves represent 75:25 lipid:lipoquinone films, blue dotted curves represent 50:50 lipid:lipoquinone films, and green dash-dot curves represent 25:75 lipid:lipoquinone films. Curves are the average of at least three measurements. Error bars are the standard deviation of the area at every 5 mN/m of surface pressure. MK-2 data were reproduced with permission from Koehn *et al.* 2018.

condensed phase, which suggests a reorganization of the monolayer. All mixed DPPE monolayers demonstrated at least a 9% increase in area per molecule at physiological surface pressure (Liebeskind, Baysdon et al. 1980) (30-35 mN/m) without the normalized curves overlapping with the control (see Tables S3 and S4). This indicates that UQ-2 is in the interface and spreading the DPPE molecules apart. UQ-2 was not compressed out of the monolayer at physiological surface pressure for DPPE.

3.2.7.2. Comparison of UQ-2 and MK-2 in Langmuir Monolayers

Interestingly, UQ-2 remains in the DPPC interface at physiological surface pressure, whereas MK-2 was likely to be compressed out. There is also a more distinct hump in the 25:75 DPPC:MK-2 curve at 25 mN/m than that of the 25:75 DPPC:UQ-2. In combination with the fact that mixed DPPC:UQ-2 curves do not overlap the control; we might conclude that UQ-2 is more likely to reside in the interface than MK-2. This is logical, as MK is more hydrophobic than UQ.

Both UQ-2 and MK-2 induce a liquid-condensed phase in DPPE, but it appears with a smaller mole fraction of MK-2 than UQ-2. As with DPPC, UQ-2 is always present in the interface as the mixed monolayers are at least 9% more expanded at physiological surface pressure than the DPPE control. Again, the hydrophobicity of the naphthoquinone headgroup of MK-2 is greater than that of the benzoquinone headgroup of UQ-2 which likely explains these differences. In summary, both UQ-2 and MK-2 associated with the Langmuir monolayer interface, but UQ-2 resided closer to the interfacial water than MK-2 due to MKs more hydrophobic nature, consistent with the RM model membrane studies.

3.3.Conclusion

UQs and MKs are critical components of the ETS. UQs are found in bacteria, fungi, plants, and mammals, and MKs are mainly found in gram positive bacteria. While the interactions of these electron transport lipids with the membrane-bound protein complexes along the ETS is well-known, surprisingly their exact location and conformation within the membrane is still widely debated. In this study, we determined the location, orientation, and conformation of UQ-2, a truncated, representative analog for native UQ-10, using 1D and 2D NMR spectroscopic methods in organic solution and biological membrane-like environments. We then compared the UQ-2

results to the previously studied MK-2 to understand fundamentally how the class of lipoquinone molecules behave within membranes.

The 1D and 2D NMR studies showed that different solution environments slightly change the observed folded conformation of UQ-2. In all four solvents examined in this study (DMSO, acetonitrile, pyridine, and benzene), UQ-2 was found to adopt a folded, U-shaped conformation with a ~90° dihedral angle about the C2C3CβCγ. On the other hand, UQ-2 adopts a more open U-shaped conformation in the hydrophobic solvents, benzene and pyridine, which documents the fact that the environment will impact the conformation of the UQ-2 side chain. Once we established that UQ-2 folded in solution, we wanted to determine if a folded conformation was also adopted in a membrane-like interface. Using 2D NMR spectroscopy, we determined that UQ-2 interacts similarly to MK-2 with the RM model membrane system. Both UQ-2 and MK-2 adopt a folded, U-shaped conformation but reside at slightly different places in the membrane-like interface. Not surprisingly, and consistent with other studies (Van Cleave, Murakami et al. 2020, Van Cleave, Koehn et al. 2021), UQ-2 resides closer to the AOT-water interface than the more hydrophobic MK-2. Both lipoquinone molecules were oriented in a manner that allowed the side chain to fold back over the quinone moiety and be accommodated in the surfactant tails. It appears that regardless of lipoquinone headgroup structure, lipoquinones adopt folded conformations at membrane-like interfaces. Langmuir monolayer studies examining the interaction of UQ-2 with DPPC and DPPE phospholipids supported the results of the RM studies. Both UQ-2 and MK-2 were found to associate with the monolayer water-lipid interface, but MK-2 was more easily compressed out of the interface, which indicates UQ-2 resides closer to the interface than MK-2.

In summary, lipoquinones UQ-2 and MK-2 adopted folded conformations in solution and within membrane-like interfaces. The more polar UQ-2 was found to reside slightly closer to the

water-surfactant interface, which was supported by both the RM and Langmuir monolayer studies. It appears that the presence of a lipoquinone headgroup is important for anchoring the lipoquinone in the membrane interface and for allowing the isoprenyl side chain to adopt some variation of a folded conformation that can be accommodated within the lipid tails due to the orientation of the lipoquinone within the interface. Varying the structure of the lipoquinone (UQ vs MK) only modestly changed the location while residing in the RM interface. However, since lipoquinones are redox-active and the polarity of the headgroup changes upon reduction to the quinol form, structural differences in the headgroup likely facilitate locomotion of headgroup within the interface between membrane-bound enzymes in the ETS (Van Cleave, Murakami et al. 2020). Taken together, the results of this study and others support a model where the headgroups of the longer, native lipoquinones, such as UQ-10 and MK-9, reside close to the water-lipid interface with the side chains folded but penetrating through the acyl tails into the midplane of the membrane bilayer. The location, orientation, and conformation of lipoquinones are critical for their function in generating cellular energy within membrane ETS and the studies described herein shed light on the behavior of lipoquinones within membrane-like environments.

3.4. Experimental

3.4.1. General Materials

The following chemicals were used without further purification for the synthetic work: Ultra-high purity argon (99.9%, Airgas), 3,4,5-trimethoxytoluene (97%, Aldrich), α,α-dichloromethyl methyl ether (98%, Aldrich), Dichloromethane (DCM, Stabilized, 99.9%, Fisher Scientific), $TiCl_4$ (99.9%, Aldrich), *n*-pentane (98%, Merck), Ethyl Acetate (99.9%, Fisher), Diethyl ether (≥99.0%, Merck), $NaHCO_3$ (99.7%, Merck), NaCl (Fisher), Na_2SO_4 (Fisher), Methanol (Aldrich), 30% aq. H_2O_2 solution (Sigma-Aldrich), H_2SO_4 (Fisher), SiO_2 (SiliCycle® SilicaFlash® F60, 43-60μm 60Å), 60% NaH dispersion in mineral oil (Aldrich), THF (Fisher),

Geranyl Bromide (95%, Aldrich), NH_4Cl (99.7%, Fisher), BF_3 diethyl etherate (≥46.5%, Aldrich), $MgSO_4$ (98%, Merck), Acetonitrile (99.9%, Fisher) and $FeCl_3$ hexahydrate (99.9%, Fisher). The following chemicals were used without further purification for the spectroscopic studies: D_2O (99.9%, Cambridge Isotope Laboratories), d_1-chloroform (99.8%, Cambridge Isotope Laboratories), d_3-acetonitrile (99.8%, Aldrich), d_6-DMSO (99.9%, Cambridge Isotope Laboratories), d_5-pyridine (99.8%, Merck), d_6-benzene (99.5%, Cambridge Isotope Laboratories), isooctane (99.8%, Aldrich), and AOT (≥99%, Aldrich). The following materials were used for the trough work: Sodium phosphate monobasic monohydrate (≥98%) and chloroform (≥99.8%) were purchased from Sigma Aldrich. Sodium phosphate dibasic anhydrous (≥99%) and methanol (≥99.9%) were purchased from Fisher Scientific. 1,2-dipalmitoyl-*sn*-glycero-3-phosphocholine (DPPC, >99%) and 1,2-dipalmitoyl-*sn*-glycero-3-phosphoethanolamine (DPPE, >99%) were purchased from Avanti Polar Lipids. Distilled deionized water (DDI H_2O) was purified with a Barnsted E-pure system (~18 MΩ-cm).

3.4.2. General Methods

All reactions were carried out under an argon atmosphere unless otherwise noted. All reagents were used as purchased unless otherwise noted. Solvents were dried by passing through an alumina drying column (Solv-Tek Inc.) under argon pressure (DCM, THF, Diethyl Ether).

3.4.3. Syntheses

3.4.3.1. Preparation of 2,3,4-trimethoxy-6-methylbenzaldehyde (2).

To a dry 500 mL round bottom Schlenk flask was added dry dichloromethane (DCM) (150 mL) followed by 3,4,5-trimethoxytoluene **1** (9.97 g, 54.7 mmol) and α,α-dichloromethyl methyl ether (12.58 g, 109.5 mmol, 2 eq.) and then cooled to 0 °C. Then, $TiCl_4$ (273.6 mmol, 137 mL, 2.0 M in dry DCM, 2.5 eq. to α,α-dichloromethyl methyl ether) was added dropwise over 30 min. via a 250 mL addition funnel under argon at 0 °C. After addition was complete, the red reaction

mixture was stirred at ambient temperature for 20 hrs. Thin-layer chromatography (TLC) (9:1 *n*-pentane/EtOAc) showed the reaction was complete. The reaction was then very slowly quenched with ice until the reaction color turned light blue-gray. The DCM was removed under reduced pressure at ambient temperature and the resulting off-yellow liquid was extracted with diethyl ether (3 x 100 mL). The combined organic extracts were washed with sat. $NaHCO_3$ (200 mL), washed with brine (3 x 100 mL), dried over anhydrous Na_2SO_4, and then the solvent was removed under reduced pressure at ambient temperature. The product was dried under reduced pressure (~125 Torr) for 1 h, which yielded an off-white crystalline solid (11.40 g, 54.2 mmol, 99.1%) that was pure. ^{1}H NMR (400 MHz, $CDCl_3$) δ: 10.40 (s, 1H), 6.50 (s, 1H), 3.98 (s, 3H), 3.92 (s, 3H), 3.86 (s, 3H), 2.56 (s, 3H). ^{13}C NMR (101 MHz, $CDCl_3$) δ: 191.18, 158.46, 157.78, 139.80, 138.26, 121.48, 110.53, 62.50, 61.12, 56.15, 21.91. HRMS (ESI, OTOF) m/z: [$(M+H)^+$] Calcd for $C_{11}H_{15}O_4$ 211.0965; Found 211.0965.

3.4.3.2. Preparation of 2,3,4-trimethoxy-6-methylphenol (3).

To a 250 mL round bottom Schlenk flask was added 2,3,4-trimethoxy-6-methylbenzaldehyde **2** (11.37 g, 54.1 mmol), MeOH (110 mL), and 30% aq. H_2O_2 solution (7.97 g, 70.3 mmol, 1.3 eq.). Then, conc. H_2SO_4 (1.08 mL) was added dropwise resulting in a red-orange reaction mixture. After 2.5 h of stirring at ambient temperature under argon, the ^{1}H NMR spectrum showed no aldehyde peak present. The reaction mixture was poured into sat. $NaHCO_3$ (100 mL) and then extracted with DCM (3 x 100 mL). The combined organic extracts were washed with sat. $NaHCO_3$ (100 mL), washed with brine (100 mL), dried over anhydrous Na_2SO_4, and the solvent was evaporated under reduced pressure (~125 Torr) at ambient temperature to yield 10.55 g crude red oil. The product was then purified by flash column chromatography (7:1 *n*-pentane/EtOAc, 600 mL SiO_2, 70 mm column) to yield the desired product as an off-white crystalline solid (9.75

g, 49.2 mmol, 90.9%). ^{1}H NMR ($CDCl_3$) δ: 6.43 (s, 1H), 5.43 (s, 1H), 3.95 (s, 3H), 3.86 (s, 3H), 3.80 (s, 3H), 2.21 (s, 3H). ^{13}C NMR (101 MHz, $CDCl_3$) δ:146.17, 141.24, 140.14, 140.09, 118.08, 109.63, 61.34, 61.11, 56.75, 15.65. HRMS (ESI, OTOF) m/z: [$(M+H)^+$] Calcd for $C_{10}H_{15}O_4$ 199.0965; Found 199.0951.

3.4.3.3. Preparation of Geranyl 2,3,4-trimethoxy-6-methylphenyl Ether (6).

NaH (2.95 g of 60% NaH dispersion in mineral oil washed with *n*-pentane that was first dried over activated neutral alumina, 73.8 mmol) was added to a dry 500 mL round bottom Schlenk flask containing a solution of 2,3,4-trimethoxy-6-methylphenol **3** (9.75 g, 49.2 mmol) dissolved in dry THF (150 mL). The mixture was stirred at ambient temperature for 35 min. The solvent was removed under reduced pressure at 25 °C until an off-white powder was obtained. To a dry 500 mL round-bottom Schlenk flask was added the crude powder dissolved in anhydrous THF (75 mL) and then the mixture was cooled in an ice-H_2O bath. Then, a solution of geranyl bromide (16.02 g, 73.8 mmol, 1.5 eq.) in dry THF (75 mL) was added dropwise over 15 min. via an addition funnel under argon. The mixture was then warmed to ambient temperature and stirred for 21.5 hrs. under argon. The resulting yellow reaction mixture was slowly quenched with 5% aq. NH_4Cl solution (100 mL) and then extracted with diethyl ether (3 x 100 mL). The combined yellow organic extracts were washed with sat. $NaHCO_3$ (100 mL), washed with brine (100 mL), dried over anhydrous Na_2SO_4, and then the solvent was removed under reduced pressure (~125 Torr) at ambient temperature to yield 22.4 g crude yellow oil. The crude oil was purified by flash column chromatography (9:1 *n*-pentane/EtOAc, 1200 mL SiO_2, 70 mm column) to yield a light-yellow oil (9.75 g, 29.2 mmol, 59.4 %). ^{1}H NMR ($CDCl_3$) δ: 6.44 (s, 1H), 5.55 (t, J = 7.2 Hz, 1H), 5.10 (t, J = 6.3 Hz, 1H), 4.45 (d, J = 7.1 Hz, 2H), 3.93 (s, 3H), 3.86 (s, 3H), 3.81 (s, 3H), 2.22 (s, 3H), 2.04-2.12 (m, 4H), 1.69 (s, 6H), 1.61 (s, 3H). ^{13}C NMR (101 MHz, $CDCl_3$) δ: 149.19, 147.42, 144.52,

141.48, 140.97, 131.81, 126.54, 124.11, 120.48, 108.45, 69.74, 61.37, 61.23, 56.28, 39.79, 26.53, 25.83, 17.83, 16.47, 16.43. HRMS (ESI, QTOF) m/z: [$(M+H)^+$] Calcd for $C_{20}H_{31}O_4$ 335.2217; Found 335.2220

3.4.3.4. Preparation of 5-Geranyl-2,3,4-trimethoxy-6-methyl-phenol (7).

To a 500 mL round bottom Schlenk flask was added geranyl 2,3,4-trimethoxy-6-methylphenyl Ether **6** (9.73 g, 29.1 mmol) dissolved in dry diethyl ether (120 mL). Then, the mixture was treated with fresh BF_3 etherate (36.9 mL, 46.5% BF_3 etherate solution, 291.0 mmol, 10 eq.) added dropwise over 5 min. and then stirred under argon at ambient temperature for 30 min. After exactly 30 min., the brown colored reaction was quenched with sat. NaCl (100 mL) very slowly over 8 min. and then the mixture was extracted with diethyl ether (3 x 100 mL). The combined light yellow organic extracts were washed with sat. $NaHCO_3$ (50 mL, releases CO_2), washed with brine (100 mL), dried over anhydrous $MgSO_4$, vacuum filtered, and then the solvent was removed under reduced pressure (~125 Torr) at ambient temperature to yield 9.41 g crude brown oil. The product was purified by flash column chromatography (9:1 *n*-pentane/EtOAc, 800 mL SiO_2, 70 mm) to yield the desired product (4.67 g, 14.0 mmol, 48.1%) as a light-yellow oil. ^1H NMR ($CDCl_3$) δ: 5.60 (s, 1H), 5.05 (q, J=6.5, 2H), 3.93 (s, 3H), 3.91 (s, 3H), 3.75 (s, 3H), 3.33 (d, J=6.5, 2H), 2.13 (s, 3H), 2.07 (q, J=7.2, 2H), 1.98 (m, 2H), 1.76 (s, 3H), 1.65 (s 3H), 1.57 (s, 3H). ^{13}C NMR (101 MHz, $CDCl_3$) δ: 144.49, 143.61, 143.44, 137.85, 135.12, 131.48, 129.82, 124.43, 123.18, 117.68, 61.44, 61.32, 60.92, 39.83, 26.78, 25, 82, 25.66, 17.82, 16.34, 11.48. HRMS (ESI, QTOF) m/z: [$(M+Na)^+$] Calcd for $C_{20}H_{31}O_4Na$ 357.2036; Found 357.2004.

3.4.3.5. Preparation of Ubiquinone-2 (8).

To a 50 mL round bottom flask was added 5-geranyl-2,3,4-trimethoxy-6-methylphenol **7** (0.137 g, 0.410 mmol), followed by DCM (2 mL) and ACN (2 mL) and then

cooled to 0 °C. An excess of $FeCl_3$ (1.11 g, 4.10 mmol, 10 eq.) dissolved in ACN (4 mL) was then added. The open atmosphere mixture was stirred at 0 °C for 35 min. Then, DDI H_2O (30 mL) and sat. aq. $NaHCO_3$ (30 mL) were added to the orange reaction mixture and then extracted with diethyl ether (3 x 100 mL). The combined organic extracts were washed with sat. $NaHCO_3$ (50 mL), washed with brine (50 mL), dried over anhydrous Na_2SO_4, and then the solvent was removed under reduced pressure at ambient temperature to yield UQ-2 as a red oil and practically pure (0.125 g, 0.393 mmol, 95.9%). ^1H NMR ($CDCl_3$) δ: 5.03 (t, J=6.8, 1H), 4.92 (t, J=7.0, 1H), 3.99 (s, 3H), 3.98 (s, 3H), 3.18 (d, J= 7.0, 2H), 2.01 (m, 8H), 1.72 (s, 3H), 1.64 (s, 3H), 1.57 (s, 3H). ^{13}C NMR (101 MHz, $CDCl_3$) δ: 184.91, 184.05, 144. 53, 144. 38, 141.84, 139.01, 137.66, 131.68, 124.13, 199.08, 61.28, 39.82, 26.66, 25.81, 25.43, 17.82, 16.43, 12.07. HRMS (DART) m/z: [$(M+H)^+$] Calcd for $C_{19}H_{27}O_4$ 319.1904; Found 319.1935.

3.4.4. Mass spectrometry.

High resolution mass spectrometry (HRMS) experiments were carried out using one of the following instruments: (1) an Agilent 6220 TOF LC/MS ("OTOF") interfaced to an Agilent 1200 HPLC, (2) a Maxis QTOF ("QTOF") with electrospray (ESI) mode, and (3) a Maxis QTOF in positive DART mode (DART) using jeffamine as an internal calibration standard.

3.4.5. NMR Spectroscopic Studies.

1D and 2D ^1H studies were carried out both in organic solvents and a RM system. ^1H and ^{13}C spectra were recorded using either a Varian Model MR400 or Model Inova400 operating at 400 MHz and 101 MHz, respectively. Chemical shift values (δ) are reported in ppm and referenced against the internal solvent peaks in ^1H NMR ($CDCl_3$, δ at 7.26 ppm; d_3-acetonitrile δ at 1.94 ppm; d_6-DMSO, δ at 2.50 ppm; d_6-benzene, δ at 7.16 ppm; d_5-pyridine, δ at 8.74 ppm; D_2O, δ at 4.79 ppm;) and in ^{13}C NMR (d_6-DMSO, δ at 39.52 ppm; d_6-benzene, δ at 128.06 ppm). All NMR spectra

were recorded at either 22 °C or 26 °C. When samples were prepared for RM NMR experiments, deuterium oxide was used instead of H_2O, and the pH was adjusted to consider the presence of deuterium (pD=0.4 + pH)(Samart, Beuining et al. 2014).

For 1D & 2D NMR spectroscopic studies, a sample for analytical characterization of UQ-2 was prepared by using normal phase preparative thin layer chromatography (TLC) (10:1 *n*-pentane/EtOAc). First, ~10 mg of UQ-2 (dissolved in minimal amount of DCM) was loaded onto a preparative TLC plate and then eluted (10:1 *n*-pentane/EtOAc, 45 min.). The plate was briefly dried of eluent solvent and eluted a second time (10:1 *n*-pentane/EtOAc, 45 min.). The orange band was illuminated under UV light and while illuminated, the band was divided into a top half and a bottom half. The bottom half was carefully removed with a razor blade, extracted with DCM, filtered through a disposable Pasteur pipette filled with glass wool (pre-rinsed with DCM) and concentrated under reduced pressure at ambient temperature to provide 6 mg of UQ-2 as a red oil for NMR spectroscopic studies.

3.4.5.1. Solution 1D ^{1}H NMR Spectroscopic Studies of UQ-2.

Samples were prepared by dissolving 5.0 mg of UQ-2 in 0.5 mL of either d_1-chloroform, d_6-DMSO, d_5-pyridine, d_3-acetonitrile, and d_6-benzene, respectively. The NMR instrument was locked onto the respective deuterium signal in the deuterated solvent used. NMR spectra were then collected using 32 scans for each sample. The data was processed using MestReNova NMR processing software version 10.0.1. The spectra were manually phased and then the baseline was corrected using a Bernstein Polynomial Fit (polynomial order 3). The obtained spectra were referenced to the internal solvent peak.

3.4.5.2. Sample Preparation for ^{1}H-^{1}H 2D NOESY and ^{1}H-^{1}H 2D ROESY NMR Spectroscopic Studies of UQ-2.

To prepare the samples in d_5-pyridine, d_3-acetonitrile, and d_6-DMSO, 3.2m g of UQ-2 was dissolved in 0.5 mL of solvent to yield a 20 mM solution of UQ-2. The NMR tubes containing the UQ-2 solution were purged with argon prior to data collection. To prepare a 100 mM solution of UQ-2 in $CDCl_3$, 15.9 mg of UQ-2 was dissolved in 0.5 mL $CDCl_3$. To prepare a 20 mM sample, 3.2 mg of UQ-2 was dissolved in 0.5 mL of each respective solvent (d_1-chloroform, d_6-DMSO, d_5-pyridine, d_3-acetonitrile, and d_6-benzene).

3.4.5.3. ^{1}H-^{1}H 2D NOESY and ^{1}H-^{1}H 2D ROESY NMR Spectroscopic Solution Experiments of UQ-2.

^{1}H-^{1}H 2D NOESY NMR and ^{1}H-^{1}H 2D ROESY NMR spectroscopic experiments were conducted using a 400 MHz Varian MR400 NMR at 26 °C. A standard NOESY pulse sequence was used consisting of 256 transients with 16 scans in the f1 domain using a 500 ms mixing time, 45° pulse angle, and a 1.5 sec. relaxation delay. A standard ROESYAD pulse sequence was used consisting of 256 transients with 16 scans in the f1 domain using a 400 ms mixing time, 45° pulse angle, and a 2.0 sec. relaxation delay. The NMR was locked onto either d_5-pyridine, d_6-benzene, d_3-acetonitrile, or d_6-DMSO. The resulting spectrum was processed using MestReNova NMR software version 10.0.1 (see Appendix I for details). The spectra were referenced to the internal solvent peak.

3.4.5.4. Sample Preparation for RM NMR Spectroscopic Studies of UQ-2.

A 0.50 M AOT stock solution was made by dissolving AOT (5.56 g, 12.5 mmol) in isooctane (25.0 mL). Empty RMs were made by mixing 0.50 M AOT stock solution with a D_2O water pool, and then vortexed. UQ-2 RMs were made in a similar matter. The only difference being a 14.3 mM for UQ-2 stock solution was made by dissolving 45.4 mg of UQ-2 in 10.0 mL of 0.50 M AOT/isooctane solution. The RM's were then prepared using the UQ-2 stock solution.

First, 2.0 mL samples were made using specific amounts of the 14.3 mM UQ-2 stock solution and then diluting the sample with the 500 mM AOT/isooctane solution. From the 2.0 ml solutions, 1.0 mL RM samples were prepared using the designated amounts of 2.0 mL sample and then adding the proper amount of D_2O with pH 7.0 (see General Methods for pH measurements) for UQ-2 to form the desired size RM. The samples were then vortexed until clear. The overall concentrations for 1.0 mL UQ-2 RM samples are as follows: w_0 4, 13.8 mM; w_0 8, 6.4 mM; w_0 12, 3.5 mM; w_0 16, 2.0 mM; and w_0 20, 1.4 mM.

3.4.5.4. 1D ^{1}H NMR Spectroscopic Studies of AOT/isooctane RMs Containing UQ-2.

NMR spectra of various size RMs and in isooctane and D_2O were obtained using a Varian Inova 400 MHz instrument at 22 °C using routine parameters (pulse angle: 45°, relaxation delay of 1 sec.) using 64 scans. The NMR instrument was locked onto 10% D_2O signal for the RM samples and D_2O for the sample in D_2O. The 1D ^{1}H spectra of UQ-2 in isooctane were doped with 5% d_6-benzene for the NMR instrument to lock onto and to achieve properly shimmed spectra. The spectral data was processed using MestReNova NMR processing software version 10.0.1. The spectra were manually phased and then the baseline was corrected using a multipoint baseline correction (cubic splines). The spectrum in D_2O was referenced to the internal D_2O peak and the spectra in isooctane and RM samples were referenced to the isooctane methyl peak (0.904 ppm) as previously reported (Samart, Beuining et al. 2014).

3.4.5.6. Sample Preparation for ^{1}H-^{1}H 2D NOESY and ROESY NMR Spectroscopic Studies of UQ-2 in AOT/isooctane RMs.

A 0.50 M AOT stock solution was made by dissolving AOT (5.56 g, 12.5 mmol) in isooctane (25.0 mL). A 1 mL stock solution of 112 mM UQ-2 in AOT/isooctane was made by dissolving 35.7 mg of UQ-2 in 1 mL isooctane/AOT stock solution. To make a w_0 12 RM, 893 μL of 112 mM UQ-2 AOT/isooctane stock solution and 107 μL of D_2O at pH 7 were mixed together

and then vortexed. This final mixture results in a w_0 12 RM microemulsion with an overall concentration of UQ-2 being ~100 mM (~29 molecules per RM).

3.4.5.7. ^{1}H-^{1}H 2D NOESY NMR Spectroscopic Studies of UQ-2 in a w_0 12 AOT/isooctane RM.

2D NMR spectra were obtained using similar conditions used previously (Yamago, Hashidume et al. 2000, Koehn, Magallanes et al. 2018) using a 400 MHz Varian NMR at 26 °C. A standard NOESY pulse sequence was used consisting of 256 transients with 16 scans in the f1 direction using a 200 ms mixing time, 45° pulse angle, and a relaxation delay of 1.5 sec. The NMR instrument was locked onto 10% D_2O signal. The resulting spectrum was processed using MestReNova NMR software version 10.0.1. (see Supporting Information for details). The spectrum was referenced to the isooctane methyl peak at 0.904 ppm as previously reported (Samart, Beuining et al. 2014, Koehn, Crick et al. 2018). The 3D structure illustration within a RM was drawn using ChemBioD Ultra 12.0 and ChemBio3D Ultra 12.0 based on spectral parameters described under results.

3.4.6. Langmuir Monolayer Compression Isotherm Methods

3.4.6.1. Instrument and Cleaning

All Langmuir monolayer studies were performed on a Kibron μTrough XS equipped with a Teflon ribbon barrier (hydrophobic) as described previously (Van Cleave, Koehn et al. 2021). The trough bed was cleaned between runs by scrubbing three times with isopropanol, then scrubbing three times with absolute EtOH, and then rinsing with DDI H_2O. The ribbon was cleaned by a rinse with isopropanol, a rinse with absolute EtOH, and then a rinse with DDI H_2O.

3.4.6.2. Preparation of the Subphase

The subphase consisted of approximately 50 mL of 20 mM sodium phosphate buffer (pH 7.40 ± 0.02). The pH was adjusted using 1.0 M HCl or NaOH. The subphase surface was cleaned

with vacuum aspiration until the surface pressure remained at 0.0 ± 0.5 mN/m throughout a quick compression.

3.4.6.3. Preparation of Lipid Solutions

Phospholipid solutions were prepared by dissolving powdered lipid (0.018 g DPPC, 0.017 g DPPE) into 25 mL of 9:1 chloroform/MeOH (v/v) to yield a 1 mM phospholipid stock solution. A 1 mM UQ-2 solution was prepared the same as the phospholipids, but with 0.0016 g UQ-2 dissolved into 5 mL of the chloroform/methanol solution. Stock solutions were stored at -20˚ C. Mixed monolayer were prepared immediately before experiments by adding appropriate amount of phospholipid stock and UQ-2 stock to a small glass vial and vortexing for ~ 30 seconds. Mixed monolayers consisted of 25:72, 50:50, and 75:25 UQ-2:phospholipid (mol fraction).

3.4.6.4. Formation and Compression of Monolayers

Monolayers consisted of pure DPPC, pure DPPE, pure UQ-2, or varying phospholipid:UQ-2 molar fractions (25:75, 50:50, 75:25). Films were prepared by adding 20 µL lipid stock solutions or mixtures (40 µl were used for UQ-2 and 75:25 UQ-2:phospholipid to obtain full compression) drop-wise to the surface of the subphase and were equilibrated for 15 minutes. Monolayers were compressed at a speed of 10 mm/min (5 mm/min from two sides). Surface pressure measurements were made via a modified Wilhelmy plate method where a wire probe was used instead of a plate. Surface pressure was calculated from surface tension with equation 1, where π is surface pressure (mN/m), γ_o is the surface tension of the subphase (72.8 mN/m), and γ is the surface tension after the addition of the monolayer.

$$\pi = \gamma_o - \gamma \quad (1)$$

The averages of triplicate isotherms were worked up in Excel. The averages were then normalized to the amount of phospholipid according to equation 2, where A_N is the normalized

area per phospholipid (Å^2), A is the experimental area per molecule (Å^2) (Van Cleave, Koehn et al. 2021), and x is the mol fraction of phospholipid (0.25, 0.5, or 0.75). This method of analysis was developed from a previous study (Masaki, Hasimoto et al. 1984).

$$A_N = A(x^{-1}) \quad (2)$$

Normalized isotherms were plotted with Origin 2021. Reported error bars are the standard deviations of the experimental area.

References

Afri, M., B. Ehrenberg, Y. Talmon, J. Schmidt, Y. Cohen and A. A. Frimer (2004). "Active oxygen chemistry within the liposomal bilayer Part III: Locating vitamin E, ubiquinol and ubiquinone, and their derivatives in the lipid bilayer." Chem. Phys. Lipids **131**(1): 107-121.

Bernardo, S. D., R. Fato, R. Casadio, P. Fariselli and G. Lenaz (1998). "A high diffusion coefficient for coenzyme Q10 might be related to a folded structure." FEBS Lett. **426**: 77-80.

Bovicelli, P., G. Borioni, D. Fabbrini and M. Barontini (2008). "New Efficient Synthesis of Ubiquinones." Synth. Commun. **38**(3): 391-400.

Bovicelli, P., G. Borioni, D. Fabbrini and M. Barontini (2008). "New Efficient Synthesis of Ubiquinones." Synth. Commun. **38**: 391-400.

Ceccarelli, M., P. Procacci and M. Marchi (2003). "An Ab Initio Force Field for the Cofactors of Bacterial Photosynthesis." J. Comput. Chem. **24**: 129-142.

Chazotte, B., E.-S. Wu and C. R. Hackenbrock (1991). "The mobility of a fluorescent ubiquinone in model lipid mebranes. Relevance to mitochondrial electron transport." Biochim. Biophys. Acta Bioenerg. **1058**: 400-409.

Chenard, B. L., M. J. Manning, P. W. Raynolds and J. S. Swenton (1980). "Organocopper chemistry of quinone bisketals. Application to the synthesis of isoprenoid quinone systems." J. Org. Chem. **45**(3): 378-384.

Coman, S. M., V. I. Parvulescu, S. Wuttke and E. Kemnitz (2010). "Synthesis of Vitamin K_1 and K_1-Chromanol by Friedel–Crafts Alkylation in Heterogeneous Catalysis." ChemCatChem **2**(1): 92-97.

Cornell, B. A., M. A. Keniry, A. Post, R. N. Robertson, L. E. Weir and P. W. Westerman (1987). "Location and activity of ubiquinone-10 and ubiquinone analogues in Model and Biological Membranes." Biochemistry **26**(24): 7702-7707.

Dötz, K. H. (1984). "Carbenkomplexe in der Organischen Synthese." Angew. Chem. **96**(8): 573-594.

Dötz, K. H., I. Pruskil and I. Muhlemeier (1982). "Vitamin-Synthesen mit Carben-Komplexen, II. Carbonyl(carben)-Komplex-induzierte Synthese von Vitaminen der K1- und K2-Reihe." Chem. Ber. **115**: 1278.

Eddine, M. S., F. Biaso, J. Rendon, E. Pilet, B. Guigliarelli, A. Magalon and S. Grimaldi (2020). "1,2H hyperfine spectroscopy ad DFT modeling unveil the demethylmenasemiquinone binding mode to E. coli nitrate reductase A (NarGHI)." Biochim Biophys Acta- Bioenerg. **1861**: 148203.

Feng, S., R. Wang, R. W. PAstor, J. B. Klauda and W. Im (2021). "Location and Conformational Enzemble of Menaquione and Menaquinol, and Protein-Lipid Modulations in Archael Membranes." J. Phys. Chem. B **125**: 4714-4725.

Galassi, V. V. and G. M. Arantes (2015). "Partition, orientation and mobility of ubiquinones in a lipid bilayer." Biochim. Biophys. Acta **1847**: 1560-1573.

Gómez-Murcia, V., A. Torrecillas, A. M. de Godos, S. Corbalán-García and J. C. Gómez-Fernández (2016). "Both idebenone and idebenol are localized near the lipid–water interface of the membrane and increase its fluidity." Biochim. Biophys. Acta, Biomembr. **1858**(6): 1071-1081.

Gupta, C., U. Khaniya, C. K. Chan, F. Dehez, M. Shekhar, M. R. Gunner, L. Sazanov, C. Chipot and A. Singharoy (2020). "Charge Transfer and Chemo-Mechanical Coupling in Respiratory Complex 1." J. Am. Chem. Soc. **142**: 9220-9230.

Hauss, T., S. Dante, T. H. Haines and N. A. Dencher (2005). "Localization of coenzyme Q10 in the center of a deuterated lipid mebrane by neutron diffraction." Biochim Biophys Acta **1710**: 57-62.

Ismail, A., V. Leroux, M. Smadja, L. Gonzalez, M. Lombard, F. Pierrel, C. Mellot-Draznieks and M. Fontecave (2016). "Coenzyme Q Biosynthesis: Evidence for a Substrate Access Channel in the FAD-Dependent Monooxygenase Coq6." PloS Comput. Biol **12**(1): 1-27.

Joela, H., S. Kasa, P. Lehtovuori and M. Bech (1997). "EPR, ENDOR, and TRIPLE Resonance and MO Studies on Ubiquinones (Q-n): Comparison of Radical Anions and Cations of Coenzymes Q-10 and Q-6 with the Model Compounds Q-2 and Q-0." Acta Chem. Scand. **51**: 233-241.

Jones, C. R., C. P. Butts and J. N. Harvey (2011). "Accuracy in Determining Interproton Distances using Nuclear Overhauser Effect Data from a Flexible Molecule." Bellstein J. Org. Chem **7**: 145-150.

Jong, D. H. d., N. Liguori, T. v. d. Berg, C. Arnarez, X. Periole and S. J. Marrink (2015). "Atomistic and Coarse Grain Topologies for the Cofactors Associated with the Photosystem II Core Complex." J. Phys. Chem. B **119**: 7791-7803.

Kaurola, P., V. Sharma, A. Vonk, I. Vattulainen and T. Rog (2016). "Distribution and dynamics of quinones in the lipid bilayer mimicking the inner membrane of mitochondria." Biochim. Biophys. Acta **1858**(9): 2116-2122.

Kawamukai, M. (2018). "Biosynthesis and applications of prenylquinones." Biosci. Biotechnol. Biochem. **82**(6): 963-977.

Kingsley, P. B. and G. W. Feigenson (1981). "1H-NMR Study of the Location and motion of ubiquinone in predeuterated phosphatidylcholine bilayers." Biochem. Biophys. Acta **635**: 602-618.

Koehn, J. T., C. N. Beuning, B. J. Peters, S. K. Dellinger, C. Van Cleave, D. C. Crick and D. C. Crans (2019). "Investigating Substrate Analogues for Mycobacterial MenJ: Truncated and Partially Saturated Menaquinones." Biochemistry **58**(12): 1596-1615.

Koehn, J. T., D. C. Crick and D. C. Crans (2018). "Synthesis and Characterization of Partially and Fully Saturated Menaquinone Derivatives." ACS Omega **3**(11): 14889-14901.

Koehn, J. T., E. S. Magallanes, B. J. Peters, C. N. Beuning, A. A. Haase, M. J. Zhu, C. D. Rithner, D. C. Crick and D. C. Crans (2018). "A Synthetic Isoprenoid Lipoquinone, Menaquinone-2, Adopts a Folded Conformation in Solution and at a Model Membrane Interface." J. Org. Chem. **83**(1): 275-288.

Lenaz, G., R. Fato, S. D. Bernardo, D. Jarreta, A. Costa, M. L. Genova and G. P. Castelli (1999). "Localization and mobility of coenzyme Q in lipid bilayers and membranes." BioFactors **9**: 87-93.

Lenaz, G., B. Samori, R. Fato, M. Battino, G. P. Castelli and I. Domini (1992). "Localization and preferred orientations of ubiquinone homologs in model bilayers." Biochim. Cell. Biol. **70**(504-514).

Liebeskind, L. S., S. L. Baysdon and M. S. South (1980). "An organotransition-metal synthesis of naphthoquinones." J. Am. Chem. Soc. **102**(24): 7397-7398.

Liebeskind, L. S. and B. S. Foster (1990). "Stannylquinones. Synthesis and utilization as quinone carbanion synthetic equivalents." J. Am. Chem. Soc. **112**(23): 8612-8613.

Lu, L. and F. Chen (2004). "A Novel and Convenient Synthesis of Coenzyme Q1." Syn. Commun. **34**(22): 4049-4053.

Maitra, A. (1984). "Determination of size paramters of water-Areosol OT-oil reverse micelles from their nuclear magnetic resonance data." J. Phys. Chem. **88**(21): 5122-5125.

Masaki, Y., K. Hasimoto and K. Kaji (1984). "Synthetic Studies of Isoprenoidquinones II. Syntheses of Ubiquinone-10, Phylloquinone, and Menaquinone-4 by a Chain-Extending Method Utilizing Terminally Functionalized Isoprenoidhydroquinones." Chem. Pharm. Bull. **32**(10): 3959-3967.

Matsumoto, M., K. Kaobayashi and Y. Hotta (1984). "Acid-Cataluzed Oxidation of Benzaldehydes to Phenols by Hydrogen Peroxide." J. Org. Chem. **49**: 4740-4741.

Matsumoto, M., H. Kobayashi and Y. Hotta (1984). "Acid-Catalyzed Oxidation of Benzaldehydes to Phenols by Hydrogen Peroxide." J. Org. Chem. **49**: 4740-4741.

Metz, G., K. P. Howard, W. B. S. v. Liemt, J. H. Prestegard, J. Lugtenburg and S. O. Smith (1995). "NMR Studies of ubiquinone locationin oriented model membranes: evidence for a single motionally-averaged population." J. Am. Chem. Soc. **117**: 564-565.

Michaelis, L. and M. J. Moore (1985). "Location of ubiquinone-10 (CoQ-10) in phospholipid vesicles." Biochim Biophys Acta **821**(121-129).

Murgolo, N. J., A. Patel, S. S. Stivala and T. K. Wong (1989). "The Conformation of Dolichol." Biochem. **28**(253-260).

Naruta, Y. (1980). "Allylation of quinones with allyltin reagents." J. Am. Chem. Soc. **102**(11): 3774-3783.

Nilsson, J. A., L. A. Eriksson and A. Laaksonen (2001). "Molecular dynamics simulations of plastoquinone in solution." Mol. Phys. **99**(3): 247-253.

Nilsson, J. A., A. Lyubartsev, L. A. Eriksson and A. Laaksonen (2001). "Molecular dynamics simulations of ubiquinone; a survey over torsional potentials and hydrogen bonds." Mol. Phys **99**(21): 1795-1804.

Nowicka, B. and J. Kruk (2010). "Occurrence, biosynthesis and function of isoprenoid quinones." Biochim Biophys Acta **1797**(9): 1587-1605.

Ondarroa, M. and P. J. Quinn (1986). "Proton magnetic resonance spectroscopic studies of the interaction of ubiquinone-10 with phospholipid model membranes." FEBS **155**(2): 353-361.

Quirk, A., M. J. Lardner, Z. Tun and I. J. Burgess (2016). "Surface Enhanved Infrared Spectroscopy and Neutron Reflectivity Studies of Ubiquinone in Hybrid Bulayer Membranes under Potential Control." Langmuir **32**: 2225-2235.

Raynolds, P. W., M. J. Manning and J. S. Swenton (1977). "Utilization of quinone bisacetal organocopper compounds in the synthesis of isoprenoid systems." ChemComm(14): 499-500.

Rüttimann, A. (1986). "Recent Advances in the Synthesis of K-Vitamins." Chimia **40**(9): 290-306.

Salgado, J., J. Villalain and J. C. Gomez-Fernandez (1993). "Magic angle spinning 13C-NMR spin-lattice relaxation study of the location and effects of a-tocopherol, ubiquinone-10, and ubiquinol-10 in unsonicated model membranes." Eur. Biophys. J. **22**: 151-155.

Samart, N., C. Beuining, K. J. Haller, C. D. Rithner and D. C. Crans (2014). "Interaction of a Biguanide Compound with Membrane Model Interface Systems: Probing the Properties of Antimalaria and Antidiabetic Compounds." Langmuir **30**(29): 8697-8706.

Singharoy, A., C. Maffeo, K. H. Delgado-Magnero, E. Tajkhorshid, A. Aksimentiev and K. Schulten (2020). "Atoms to Phenotypes: Molecular Design Principles of Cellular Energy Metabolism." Cell **179**: 1098-1111.

Soderhall, J. A. and A. Laaksonen (2001). "Molceular dynamics simulations of ubiquinone inside a lipid bilayer." J. Phys. Chem. B **105**: 9308-9315.

Stidham, M. A., T. J. McIntosh and J. N. Siedow (1984). "On the locatization of ubiquinones in phosphatidylcholine bilayers." Biochim Biophys Acta **767**: 423-431.

Teixeira, M. H. and G. M. Arantes (2019). "Effect of lipid composition on membrane distribution and permeability of natural quinones." RSC Adv. **9**: 16892.

Tekin, E. D. and S. Erkoc (2010). "Structural and electronic features of the ubiquinone and ubiquinol molecules: molecular dynamics and quantum chemical treatments." Molecular Simulation **36**(10): 763-771.

Trumpower, B. L. (1981). "New Concepts on the Role of Ubiquinone in the Mitochondrial Respiratory Chain." J. Bioenerg. Biomem. **13**(1/2): 1-24.

Tso, H.-H. and Y.-J. Chen (1995). "A convenient one-flask synthesis of vitamin K." J. Chem. Res. Synop. **3**: 104-105.

Ulrich, E. L., M. E. Girvin, W. A. Cramer and J. L. Markley (1985). "Location and mobility of ubiquinones of different chain lengths in artificial membrane vesicles." Biochemistry **24**(10): 2501-2508.

Van Cleave, C., J. T. Koehn, C. S. Pereira, A. A. Haase, B. J. Peters, S. W. Croslow, K. G. McLaughlin, K. R. Wrest, A. L. Goach, D. C. Crick, G. M. Arantes and D. C. Crans (2021). "Interactions of truncated menaquinones in lipid monolayers and bilayers." Int. J. Mol. Sci **22**: 1-22.

Van Cleave, C., H. A. Murakami, N. Samart, J. T. Koehn, P. M. Jr, H. D. Kreckel, E. J. Cope, A. Basile, D. C. Crick and D. C. Crans (2020). "Location of menaquinone and menaquinol headgroups in model membranes." Can. J. Chem. **98**(6): 307-317.

Van Horn, W. D., M. E. Ogilvie and P. F. Flynn (2008). "Use of reverse micelles in membrane protein structural biology." J. Biomol. NMR. **40**(3): 203-211.

Woodward, R. B. and K. Bloch (1953). "The Cyclization of Squalene in Cholesterol Synthesis." J. Am. Chem. Soc. **75**(8): 2023-2024.

Yamago, S., M. Hashidume and J.-i. Yoshida (2000). "Radical-Mediated Synthesis of Substituted Quinones with Organotellurium Compounds." Chem. Lett. **29**(11): 1234-1235.

Zahn, T. J., M. Eilers, Z. Guo, M. B. Ksbati, M. Simon, J. D. Scholten, S. O. Smith and R. A. Gibbs (2000). "Evaluation of Isoprenoid Conformation in Solution and in the Active Site of Protein-Farnesyl Transferase Using Carbon-13 Labeling in COnjuction with Solution- and Solid-State NMR." J. Am. Chem. Soc. **122**(30): 7153-7164.

Chapter 4:
Synthesis of Naphthoquinone Derivatives: Menaquinones, Lipoquinones, and other Vitamin K Derivatives

4.1. Introduction

Menaquinones are hydrophobic, isoprenoid molecules containing a methylated naphthoquinone unit and an isoprene side chain which constitutes a subgroup of lipoquinones (Collins and Jones 1981, Kroppenstedt and Mannheim 1989, Nakagawa, Hirota et al. 2010, Upadhyay, Fontes et al. 2015, Bergdoll, Ten Brink et al. 2016, Epand, Walker et al. 2016, Vilcheze, Hartman et al. 2017). There are two major structural subgroups of lipoquinones. Ubiquinones (or benzoquinones, U) are generally found in eukaryotes and Gram-negative prokaryotes, and menaquinones (or naphthoquinones, MK) generally found in Gram-positive prokaryotes. In humans, menaquinones have several biological properties, including facilitating blood coagulation. In bacteria, menaquinones are essential molecules that shuttle electrons between the membrane-bound protein complexes acting as electron acceptors and donors in the respiratory electron transport system and consequently resulting in ATP synthesis. Menaquinones are also referred to as vitamin K_2, a subgroup of the class of compounds categorized as vitamin K. The preparation and studies of some of these compounds have been extensive and include the preparation both by fermentation and synthesis (Mahdinia, Demirci et al. 2017, Tarento, McClure et al. 2019, Zhang, Wu et al. 2020). The major structural variation in menaquinones involves the isoprene side chain; that is the number of isoprene units and saturation in the side chain (Dunphy and Brodie 1971). Although these minor structural changes are deceptively simple, the specific stereochemistry of each is required to maintain their biological action. Hence, the synthesis of

these compounds requires attention to detail and often meticulous purification, which consequently leads to a decrease in yields of the desired compounds. In the following review, we will summarize reported methods and discuss the advantages and disadvantages of each, as well as identify the most suitable methods within each synthetic strategy.

Vitamin K_2 and vitamin K_1 (also referred to as phylloquinone) are natural vitamins and together make up the family of compounds known as vitamins K. The variety of the structures of vitamin K_2 depend on the number of isoprene units in the side chain. In Figure 4.1, we show the structures of menadione (vitamin K_3) **1**, menadiol **2**, vitamin K_1, and menaquinone (MK) derivatives with 1 to 9 isoprene groups in the side chain. The abbreviation used for the menaquinones in this manuscript will indicate the number of isoprene units in the side chain. For example, MK-1 describes a menaquinone with one isoprene unit, and MK-9, the major MK-derivative found in the *Mycobacteria*, contains nine isoprene units (Koehn, Magallanes et al. 2018). If the MK-derivative contains isoprene units that are saturated, it will be indicated by the addition of a Roman numeral to specify the location of the isoprene unit numbered from the naphthoquinone. For example, MK-9(II-H_2) is the major MK-derivative active as the electron transport agent in the *Mycobacterium tuberculosis.* It is a MK-9 derivative with the second isoprene group saturated (Upadhyay, Fontes et al. 2015). When more than one isoprene units are saturated, such as the three units in vitamin K_1, the nomenclature will identify the location of the

saturations using Roman numerals and the number of H-atoms added, such as MK-4(II,III,IV-H_6) indicating the first isoprene unit is still unsaturated (Dunphy and Brodie 1971).

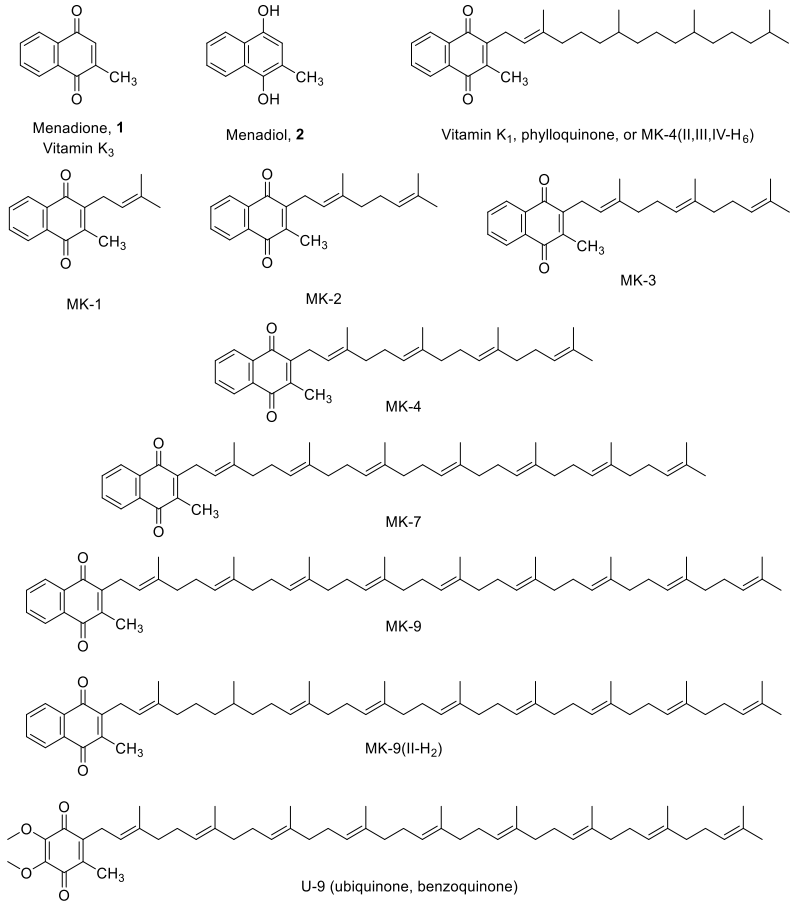

Figure 4.1. Common menaquinones and ubiquinones.

The biological activities of these compounds have been studied in-depth, and most reviews that been reported have a biological-biomedical focus. In general, terpenes and isoprenoid compounds have been widely reviewed for many uses, including pharmaceutical, flavor fragrance, and possible applications in biofuel industries (Tetali 2019). Naphthoquinones have been assessed for their biological activity against cancer (Ferreira, Ferreira et al. 2016), cardiovascular disease (Ingles, Cruz Rodriguez et al. 2020), tuberculosis (Gengenbacher and Kaufmann 2012, Bahuguna and Rawat 2020), diabetes (Karamzad, Maleki et al. 2020), kidney function (Turner, Adams et al. 2018), and age-related diseases (Simes, Viegas et al. 2020). The most well-known members of the

naphthoquinone family are the compounds known as vitamin K. Much work has been done in this area comparing the health effects of synthetic vitamin K analogs to naturally derived analogs (Schurgers, Teunissen et al. 2007). The biosynthesis of vitamin K analogs have been mapped out within bacteria (Bentley and Meganathan 1982), particularly with respect to intestinal bacteria in relation to coagulation homeostasis (Conly and Stein 1992), and discovery of possible drug targets to inhibit electron transport systems (Kurosu and Begari 2010). Another important effect caused by vitamin K_1 is the regulation of calcium uptake, particularly in bone of humans and other mammals (Cockayne, Adamson et al. 2006).

In addition, menaquinones are hydrophobic molecules that shuttle electrons between the membrane-bound protein complexes acting as electron acceptors and donors in the respiratory electron transport system facilitating oxidative phosphorylation in bacteria (Bentley and Meganathan 1982, Gengenbacher and Kaufmann 2012). In *Mycobacteria,* a menaquinone headgroup is required, whereas in a bacterium such as *E. Coli,* both menaquinones and ubiquinones (U-9, Figure 4.1) are able to serve this function (Upadhyay, Fontes et al. 2015). In the case of *Mycobacterium smegmatis,* MK-9(II-H_2) was proposed as a contextual virulent factor (Upadhyay, Fontes et al. 2015), but this suggestion was later rejected when the presence of inactive MenJ protein was shown to prevent infection by the bacterium. Thus, the protein rather than the substrate was found to be the contextual virulent factor (Kumar, Koehn et al. 2020). Development of inhibitors for the biosynthesis of menaquinones or other isoprene-derivatives has been explored as potential treatments (Debnath, Siricilla et al. 2012, Abe, Ozaki et al. 2020).

4.1.1. Properties and Biological Function of Menaquinones

The structural and redox properties of menaquinones are key for their biological function. The quinone group of the menaquinones is reduced through a two-electron transport system to form a radical anion after the addition of the first electron (Dryhurst, Kadish et al. 1982, Prince, Dutton et al. 1983, Guin, Das et al. 2011). After addition of the second electron, a dianion catecholate is formed, which then forms a catechol in the presence of a protic solvent (Figure 4.2). The two intermediates are sufficiently long-lived to be observed in aprotic solvents because the proton transfer step is slow. However, in a protic solvent the proton transfer is faster, and protonation of the intermediate radical ion occurs quickly, and the second intermediate is not long-lived enough to be observed using electrochemistry. For MK-derivatives in cellular systems, the

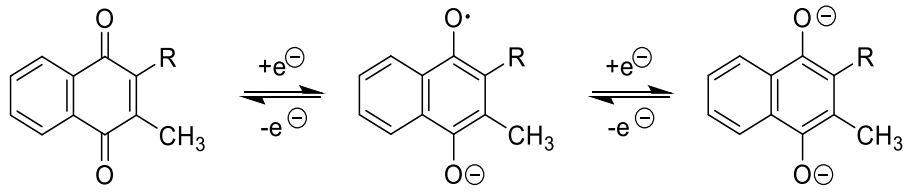

Figure 4.2. The redox reaction of menaquinones showing the two steps observed in aprotic organic solvent; in the presence of a protic solvent, it occurs in only one step, but the overall reaction is conserved.

presence of H_2O renders the redox chemistry a one step process. Even though menaquinones are located in the membrane, H_2O is an accessible proton source. It is highly likely that the redox reaction involving fewer intermediates is important for the biological properties of these compounds. Our group has been investigating the redox properties of some menaquinone systems and found distinctly different properties in organic solvents where the MK-derivatives are soluble (Koehn, Magallanes et al. 2018), compared to aqueous systems where the menaquinone will be interacting with a membrane or a model membrane system, such as a liposome (Jaworski, Leniewska et al. 1979).

The location of menaquinones in biological systems is associated with the membrane due to their hydrophobicity. These compounds have been presumed to reside inside the membrane; however, few studies have been done to investigate the specific interaction. Some computational studies have examined the association with the membrane because it is critical to understand the interaction for the electron transport action of menaquinones in bacterial systems (Gómez-Murcia, Torrecillas et al. 2016); however, less work has been done experimentally. A range of studies have been performed with ubiquinone derivatives, and evidence for the membrane association has been reported both in computational and experimental systems (Quinn and Esfahani 1980, Roche, Peretti et al. 2007, Kaurola, Sharma et al. 2016). On the other hand, significantly less work has been done with the menaquinone system, but so far, the reports support the presumptions often that the menaquinone is associated with the membrane.

Despite the polarity of the quinone group, these molecules are very hydrophobic, even though this property does vary with the length and the nature of the isoprene side group. We have recently found by synthesis of truncated MK-derivatives that only MK-1, MK-2, and MK-3, including derivatives with fully or partially saturated counterparts, are soluble in aqueous solution (Koehn, Crick et al. 2018, Koehn, Magallanes et al. 2018, Koehn, Beuning et al. 2019). This means that assays with MK-4, even though it is known as an enzyme substrate *in vivo*, may not demonstrate enzyme activity even if the aqueous assay includes surfactants (Upadhyay, Kumar et al. 2018). This experiment was attempted for MenJ, the membrane bound enzyme reported to stereospecifically hydrogenate the second isoprene unit of MK-9 in *Mycobacterium tuberculosis* and *Mycobacterium smegmatis*. The inability of the isolated enzyme to saturate MK-4 was attributed to the poor solubility of MK-4 in vitro since it was following the study that demonstrated in vivo activity. These experiments document the need for use of the truncated MK-derivatives

and caution the use of computational methods for evaluation of these systems. For example, the anticancer properties of MK-1 through MK-7 were investigated with a series of five cancer cell lines (Ishihara and Sakagami 2007). MK-1, MK-2, and MK-3 were shown to be cytotoxic, however, MK-4, MK-5, MK-6, and MK-7 did not exhibit any cytotoxic activity against any of the cell five cell lines. Based on the studies with MenJ, it seems likely that the anticancer effects of longer MK-derivatives are a consequence of the physical properties of these derivatives, and any correlations and conclusions regarding the measured activities are not based on the true cytotoxicity of these compounds, but a reflection of their hydrophobicity.

Due to the distinct hydrophobicity of menaquinones, assaying these substrates in vitro is often critical and/or convenient in biological studies. Since assays are often done in aqueous solution, this can cause problems if the substrates are menaquinones with longer isoprene side chains, because the longer naturally occurring MK-derivatives are often insoluble in aqueous solution. Contrary to common belief, the addition of surfactants in such assays is often insufficient to solubilize these compounds. The approach we have used to overcome this challenge is to synthesize water soluble, truncated MK-substrates (Siricilla, Mitachi et al. 2014). To this end, the small, truncated MK-derivatives, MK-1 through MK-3, are somewhat soluble in aqueous assays with added surfactants, which makes these MK-derivatives excellent substrates for biological studies. We have recently used this approach in studies of MenJ documenting the effectiveness of this approach (Kumar, Koehn et al. 2020).

4.1.2. Synthetic Strategy for the Preparation of Menaquinones

Contemplating the many synthetic strategies available, consideration of the structure and the application of the MK-derivatives may be important when choosing the appropriate method for synthesis. So far, our group has focused on the preparation of truncated MK-derivatives, where

the syntheses are relatively short and direct (Koehn, Crick et al. 2018, Koehn, Magallanes et al. 2018, Koehn, Beuning et al. 2019). Therein, we used Friedel-Crafts alkylation using $BF_3{\cdot}OEt_2$ as a Lewis acid catalyst. This use of electrophilic aromatic substitution is one of the most common across the literature for the synthesis of this family of compounds. This is most likely because it occurs over two steps from commercially available starting materials. For example, for our synthesis of MK-2, we begin by reducing menadione **1** with 10% $Na_2S_2O_4$ at room temperature for 30 min to produce menadiol **2** in ~84% yield (Figure 4.3) (Koehn, Magallanes et al. 2018). Then menadiol **2** underwent alkylation with commercially available geraniol in the presence of $BF_3{\cdot}OEt_2$, producing MK-2 in 20.1% yield. This approach may be direct, but it generally results in low yields (< 30%) and a mixture of isomers. Although biological studies do not require very much sample, consistently low yielding reactions are not suitable for multi-step syntheses at large scales, such as longer MK-derivatives where the key step is a Friedel-Crafts alkylation.

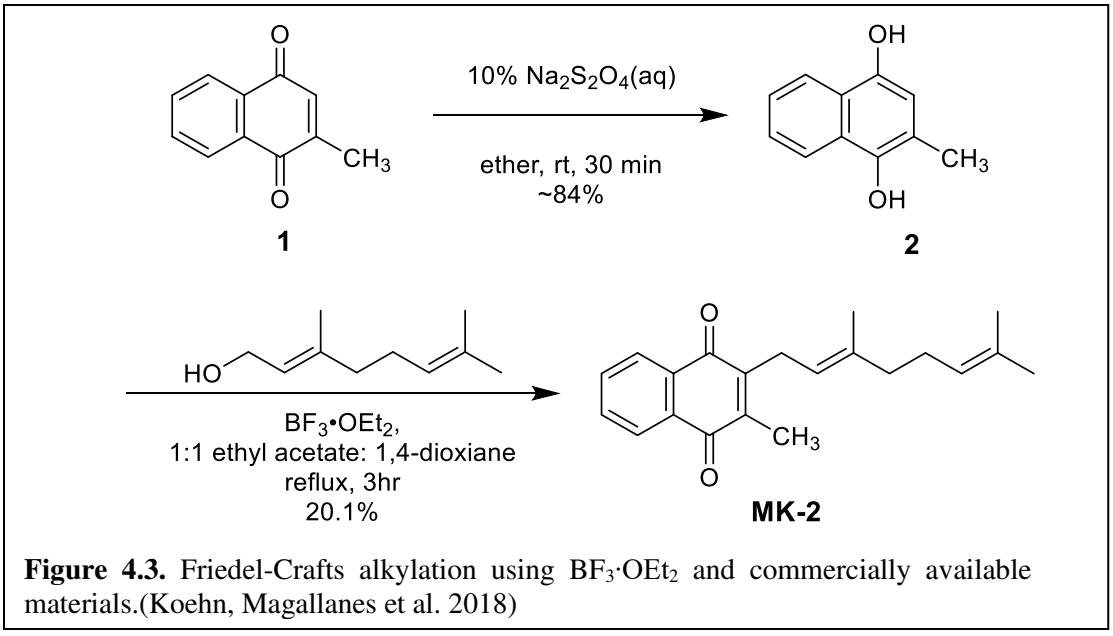

Figure 4.3. Friedel-Crafts alkylation using $BF_3{\cdot}OEt_2$ and commercially available materials.(Koehn, Magallanes et al. 2018)

Two reviews (Rüttimann , Daines, Payne et al.) have been published that focus on the synthesis of the biologically relevant vitamin K_1. In this review, we summarize the syntheses of MK-derivatives reported in recent history. This includes menaquinones of varying side chain

lengths, which include many types of vitamin K_2 derivatives, as well as vitamin K_1. This review will highlight the five most common synthetic strategies used for preparation of truncated and full-length MK-derivatives: nucleophilic ring methods, metal-mediated and radical reactions, electrophilic ring methods, pericyclic reactions, and side chain extensions (Figure 4.4). Each class

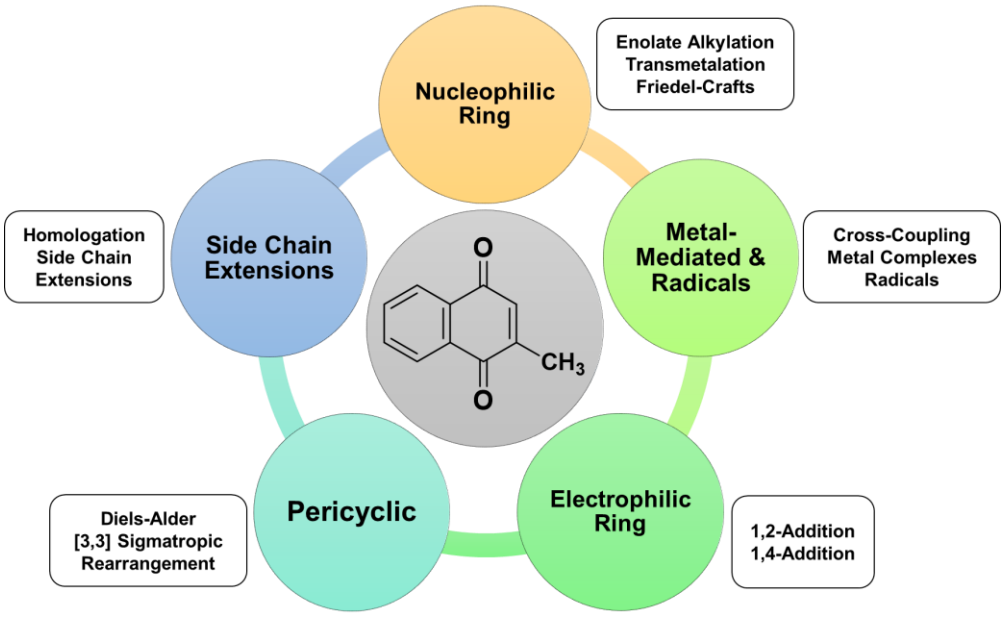

Figure 4.4. 5 Main synthetic strategies from across the literature for the synthesis of menaquinone derivatives.

of reactions will be summarized, identifying the advantages and disadvantages of each. This will allow an evaluation of each strategy based on the overall yields of the synthesis, regioselectivity, and the stereoretention of the first isoprene (α) unit from the ring. Other comparisons concerning the number of steps, competing side reactions, and safety will also be presented, which will result in a summary identifying the most attractive synthetic strategies from each category for preparation of this class of compounds.

4.2. Nucleophilic Ring Methods

4.2.1. Enolate Alkylation

In 1974, Snyder and Rapoport published a comprehensive report detailing their attempts to synthesize menaquinones (Snyder and Rapoport). The main goal of their syntheses was to retain the stereochemistry of α-isoprene double bond. The first approach used enolate chemistry to alkylate the C3 position of menadiol **2**. Beginning with menadiol **3a**, the potassium salt **4a** was formed using potassium hydride or potassium methoxide (Figure 4.5). It was suspected that

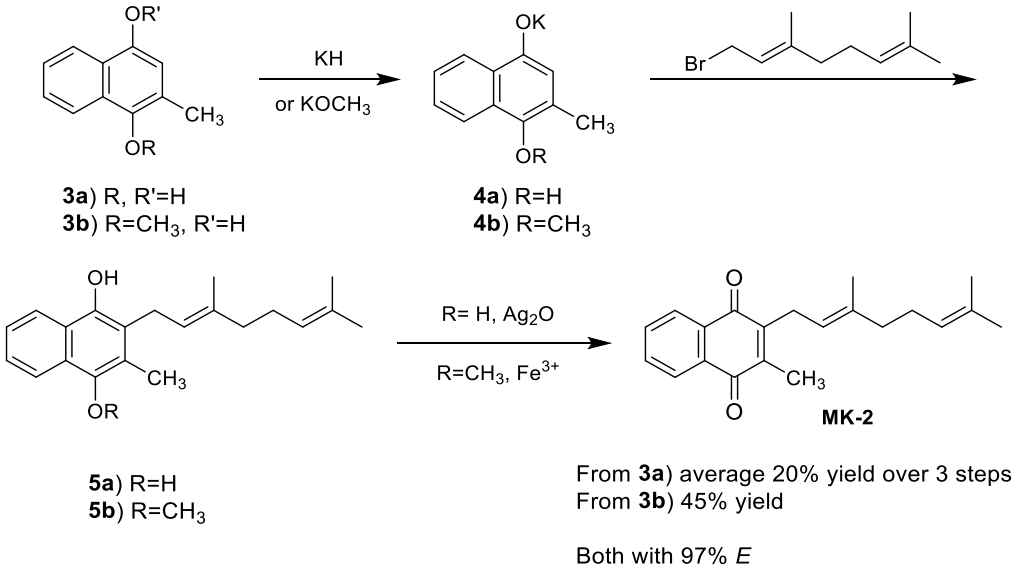

Figure 4.5. Synthesis of MK-2 via enolate alkylation (Snyder and Rapoport 1974)

Claisen alkylation had occurred, but upon further analysis it was concluded that the reaction proceeded via enolate alkylation to form **5a** with 97:3 *E/Z*. Oxidation of the ring in the presence of Ag_2O formed MK-2 in an average of 20% yield over three steps. The authors postulated the lower yield was due to competing Friedel-Crafts alkylation occurring on the C2 position. To prevent competition, the authors redeveloped the route using C1 methyl ether protected menadiol **3b**. Conversion of **3b** to MK-2 yielded 45% with 97% *E* alkene (Figure 4.5). Despite the improved yield, the synthesis of **3b** was more complicated than the authors originally thought. Therefore, this route was abandoned for one with more accessible starting materials.

A few years later, Tabushi et al. published on the allylation of naphthoquinones using β-cyclodextrin as an inclusion catalyst, especially for synthesis of vitamin K_1 (Tabushi, Fujita et al. , Tabushi, Yamamura et al.). Menadiol **2** was alkylated at the C3 position in mild basic conditions, borate buffer (pH 9), with and without β-cyclodextrin (Figure 4.6a). The yields of MK-1 were found to be 40% and 15%, respectively, showing a significant decrease in yield without β-cyclodextrin. The only byproduct observed was menadione **1** in 49% and 28% yield, respectively.

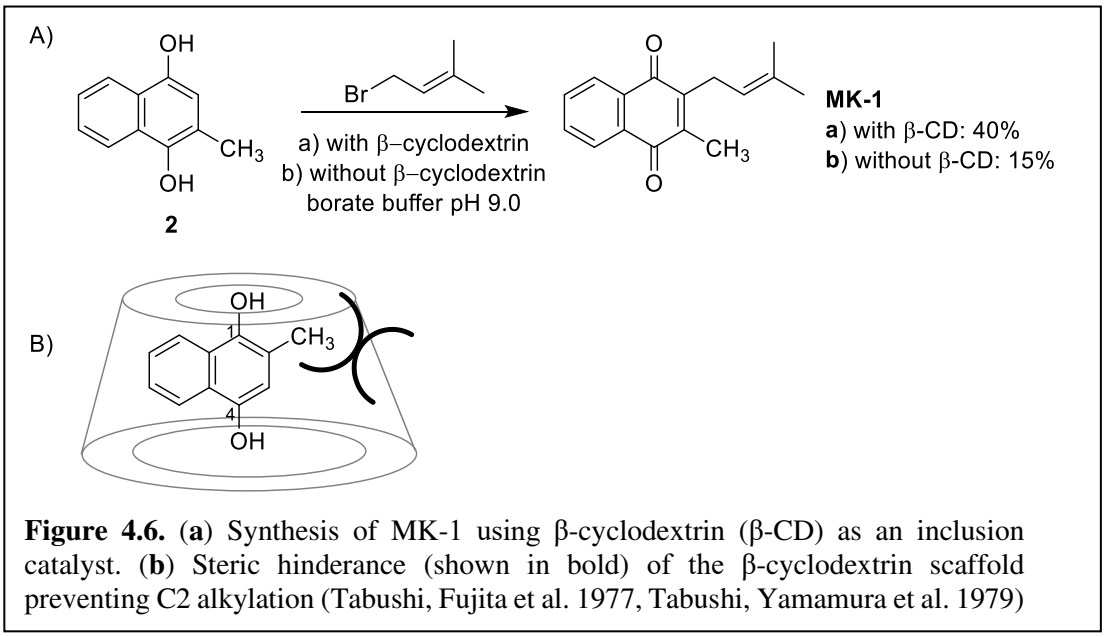

Figure 4.6. (**a**) Synthesis of MK-1 using β-cyclodextrin (β-CD) as an inclusion catalyst. (**b**) Steric hinderance (shown in bold) of the β-cyclodextrin scaffold preventing C2 alkylation (Tabushi, Fujita et al. 1977, Tabushi, Yamamura et al. 1979)

The results strongly indicate that β-cyclodextrin played a significant role catalyzing this reaction. The authors noted the selectivity of the alkylation behaved as if it were a ligase and or oxidase. Due to the semi-conical structure of β-cyclodextrin, menadiol is surrounded by the hydrophobic cavity. The C1 and C4 hydroxy groups interact with the hydrophilic exterior (Figure 4.6b). The C1 hydroxy group hypothesized to be hydrogen bonding on the narrower end of the scaffold. The hydrogen bonding interactions were found to lower the pKa of the opposite hydroxy group at the C4 position. Unbound menadiol has a pKa of 9.45, and bound menadiol was calculated to have a pKa of ~8.90 (Tabushi, Yamamura et al.). The decrease in pKa was said to enhance the nucleophilicity of the partially charged carbanion on the C3 position. Deprotonation of the C4

hydroxy group in pH 9 medium created a more nucleophilic enolate, alkylating at the C3 position. The authors did not observe any C2-alkylated product in their trials. They postulated the sterically hindered, semi-conical shape of the β-cyclodextrin scaffold prevented C2 alkylation (Figure 4.6b). Menadione **1** was the only other product formed. In both trials, **1** was produced in higher yields than MK-1. In protic solvents, menadiol **2** will spontaneously oxidize to form menadione **1**. In the presence of an enzyme-like cavity of β-cyclodextrin, the transformation was most likely accelerated in the buffer solution. Although menadione **1** was formed in higher yields, it can be recovered and recycled for subsequent use.

4.2. Transmetalation

After marginal success with enolate alkylations, Snyder and Rapoport shifted their focus towards more direct nucleophilic methods (Snyder and Rapoport). Bismethyl ether 2-bromomenadiol **6** was transformed into 2-metallo derivatives using lithium, magnesium, and copper to react with a variety of electrophiles (Figure 4.7). The authors were originally interested in using aldehydes as electrophiles; however, their attempts were unsuccessful. Removal of the

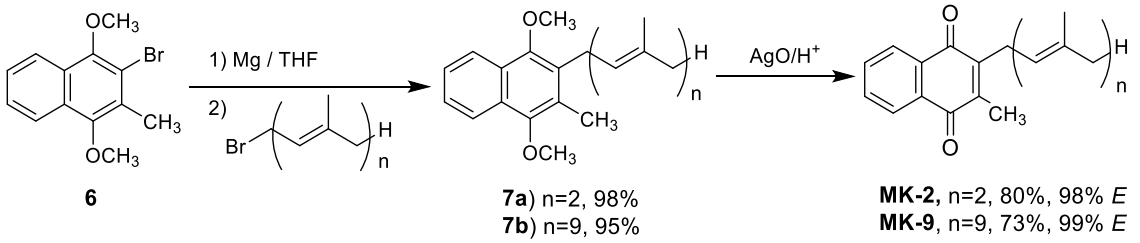

Figure 4.7. Synthesis of MK-2 and MK-9 using Grignard reagents (Snyder and Rapoport 1974).

resultant benzyl alcohol led to the formation of a vinyl alkene or isomerization of the α-isoprene double bond. To avoid this, prenyl halide substrates were used instead. Preliminary reactions were performed to assess the stereoretention of the α-isoprene double bond for each 2-metallo derivative. All three 2-metallo derivatives left the α-isoprene double bond virtually unaffected. Organolithium yields were 10% and 65% for geranyl chloride and bromide, respectively, leading

to the exclusive use of prenyl bromide electrophiles. Lithium organocuprate and organocuprate yields were 74% and 82%, respectively. The Grignard reagent was formed in 92% yield. Snyder and Rapoport continued their studies using the Grignard reagent.

To examine the utility of this method, the authors synthesized MK-2 and MK-9 (Figure 4.7). The Grignard reagent was produced by stirring **6** with Mg turnings in dry THF. Geranyl bromide and solanesyl bromide were added to the solution, resulting in the respective alkylated products, **7a** and **7b**. Removal of the bismethyl ethers and oxidation of the ring were achieved with AgO in acidic conditions yielding 80% and 73% for MK-2 and MK-9, respectively. Both products retained the stereochemistry of the α-isoprene double bond, each with ≥ 98% *E* alkene.

Unlike Snyder and Rapoport, Saá and coworkers were successful using aldehydes as electrophiles in the early 1990s. This challenge was overcome with the use of stereocontrolled Birch hydrogenolysis conditions (BIHY) to selectively remove silyl ether protected *(E)*- or *(Z)*-α-alkenylbenzyl alcohols (Ballester, Saá et al. , Ballester, Capo et al. , Garcias, Ballester et al.). The authors applied this method towards the synthesis of MK-2 and MK-4 (Figure 4.8). Using the same starting material as Snyder and Rapoport, bismethyl ether 2-bromomenadiol **6** underwent lithium-bromide exchange to form the organolithium reagent. Commercially available aldehydes, citral **8a** (68:32 *E/Z*) and geranylgeranial **8b** (≥ 95% *E*), were used without further purification to assess the stereoretentive abilities of BIHY conditions. Upon nucleophilic attack, the resultant benzylic alcohols **9a** and **9b** were formed in ~65% and 58% yield, respectively. The alcohols were protected with TMSCl in the presence of HMDS, as used in previous reports (Ballester, Saá et al. 1990, Ballester, Capo et al. 1993). In the literature, the authors used the abbreviation “HMDSZ” instead of “HMDS”, which is now a more commonly used abbreviation. The protected alcohol was then

reduced in the presence of lithium metal and liquid ammonia to produce the free methylene **10**. With this method, the resulting stereochemistry of **10a** and **10b** α-isoprene double bonds were

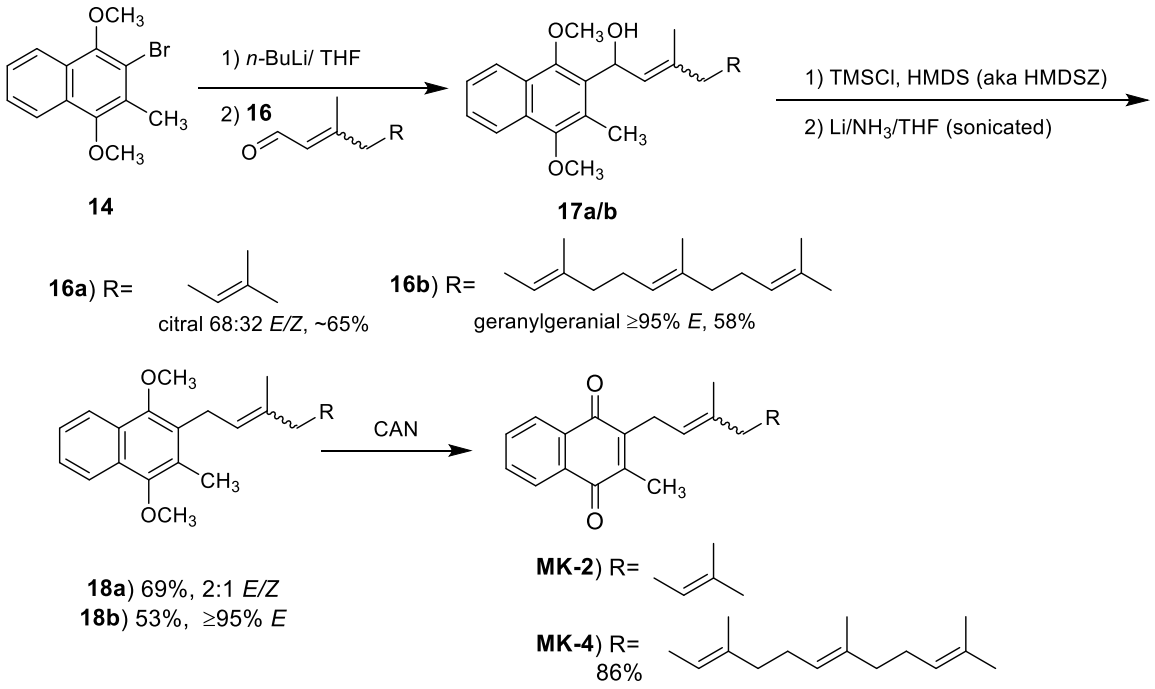

Figure 4.8. Synthesis of MK-2 and MK-4 using BIHY conditions (Ballester, Saá et al. , Ballester, Capo et al. , Garcias, Ballester et al.).

determined to be 2:1 *E/Z* and ≥95% *E* alkene, respectively. These results reflect the stereochemistry of the aldehyde precursors and demonstrate the remarkable stereoretention of BIHY. The methyl ether protecting groups were removed using CAN to produce MK-2 and MK-4. Only the reported yield was for MK-4 in 86%.

Further improvement upon the strategies established by Snyder and Rapoport was reported by Swenton and coworkers in 1977 (Raynolds, Manning et al.). Therein, preliminary results were published using electrolysis to protect bismethyl 2-bromomenadiol **6** as bismethyl ketals. The authors used lithium organocuprate nucleophiles instead of Grignard reagents. In 1980, the authors published a complete study towards the synthesis of menaquinones (Chenard, Manning et al.). Bismethyl ether 2-bromomenadiol **6** underwent electrolysis in a divided cell with 2% KOH and methanol, producing bisketal **11** (Figure 4.9). Lithium-bromide exchange in THF and subsequent transmetalation with cuprous iodide produced the desired lithium organocuprate dimer **12**. The corresponding electrophiles, prenyl bromide **13a** and geranyl bromide **13b**, were added to the solution and immediately carried forward to hydrolysis without purification. MK-1 and MK-2 were formed in 92% and 96% yield, respectively. The authors did not observe any evidence of the *Z* isomer in NMR; however, its absence could not be concluded.

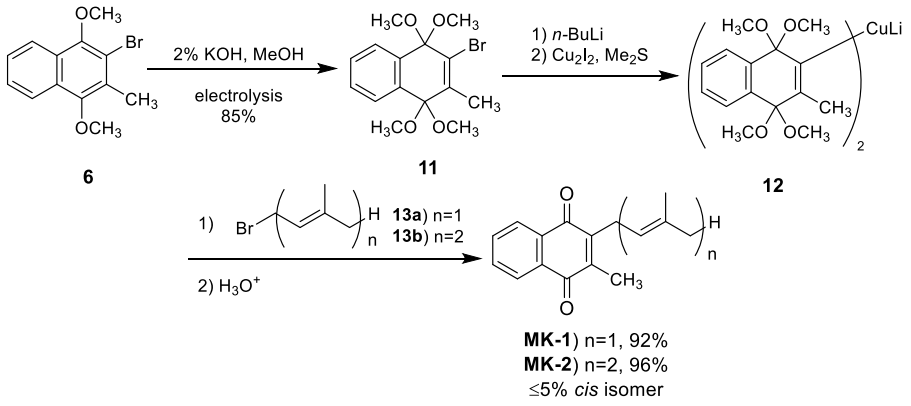

Figure 4.9. Synthesis of MK-1 and MK-2 featuring electrolysis as a protection method (Raynolds, Manning et al. , Chenard, Manning et al.).

4.2.3. Friedel-Crafts Alkylation

Throughout all the strategies described in this report, the Friedel-Crafts alkylation is by far the most popular across the literature. The most common Lewis acid catalyst used for this specific transformation is $BF_3{\cdot}OEt_2$, which became popular after Lindlar's 1953 patent detailing its

usage(Lindlar). Two more reports of its use specifically towards the synthesis of vitamin K_1 were published in the following year. First, Isler and Doebel detailed the synthesis of vitamin K_1 and various other racemic derivatives (Isler and Doebel). Second, Hirschmann et al. reported the comparison of different Lewis and Brønsted-Lowry acid catalysts towards the synthesis of vitamin K_1 (Hirschmann, Miller et al.) in an effort to improve upon existing reported methods at the time (Klose and Almquist , Almquist and Klose 1939, Binkley, Cheney et al. 1939, Fieser 1939, Fieser, Campbell et al. 1939, Fieser, Campbell et al. 1939, Isler). Most notably among those methods, Fieser reported the condensation of menadiol and phytol in the presence of oxalic acid with overall yields of 25–30% (Fieser). Much of the yield was lost to undesired side products, such as phytadiene and the C2-alkylated product (Tishler, Fieser et al.). Many of the early reports do not use protecting groups or other functional handles to induce regioselectivity.

To address the regioselectivity challenge, Hirschmann et al. designed monoacetate **14** to influence C3 alkylation (Figure 4.10). Monoacetate **14** underwent condensation with phytol in the presence of an acid catalyst to form alkylated product **15**. Potassium acid sulfate, oxalic acid,

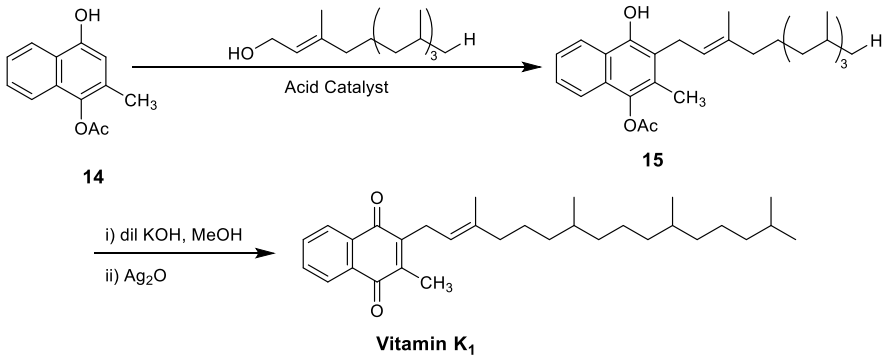

Figure 4.10. Synthesis of vitamin K_1 using Friedel-Crafts alkylation with different acid catalysts (Hirschmann, Miller et al.).

Duolite C-60 cation exchange resin, and $BF_3{\cdot}OEt_2$ produced varied results, as outlined in Table 4.1. Removal of the acetate protecting group was achieved using Claisen alkali conditions (dilute KOH in methanol), and oxidation with Ag_2O work up formed vitamin K_1.

Table 4.1. Yields for different acid catalysts used in the synthesis of vitamin K_1 (Hirschmann, Miller et al.).

Acid Catalyst	% Yield[1]
$KHSO_4$	55%
Oxalic Acid	N/A[2]
Duolite C-60	8%
$BF_3{\cdot}OEt_2$	66.5%

[1.] Over two steps. [2.] No yield reported.

In 1990, Schmid et al. published a comprehensive report on the synthesis and analysis of all four stereoisomers of (*E*)-vitamin K_1 (Schmid, Antoulas et al. 1990). The synthesis of the naturally occurring stereoisomer showcased a unique transformation using $BF_3{\cdot}OEt_2$ as the catalyst (Figure 4.11). Starting with monoacetate **14**, the free phenol was alkylated with phytyl chloride **16** and potassium carbonate in 79–87% yield with 99.5% *E* alkene. In the presence of $BF_3{\cdot}OEt_2$, the

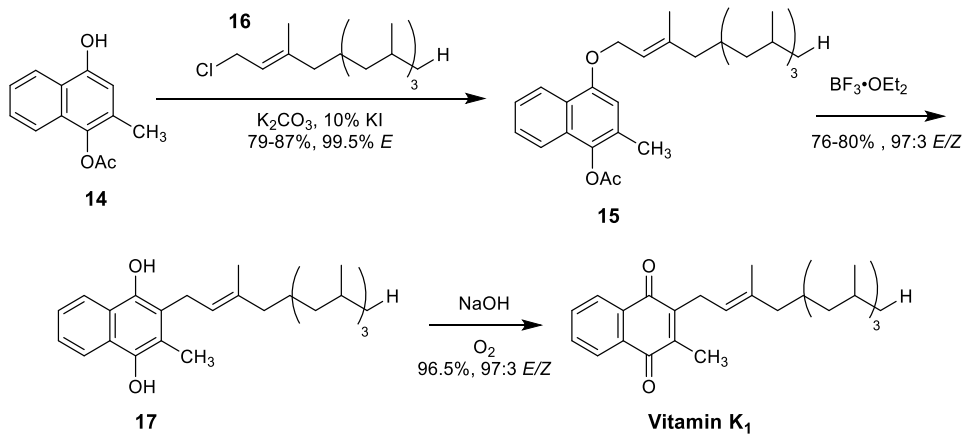

Figure 4.11. Synthesis of vitamin K_1 featuring an intramolecular Friedel-Crafts alkylation (Schmid, Antoulas et al. 1990).

O-alkylated product **15** was thought to have undergone a Claisen rearrangement to form C-alkylated product **17**, but upon further analysis, the reaction was determined to proceed via and intramolecular Friedel-Crafts mechanism. The C-alkylated product **17** was formed in 76–80%

yield and the *E/Z* ratio was found to be 97:3. This kind of intramolecular transformation was first reported by Yoshizawa et al. in 1982 on ubiquinone derivatives (Yoshizawa, Toyofuku et al. 1982). Removal of the acetyl group in basic conditions produced vitamin K_1 in 96.5% yield based on HPLC. The *E/Z* ratio of the α-isoprene double bond was determined to be 97:3, unchanged from the previous step. In 2003, the authors of a vitamin K_1 syntheses review (Daines, Payne et al.) commented that this route has received little attention.

Allyl alcohols have a reputation for being intrinsically unstable towards alcohol rearrangement. To circumvent this issue, Min et al. used prenyl chlorides instead (Min, Lee et al.). Menadiol dimethyl ether **18** was reacted with prenyl chloride **19** in presence of $BF_3{\cdot}OEt_2$ to form sulfonyl intermediate **20** (Figures 4.12). Truncated prenyl chain **19** allowed for further

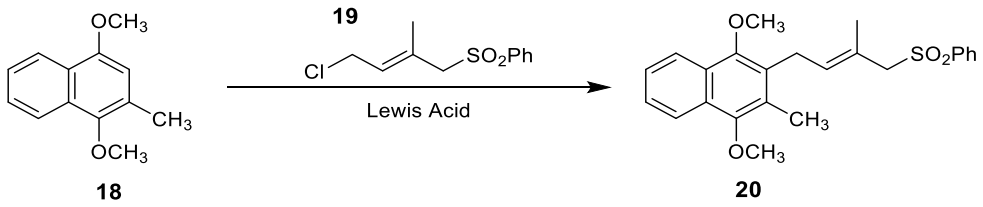

Figure 4.12. Synthesis of truncated MK-derivatives using Friedel-Crafts alkylation (Min, Lee et al. 2003)

functionalization of the side chain to make more diverse analogs, which will be discussed in detail later in Section 6.2. The authors assessed the efficacy of a large scope of Lewis acids, which are summarized in Table 4.2. Based on these results, $AlCl_3$ performed the best with 72% yield and all *E* configuration of the α-isoprene double bonds.

Table 4.2. Friedel-Crafts alkylation of **18** with sulfonyl **19** to form **20** (Min, Lee et al.).

Lewis Acid[1]	% of 20 (*E/Z*)
$BF_3{\cdot}OEt_2$	0 (-)
$MgBr_2$	0 (-)
$TiCl_4$	-[2](-)
$FeCl_3$	55 (4:1)
Et_2AlCl	56 (7:1)
$SnCl_4$	56 (*E*)
$ZnBr_2$	60 (7:1)
$ZnCl_2$	67 (7:1)
$AlCl_3$	72 (E)

1.2 equiv of Lewis acid was used. [2.] Decomposition of the starting materials was observed.

Despite the historical popularity of $BF_3{\cdot}OEt_2$, the competition between C2/C3 alkylation continued to be a persistent challenge. Various types of protecting groups have been used to prevent competition with varying success. Due to competing side reactions, its use in industrial applications has been accused of being wasteful, inspiring researchers to identify new, more sustainable Lewis acids to minimize byproducts and maximize yield. Coman et al. developed a new class of heterogenous, partly hydroxylated magnesium and aluminum fluorides to address such concerns (Coman, Parvulescu et al.). The authors predict that this class of catalysts will replace homogenous $BF_3{\cdot}OEt_2$ in industrial applications. Vitamin K_1 was synthesized to illustrate this concept starting with menadiol **2** and isophytol **21** (Figure 4.13). The reactions resulted in 100% conversion of the starting material with each catalyst. The yields were low and showed considerable formation of byproducts, mainly chromanol and C2-alkylated product, as shown in

Table 4.3. The catalyst, MgF_2-57 provided the best results with respect to vitamin K_1, yielding 26.5%, which is comparable to $BF_3 \cdot OEt_2$.

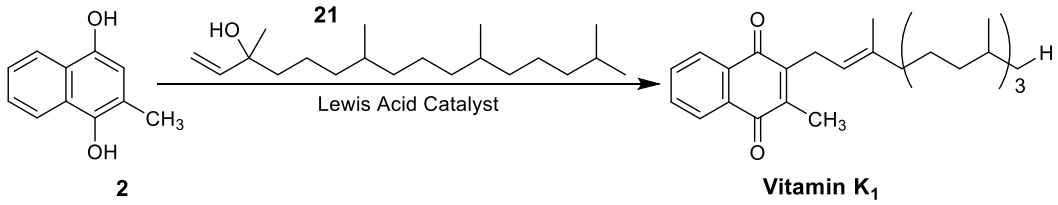

Figure 4.13. Synthesis of vitamin K_1 using partly hydroxylated magnesium and aluminum fluorides (Coman, Parvulescu et al.).

Table 4.3. The catalytic results in the synthesis of vitamin K_1, K_1-chromanol, and C2-alkylated product from menadiol (Coman, Parvulescu et al.).

Catalyst	% of Vitamin K_1	% of K_1 chromanol	% of C2 product
MgF_2-40	21.2	5.9	58.8
MgF_2-57	26.5	21.0	43.7
MgF_2-71	15.6	20.8	52.9
MgF_2-87[1]	0	0	0
AlF_2-50	7.6	42	41.2

[1.] 0% conversion.

Recently, we synthesized fully and partially saturated MK-derivatives in an effort to understand their structural and electrochemical properties in model membranes (Koehn, Crick et al. , Koehn, Magallanes et al. 2018, Koehn, Beuning et al.). For the synthesis of MK-2(II-H_2), the condensation of isophytol **22** and menadiol **2** was accomplished in 11% yield using MgF_2-48, a Coman et al. inspired catalyst (Figure 4.14). Before purification, the crude yield was determined to be 60%, consisting of regio- and stereoisomers. The regioisomers separated readily via column

chromatography; however, the E/Z isomers of the C3-product required thorough purification using preparative TLC. Therefore, these stereoisomers are purified on demand for the biological studies.

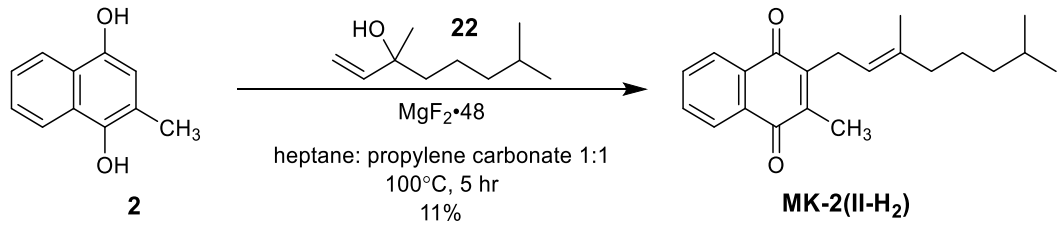

Figure 4.14. Synthesis of MK-2(II-H_2) using using MgF_2-48 as a catalyst (Koehn, Crick et al. 2018)

4.2.4. Summary

The three main nucleophilic ring methods throughout the literature include enolate alkylation, transmetalation of bromonaphthoquinone derivatives, and Friedel-Crafts alkylation. The advantages and disadvantages of each have been outlined in Table 4.4. Out of all nine methods presented, only three of them reported overall yields greater than 80%. These methods were Snyder and Rapoport's aryl-Grignard reaction with prenyl bromides, Swenton and coworker's use of electrolytically protected lithium organocuprate, and Schmid et al.'s unique intramolecular Friedel-Crafts alkylation. The first two methods also demonstrated exemplary regiocontrol due to lithium-bromide exchange with bismethyl ether 2-bromomenadiol **6**. The other methods produced regioisomers owing to prominent competition between C2 and C3 alkylation. Many methods did not utilize protecting groups or directing group manipulations to influence regiocontrol. For most of these methods, the chosen electrophiles were prenyl halides, which left the α-isoprene double bond virtually undisturbed. However, in the case of Tabushi et al., the authors only synthesized MK-1; therefore, the stereochemical implications of the method were not addressed.

Table 4.4. Summary of nucleophilic ring methods.

Methods	Advantages	Disadvantages
Section 2.1. Enolate Alkylations		
Snyder and Rapoport Enolate Alkylation (Snyder and Rapoport 1974)	-Stereoretention of α-isoprene double bond (97% *E*-alkene) -3 step synthesis (not including starting material)	-Low yields (20–45%) -C2 alkylation competition via Friedel-Crafts alkylation -Unviable synthesis of starting material
Tabushi et al. β-cyclodextrin inclusion catalyst (Tabushi, Fujita et al. 1977, Tabushi, Yamamura et al. 1979)	-Regiocontrol via sterically hindered nature of β-cyclodextrin -Menadione is the only byproduct -1 step synthesis	-Low yields (40% with inclusion catalyst) -Competition between C3 alkylation and C3 protonation -Only synthesized MK-1
Section 2.2. Transmetalations		
Snyder and Rapoport Grignard reaction (Snyder and Rapoport 1974)	-Regiocontrol through lithium-bromide exchange -Stereoretention of the α-isoprene double bond (≥ 95%) -Alkylation step is high yielding (> 95%) -3 step synthesis (not including starting material)	-Need to prepare starting material 6

Table 4.4. *Cont.*

Saá and coworkers BIHY Reduction (Ballester, Saá et al. 1990, Ballester, Capo et al. 1993, Garcias, Ballester et al. 1994)	-Stereoretention of the α-isoprene double bond during BIHY reduction	-Moderate yields for nucleophilic addition (58–65%) and BIHY reduction(53–70%) -5 step synthesis (not including starting material)
Swenton and coworkers Electrolysis & Lithium Organocuprate (Raynolds, Manning et al. 1977, Chenard, Manning et al. 1980)	-Unique use of electrolysis as a protection method -High yields for all reported steps (≥ 85%) -Regiocontrol through lithium bromide exchange -Stereoretention of α-isoprene double bond (< 5% *Z*-alkene estimated) -Deprotection of bisketals to menaquinone ring structure via hydrolysis, no oxidation required	-Lithium organocuprate nucleophile only used one of two bisketal rings—poor atom economy -Difficult purification because of unreacted starting materials -5-step synthesis (not including starting material)
2.3. Friedel-Crafts Alkylation		
Hirschmann et al. Friedel-Crafts Alkylation Lewis Acid Analysis (Hirschmann, Miller et al. 1954)	-Favors C3 alkylation over C2 due to monoacetate **14** -Avoided formation of undesired byproducts (phytadiene and chromanol) -Monoacetate **14** was the only recoverable byproduct	-Low to moderate yields (8–66.5%) depending on acid catalyst used (Table 4.1) -Stereoretention of the α-isoprene double bond was not discussed

	-2 step synthesis (not including starting material)	
Schmid et al. Intramolecular Friedel-Crafts (Schmid, Antoulas et al. 1990)	-Features unique intramolecular Friedel-Crafts alkylation at C3 position -High yields (76–96.5%) throughout all steps -Stereoretention of α-isoprene double bond -3 step synthesis (not including starting material)	-Need to prepare starting material **22**
Min et al. Friedel-Crafts Alkylation Lewis Acid Analysis (Min, Lee et al. 2003)	-Stereoretention of α-isoprene double bond with $AlCl_3$ -Produced a functional handle for chain extension methods -1 step synthesis (not including starting material)	-Low to moderate yields (0–72%) depending on Lewis acid used
Coman et al. (Coman, Parvulescu et al. 2010) and Koehn et al. (Koehn, Crick et al. 2018) Heterogenous Lewis Acid Catalysts	-Predicted industrial benefit to replace $BF_3{\cdot}OEt_2$ -Performed without protecting groups, but could benefit from them -1 step synthesis (not including starting material)	-Universally low yields (0–26.5%) -Poor regiocontrol to prevent C2 alkylation -Difficult purification -Synthesis of partly hydroxylated metal fluorides requires the use of dangerous aqueous HF (Wuttke, Coman et al. , Scholz, Stosiek et al.)

4.3. Metal-Mediated and Radical Reactions

4.3.1. Cross-Coupling

After the incorporation of transmetalation, synthetic efforts were shifted to investigate cross-coupling reactions. In 1973, Sato et al. used π-allylnickel chemistry to synthesize vitamin K_1 and MK-9 after initial success with MK-1 (Sato, Inoue et al.). For this method, π-allylnickel complexes **24** and **28** were formed in situ using allyl bromides **23** and **27** with $Ni(CO)_4$ (Figures 4.15A and 4.16A). Vitamin K_1 was synthesized from diacetate **25** and π-allyl complex **24** in MPD at 50 °C for 5 h to form the expected alkylated product **26** in 75% yield (Figure 4.15B). The acetate protecting groups were removed in mild basic conditions, and the oxidation was achieved using

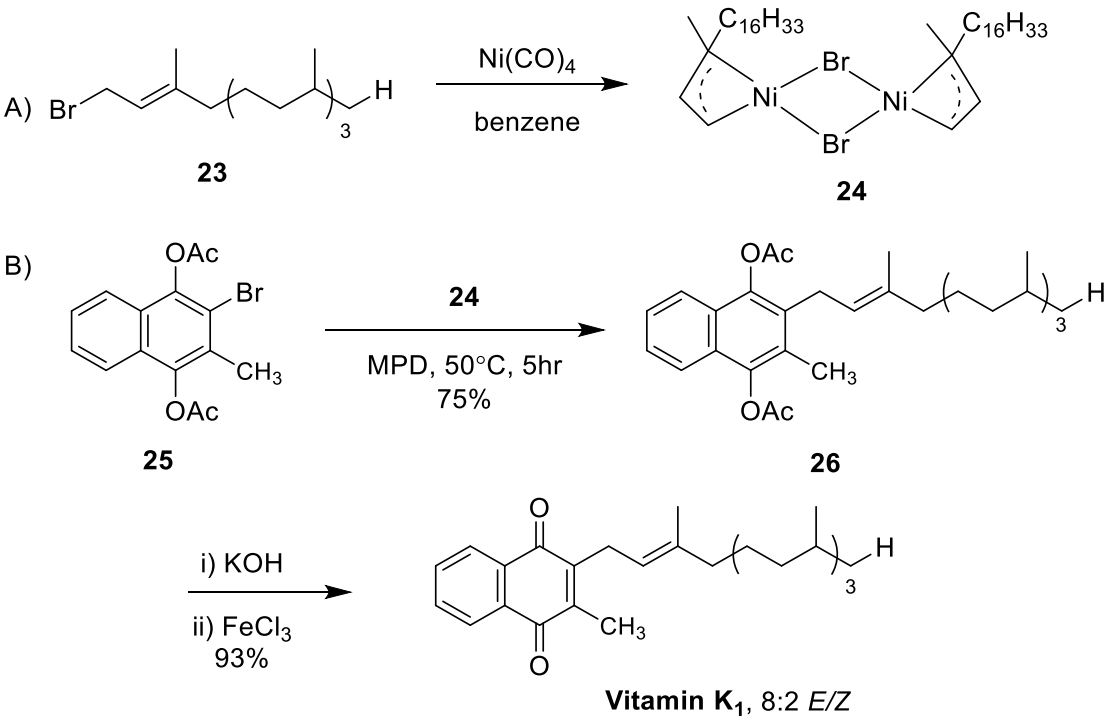

Figure 4.15. (**A**) Formation of π-allylnickel complex. (**B**) Synthesis of vitamin K_1 using π-allylnickel cross-coupling (Sato, Inoue et al.).

$FeCl_3$, producing vitamin K_1 in 93% over two steps. The observed *E/Z* ratio was 8:2 with respect to the α-isoprene double bond. For MK-9, the same starting material diacetate **25** and π-allyl complex **28** were heated to 50 °C for 16 h to form alkylated product **29** in 52% yield (Figure

4.16A). MK-9 was produced in 85% yield and 7:3 *E/Z* using the same methods of deprotection and oxidation (Figure 4.16B).

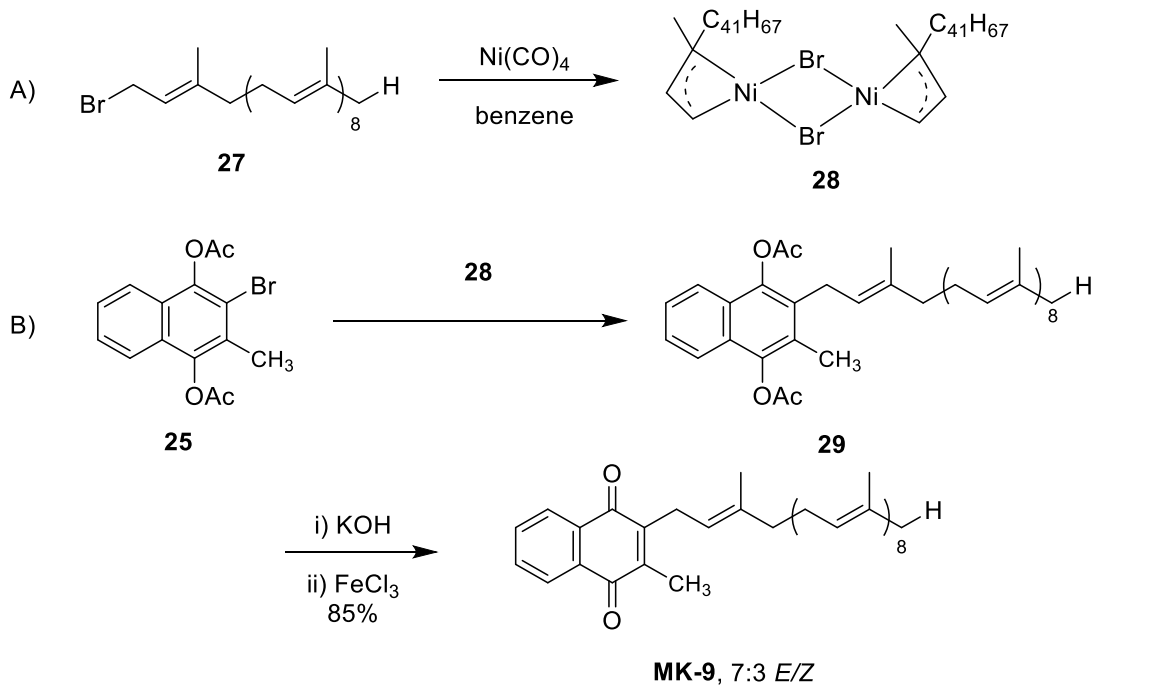

Figure 4.16. (**A**) Formation of π-allylnickel complex. (**B**) Synthesis of MK-9 using π-allylnickel cross-coupling (Sato, Inoue et al.).

Stille et al. published the synthesis of vitamin K_1 using trimethylstannane derivatives to cross couple phytyl bromide in 1983 (Godschalx and Stille). 2-Bromomenadiol **30** was protected with TBSCl in 95% yield (Figure 4.17). Lithiation with *t*-BuLi and transmetalation with trimethyltin chloride formed **31** in 77% yield over two steps. Phytyl bromide was then coupled with **31** in the presence of $ZnCl_2$ forming **32**. PCC was used to deprotect and oxidize the ring to form vitamin K_1 in 40% yield over two steps.

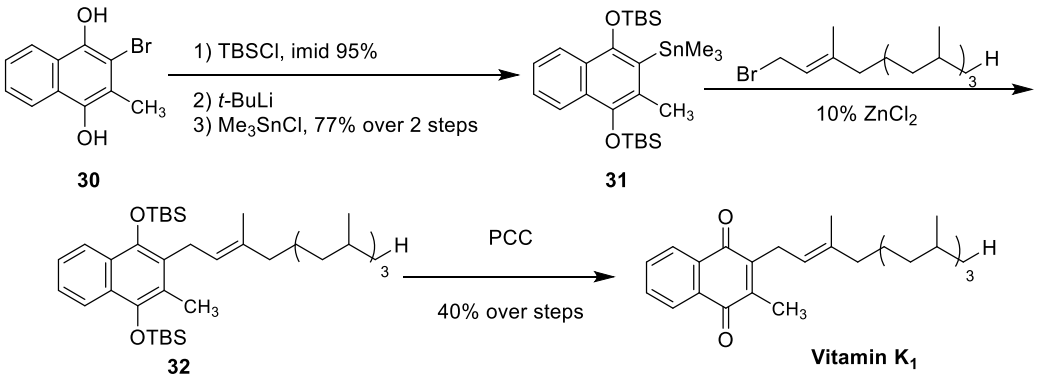

Figure 4.17. Synthesis of vitamin K_1 using Stille organostannane chemistry (Godschalx and Stille).

In 1990, Liebeskind and Foster discovered an unexpected transformation that appeared useful towards the synthesis of MK-derivatives (Liebeskind and Foster), which was previously mentioned in a review of syntheses of vitamin K and analogs (Daines, Payne et al. 2003). MK-1 was synthesized using ring-strained dione **33** and propyne, forming alcohol **34** (Figure 4.18). Then

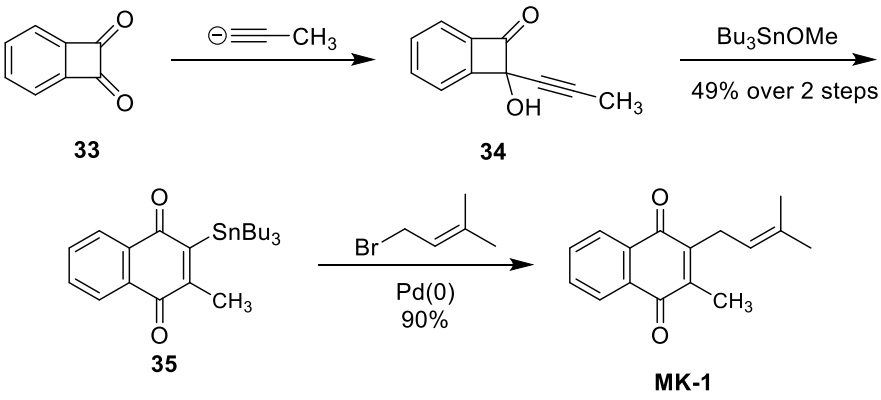

Figure 4.18. Synthesis of MK-1 featuring Liebeskind-Moore rearrangement to ring expansion (Liebeskind and Foster).

alcohol **34** underwent a Liebeskind-Moore rearrangement in the presence of Bu_3SnOMe to form the stannylated product **35** in 49% over two steps. From there, MK-1 was synthesized in 90% yield using Stille cross-coupling conditions with Pd(0) and prenyl bromide.

4.3.2. . Coordination Complex

An intriguing approach to the synthesis of MK-derivatives was developed by Dötz et al. in 1986. Using pentacarbonyl(methoxyphenylcarbene)chromium(0) complex **36** and an alkyne (Figure 4. 19), the quinone ring was formed via carbonylation (Dötz, Pruskil et al. 1982, Dötz 1984, Rüttimann 1986). This approach provided access to several different naphthoquinone derivatives using functionalized alkynes. The authors synthesized vitamin K_1 and MK-1 through MK-3 to illustrate this transformation. Phenyllithium reacted with one of the carbonyl ligands

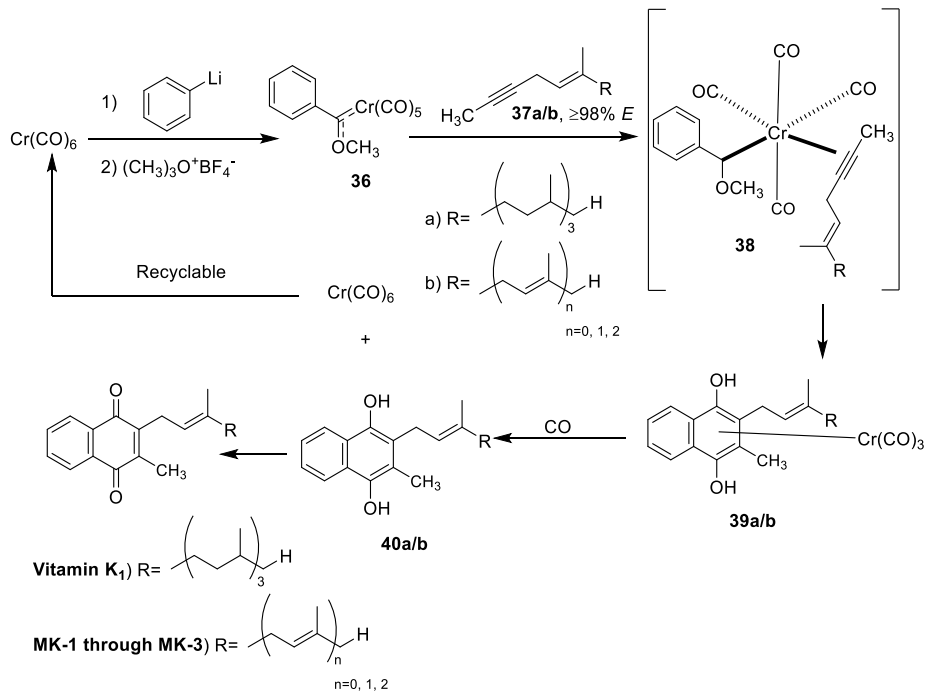

Figure 4.19. Synthesis of MK-derivatives using unique $Cr(CO)_6$ mediated ring formation (Liebeskind, Baysdon et al. , Dötz, Pruskil et al. 1982, Dötz 1984, Liebeskind, Baysdon et al. , Rüttimann 1986).

(CO) on $Cr(CO)_6$, and then was methylated by trimethyloxonium tetrafluoroborate to form complex **36**. Vitamin K_1 and MK-1 through MK-3 were formed by using alkynes **37a** or **37b**, respectively. Upon addition, the alkyne displaced another molecule of CO, to form intermediate complex **38**. The resulting menadiol ring **39a/b** was coordinated to $Cr(CO)_3$. To make this route more sustainable, the authors determined $Cr(CO)_6$ could be regenerated by pressurizing the system

with CO to displace $Cr(CO)_3$ and liberate the alkylated product **40a/b**. Oxidation with standard oxidizing agents afforded the menaquinone products accordingly. The yields of each reaction were not reported in Rüttimann's 1986 review (Rüttimann).

In 1980, Liebeskind et al. designed a synthesis of naphthoquinones using bis(triphenylphosphine)phthaloylcobalt complex 41 (Figure 4.20A). Ring formation was achieved upon addition of an alkyne in the presence of $AgBF_4$ (Liebeskind, Baysdon et al.). In 1986, an update was published wherein the authors describe an improved cobalt complex to increase the yield of the reaction and minimize the amount of AgBF4 required (Liebeskind, Baysdon et al.). The updated complex 42 replaced the triphenylphosphine ligands with pyridine and dimethylglyoxime (Figure 4.20B).

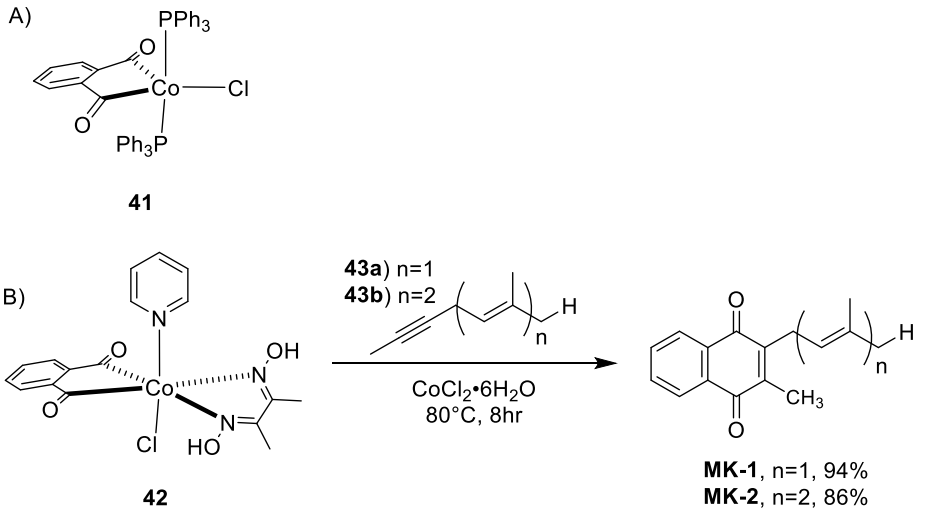

Figure 4.20. (**A**) Original cobalt complex synthesized by Liebeskind et al. for this transformation. (**B**) Synthesis of MK-1 and MK-2 using the updated catalyst (Liebeskind, Baysdon et al. 1980, Liebeskind, Baysdon et al. 1986)

This new complex was more tolerant towards different Lewis acids as well as hydrated salts, which was demonstrated by the formation of **44** using complex **42**, as shown in Table 4.5. MK-1 and MK-2 were synthesized using alkynes **43a** and **43b**, cobalt complex **42** and Lewis acid

in the form of $CoCl_2 \cdot 6H_2O$ at 80 °C producing MK-1 and MK-2 in 94% and 86% yield, respectively.

Table 4.5. Effects of Additives on 2,3-diethyl-1,4-naphthoquinone **44** formation at 80 °C (Liebeskind, Baysdon et al.).

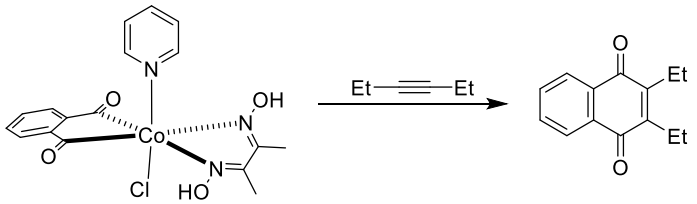

42 **44**

Additive	**GC Yield % of 44**		
(1 equiv)	**2 hr**	**5 hr**	**18 hr**
None	25	52	77
$AgBF_4$	80	82	-
$BF_3 \cdot OEt_2$	74	79	82
$SnCl_2$	41	39	70
$CoCl_2 \cdot 6H_2O$	59	83	91
$CoCl_2$(anhyd)	61	86	86
p-CH_3PhSO_3H	14	31	76
CH_3CO_2H	23	47	74

4.3.3. Radical Reactions

4.3.3.1. Metal-Mediated Radical Reactions

In 1972, Jacobsen and Torssell reported the use of allyl radicals produced via decarboxylation of carboxylic acids to alkylate quinones. Upon mixing silver nitrate and ammonium peroxodisulfite, Ag^+ and $S_2O_8^2$ produce the radical, Ag^{2+} as shown in Equation (1). Then Ag^{2+} abstracts an electron from the carboxylic acid to produce CO_2 and a radical species **R**

as shown in Equation (2) (Jacobsen and Torssell). The authors were concerned about possible

$$Ag^{+} + S_2O_8^{2-} \rightarrow Ag^{2+} + SO_4^{\cdot -} + SO_4^{2-} \quad (1)$$

$$Ag^{2+} + RCOOH \rightarrow R^{\cdot} + CO_2 + H^{+} + Ag^{+} \quad (2)$$

rearrangement of the position of isoprene double bond (Jacobsen and Torssell). 4-Methyl-3-pentenoic acid **45** formed the 3,3-dimethylallyl radical **46**, which resonates between α,α and γ,γ positions (Figure 4.21A). The more stable tertiary radical, α,α-dimethylallylquinone, was expected; however, only γ,γ-dimethylallylquinone was observed, favoring the more stable alkene. MK-1 was produced in 70% yield using **45** (Figure 4.21B), leaving the question of *E/Z* alkene isomerization unanswered:

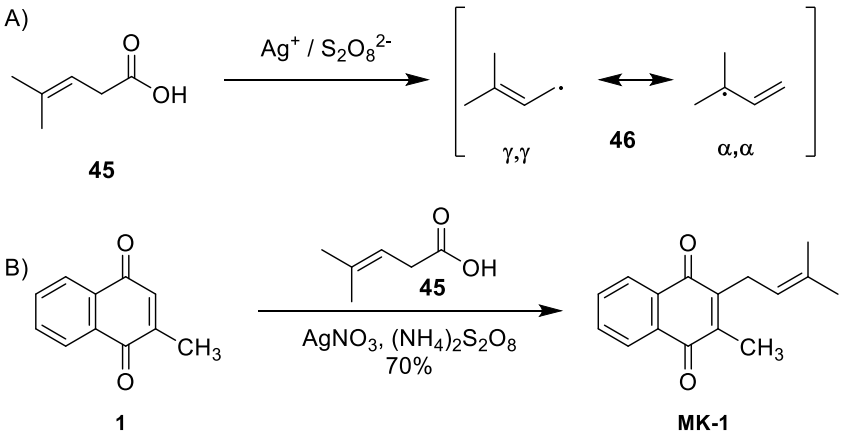

Figure 4.21. (**A**) Radical formation via decarboxylation. (**B**) Synthesis of MK-1 using this method (Jacobsen and Torssell , Jacobsen and Torssell).

The question of α-isoprene double bond stereoretention was later answered by Yamago et al. in 2000 with preliminary results of the radical coupling of quinones with organotellurium reagents (Yamago, Hashidume et al. , Yamago, Hashidume et al.). Geranyl bromide (73:23 *E/Z*) **47** was converted to the corresponding tolyltelluride **48** in 41% yield with complete retention of stereochemistry (Figure 4.22A). Then the tolyltelluride **48** was photochemically coupled to menadione **1** to produce MK-2 in 44% yield with complete retention of stereochemistry (Figure

4.22B). This reaction was previously mentioned in a review by Daines et al. in 2003 (Daines, Payne et al. 2003).

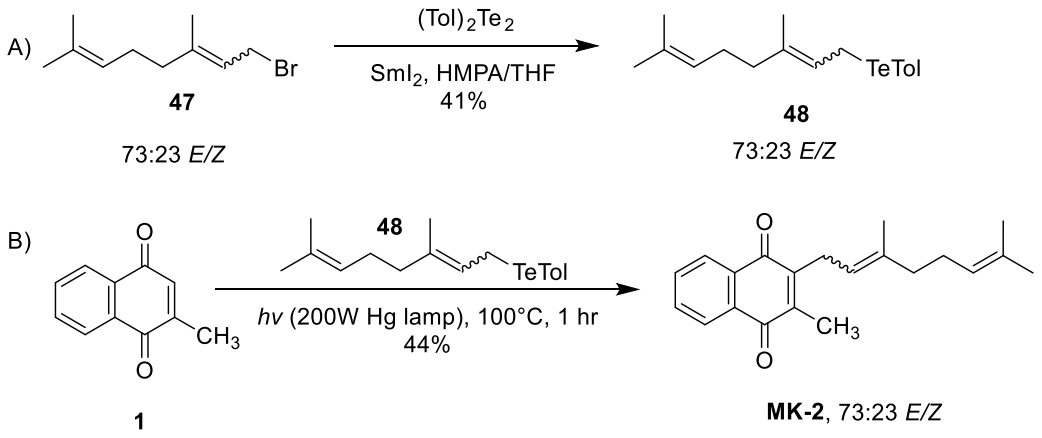

Figure 4.22. (**A**) Synthesis of geranyltelluride reagents. (**B**) Synthesis of MK-2 with organotelluride radical alkylation (Yamago, Hashidume et al. , Yamago, Hashidume et al.).

4.3.3.2. Non-Metal-Mediated Radical Reactions

In 2019, we continued our pursuit to synthesize menaquinone analogs with various levels of saturation within the side chain (Koehn, Crick et al.). For analogs with the first isoprene unit saturated, we employed chemistry developed by Coppa et al. in 1991. Therein, different methods for homolytic methylation of quinones with alkyl iodides were discussed (Coppa, Fontana et al.

1991). In one such method, menadione **1** reacted with a saturated alkyl iodide in the presence of benzoyl peroxide to form the C3-alkylated product **49** (Figure 4.23A).

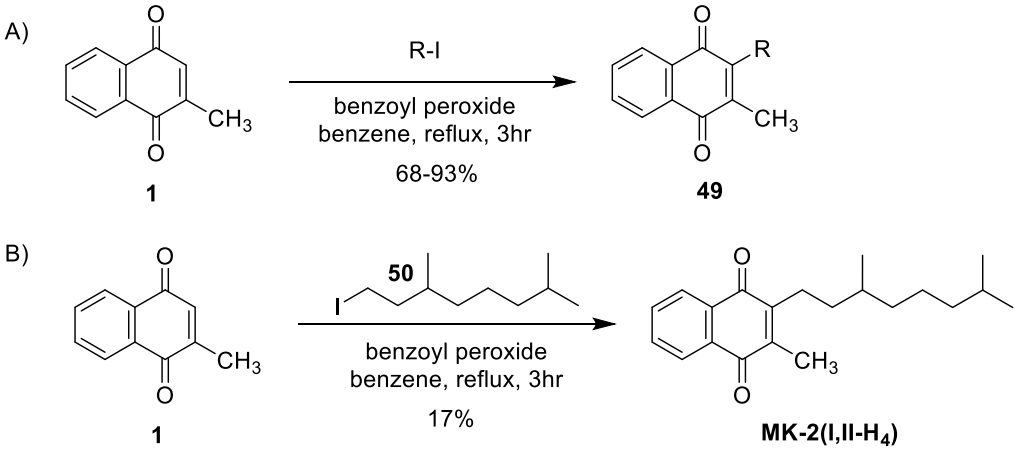

Figure 4.23. (**A**) General synthesis of menaquinones with alkyl iodides (Coppa, Fontana et al. 1991). (**B**) Synthesis of MK-2 (I,II-H_4) (Koehn, Crick et al.).

The results varied, with yields ranging from 68 to 93%. Prominent competition between the C3-alkylated product and the C3-self-coupling aryl product was observed, showing 32–94% the C3 aryl product in some trials. We saw the parallels between the substrates used by Coppa et al. and the saturated prenyl side chains required for our studies. Menadione **1** was coupled with alkyl iodide **50** to synthesize MK-2(I,II-H_4) in 17% yield (Figure 4.23B).

4.3.4. Summary

The three main metal-mediated and radical methods reported in the literature included organometallic cross-coupling, the use of coordination complexes, and both metal and non-metal mediated radical reactions. The advantages and disadvantages of each have been outlined in Table 4.6. Only four methods reported moderate to high yields (65–100%) across the synthesis. Liebeskind and Foster used Stille coupling for the key alkylation step (90%). Liebeskind et al., again, reported high yields (77%) using the updated cobalt complex to aid the cycloaddition of alkynes to the coordinated phthaloyl group. Jacobsen and Torssell achieved moderate yields (70%)

in the alkylation of quinones with radicals generated by the decarboxylation of prenyl carboxylic acids. Lastly, Coppa et al. also used radical alkylation of quinones using short-chain alkyl iodides in the presence of benzoyl peroxide. Regiocontrol for these methods was achieved in three ways: 1) transmetalation of organolithium reagents to different organometallates; 2) asymmetric alkynes coordinating to symmetric complexes; and 3) selective abstraction of aryl hydrogens adjacent to the carbonyl. Complete stereoretention was observed during Stille et al.'s cross-coupling of arylstannanes and phytyl bromide in the presence of $ZnCl_2$, Dötz et al.'s cycloaddition using stereopure alkynes, and Yamago et al.'s radical organotelluride alkylation. Like the nucleophilic methods above, several syntheses only produced MK-1; therefore, the stereochemical implications of the method were not addressed.

Table 4.6. Summary of metal-mediated reactions.

Methods	Advantages	Disadvantages
	4.3.1. Cross-Coupling	
Sato et al. π-Allylnickel Cross Coupling (Sato, Inoue et al. 1973)	-No coordination complex synthesis required - π-allyl complex is formed *in situ* -Moderate to high yields (52–93%) across the syntheses -*E/Z* ratio of the α-isoprene double bond (7:3 *E/Z* for MK-9) -3 step synthesis (not including starting material)	-The yields drop at the cross-coupling, especially for the much longer prenyl side chains, MK-9 (52%) -Authors note *E/Z* ratio is tunable depending on the solvent, but the yields drop as a result

Stille et al. Aryl Stannane Cross Coupling (Godschalx and Stille 1983)	-High yields (77%) for the formation of the arylstannane -The regiochemistry of the system is controlled by transmetalation at C3 position -Allylic transposition was not observed in analogous syntheses of myrcene (Godschalx and Stille)	-Low yield for cross-coupling (40% over two steps) -Requires the use of *t*-BuLi -5 step synthesis (not including starting material)
4.3.2. Coordination Complex		
Liebeskind and Foster Ring Expansion to Stille Coupling (Liebeskind and Foster 1990)	-Stille coupling achieved high yields (90%) -3 step synthesis (not including starting material)	Low yield for key Liebeskind-Moore rearrangement (49% over two steps) -Only synthesized MK-1
Dötz et al. Chromium Complex Carbonylation (Dötz, Pruskil et al. 1982, Dötz 1984)	-No coordination complex synthesis required -*E/Z* ratio of the α-isoprene double bonds was retained throughout the synthesis -The regiochemistry of the system is controlled by the alkynes **37a** and **37b** -$Cr(CO)_6$ is recyclable	-Known adverse health effects related to hexavalent chromium -No yields reported in Rüttimann's 1986 review (Rüttimann 1986) -5 step synthesis (not including starting material)

Table 4. 6. *Cont.*

Liebeskind et al. Cobalt Complex Cycloaddition (Liebeskind, Baysdon et al. 1986)	-High yields (> 86%) -Simple coordination complex synthesis required using commercially available materials -The regiochemistry of the system is controlled by the alkynes **43a** and **43b** -1 step synthesis (not including catalyst)	-The authors did not address α-isoprene double bonds isomerization
4.3.3. Radical Reactions		
Jacobsen & Torssell Radical Decarboxylation (Jacobsen and Torssell 1973)	-Moderate yields (70%) -Regiocontrolled through aryl hydrogen abstraction -Selective for γ,γ-alkene product of MK-1 -1 step synthesis	-Only synthesized MK-1

Yamago et al. Radical Organotelluride (Yamago, Hashidume et al. 2000, Yamago, Hashidume et al. 2002)	-Regiocontrolled through aryl hydrogen abstraction -Stereoretention of the α-isoprene double bond across all steps -2 step synthesis	-Low yields for both formation of tolyltelluride and radical coupling (~40%) -Known adverse health effects related to working with tellurium and tellurium compounds
Coppa et al. (Coppa, Fontana et al. 1991) & Koehn et al. (Koehn, Crick et al. 2018) Benzoyl Peroxide Initiated Radical Alkylation	-Moderate to high yields of straight chain alkyl iodides (68–93%) (Coppa, Fontana et al. 1991) -1 step synthesis (not including starting material)	-Koehn et al. reported very low yields (17%) for this transformation with a branched alkane -Substantial α-isoprene double bond isomerism -Competing reactions interfere with C3-alkylated product (C3-C3, and C2 alkylation)

4.4. Electrophilic Ring Methods

4.4.1. 1,2-Addition versus 1,4-Addition

In the late 1970s and early 1980s, Naruta published two reports independently and published one with Maruyuma, reporting the use of prenyl stannanes for the synthesis of biologically important quinones, focusing on vitamin K_1 and MK-2 (Maruyama and Naruta 1978, Naruta 1980, Naruta 1980). Using menadione **1**, *trans* and *cis* isomers with respect to the α-isoprene double bond were synthesized using geranyl and neryl trimethylstannanes, **51a** and **51b**, respectively, in the presence of $BF_3{\cdot}OEt_2$ (Figure 4.24A). The yields were 30% and 41% for the

respective *trans* and *cis* products with the configuration of the double bond mostly maintained for each product. *Trans*-MK-2 was found to have 95% *E* alkene, and the *cis* isomer was found to have 76% *Z* alkene. Using the same conditions, vitamin K_1 was synthesized in 48% using phytyl trimethylstannane **52** (> 95% *E*) (Figure 4.24B). The product was found to have 96% *E* alkene configuration, showing complete stereoretention.

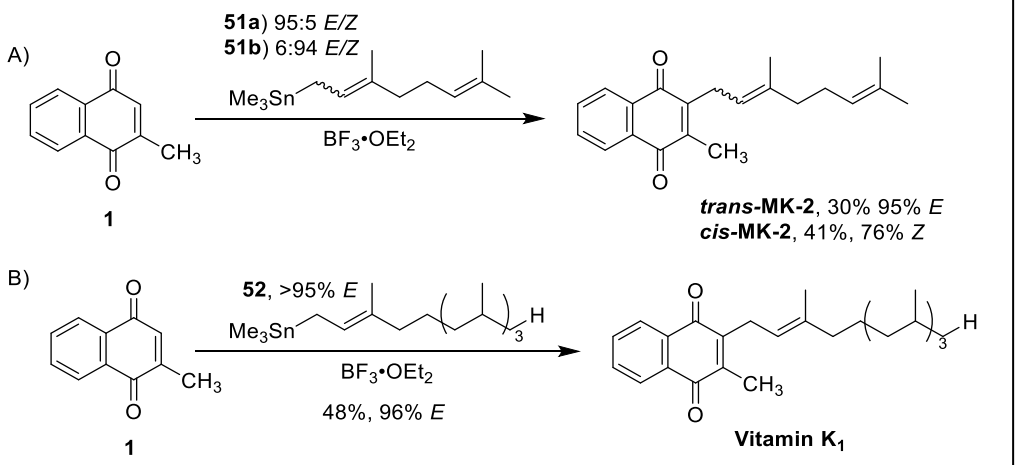

Figure 4.24. The synthesis of (**A**) MK-2 and (**B**) vitamin K_1 using alkylstannanes (Maruyama and Naruta , Naruta 1980, Naruta 1980).

Although the major product for all trials was the 1,4-addition product, 1,2-addition accounted for a large portion of the undesired byproducts. For *cis*-MK-2 and vitamin K_1, the C2 isomer was isolated in 13% and 14% yield, respectively. The 1,2 addition is hypothesized to add the least hindered carbonyl carbon of menadione **1**, which then undergoes a [3,3] sigmatropic rearrangement, similarly described by Araki et al. (Araki, Katsumura et al.) and Evans and Hoffmann (Evans and Hoffman 1976) in Section 4.3. The rearrangement places the prenyl chain on the C2 carbon with the preexisting methyl group. In addition to prominent mechanistic competition, the yields are low across all steps. This method does, however, feature complete retention of stereochemistry of the α-isoprene double bond, as detailed in Table 4.7.

Table 4.7. Summary of electrophilic ring methods.

Methods	Advantages	Disadvantages
4.4.1. 1,2-Addition vs. 1,4-Addition		
Naruta and Maruyuma. Organostannane Michael Addition (Maruyama and Naruta 1978, Naruta 1980, Naruta 1980)	-Stereoretention of the α-isoprene double bond -1 step synthesis (not including starting materials)	-Low yields for both formations (30–48%) -Prominent competition between C2 and C3 alkylation

4.5. Pericyclic Reactions

4.5.1. Diels-Alder Reactions

In a review published by Rüttimann in 1986 (Rüttimann), synthetic advancements of the preparation of vitamin K_1 were presented, detailing methods from traditional substitutions, organometallic reactions, and pericyclic reactions. Therein, Rüttimann and coworkers explored the use of Diels-Alder reactions to form the naphthoquinone unit of vitamin K in a previously unpublished synthesis inspired by the work of Troll and Schmid. (Troll and Schmid 1984). Dihydroisobenzofurane **53** was reacted with activated alkyne dienophile **54** (96:4 *E/Z*) at 80 °C overnight to form the Diels-Alder adduct **55** (Figure 4.25). Deprotection of the silyl ethers was achieved using methanol, and reduction of C2 methyl ester to a methyl group with sodium bis(2-

methoxyethoxy)aluminum hydride in toluene under reflux formed the substituted menadiol. Oxidation with air in slightly acidic conditions produced vitamin K_1 in ~50% yield over four steps. The configuration of the isoprene double bond was not disturbed, resulting in 93-96% *E* alkene.

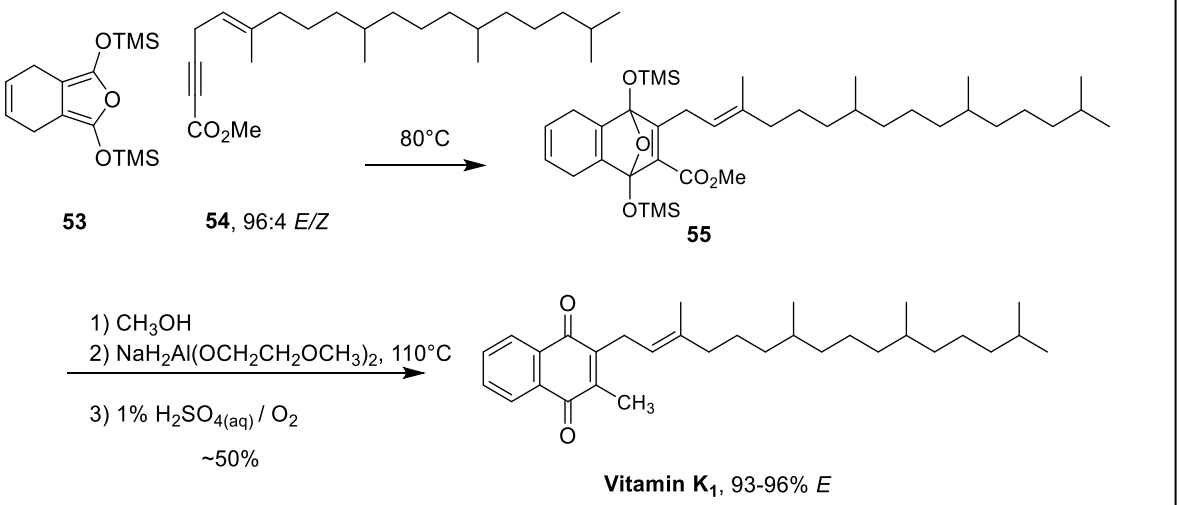

Figure 4.25. Previously unpublished synthesis of vitamin K_1 inspired by Troll & Schmid (Rüttimann).

Using insights gained from the previous route, Rüttimann continued to explore the use of Diels-Alder reactions to synthesize vitamin K_1. He and Büchi designed an auxiliary-directed route using cyclopentadiene as the corresponding diene (Figure 4.26) (Büchi and Rüttimann). *Endo*-Diels-Alder adduct **56** was formed at room temperature using menadione **1** and cyclopentadiene in 93% yield. Formation of adduct **56** switched the C3 hybridization from sp^2 to sp^3, decreasing the pKa. Upon deprotonation by a strong base (e.g., potassium amide, sodium amide, or potassium *t*-butoxide (which is referred to as potassium *t*-butanolate in the source literature)) a stable carbanion is formed, allowing regioselective alkylation at the C3 position with a variety of electrophiles.

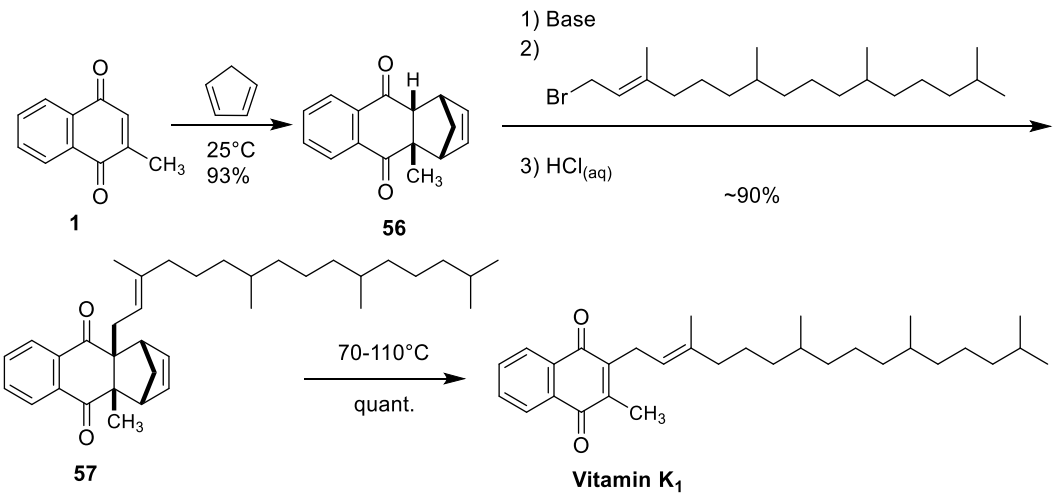

Figure 4.26. Synthesis of vitamin K_1 using Diels-Alder approach with cyclopentadiene auxiliary (Büchi and Rüttimann 1986, Rüttimann).

Alkylation with phytyl bromide (≥ 98% *E*) gave the predicted product **57**. The authors found that some *O*-alkylation product was formed in trace amounts, however it was cleaved with acidic aqueous work up and easily separated. Alkylated adduct **57** was formed in approximately 90% yield over three steps. Due to the intrinsic instability of adduct **57**, slow decomposition was observed at room temperature. Retro-Diels-Alder reaction was induced at high temperatures to remove the auxiliary group quickly, producing vitamin K_1 in quantitative yield (Büchi and Rüttimann).

4.5.2. Anionic Diels-Alder Reactions

In contrast to traditional Diels-Alder reactions where neutral species form adducts, anionic Diels-Alder reactions have been another useful method to form the naphthoquinone unit. In 1995, Tso and Chen. published a one-pot synthesis applicable towards the synthesis of vitamin K_1, and MKs-1, 2, and 9 (Figure 4.27) (Tso and Chen 1995). The dienophiles used were alkenyl sulfones **60a–d**, which were readily prepared from the corresponding allyl phenylsulfone **58** and allyl bromides **59a–d** for vitamin K_1, MK-1, MK-2, and MK-9, respectively. Isobenzofuranone **61** was

deprotonated with NaHMDS, then **60a-d** were attacked forming the intermediate **62**. Elimination of the benzenesulfonate produced the desired products vitamin K_1, MK-1, MK-2, and MK-9 in moderate yields, 60–64%. The configuration of the α-isoprene unit was found to be > 98% *E* alkene for all substrates.

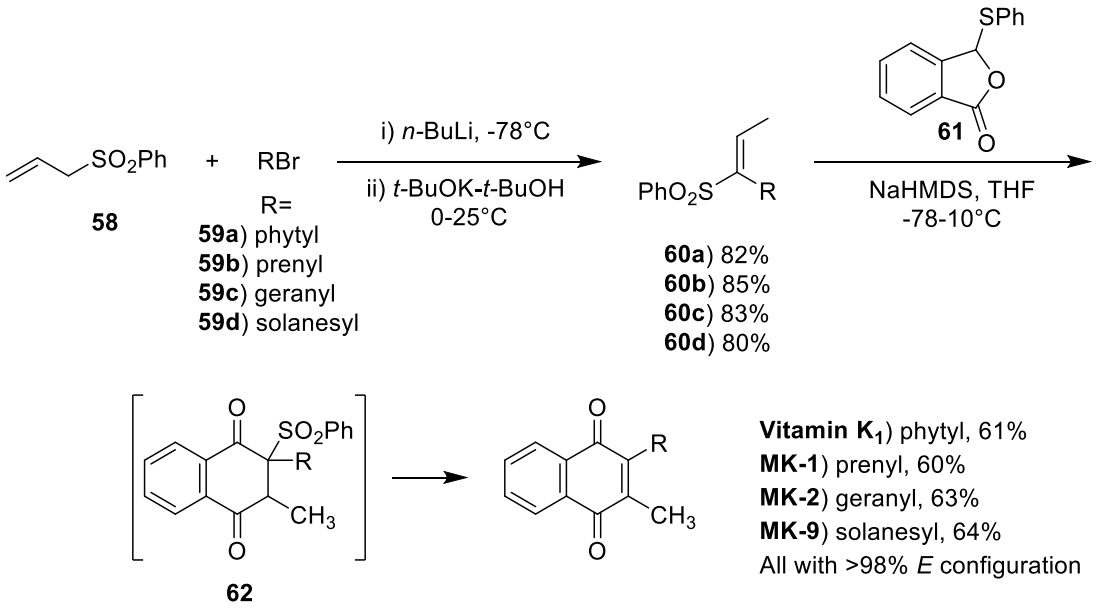

Figure 4.27. Synthesis of vitamin K_1, MK-1, 2, and 9 using anionic Diels-Alder approach (Tso and Chen 1995).

Nearly twenty years later, Mal et al. suggested a better atom economy could be obtained in comparison to the work done by Tso and Chen. In an effort to improve the atom economy of anionic Diels-Alder reactions, the authors replaced the phenylsulfone moiety with a nitrile **63** (Figure 4.28) (Mal, Ghosh et al.). Using this method, the authors synthesized different C3-alkylated MK-derivatives using specifically designed dienophiles. For the synthesis of MK-1 and MK-2, methyl acrylate derivatives **64a** and **64b** were used. It is important to note the synthesis of **64b** produced a mixture of ~3:1 of *E/Z* isomers with respect to the methyl acrylate alkene, as determined by NMR. It is unclear to us whether that refers to stereochemical composition of the methyl acrylate alkene or the geranyl side chain of **64b**. Isobenzofuranone **63** was deprotonated

with LiO*t*-Bu at −78 °C in THF, and then formed the adduct **65a/b** with dienophiles **64a/b** in 73% and 65% yield, respectively. Demethylcarboxylation of adducts **65a/b** was achieved using a second round of LiO*t*-Bu in THF under reflux to form MK-1 and MK-2 in 55% and 40% yield, respectively. The ratio of *E/Z* ratio of MK-2 was found to be 5:3.

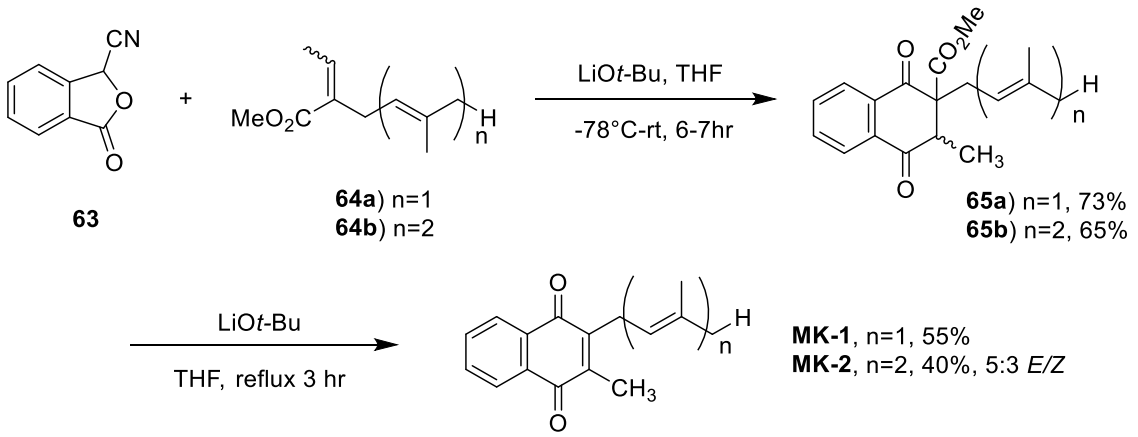

Figure 4.28. Synthesis of MK-1 and MK-2 using anionic Diels-Alder approach with improved atom economy (Mal, Ghosh et al.).

4.5.3. [3,3] Sigmatropic Rearrangements- Cope

[3,3] Sigmatropic rearrangements were also used to synthesize menaquinones, as shown in Daines et al. 2003 review (Daines, Payne et al. 2003). In 1976, Evans and Hoffmann took advantage of the Cope rearrangement to synthesize MK-1 (Figure 4.29A) (Evans and Hoffman 1976). Using masked ketone **66**, the unprotected carbonyl was attacked with prenylmagnesium bromide, forming ketone **67** in one step. Interestingly, the authors discovered that prenylmagnesium bromide added to the carbonyl in a reverse prenylated fashion **68a** (Figure 4.29B). The C1-reverse prenylated product **68a** set the transition state **68b** for a Cope rearrangement, **68b** to **69a**, producing C3-prenylated product **69a**. Upon quenching with saturated NH_4Cl, as shown in intermediate **69b**, the C3 methoxy group was removed to reform ketone **67** (Figure 4.29B). Deprotection of the masked ketone was achieved using AgF in mild conditions to

form MK-1 in 71% yield over two steps. Since MK-1 was the only product synthesized, there *E/Z* ratio of the α-isoprene double bond was not considered, nor were the effects of this synthesis on longer prenyl chains.

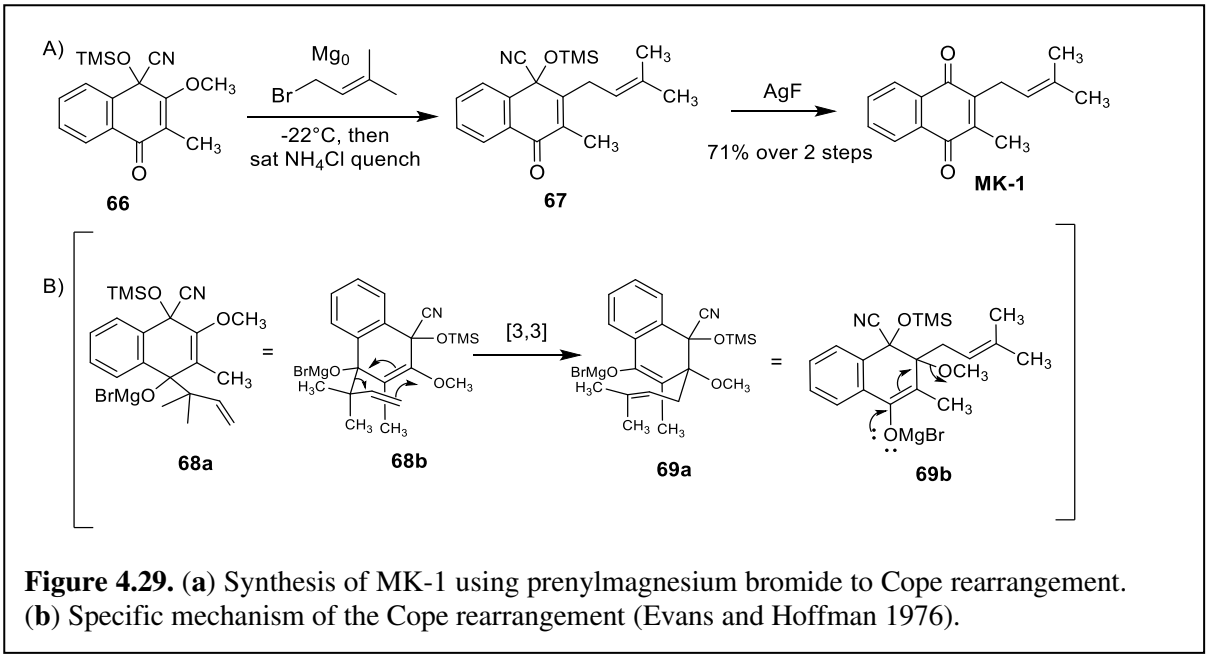

Figure 4.29. (**a**) Synthesis of MK-1 using prenylmagnesium bromide to Cope rearrangement. (**b**) Specific mechanism of the Cope rearrangement (Evans and Hoffman 1976).

In contrast to more conventional alkylating reagents, Araki et al. used organoindium reagents for the allylation of various quinones (Araki, Katsumura et al.). Throughout many trials with a wide scope of benzo- and naphthoquinone derivatives, organoindium reagents were found to selectively add to the least hindered carbonyl in 1,2-addition (Figure 4.30A). Therefore, when choosing between the C1 and C4 carbonyl groups, 2-bromomenadione **70** was attacked at the less hindered C1 ketone with prenylindium **71** to form reverse prenylated intermediate **72a** (Figure 4.30B). Following addition, the reverse prenyl group underwent a Cope rearrangement, **72b** to **73a**, analogous to the system reported by Evans and Hoffmann. After oxidation with Ag_2O, MK-1 was produced in 67% over two steps. This synthesis did not address the possibility of alkene isomerization, however, in other trials reported in the same paper (Araki, Katsumura et al.), the authors reported geranylindium **74a** and nerylindium **74b** rearrangements on menadione **1**, producing **75a** and **75b** in 85% and 95% yield, respectively (Figure 4.30C). Each product showed

a total loss of stereoretention, ~50/50 *E/Z*. The authors hypothesized the same trend would have been seen using 2-bromomenadione **70**; therefore, stereocontrol of the α-isoprene double bond continues to be an important challenge with Cope rearrangements.

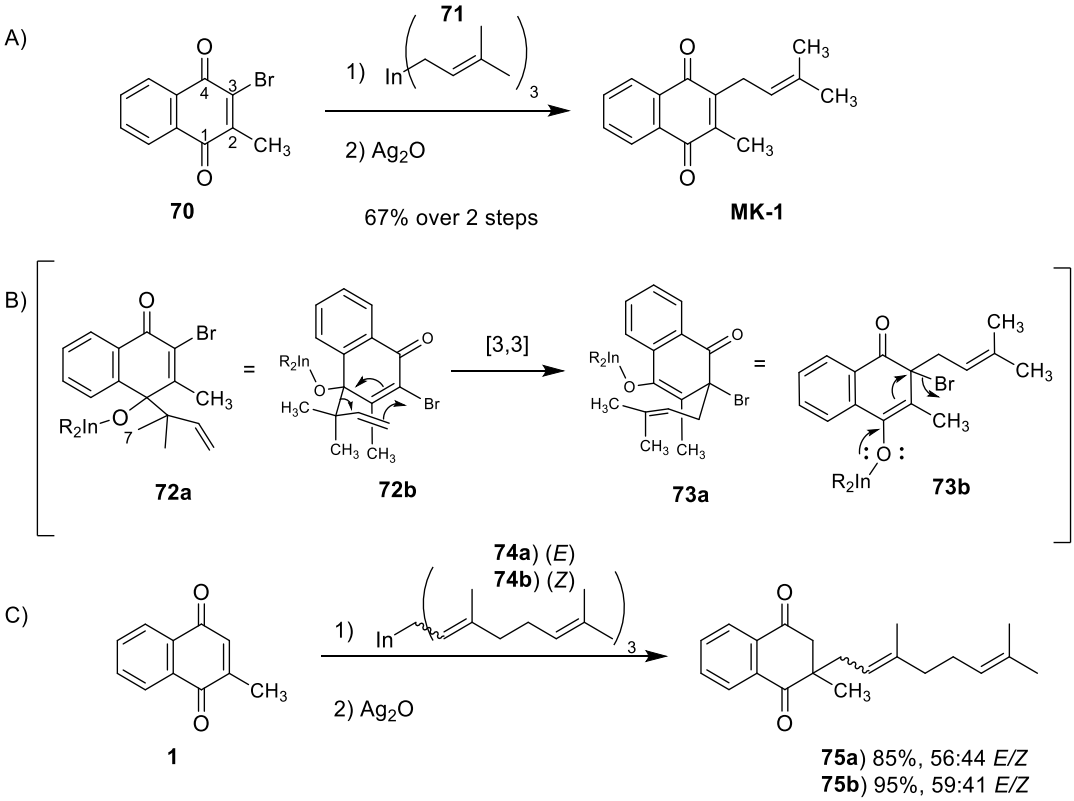

Figure 4.30. (**A**) Synthesis of MK-1 using organoindium reagents. (**B**) Closer look into the Cope rearrangement. (**C**) Attempted synthesis of MK-2 using geranyl **74a** and neryl **74b** organoindium rearrangement. (Araki, Katsumura et al.).

4.5.4. Summary

Across the literature, the common types of pericyclic reactions are Diels-Alder cycloadditions and [3,3] sigmatropic rearrangements, specifically Cope rearrangements. The advantages and disadvantages of each method have been outlined in Table 4.8. Rüttimann et al. achieved high yields with a cyclopentadiene auxiliary-directed Diels-Alder reaction. For all methods described in this section, the asymmetry of certain reagents controlled the regioselectivity of the reaction. For example, the asymmetry of the dienophiles involved in the Diels-Alder reactions controlled the regiochemistry of the adduct. The Cope rearrangement reactions were

regiocontrolled by using starting materials with leaving groups on the desired position, protecting groups, and by taking advantage of steric hinderance. For all Diels-Alder reactions described, except for the work done by Mal et al., complete retention of stereochemistry was observed for the α-isoprene double bond. In the case of Mal et al., the reported *E/Z* ratio for dienophile **64b** was ~3:1 *E/Z* by NMR for the methyl acrylate dienophile. The *E/Z* ratio of the product MK-2 was found to be 5:3 *E/Z*. It is unclear to us whether this was a result of the Diels-Alder reaction or due to isomeric starting material. For all Cope rearrangements, it can be inferred that a complete loss of stereocontrol would be observed due to the reverse-prenyl addition to the carbonyl, as observed by Araki et al. using geranyl and nerylindium reagents with menadione **1**.

Table 4.8. Summary of pericyclic reactions.

Methods	Advantages	Disadvantages
	4.5.1. Diels-Alder	
Rüttimann et al. Diels-Alder Reaction inspired by Troll & Schmid (Rüttimann 1986)	-High regiocontrol through the symmetry of dihydroisobenzofurane diene -Stereoretention of α-isoprene double bond (≥ 93%)	-Overall low yields (~50% over four steps) -Synthesis of starting materials -4 step synthesis (not including starting material)
Rüttimann et al. Auxiliary-Directed Diels-Alder (Rüttimann 1986)	-Uses commercially available starting materials (menadione and cyclopentadiene) -High regiocontrol through adduct **66** -Stereoretention of α-isoprene double bond -Cyclopentadiene can be recycled	-Slight competition between C-alkylation and O-alkylation -5 step synthesis

	-High yields throughout the synthesis (≥ 90%)	

4.5.2. Anionic Diels-Alder

Tso and Chen Anionic Diels-Alder (Tso and Chen 1995)	-One-pot synthesis -High regiocontrol through asymmetry of dienophile -Stereoretention of α-isoprene double bond across all steps (> 98%) -3 step synthesis (not including starting material)	-Moderate yields (60–64%) -Requires the synthesis of starting materials
Mal et al. Anionic Diels-Alder with Improved Atom Economy (Mal, Ghosh et al. 2015)	-Improved atom economy -High regiocontrol through asymmetry of dienophile -2 step synthesis (not including starting material)	-Low to moderate yields (40–73%) -5:3 E/Z ratio -Unclear if it is due to stereochemistry of starting material or caused by the reaction

4.5.3. [3,3] Sigmatropic Rearrangements- Cope

Evans and Hoffmann Grignard-Promoted Cope Rearrangement (Evans and Hoffman 1976)	-Regiocontrol achieved through protected naphthoquinone -Cope rearrangement to achieve C3 alkylation Moderate yields (71% over two steps) -2 step synthesis (not including starting material)	-No consideration of the isomerization of the isoprene double bond
Araki et al. Organoindium-Promoted Cope Rearrangement	-Regiocontrol achieved through less hindered 1,2-addition of organoindium reagent	No stereoretention observed in Cope rearrangement

(Araki, Katsumura et al. 1991)	-No protecting groups required -Cope rearrangement to achieve C3 alkylation -Moderate yields (67% over two steps) -2 step synthesis (not including starting material)

4.6. Homologation & Side Chain Extension Methods

4.6.1. Homologation

In 1998, Lipshutz et al. designed a route to install a one carbon functional handle at the C3 position to enable the synthesis of a wide variety of MK-derivatives (Lipshutz, Kim et al. 1998). Menadione **1** was reacted with formaldehyde and hydrogen chloride gas to form 3-chloromethylmenadione **76** in 87% yield (Figure 4.31). The introduction of the chloromethyl group allows for reactions that were previously less approachable, like S_N2 substitutions and organometallic cross-couplings. Using 3-chloromethylmenadione **76** as the starting material, the authors used Negishi cross-coupling conditions to take advantage of the stereoselective installation of alkenes based on the configuration of the organoalane species (Van Horn and Negishi 1978, Negishi 1981, Matsushita and Negishi 1984, Negishi, Van Horn et al. 1985). For example, phytyl alkyne **79** underwent Negishi carboalumination to form organoalane **77** (Figure 4.32). Vitamin K_1 and MK-3 were synthesized using this method (Figure 4.31). For the synthesis of vitamin K_1, 3-chloromethylmenadione **76** was coupled with phytylalane **77** in the presence of the nickel catalyst which is formed in situ using nickel (II) chloride, triphenylphosphine, and *n*-BuLi. Vitamin K_1 was

formed in 88% with exclusively *E* configuration. MK-3 was prepared similarly, but instead with farnesylalane **78**, in 93% yield with *E* configuration at the α-isoprene double bond.

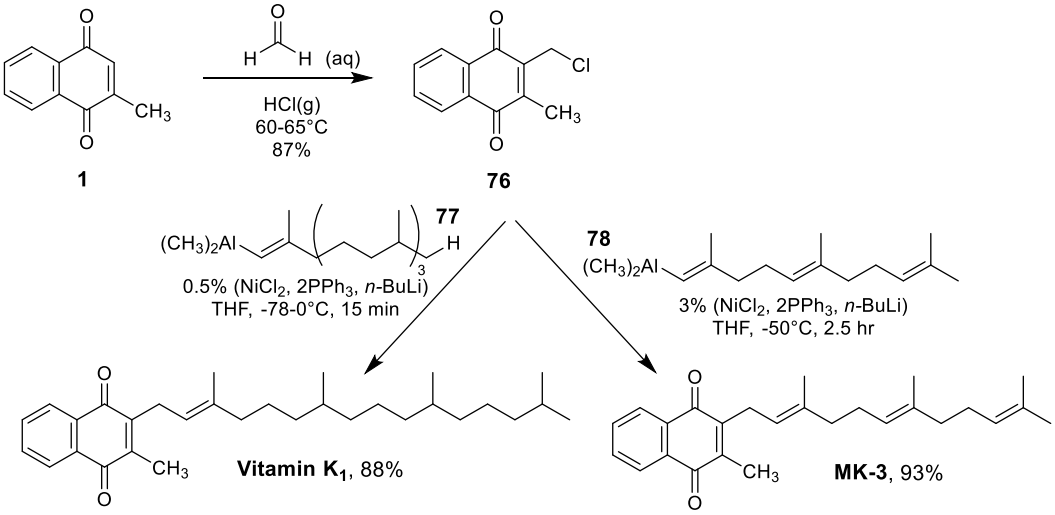

Figure 4.31. Synthesis of MK-3 and vitamin K_1 via C3 homologation and Negishi cross-coupling conditions (Lipshutz, Kim et al. 1998).

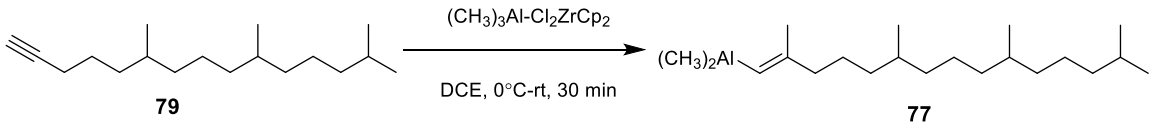

Figure 4.32. Negishi carboalumination of phytyl alkyne (Van Horn and Negishi 1978, Negishi 1981, Matsushita and Negishi 1984, Negishi, Van Horn et al. 1985).

In 2015, Mehta et al. published a patent covering the synthesis of stereospecific quinone derivatives (Mehta, Mohan et al. 2015). Therein, the authors described methods used for the synthesis of the various lengths of prenyl side chains using a series of homologation and side chain extension reactions featuring stereoselective alkene syntheses, such as Wittig, Horner-Wadsworth-Emmons, and Still-Gennari. For the synthesis of MK-7, 1,4-dimethoxynaphthoquinol **18** reacted with dichloro(methoxy)methane and $TiCl_4$ to form the C3 aldehyde **80** in 95% yield (Figure 4.33). Wittig homologation of **80** was achieved using ylide **81** followed by mild acid hydrolysis to form aldehyde **82**. Using phosphonate ester **83**, aldehyde **82** underwent a Horner-Wadsworth-Emmons

reaction to form the desired *E* alkene in 85% yield. The authors noted the use of Still-Gennari conditions for the synthesis of the *Z* alkene where appropriate. The ester was reduced to the alcohol using DIBAL-H in 91% yield, and then immediately oxidized to aldehyde **84** using PCC in 88%

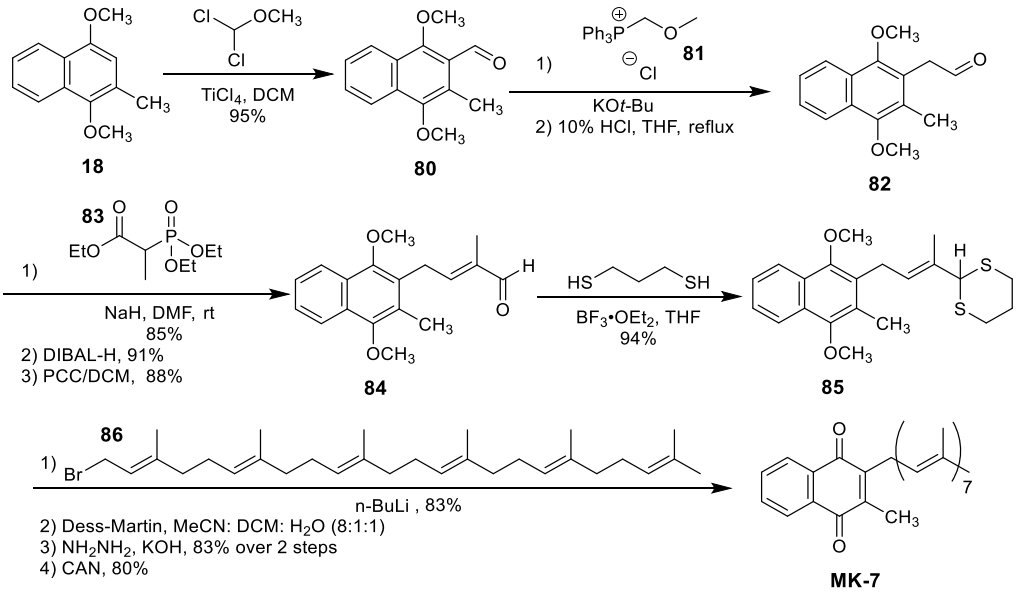

Figure 4.33. Synthesis of MK-7 using dithiane anion side chain extensions (Mehta, Mohan et al. 2015).

yield. The resulting aldehyde **84** was protected as dithiane **85** in 94% yield. Deprotonation of the methine hydrogen of **85** with *n*-BuLi created a stable anionic nucleophile. Farnesylfarnesyl bromide **86** was used to form the C3-alkylated product in 83%. The dithiane protected carbonyl was deprotected using Dess-Martin periodinane and then reduced using Wolff-Kishner conditions, producing the hydrocarbon prenyl side chain in 82% yield over two steps. Oxidation with CAN formed MK-7 in 80% yield. The authors achieved the synthesis of MK-7 in two different iterations: 1) when the entire chain was added in one step (Figure 4.33), and 2) when the side chain was added on smaller segments using the same methodology, which is similarly used in Masaki et al.'s work in Section 6.2.

4.6.2. Side Chain Extensions

Another popular method across the literature is the continued functionalization of truncated prenyl chains that were installed using the previously described methods. In 1984, Masaki et al. developed a synthetic route to lengthen the prenyl chain starting with prenyl bromides (Figure 4.34) (Masaki, Hasimoto et al. 1984, Masaki, Hasimoto et al.). This served as the starting material

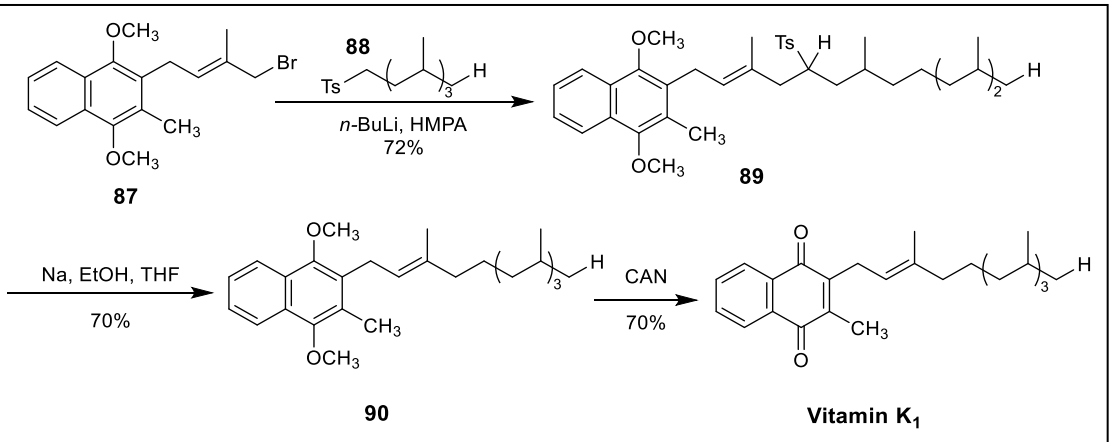

Figure 4.34. Synthesis of vitamin K_1 using tosylate extension methods (Masaki, Hasimoto et al. 1984, Masaki, Hasimoto et al.).

for the synthesis of vitamin K_1 and MK-4. The common electrophiles across all trials were prenyl bromides **92**, synthesized in 70-90% yield from the corresponding prenyl alcohols **91** using PBr_3 (Figure 4.35). For the synthesis of vitamin K_1 (Figure 4.34), prenyl bromide **87** was coupled to

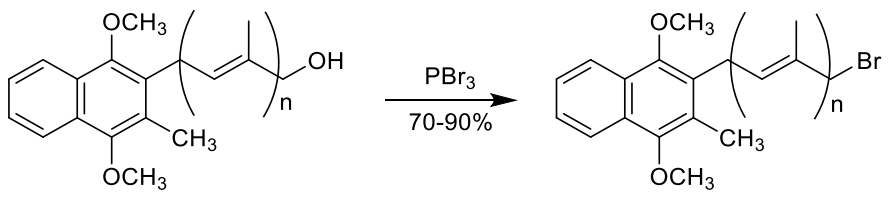

Figure 4.35. Conversion of prenyl alcohols to respective prenyl bromides (Masaki, Hasimoto et al. 1984, Masaki, Hasimoto et al.).

tosylate **88**. Deprotonation of the tosylate methine hydrogen created a stable anion to attack **87** to form the alkylated product **89** in 72% yield. Removal of the tosyl group was achieved using

modified Bauvault-Blanc desulfurization conditions in 70% yield. Deprotection of tosylate **89** obtained **90** in 70% yield, and thus vitamin K_1 was produced in 70% yield in the presence of CAN. For the synthesis of MK-4, Masaki et al. approached the synthesis with two different iterations (Figure 4.36). Starting with benzyl ether protected polyprenyl bromide **93a** and **93b**, the same

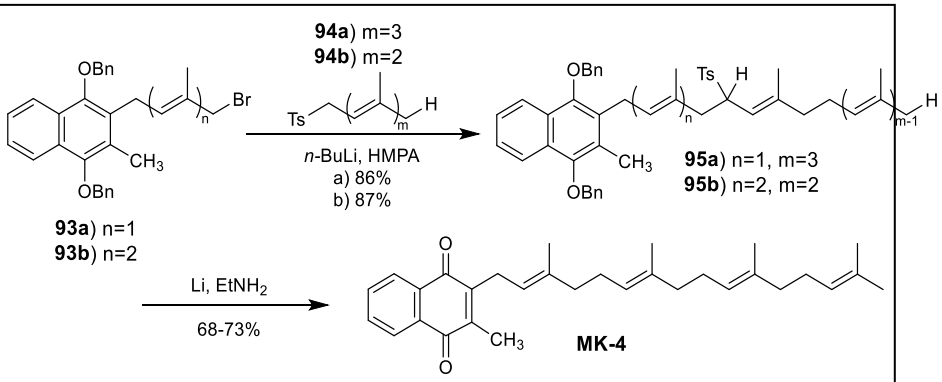

Figure 4.36. Synthesis of MK-4 using tosylate extension methods (Masaki, Hasimoto et al. 1984, Masaki, Hasimoto et al.).

alkylating conditions were used to extend the chain using tosylates **94a** and **94b** to form products **95a** and **95b** in 86% and 87% yield, respectively. Desulfurization of the prenyl chain produced the hydrocarbon side chain of MK-4 in 68-73% yield. The authors noted HPLC analysis showed isomeric byproducts in 5-7%, likely formed during the desulfurization step.

In contrast to Masaki et al.'s. approach with tosylates, Schmid et al. used organocuprate reagents as nucleophiles to install the remaining hydrocarbon chain for vitamin K_1 (Schmid, Antoulas et al. 1990). Installation of the first prenyl group was achieved via coupling of organocuprate reagent of bismethyl ether 2-bromomenadiol **6** with isoprene oxide in a 1,4-addition (Figure 4.37). The resulting alcohol was protected as ester **96**. This reaction yielded 90% over two steps with 93:7 *E/Z* configuration. The rest of the phytyl chain was installed using the organocuprate reagent formed with hexahydrofarnesyl bromide **97**, performing a S_N2 substitution with the ester protecting group, forming the extended side chain in 51–79% yield. Oxidation of the ring was achieved with CAN with 77–86% yield to form vitamin K_1.

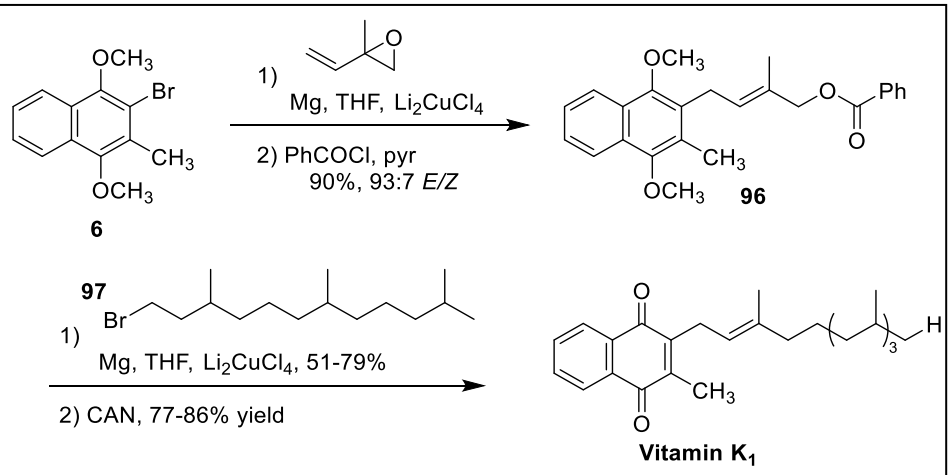

Figure 4.37. Synthesis of vitamin K_1 using organocuprate reagents to extend the length of the side chain (Schmid, Antoulas et al. 1990).

4.6.3. Summary

Homologation and side chain extension methods comprise a separate category from the others despite the use of similar techniques because they provide a functional handle that enables more diverse reactions than were previously less accessible. Homologation describes the addition of one carbon-containing group to the C3 position, which is then further functionalized to synthesize the rest of side chain. Side chain extension methods have one or two isoprene units attached to the ring which were installed using previously described methods to then add the

remainder of the chain using a different method, allowing for continued iterative additions. The advantages and disadvantages of each method have been outlined in Table 4.9. Nearly all described methods produced moderate to high yields throughout all steps, except for the organocuprate substitution demonstrated by Schmid et al., which produced low yields compared to the rest of the synthesis. Regiocontrol for these methods was achieved by the preinstalled carbons or prenyl chains connected to the ring which make the subsequent reactions chemoselective. Stereoretention of the α-isoprene double bond was achieved in three ways: 1) using stereospecific methodology, like Negishi carboalumination and cross-coupling; 2) stereoselective alkene syntheses; and 3) taking advantage of the stereochemical outcome of S_N2 substitutions.

Table 4.9. Summary of homologation and side chain extension methods.

Methods	Advantages	Disadvantages
	4.6.1. Homologation	
Lipshutz et al. Homologation to Negishi Cross-Coupling (Lipshutz, Kim et al. 1998)	-High yields throughout the synthesis (87–93%) -Method is applicable to a wide scope of benzo- and naphthoquinones -Stereochemistry of the α-isoprene double bond is defined by the configuration of the organoalane -Regiocontrolled by the installation of the chloromethyl group at the C3 position -No extraneous coordination complex synthesis required -3 step synthesis (including starting material)	-Requires the use of hydrogen chloride gas

Mehta et al. Stereoselective Alkene Syntheses (Mehta, Mohan et al. 2015)	-High yields throughout the synthesis for all reported steps (80–95%) -Strict use of stereoselective alkene syntheses -Methodology is applicable to full side chain extensions and smaller segments	-Requires the use of protecting groups and oxidation manipulations -11 step synthesis (not including starting material)
	4.6.2. Side Chain Extension	
Masaki et al. Tosylate Substitution (Masaki, Hasimoto et al. 1984, Masaki, Hasimoto et al. 1984)	-Moderate to high yields throughout the synthesis (68–90%) Stereoretention of the α-isoprene double bond with minor isomerization (5–7%) Methodology is applicable to full side chain extensions and smaller segments	-4 step synthesis (not including starting material)
Schmid et al. Organocuprate Substitution (Schmid, Antoulas et al. 1990)	-Achieved regio- and stereocontrol using isoprene oxide in a 1,4-addition -Stereoretention of the α-isoprene double bond (97:3) -Iterative methodology	-Low to moderate yields (51–79%) for alkylation step -4 step synthesis (not including starting material)

4.7. Conclusions

Menaquinones are a biologically important class of isoprenoid compounds that comprise of a methylated naphthoquinone unit and an isoprene side chain of various lengths and levels of saturation. The intrinsic hydrophobicity of these compounds makes it exceedingly difficult to analyze the activity in aqueous-based in vitro assays and growth studies. The moderately water soluble, truncated derivatives, MK-1 through MK-3, have made it possible to test and measure the activities of these compounds, especially in membrane-associated proteins. The most popular

method used to synthesize menaquinones and derivatives has been $BF_3 \cdot OEt_2$-catalyzed Friedel-Crafts reaction. This reaction typically occurs over two steps from commercially available starting material, but it generally produces low yields and a mixture of isomers. Although Friedel-Crafts alkylation is the conventional, concise method, in this review we aimed to compile and evaluate syntheses of menaquinones from all the literature to summarize the advantages and disadvantages of each route based on overall yield, regioselectivity, and stereoretention of the α-isoprene double bond, as shown in Tables 4.4, 6–9.

We further evaluated the reactions to consider the number of steps in the synthesis, minimization of side reactions, and overall safety to highlight one representative method in each category, as outlined in Table 4.10. With examination of Table 4.10, it is possible to compare the syntheses across different approaches. As a representative of the nucleophilic ring methods, Swenton and coworkers were chosen for the clean use of electrolysis to protect the quinone as bismethyl ketals. Simple acid hydrolysis deprotection of the ketals reformed the carbonyls of the quinone without oxidizing agents. As a representative of the metal-mediated and radical reactions, Liebeskind et al. were chosen for the easily synthesized cobalt complex and internal alkynes. The updated cobalt complex was found to be more tolerant toward a wide scope of Lewis acid catalysts, and, as a result, decreased the amount of catalyst required to synthesize the product. Rüttimann and Büchi designed an auxiliary-directed Diels-Alder reaction using commercially available materials, cyclopentadiene and menadione. Alkylation of the adduct occurred chemoselectively, and then facile retro-Diels-Alder formed the desired product in high yields and excellent regioselectivity. Lipshutz et al. used homologation and Negishi carboalumination and cross-coupling as side chain extension methods to attach the prenyl side chain. The stereochemistry of the α-isoprene double bond was easily installed using Negishi carboalumination of the

corresponding terminal alkyne. Finally, the representative electrophilic ring strategy was done in one synthesis of menaquinones using Michael additions was presented. The method developed by Naruta and Maruyuma retained the stereochemistry of α-isoprene double bond but was not regioselective due to competing 1,2- and 1,4-addition mechanisms.

Although the methods described in Table 4.10 are short, high yielding, and selective, there are a few more methods that should be considered if a new synthetic target can accommodate a longer synthesis or the processes in Table 4.10 are incompatible for the particular target. The homologation method developed by Mehta et al. uses two one-carbon installations at the beginning to synthesize provide a functional handle to stereoselectively install the α-isoprene double bond, and thus can be a strong competitor to the other reactions. Even though many of the methods described have great success using prenyl halides, the reagents are expensive, particularly in comparison to synthesizing MK-derivatives from cheap prenyl alcohols. Saá & coworkers were successful in using commercially available prenyl aldehydes as electrophiles (no distillation necessary). Reduction of the resultant benzyl alcohol was achieved using Birch hydrogenolysis conditions to maintain the stereochemistry of the α-isoprene double bond. Despite the notorious use of Friedel-Crafts alkylations, Schmid et al. discovered a unique intramolecular Friedel-Crafts alkylation beginning with the *O*-alkylated product using $BF_3{\cdot}OEt_2$. This route adds two steps, not including synthesis of the starting material and one protecting group, but the additional steps improved the overall yield, as well as the regio- and stereochemistry. Lastly, even though Jacobsen and Torssell only synthesized MK-1, their method would most likely tolerate polyprenylcarboxylic acids based on the stereoretentive results of radical coupling with organotellurides reported by Yamago et al.

With respect to Michael additions, the method developed by Naruta and Maruyuma was plagued by competing mechanisms (1,2- vs. 1,4-addition). It appears that alkylstannanes are not chemoselective enough to produce the Michael product for C-C bonds; however, many advancements have been made regarding Michael additions in general, suggesting more regioselective Michael additions may now be available for the synthesis of menaquinone and derivatives. Recently, Michael additions have been successfully used to synthesize C-N bonds using primary amines to form new analogues for biological testing. Recently, Salunke-Gawali and coworkers have used *n*-alkylamines and aminophenols to synthesize naphthoquinone derivatives which have been reported to assess their antiproliferative and antibacterial activities (Kathawate, Joshi et al. 2014, Chadar, Camilles et al. 2015). Salunke-Gawali and coworkers used single crystal x-ray crystallography to determine the structures of these compounds. The incorporation of C-N bonds introduces more hydrogen bonding sites for both intra- and intermolecular interactions. Similarly, Zacconi et al. synthesized naphthoquinone derivatives using benzylamine and 2-phenylethylamine to evaluate their isothermal solubility in supercritical carbon dioxide (Zacconi, Nuñez et al. 2016). All these MK-derived compounds were solids, compared to the typical oil produced for the all-C-atoms MK-derivatives. It would be of great interest to synthesize truncated menaquinones with *N*-containing isoprenyl side chains and study their redox potentials, solubility, and potential solid-state structure compared to the compounds already reported. However, as demonstrated by this review, many attractive strategies are available that could be used to synthesize potential targets even if specific geometries are required.

Table 4.10. Summary of the best reactions within each strategy to be compared to each other.

Strategy-	Advantages	Disadvantages
Nucleophilic Ring *4.2.2. Transmetalation* Swenton and coworkers Electrolysis and Lithium Organocuprate (Raynolds, Manning et al. 1977, Chenard, Manning et al. 1980)	-Unique use of electrolysis as a protection method -High yields for all reported steps (≥ 85%) -Regiocontrol through lithium bromide exchange -Stereoretention of α-isoprene double bond (< 5% *Z* alkene estimated) -Deprotection of bisketals to menaquinone ring structure via hydrolysis, no oxidation required	-Lithium organocuprate nucleophile only used one of two bisketal rings—poor atom economy -Difficult purification because of unreacted starting materials -5 step synthesis (not including starting material)
Metal-Mediated *4.3.2. Coordination Complex* Liebeskind et al. Cobalt Complex Cycloaddition (Liebeskind, Baysdon et al. 1986)	-High yields (> 86%) -Simple coordination complex synthesis required using commercially available materials -The regiochemistry of the system is controlled by the alkynes **43a** and **43b** -1 step synthesis (not including catalyst)	-The authors did not address α-isoprene double bonds isomerization
Electrophilic Ring *4.4.1. 1,2- vs 1,4-Addition* Naruta and Maruyuma Organostannane Michael Addition (Maruyama and Naruta 1978, Naruta 1980)	-Stereoretention of the α-isoprene double bond	-Low yields for both formations (30–48%) -Prominent competition between C2 and C3 alkylation

Pericyclic *4.5.1. Diels-Adler* Rüttimann et al. Auxiliary-Directed Diels-Alder (Rüttimann 1986)	-Uses commercially available starting materials (menadione and cyclopentadiene) -High regiocontrol through adduct **66** -Stereoretention of α-isoprene double bond -Cyclopentadiene can be recycled -High yields throughout the synthesis (≥ 90%)	-Slight competition between C-alkylation and O-alkylation
Homologation & Side Chain Extensions *4.6.1. Homologation* Lipshutz et al. Homologation to Negishi Cross-Coupling (Lipshutz, Kim et al. 1998)	-High yields throughout the synthesis (87–93%) -Method is applicable to a wide scope of benzo- and naphthoquinones -Stereochemistry of the α-isoprene double bond is defined by the configuration of the organoalane -Regiocontrolled by the installation of the chloromethyl group at the C3 position -No extraneous coordination complex synthesis required	-Requires the use of hydrogen chloride gas

References

Abe, T., S. Ozaki, D. Ueda and T. Sato (2020). "Insight into Isoprenoid Biosynthesis by Functional Analysis of Isoprenyl Diphosphate Synthases from Mycobacterium vanbaalenii and Mycobacterium tuberculosis." ChemBioChem **21**: 1-9.

Almquist, H. J. and A. A. Klose (1939). "SYNTHETIC AND NATURAL ANTIHEMORRHAGIC COMPOUNDS." J. Am. Chem. Soc. **61**(9): 2557-2558.

Araki, S., N. Katsumura and Y. Butsugan (1991). "Allylation of quinones by allylic indium reagents." J. Organomet. Chem. **415**(1): 7-24.

Bahuguna, A. and D. S. Rawat (2020). "An overview of new antitubercular drugs, drug candidates, and their targets." Med. Res. Rev. **40**(1): 263-292.

Ballester, P., M. Capo, X. Garcias and J. M. Saá (1993). "Synthesis of prenylated quinones by the oxidative degradation approach. Birch vs vinylogous Birch hydrogenolysis (BIHY vs VIBIHY) in controlling 2.DELTA. stereochemistry of the prenyl chain." J. Org. Chem. **58**(2): 328-334.

Ballester, P., J. Saá and M. Capo (1990). "PRENYLATION OF AROMATICS. LITHIUM-AMMONIA REDUCTION OF 0-SILYLATED TERTIARY CINNAMYL ALCOHOLS." Tetrehedron Lett. **31**(9): 1339-1342.

Bentley, R. and R. Meganathan (1982). "Biosynthesis of Vitamin K (Menaquinone) in Bacteria." Microbiol. Rev. **46**(3): 241-280.

Bergdoll, L., F. Ten Brink, W. Nitschke, D. Picot and F. Baymann (2016). "From low- to high-potential bioenergetic chains: Thermodynamic constraints of Q-cycle function." Biochim. Biophys. Acta **1857**(9): 1569-1579.

Binkley, S. B., L. C. Cheney, W. F. Holcomb, R. W. McKee, S. A. Thayer, D. W. MacCorquodale and E. A. Doisy (1939). "THE CONSTITUTION AND SYNTHESIS OF VITAMIN K_1." J. Am. Chem. Soc. **61**(9): 2558-2559.

Büchi, G. and A. Rüttimann (1986). Process For The Manufacture of Quinone Derivatives. United States of America, Hoffmann-La Roche, Inc.

Chadar, D., M. Camilles, R. Patil, A. Khan, T. Weyhermüller and S. Salunke-Gawali (2015). "Synthesis and characterization of n-alkylamino derivatives of vitamin K3: Molecular structure of 2-propylamino-3-methyl-1,4-naphthoquinone and antibacterial activities." J. Mol. Struct. **1086**: 179-189.

Chenard, B. L., M. J. Manning, P. W. Raynolds and J. S. Swenton (1980). "Organocopper chemistry of quinone bisketals. Application to the synthesis of isoprenoid quinone systems." J. Org. Chem. **45**(3): 378-384.

Cockayne, S., J. Adamson, S. Lanham-New, M. J. Shearer, S. Gilbody and D. J. Torgerson (2006). "Vitamin K and the Prevention of Fractures." Arch. Intern. Med. **166**(12): 1256-1261.

Collins, M. D. and D. Jones (1981). "Distribution of Isoprenoid Quinone Structural Types in Bacteria and Their Taxonomic Implications." Microbiol. Rev. **45**(2): 316-354.

Coman, S. M., V. I. Parvulescu, S. Wuttke and E. Kemnitz (2010). "Synthesis of Vitamin K_1 and K_1-Chromanol by Friedel–Crafts Alkylation in Heterogeneous Catalysis." ChemCatChem **2**(1): 92-97.

Conly, J. and K. Stein (1992). "The production of menaquinones (vitamin K2) by intestinal bacteria and their role in maintaining coagulation homeostasis." Prog Food Nutr Sci **16**(4): 307-343.

Coppa, F., F. Fontana, F. Minisci, M. C. Nogueira and E. Vismara (1991). "Homolytic Alkylation of Naphthoquinone and Methyl-Naphthoquinone. Enthalpic, Steric, and Polar Effects." Tetrahedron **47**(35): 7347-7352.

Daines, A. M., R. J. Payne, M. E. Humphries and A. D. Abell (2003). "The Synthesis of Naturally Occurring Vitamin K and Vitamin K Analogues." Curr. Org. Chem. **7**: 1-15.

Debnath, J., S. Siricilla, B. Wan, D. C. Crick, A. J. Lenaerts, S. G. Franzblau and M. Kurosu (2012). "Discovery of selective menaquinone biosynthesis inhibitors against Mycobacterium tuberculosis." J. Med. Chem. **55**(8): 3739-3755.

Dötz, K. H. (1984). "Carbenkomplexe in der Organischen Synthese." Angew. Chem. **96**(8): 573-594.

Dötz, K. H., I. Pruskil and I. Muhlemeier (1982). "Vitamin-Synthesen mit Carben-Komplexen, II. Carbonyl(carben)-Komplex-induzierte Synthese von Vitaminen der K1- und K2-Reihe." Chem. Ber. **115**: 1278.

Dryhurst, G., K. M. Kadish, F. Scheller and R. Renneberg (1982). Biological Electrochemistry, Academic Press.

Dunphy, P. J. and A. F. Brodie (1971). [233] The structure and function of quinones in respiratory metabolism. Methods Enzymol., Elsevier. **18:** 407-461.

Epand, R. M., C. Walker, R. F. Epand and N. A. Magarvey (2016). "Molecular mechanisms of membrane targeting antibiotics." Biochim. Biophys. Acta **1858**(5): 980-987.

Evans, D. A. and J. M. Hoffman (1976). "Regiospecific quinone isoprenylation. Examples of remarkably facile [3,3] sigmatropic processes." J. Am. Chem. Soc. **98**(7): 1983-1984.

Ferreira, V. F., V. Ferreira, C. Nicoletti, P. Ferreira, D. Futuro and F. da Silva (2016). "Strategies for Increasing the Solubility and Bioavailability of Anticancer Compounds: β-Lapachone and Other Naphthoquinones." Curr. Pharm. Des. **22**(39): 5899-5914

Fieser, L. F. (1939). "Synthesis of Vitamin K_1." J. Am. Chem. Soc. **61**(12): 3467-3475.

Fieser, L. F., W. P. Campbell and E. M. Fry (1939). "Synthesis of Quinones Related to Vitamins K_1 and K_2." J. Am. Chem. Soc. **61**(8): 2206-2218.

Fieser, L. F., W. P. Campbell, E. M. Fry and M. D. Gates (1939). "SYNTHETIC APPROACH TO VITAMIN K1." J. Am. Chem. Soc. **61**(9): 2559-2559.

Garcias, X., P. Ballester, M. Capo and J. M. Saá (1994). "2.DELTA.-Stereocontrolled Entry to (E)- or (Z)-Prenyl Aromatics and Quinones. Synthesis of Menaquinone-4." J. Org. Chem. **59**(17): 5093-5096.

Gengenbacher, M. and S. H. Kaufmann (2012). "Mycobacterium tuberculosis: success through dormancy." FEMS Microbiol. Rev. **36**(3): 514-532.

Godschalx, J. P. and J. K. Stille (1983). "Cross-coupling reaction of allyl bromides with organotin reagents catalyzed by zinc chloride." Tetrahedron Lett. **24**(18): 1905-1908.

Gómez-Murcia, V., A. Torrecillas, A. M. de Godos, S. Corbalán-García and J. C. Gómez-Fernández (2016). "Both idebenone and idebenol are localized near the lipid–water interface of the membrane and increase its fluidity." Biochim. Biophys. Acta, Biomembr. **1858**(6): 1071-1081.

Guin, P. S., S. Das and P. C. Mandal (2011). "Electrochemical Reduction of Quinones in Different Media: A Review." Int. J. Electrochem. **2011**: 1-22.

Hirschmann, R., R. Miller and N. L. Wendler (1954). "The Synthesis of Vitamin K1." J. Am. Chem. Soc. **76**(18): 4592-4594.

Ingles, D. P., J. B. Cruz Rodriguez and H. Garcia (2020). "Supplemental Vitamins and Minerals for Cardiovascular Disease Prevention and Treatment." Curr. Cardiol. Rep. **22**(4): 1-8.

Ishihara, M. and H. Sakagami (2007). "QSAR of Molecular Structure and Cytotoxic Activity of Vitamin K2 Derivatives with Concept of Absolute Hardness." Anticancer Res. **27**: 4059-4064.

Isler, O. (1943). Process for Producing Condensation Products of 1,4-Naphthohydroquinones. United States of America**:** 1.

Isler, O. and K. Doebel (1954). "Synthesen in der Vitamin-K-Reihe I. Über totalsynthetisches Vitamin K $_1$." Helv. Chim. Acta **37**(1): 225-233.

Jacobsen, N. and K. Torssell (1972). "Radikalische Alkylierung von Chinonen: Erzeugung von Radikalen in Redoxreaktionen." Liebigs Ann. **763**(1): 135-147.

Jacobsen, N. and K. Torssell (1973). "Synthesis of Naturally Occuring Quinones: Alkylation with the Silver Ion-Peroxydisulphite-Carboxylic Acid System." Acta Chem. Scand. **27**: 3211-3216.

Jaworski, J. S., E. Leniewska and M. K. Kalinowski (1979). "Solvent Effect on the Redox Potential of Quinone-Semiquinone Systems." J. Electroanal. Chem. Interfacial Electrochem **105**(2): 329-334.

Karamzad, N., V. Maleki, K. Carson-Chahhoud, S. Azizi, A. Sahebkar and B. P. Gargari (2020). "A systematic review on the mechanisms of vitamin K effects on the complications of diabetes and pre-diabetes." Biofactors **46**(1): 21-37.

Kathawate, L., P. V. Joshi, T. K. Dash, S. Pal, M. Nikalje, T. Weyhermüller, V. G. Puranik, V. B. Konkimalla and S. Salunke-Gawali (2014). "Reaction between lawsone and aminophenol derivatives: Synthesis, characterization, molecular structures and antiproliferative activity." J. Mol. Struct. **1075**: 397-405.

Kaurola, P., V. Sharma, A. Vonk, I. Vattulainen and T. Rog (2016). "Distribution and dynamics of quinones in the lipid bilayer mimicking the inner membrane of mitochondria." Biochim. Biophys. Acta **1858**(9): 2116-2122.

Klose, A. A. and H. J. Almquist "Synthesis of Vitamink K1." J. Biol. Chem. **132**(1): 469-471.

Koehn, J. T., C. N. Beuning, B. J. Peters, S. K. Dellinger, C. Van Cleave, D. C. Crick and D. C. Crans (2019). "Investigating Substrate Analogues for Mycobacterial MenJ: Truncated and Partially Saturated Menaquinones." Biochemistry **58**(12): 1596-1615.

Koehn, J. T., D. C. Crick and D. C. Crans (2018). "Synthesis and Characterization of Partially and Fully Saturated Menaquinone Derivatives." ACS Omega **3**(11): 14889-14901.

Koehn, J. T., E. S. Magallanes, B. J. Peters, C. N. Beuning, A. A. Haase, M. J. Zhu, C. D. Rithner, D. C. Crick and D. C. Crans (2018). "A Synthetic Isoprenoid Lipoquinone, Menaquinone-2, Adopts a Folded Conformation in Solution and at a Model Membrane Interface." J. Org. Chem. **83**(1): 275-288.

Kroppenstedt, R. M. and W. Mannheim (1989). "Lipoquinones in Members of the Family Pasteurellaceae." Int. J. Syst. Bacteriol. **39**(3): 304-308.

Kumar, S., J. T. Koehn, M. Gonzalez-Juarrero, D. C. Crans and D. C. Crick (2020). "Mycobacterium tuberculosis survival in J774A.1 cells is dependent on MenJ moonlighting activity, not its enzymatic activity." ACS Infect. Dis. **Just Accepted Manuscript**.

Kurosu, M. and E. Begari (2010). "Vitamin K2 in electron transport system: are enzymes involved in vitamin K2 biosynthesis promising drug targets?" Molecules **15**(3): 1531-1553.

Liebeskind, L. S., S. L. Baysdon, V. Goedken and R. Chidambaram (1986). "Phthaloylcobalt complexes in synthesis. Ligand modifications leading to a practical naphthoquinone synthesis." Organometallics **5**(6): 1086-1092.

Liebeskind, L. S., S. L. Baysdon and M. S. South (1980). "An organotransition-metal synthesis of naphthoquinones." J. Am. Chem. Soc. **102**(24): 7397-7398.

Liebeskind, L. S. and B. S. Foster (1990). "Stannylquinones. Synthesis and utilization as quinone carbanion synthetic equivalents." J. Am. Chem. Soc. **112**(23): 8612-8613.

Lindlar, H. (1953). Verfahren zur Herstellung von Kondensationsprodukten. Switzerland.

Lipshutz, B. H., S.-k. Kim and P. Mollard (1998). "An Expeditious Route to COQn, Vitamins K1 and K2, and Related Allylated para-Quinones Utilizing Ni(0) Catalysis." Tetrahedron **54**: 1241-1253.

Mahdinia, E., A. Demirci and A. Berenjian (2017). "Production and application of menaquinone-7 (vitamin K2): a new perspective." World J. Microbiol. Biotechnol. **33**(2): 1-7.

Mal, D., K. Ghosh and S. Jana (2015). "Synthesis of Vitamin K and Related Naphthoquinones via Demethoxycarbonylative Annulations and a Retro-Wittig Rearrangement." Org. Lett. **17**(23): 5800-5803.

Maruyama, K. and Y. Naruta (1978). "Synthesis of naturally occurring quinones. Part 3. Allylation of quinones with allyltin reagents. New synthesis of coenzyme Q1 and plastoquinone-1." J. Org. Chem. **43**(19): 3796-3798.

Masaki, Y., K. Hasimoto and K. Kaji (1984). "Synthetic Studies of Isoprenoidquinones II. Syntheses of Ubiquinone-10, Phylloquinone, and Menaquinone-4 by a Chain-Extending Method Utilizing Terminally Functionalized Isoprenoidhydroquinones." Chem. Pharm. Bull. **32**(10): 3959-3967.

Masaki, Y., K. Hasimoto, K. Sakuma and K. Kaji (1984). "Synthetic Studies on Isoprenoidquinones. I. A Facile Regio- and Stereocontrolled Synthesis." Chem. Pharm. Bull. **32**(10): 3952-3958.

Matsushita, H. and E. Negishi (1984). "PALLADIUM-CATALYZED SYNTHESIS OF 1,4-DIENES BY ALLYLATION OF ALKENYLALANES: α-FARNESENE." Org. Synth. **62**: 31-37.

Mehta, D. S., P. Mohan, M. Shastri and T. Reid (2015). Method of Preparation of Stereospecific Quinone Derivatives. United States of America.

Min, J.-H., J.-S. Lee, J.-D. Yang and S. Koo (2003). "The Friedel−Crafts Allylation of a Prenyl Group Stabilized by a Sulfone Moiety: Expeditious Syntheses of Ubiquinones and Menaquinones." J. Org. Chem. **68**(20): 7925-7927.

Nakagawa, K., Y. Hirota, N. Sawada, N. Yuge, M. Watanabe, Y. Uchino, N. Okuda, Y. Shimomura, Y. Suhara and T. Okano (2010). "Identification of UBIAD1 as a novel human menaquinone-4 biosynthetic enzyme." Nature **468**(7320): 117-121.

Naruta, Y. (1980). "Allylation of quinones with allyltin reagents." J. Am. Chem. Soc. **102**(11): 3774-3783.

Naruta, Y. (1980). "Regio- and stereoselective synthesis of coenzymes Qn (n = 2-10), vitamin K, and related polyprenylquinones." J. Org. Chem. **45**(21): 4097-4104.

Negishi, E. (1981). "Bimetallic catalytic systems containing Ti, Zr, Ni, and Pd. Their applications to selective organic syntheses." Pure Appl. Chem. **53**(12): 2333-2356.

Negishi, E., D. E. Van Horn and T. Yoshida (1985). "Controlled carbometalation. 20. Carbometalation reaction of alkynes with organoalene-zirconocene derivatives as a route to stereo-and regiodefined trisubstituted alkenes." J. Am. Chem. Soc. **107**(23): 6639-6647.

Prince, R. C., P. L. Dutton and J. M. Bruce (1983). "Menaquinones and plastoquinones in aprotic solvents." FEBS Lett. **160**(1,2): 273-276.

Quinn, P. J. and M. A. Esfahani (1980). "Ubiquinones have Surface-Active Properties Suited to Transport Electrons and Protons Across Membranes." Biochem. J. **185**: 715-722.

Raynolds, P. W., M. J. Manning and J. S. Swenton (1977). "Utilization of quinone bisacetal organocopper compounds in the synthesis of isoprenoid systems." ChemComm(14): 499-500.

Roche, Y., P. Peretti and S. Bernard (2007). "The Redox State Influences the Interactions of Ubiquinones with Phospholipid Bilayers: A DSC Study." J. Therm. Anal. Calorim. **89**(3): 867-873.

Rüttimann, A. (1986). "Recent Advances in the Synthesis of K-Vitamins." Chimia **40**(9): 290-306.

Sato, K., S. Inoue and K. Saito (1973). "A New Synthesis of Vitamin K via π-Allylnickel Intermediates." J. Chem. Soc. Perkin Trans. I: 2289-2293.

Schmid, R., S. Antoulas, A. Rüttimann, M. Schmid, M. Vecchi and H. Weiserb (1990). "Synthesis of All Four Stereoisomers of (E)-Vitamin KT (Phylloquinone), Analysis of Their Diastereoisomeric and Enantiomeric Purities and Determination of Their Biopotencies." Helv. Chim. Acta **73**(5): 1276-1299.

Scholz, G., C. Stosiek, M. Feist and E. Kemnitz (2012). "Magnesium Hydroxide Fluorides - New Materials with Adjustable Composition and Properties." Eur. J. Inorg. Chem. **2012**(14): 2337-2340.

Schurgers, L. J., K. J. Teunissen, K. Hamulyak, M. H. Knapen, H. Vik and C. Vermeer (2007). "Vitamin K-containing dietary supplements: comparison of synthetic vitamin K1 and natto-derived menaquinone-7." Blood **109**(8): 3279-3283.

Simes, D. C., C. S. B. Viegas, N. Araujo and C. Marreiros (2020). "Vitamin K as a Diet Supplement with Impact in Human Health: Current Evidence in Age-Related Diseases." Nutrients **12**(1): 138.

Siricilla, S., K. Mitachi, K. Skorupinska-Tudek, E. Swiezewska and M. Kurosu (2014). "Biosynthesis of a water-soluble lipid I analogue and a convenient assay for translocase I." Anal. Biochem. **461**: 36-45.

Snyder, C. D. and H. Rapoport (1974). "Synthesis of menaquinones." J. Am. Chem. Soc. **96**(26): 8046-8054.

Tabushi, I., K. Fujita and H. Kawakubo (1977). "One-step preparation of vitamin K1 or K2 analogs by cyclodextrin inclusion catalysis." J. Am. Chem. Soc. **99**(19): 6456-6457.

Tabushi, I., K. Yamamura, K. Fujita and H. Kawakubo (1979). "Specific inclusion catalysis by .beta.-cyclodextrin in the one-step preparation of vitamin K1 or K2 analogs." J. Am. Chem. Soc. **101**(4): 1019-1026.

Tarento, T. D. C., D. D. McClure, A. M. Talbot, H. L. Regtop, J. R. Biffin, P. Valtchev, F. Dehghani and J. M. Kavanagh (2019). "A potential biotechnological process for the sustainable production of vitamin K1." Crit. Rev. Biotechnol. **39**(1): 1-19.

Tetali, S. D. (2019). "Terpenes and isoprenoids: a wealth of compounds for global use." Planta **249**(1): 1-8.

Tishler, M., L. F. Fieser and N. L. Wendler (1940). "Nature of the By-product in the Synthesis of Vitamin K $_1$." J. Am. Chem. Soc. **62**(8): 1982-1991.

Troll, T. and K. Schmid (1984). "Darstellung und reaktionen von 1,3-bis-(trimethylsiloxy)-isobenzofuranen." Tetrahedron Lett. **25**(28): 2981-2984.

Tso, H.-H. and Y.-J. Chen (1995). "A convenient one-flask synthesis of vitamin K." J. Chem. Res. Synop. **3**: 104-105.

Turner, M. E., M. A. Adams and R. M. Holden (2018). "The Vitamin K Metabolome in Chronic Kidney Disease." Nutrients **10**(8): 1-9.

Upadhyay, A., F. L. Fontes, M. Gonzalez-Juarrero, M. R. McNeil, D. C. Crans, M. Jackson and D. C. Crick (2015). "Partial Saturation of Menaquinone in *Mycobacterium tuberculosis* : Function and Essentiality of a Novel Reductase, MenJ." ACS Cent. Sci. **1**(6): 292-302.

Upadhyay, A., S. Kumar, S. A. Rooker, J. T. Koehn, D. C. Crans, M. R. McNeil, J. S. Lott and D. C. Crick (2018). "Mycobacterial MenJ: An Oxidoreductase Involved in Menaquinone Biosynthesis." ACS Chem. Biol. **13**(9): 2498-2507.

Van Horn, D. E. and E. Negishi (1978). "Selective carbon-carbon bond formation via transition metal catalysts. 8. Controlled carbometalation. Reaction of acetylenes with organoalane-zirconocene dichloride complexes as a route to stereo- and regio-defined trisubstituted olefins." J. Am. Chem. Soc. **100**(7): 2252-2254

Vilcheze, C., T. Hartman, B. Weinrick, P. Jain, T. R. Weisbrod, L. W. Leung, J. S. Freundlich and W. R. Jacobs, Jr. (2017). "Enhanced respiration prevents drug tolerance and drug resistance in Mycobacterium tuberculosis." Proc. Natl. Acad. Sci. U. S. A. **114**(17): 4495-4500.

Wuttke, S., S. M. Coman, G. Scholz, H. Kirmse, A. Vimont, M. Daturi, S. L. M. Schroeder and E. Kemnitz (2008). "Novel Sol-Gel Synthesis of Acidic MgF2−x(OH)x Materials." Chem. Eur. J. **14**(36): 11488-11499.

Yamago, S., M. Hashidume and J.-i. Yoshida (2000). "Radical-Mediated Synthesis of Substituted Quinones with Organotellurium Compounds." Chem. Lett. **29**(11): 1234-1235.

Yamago, S., M. Hashidume and J.-i. Yoshida (2002). "A new synthetic route to substituted quinones by radical-mediated coupling of organotellurium compounds with quinones." Tetrahedron **58**(34): 6805-6813.

Yoshizawa, T., H. Toyofuku, K. Tachibana and T. Kuroda (1982). "REGIOSELECTIVE POLYPRENYL REARRANGEMENT OF POLYPRENYL 2,3,4,5-TETRASUBSTITUTED PHENYL ETHERS PROMOTED BY BORON TRIFLUORIDE." Chem. Lett. **11**(8): 1131-1134.

Zacconi, F. C., O. N. Nuñez, A. L. Cabrera, L. M. Valenzuela, J. M. del Valle and J. C. de la Fuente (2016). "Synthesis and solubility measurement in supercritical carbon dioxide of two solid derivatives of 2-methylnaphthalene-1,4-dione (menadione): 2-(Benzylamino)-3-methylnaphthalene-1,4-dione and 3-(phenethylamino)-2-methylnaphthalene-1,4-dione." J. Chem. Thermodyn. **103**: 325-332.

Zhang, C., D. Wu and H. Ren (2020). "Economical production of vitamin K2 using crude glycerol from the by-product of biodiesel." Sci. Rep. **10**(1): 1-8.

Chapter 5:
Exploratory Synthesis of Menaquinone Derivatives

5.1. Introduction

As described in Chapter 4, there are numerous reported syntheses of naphthoquinone derivatives. The majority of the literature concerns the synthesis of vitamin K_1 and vitamin K_2, a family of molecules essential for human health (Simes, Viegas et al. 2020). There have been many reported syntheses of the full-length, native naphthoquinone derivatives, such as MK-9 and UQ-10 (Figure 5.1A). There are fewer reports of the truncated derivatives, such as MK-1, MK-2 (**1**), and MK-3 (Figure 5.1B). Biological assays of MK-derivatives require complete dissolution of the

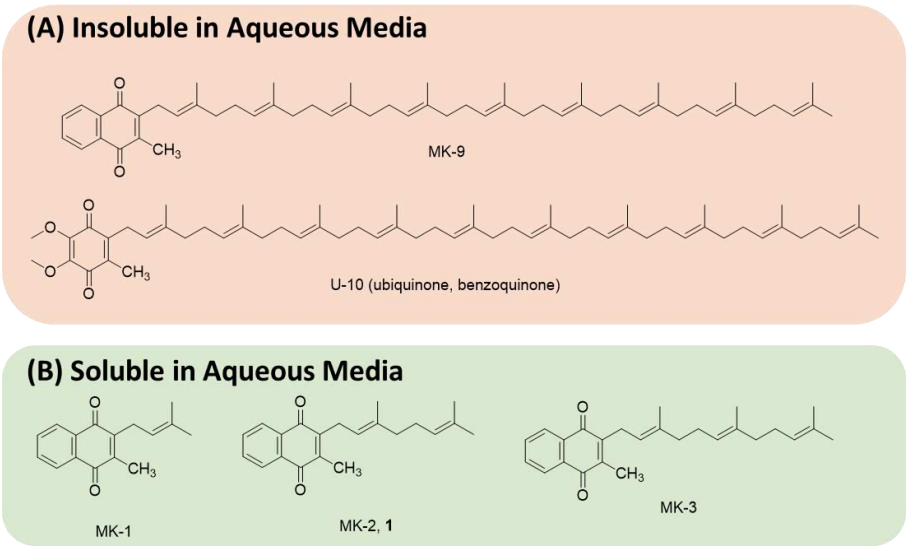

Figure 5.1. Structures of select lipoquinones derivatives. (A) The long-chain, native lipoquinone derivatives are insoluble in aqueous media. (B) Truncated lipoquinone derivatives, such as the picture MK-derivatives, are more soluble in aqueous media.

molecules. In a recent study, MK-derivatives with 1-9 isoprene units were investigated for their anticancer activities (Ishihara and Sakagami 2007). Only MK-1 through MK-4 showed any anticancer activity, and MK-5 through MK-9 showed no biological activity which led to the

assumption that they are not suitable for anticancer applications. In reality, the longer chain MK-derivatives were simply too hydrophobic to dissolve in aqueous media. Long-chain native lipoquinone derivatives are very hydrophobic (Chapter 2, Section 2.2.1) causing them to be insoluble in aqueous media (Figure 5.1A). Instead, researchers have turned to using truncated MK-derivatives, like MK-2 which are more soluble in aqueous conditions (Figure 5.1B).

Currently, the most popular method to synthesize truncated MK-derivatives is through Friedel-Crafts alkylation. At its shortest, the route consists of a 2 step sequence with easy to set up techniques. The accessibility has led to its popularity to synthesize MK-derivatives for biology-focused studies. In such studies, the syntheses were likely performed by a non-chemist researcher. The use of this method was established in the Crans group by Dr. Jordan T. Koehn, a recent Ph.D. graduate of the lab. Using Friedel-Crafts alkylation and a radical alkylation, the syntheses of MK-1 (Koehn, Beuning et al. 2019), MK-2 (**1**) (Koehn, Magallanes et al. 2018) and a series of other partially or fully saturated MK-derivatives (Koehn, Crick et al. 2018) were achieved. In general, this route begins with the reduction of menadione (**2**) in the presence of 10% $Na_2S_2O_4$ to form menadiol (**3)** (Figure 5.2). At this point, the alkylation of the headgroup depends on the identity of the sidechain. For example, the synthesis of MK-2 **(1)** was achieved through the Friedel-Crafts alkylation of geraniol in the presence of BF_3-OEt_2 in 20.1% yield (Figure 5.2B) (Koehn, Magallanes et al. 2018). Alternatively, the installation of the sidechain for MK-2(II-H_2) **(4)** was carried out with isophytol and MgF_2·48 (Figure 5.2C) (Wuttke, Coman et al. 2008, Coman, Parvulescu et al. 2010, Koehn, Crick et al. 2018). Finally, the installation of non-isoprenyl alcohols occurred via a benzoyl peroxide-promoted radical reaction between the C3 position of menadione and an alkyl iodide, as shown for MK-2 (I, II-H_4) **(5)** (Figure 5.2D).(Coppa, Fontana et al. 1991, Suhara, Wada et al. 2010, Koehn, Crick et al. 2018). Although the yields were low (~10-20%), the

amount of product synthesized in these experiments was sufficient for the conformational studies performed in organic solvent and AOT-reverse micelles (Koehn, Magallanes et al. 2018, Koehn, Beuning et al. 2019).

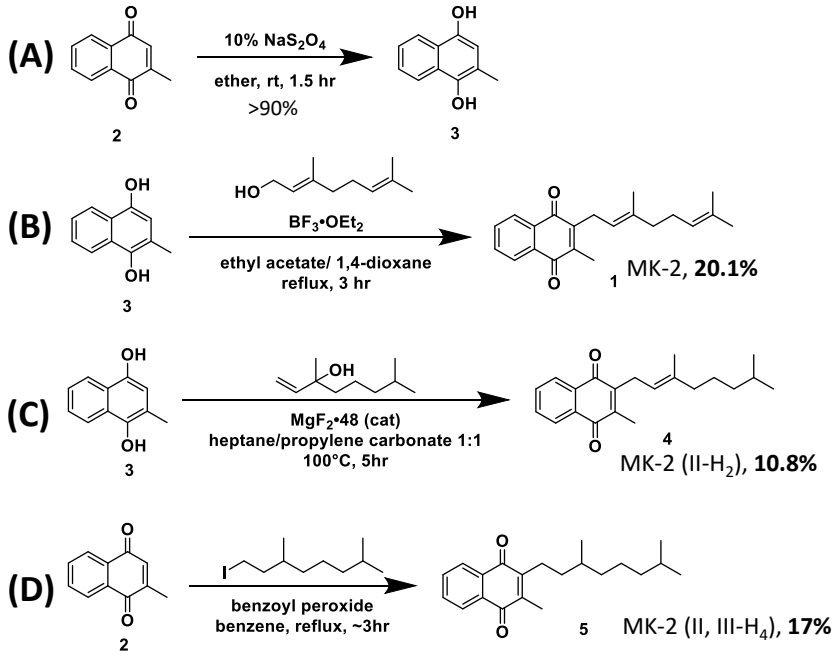

Figure 5.2. Examples of the established MK-derivative syntheses by Dr. Jordan Koehn. (A) reduction of menadione **2** to menadiol 3 (Koehn, Magallanes et al. 2018). (B) Synthesis of MK-2 (**1**) via BF_3·OEt_2-meditated Friedel-Crafts alkylation (Koehn, Magallanes et al. 2018). (C) Synthesis of MK-2(II-H_2) (**4**) via MgF_2·48-mediated Friedel-Crafts alkylation (Koehn, Crick et al. 2018). (D) Synthesis of MK-2(I,II-H_4) (**5**) via benzoyl peroxide-promoted radical reaction (Koehn, Crick et al. 2018).

In general, the Friedel-Crafts method is exceptionally low yielding because of the formation of regio- and stereoisomer byproducts. The most significant source of loss is regiochemical competition between alkylation at the C2 and C3 position on the quinone headgroup. The Lewis acid catalyst cannot discriminate between the quinone carbonyl groups to show any preference in regioselectivity. Next, the α-isoprene unit (the first isoprene unit from the headgroup) is susceptible to *E/Z* isomerization under Friedel-Crafts conditions. The formation of the carbocation electrophile is capable of rearrangement and thus isomerization from the thermodynamically favorable *E* alkene to the unfavorable *Z* alkene. Finally, the formation of an

reverse prenyl connection is also possible. It is important to note that MK-derivatives are susceptible to decomposition from exposure to light. Studies have shown UV-irradiated cells are depleted of MK-derivatives (Dunphy and Brodie 1971), and therefore, limited exposure to light in required to avoid accidental decomposition.

The trajectory of the menaquinone project within the Crans group is changing. Although we are still interested in understanding the conformation and location of menaquinones in a membrane system, we are expanding our scope to probe the structural requirements of menaquinones for prokaryotic oxidative phosphorylation. For example, studies have shown that coupled oxidative phosphorylation could be restored in membranes that had been depleted of native naphthoquinone by the addition of exogenous MK-derivatives (Dunphy and Brodie 1971). MK-derivatives capable of restoring both oxidation and phosphorylation to lipoquinone depleted membranes contain a methyl group at the C2 position of the naphthyl rings and at least one isoprene unit in the C3 position (orange areas in Figure 5.3) (Dunphy and Brodie 1971). In addition, at least one unsaturated isoprene unit in the *E*-configuration (adjacent to the naphthyl rings, like the α-isoprene) is required in the sidechain for oxidation and phosphorylation to proceed normally. If the first isoprene unit is saturated or in the *Z*-configuration, oxidation is uncoupled from phosphorylation (blue and green areas in Figure 5.3) (Brodie 1961). There appears to be no reports of eubacteria with saturation in the α-isoprene unit adjacent to the naphthyl ring system. In addition, substitution of either the C2 or C3 functional groups with other non-isoprenyl

substituents also fails to restore phosphorylation but were still capable of restoring oxidation (orange area in Figure 5.3) (Dunphy and Brodie 1971).

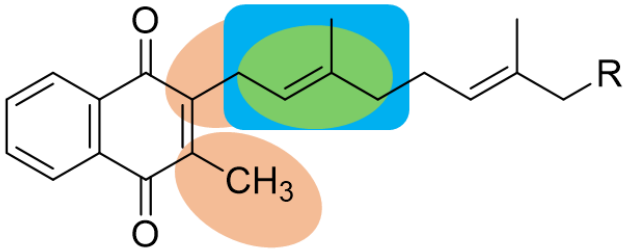

MK Characteristic	Restores Only Oxidation	Uncouples Oxidation & Phosphorylation	Restores Oxidation & Phosphorylation
C2 Methyl group			X
Any other substituents at C2/C3	X		
Unsaturated α-Isoprene Unit			X
Saturated α-Isoprene Unit		X	
E Configuration of α-Isoprene			X
Z Configuration of α-Isoprene		X	

Figure 5.3. Structural requirements for restoring oxidation, uncoupling of oxidation from phosphorylation, and restoring oxidation and phosphorylation (Brodie 1963, Dunphy and Brodie 1971). The orange areas are the headgroup substituent requirements. The blue area is the degree of saturation of the α-isoprene unit, and the green area is the configuration of the α-isoprene unit.

The alkene configuration of the sidechain is also important to restore both oxidation and phosphorylation. The structures of specific examples are shown in Figure 5.4 (on the next page). For example, MK-9 (II-H_2) and vitamin K_1 are MK-derivatives with α-isoprene units with *E* configurations, and they have been shown to restore oxidation and phosphorylation to a quinone-depleted system. The corresponding *Z* isomers have been found to only restore oxidation (Dunphy and Brodie 1971).

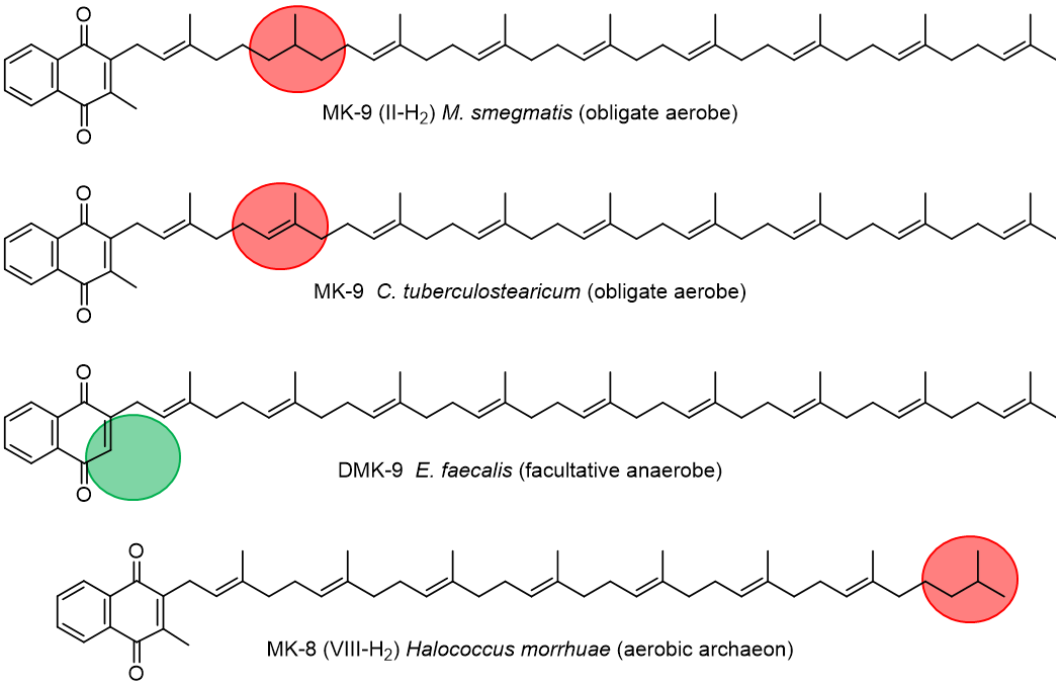

Figure 5.4. Schematic structures of MK-derivatives native to the indicated species of prokaryotes. The areas of structural variation are circled.

Of particular significance is the observation that MK-9 restores only oxidation whereas MK-9 (II-H_2) restores both oxidation and phosphorylation activities in membranes isolated from *M. phlei* (Dunphy and Brodie 1971). This suggests the presence of the saturated isoprene unit in the β-position is critical for phosphorylation in *M. phlei*. In a recent study, the gene *menJ* was found to encode for the enzyme MenJ in *M. tuberculosis* and *M. smegmatis* (Upadhyay, Fontes et al. 2015). MenJ converts MK-9 to MK-9(II-H_2) by hydrogenating the β-isoprene unit of the sidechain. This study also demonstrated that disruption of *menJ* results in a 3-fold reduction of electron transport efficiency (Upadhyay, Fontes et al. 2015).

In addition to the structural requirements of the sidechain, the substituents on the naphthoquinone headgroup are also significant. A study has shown that an inhibitor of *M. tuberculosis* demethylmenaquinone methyltransferase, an enzyme that converts demethyl-MK to MK, is bactericidal (Figure 5.4)(Sukheja, Kumar et al. 2017). However, the same compound does

not inhibit growth of non-tuberculous mycobacteria or *Staphylococcus aureus*, both of which synthesize MK from DMK.

Thus, it appears there are strict structural requirements necessary for the restoration of phosphorylation, whereas the requirements to restore oxidation are not as strict. To investigate the structural requirements across various species of bacteria, we want to synthesize a diverse library of truncated MK-derivatives to include both E and Z isomers of the α-isoprene unit and partially saturated sidechains at the α-, β-, and γ-isoprene positions (Figure 5.5). Saturated bonds at each position are intended to mimic the endogenous MK-derivatives with saturated units near the headgroup, in the middle of the sidechain, and at the end of the sidechain.

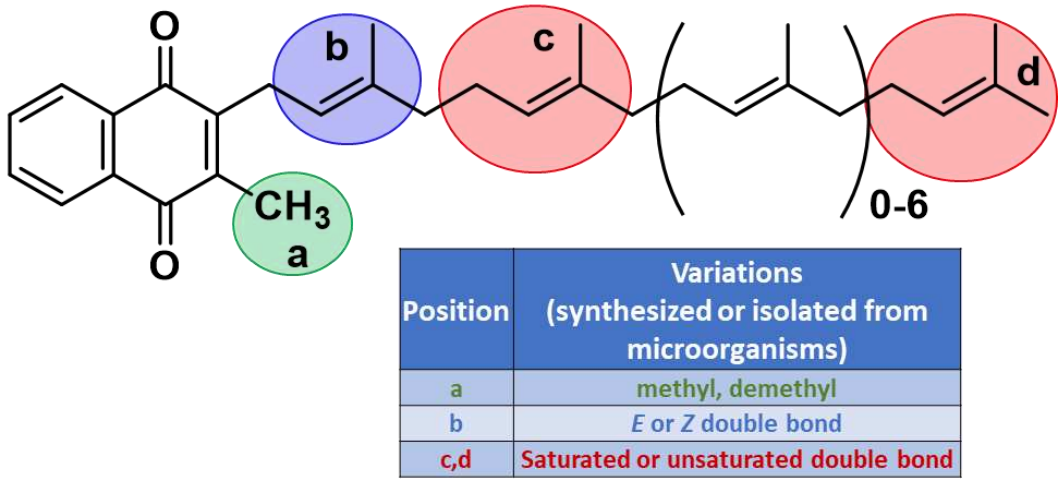

Position	Variations (synthesized or isolated from microorganisms)
a	methyl, demethyl
b	*E* or *Z* double bond
c,d	Saturated or unsaturated double bond

Figure 5.5. Structural variations of MK-derivatives that will be investigated for oxidative phosphorylation activity studies.

With this new direction in mind, using the Friedel-Crafts alkylation approach to synthesize the MK-derivatives might not be the most effective approach to achieve all derivatives in a convergent manner. In the previous perspective on the project, the Z-isomer of MK-2 was thought to be a useless byproduct. Now, having access to Z-isomers is of interest. Rather than relying on the yields of the Friedel-Crafts reaction, I designed an approach that would allow for stereopure sidechains to be coupled to the headgroup to minimize the risk of isomerization at the α-isoprene

unit and regiochemical boundaries. To overcome these pitfalls, I researched the synthetic techniques described in Chapter 4 to achieve (1) regioselective alkylation to the C3 position, (2) stereoretention of the α-isoprene unit, and (3) overall increase the yields.

In Chapter 4, Section 4.5.1, a unique Diels-Alder approach was described towards the synthesis of vitamin K_1. This approach uses an auxiliary cycloadduct between menadione and cyclopentadiene (CPD) (Figure 5.6). The formation of the menadione-cyclopentadiene cycloadduct (M-C adduct) transforms the C2/C3 sp^2 hybridized carbons into sp^3 carbona. With the

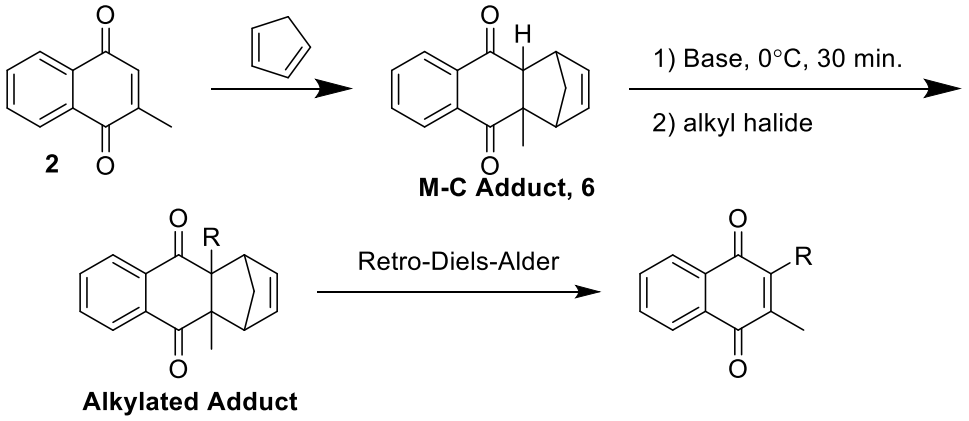

Figure 5.6. General sequence of the Diels-Alder approach to synthesizing MK-derivatives (Braasch-Turi and Crans 2020).

auxiliary group in place, the C3 position is now equipped with an acidic sp^3 C-H bond at the α-position. This sets the stage for a regioselective enolate formation between the C3 α-proton and the adjacent carbonyl group. Subsequent alkylation with an electrophilic sidechain would form a thermodynamically unstable alkylated adduct (Singh, Raju et al. 1988, Ji, Zong et al. 2003). At this point, studies have shown the tricyclic system spontaneously undergoes retro Diels-Alder, but it is promoted with heat (Singh, Raju et al. 1988, Ji, Zong et al. 2003).

Of all the methods discussed in Chapter 4, this one demonstrates the most regiocontrol with the fewest number of synthetic steps to install the isoprene sidechain. Studies have also shown the

stereochemistry of the α-isoprene unit is retained throughout the enolate alkylation to retro Diels-Alder sequence (Figure 5.6). With this in mind, a Diels-Alder approach to synthesize MK-derivatives seems to be a favorable route forward to achieve regioselectivity at the C3 position and retention of the stereochemistry of the α-isoprene unit of the sidechain.

5.2. Previous Work

My decision to pursue a Diels-Alder approach to synthesize menaquinones is supported by the synthesis of vitamin K_1 at gram scale quantities. In 1986, Rüttimann and Büchi reported a 100g scale synthesis of the cycloadduct formed between menadione **2** and cyclopentadiene, referred to as the M-C adduct **6** (Figure 5.7) (Büchi and Rüttimann 1986, Rüttimann 1986). The resulting adduct was then deprotonated with freshly prepared potassium tert-butoxide to form the corresponding enolate. Phytyl bromide was added slowly over 15 minutes at 0°C and stirred for 1 hour. The alkylated adduct **7** was then refluxed in toluene in the dark for 15 minutes to promote a retro Diels-Alder reaction to form vitamin K_1 **8** in excellent yield, >90%.

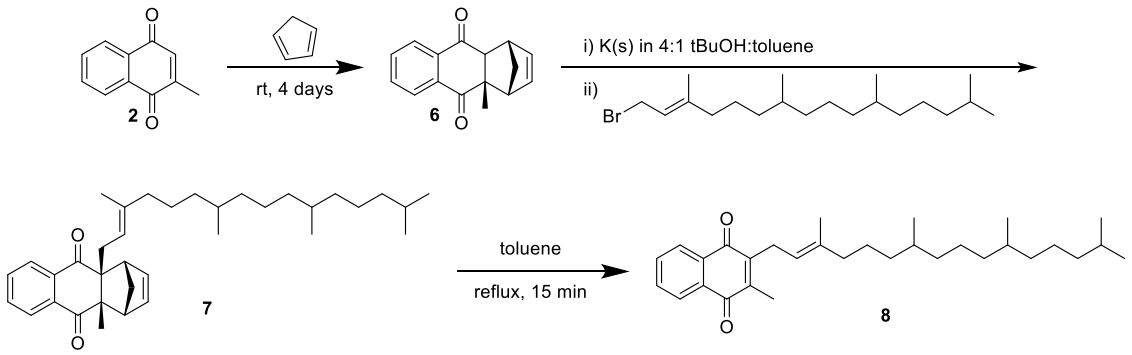

Figure 5.7. Synthesis of vitamin K_1 established by Rüttimann and Büchi (Büchi and Rüttimann 1986, Rüttimann 1986)

In 2003, Ji and coworkers reported an improved synthesis over the Rüttimann and Büchi method using micelles to catalyze the [4+2] pericyclic reaction between menadione and cyclopentadiene through the hydrophobic effect and forced proximity. Ji and coworkers were inspired by Singh and coworkers who used hexadecyltrimethylammonium bromide (CTAB, **9**) to

catalyze a Diels-Alder reaction between naphthoquinone and benzoquinone derivatives and various cyclopentadiene derivatives to generate spiro compounds along the methylene bridge of cyclopentadiene in aqueous conditions (Singh, Raju et al. 1988). The synthesis of the M-C adduct **6** is shown in Figure 5.8A. Using glacial acetic acid as a solvent instead, Ji and coworkers utilized dodecyltrimethylammonium bromide (LTAB, **10**) as the micelle catalyst to synthesize the M-C adduct in 93% yield (Figure 5.8B) (Ji, Zong et al. 2003). The enolate alkylation step followed Rüttimann and Büchi but used a different retro-Diels-Alder conditions. Instead of refluxing in toluene, the alkylated adduct **7** was dissolved in acetic acid and heated to 90°C for 15 minutes, producing vitamin K_1 **8** in 80-91% yield.

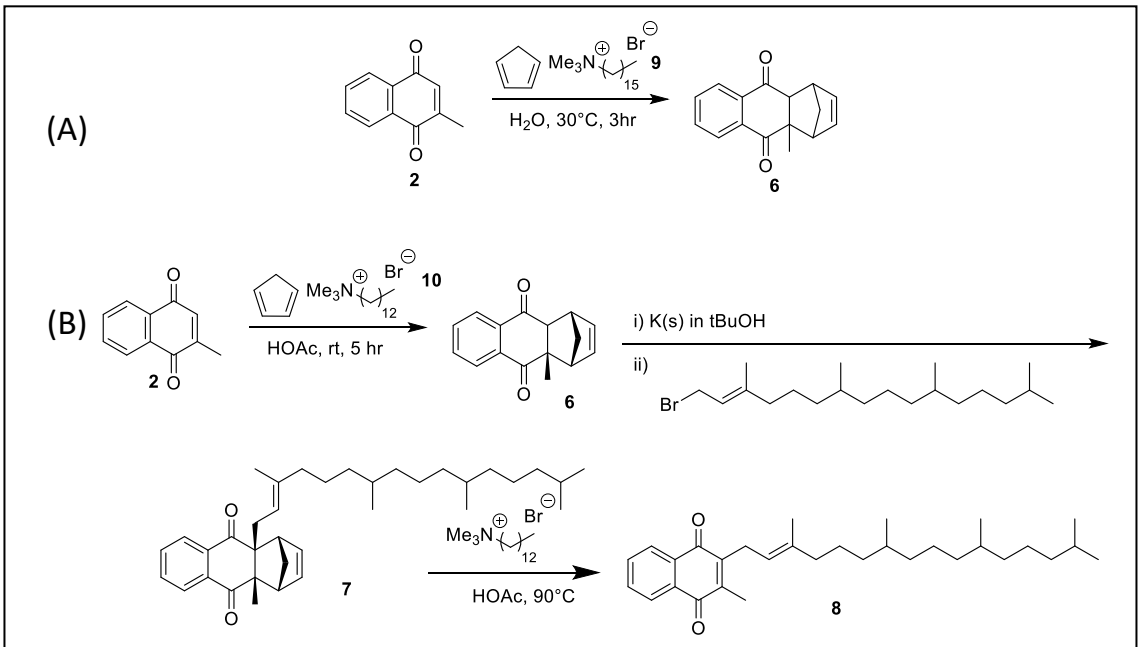

Figure 5.8. Micelle catalyzed M-C adduct formation by (A) Singh and coworkers using hexadecyltrimethylammonium bromide (CTAB) (Singh, Raju et al. 1988) and (B) the synthesis of vitamin K_1established by Ji and coworkers using dodecyltrimethylammonium bromide (LTAB) (Ji, Zong et al. 2003)

Both reports note a remarkable retention of the stereochemistry of the isoprene unit of the phytyl sidechain. Ji and coworkers synthesized vitamin K_1 with a mixture of E/Z isomers of the corresponding phytyl bromide. The ratio of geometric isomers of the phytyl bromide starting material matched the geometric ratios of the produced vitamin K_1(Ji, Zong et al. 2003). This

suggests the Diels-Alder route is suitable to maintain the stereochemistry of the desired MK-derivatives.

In addition to the synthesis of vitamin K_1, the Diels-Alder approach has been used to synthesize vitamin K_1 derivatives with diverse sidechains. Hamamura and coworkers developed a route to synthesize both naphthoquinone derivatives and MK-derivatives in a simple diverging route (Figure 5.9A) (Hamamura, Iwama et al. 1994). For example, the synthesis of both DMK-1

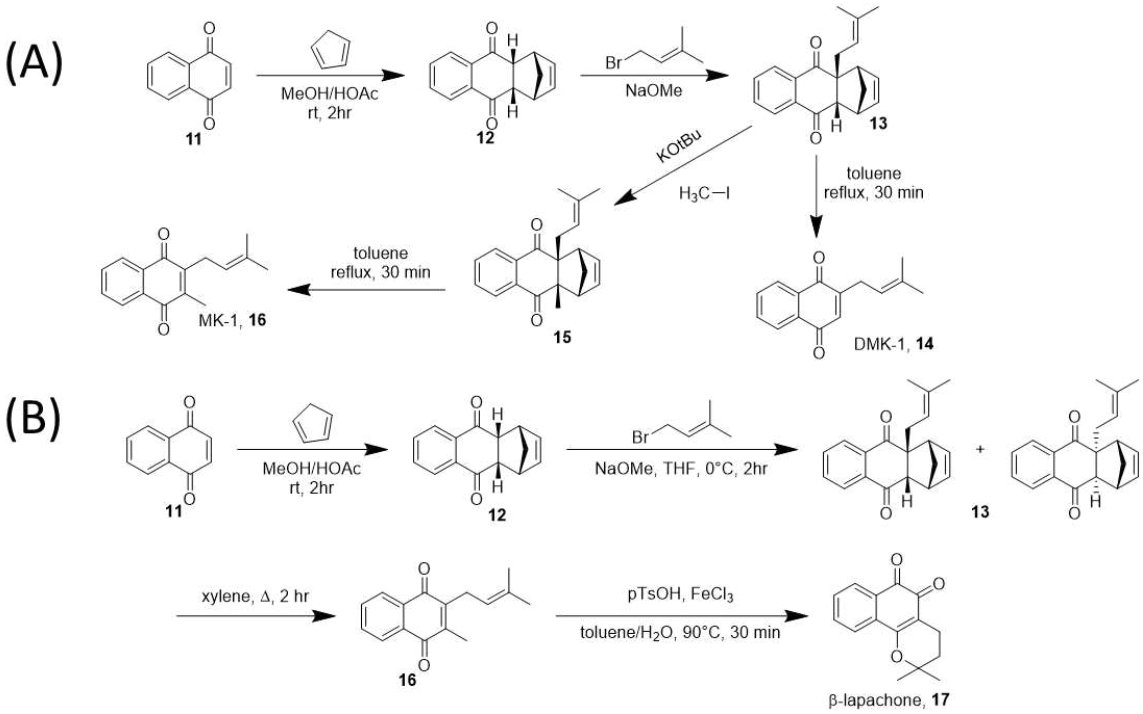

Figure 5.9. Synthesis of various vitamin K_1 derivatives using the Diels-Alder approach. (A) Example of a divergent synthesis to access DMK and MK-derivatives (Hamamura, Iwama et al. 1994). (B) Synthesis of β-lapachone (Katoh, Monma et al. 2014).

14 and MK-1 **16** would begin with forming the cycloadduct between 1,4-naphthoquinone **11** and cyclopentadiene, **12**. β-Lapachone, a vitamin K derivative (**17**), was synthesized via a cycloadduct **12** formed between 1,4-naphthoquinone and cyclopentadiene (Figure 5.9B) (Katoh, Monma et al. 2014). Therein, the enolate alkylation was achieved using sodium methoxide resulting in a diastereomeric mixture. Retro Diels-Alder was achieved through reflux in xylene.

In addition, the Diels-Alder approach has been used to attach non-isoprenyl sidechains. Teitelbaum and coworkers followed Ji and coworkers procedure to form the M-C adduct **6** and attached the sidechain to the headgroup using potassium tert-butoxide(Figure 5.10A) (Teitelbaum, Scian et al. 2015). A series of ω-oxidations to the β-isoprene unit of the sidechain created a series of vitamin K carboxylic acid metabolites for biological study (Teitelbaum, Scian et al. 2015).

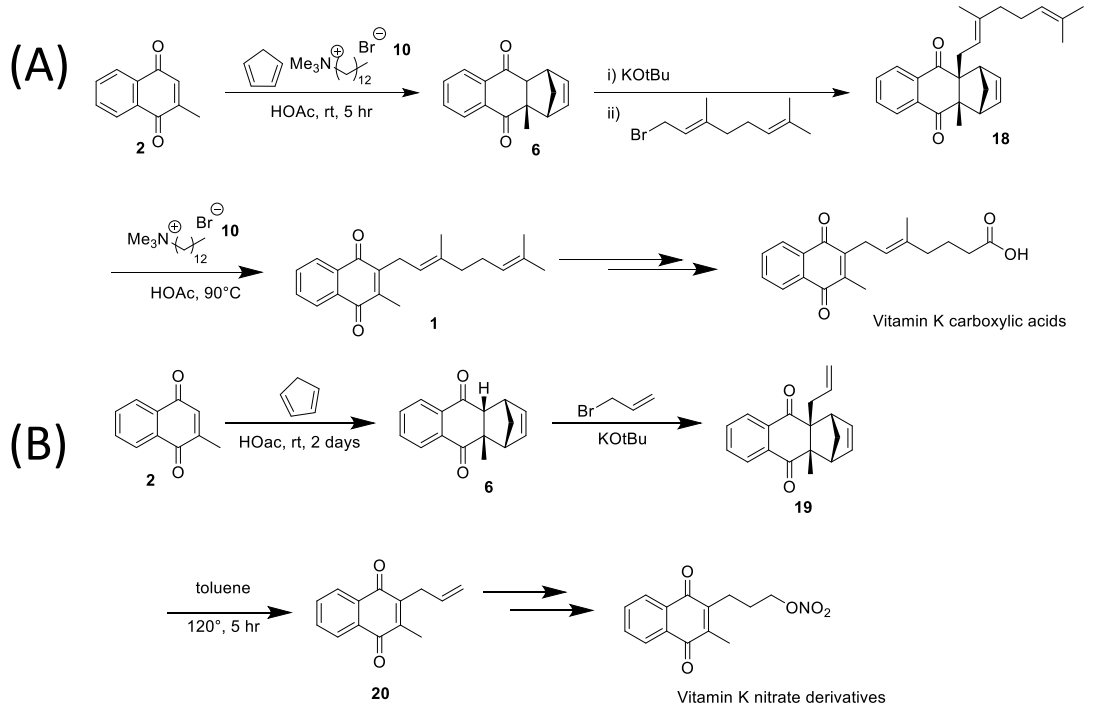

Figure 5.10. Synthesis of various vitamin K_1 derivatives using the Diels-Alder approach. (A) Synthesis of vitamin K_1 carboxylic acid derivatives (Teitelbaum, Scian et al. 2015). (B) Synthesis of vitamin K_1 nitrate derivatives (Ongini, Almirante et al. 2014).

Ongini and coworkers synthesized an allyl derivative using the Diels-Alder route to eventually synthesize a saturated sidechain with terminal nitrate substituent (Ongini, Almirante et al. 2014) (Figure 5.10B).

5.3 Retrosynthetic Analysis

A convergent synthesis was devised to access a diverse library of MK-derivatives to support the structure-activity relationship studies described in Section 5.1. The generic MK-derivative could be achieved via a convergent Diels-Alder approach in a three step sequence via the coupling of the M-C adduct (in the grey box in Figure 5.11) to the Prenyl Fragment (shown in red in Figure 5.11). The M-C adduct breaks down into commercially available menadione and cyclopentadiene, and it will be used universally to introduce the menaquinone headgroup. The

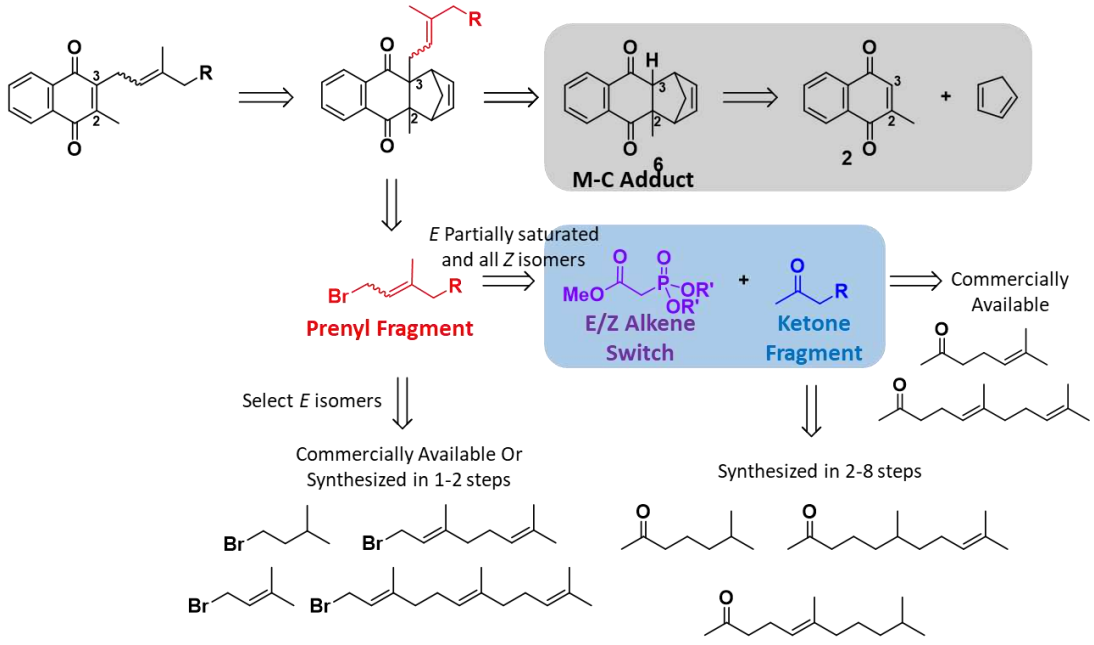

Figure 5.11. Retrosynthetic analysis of MK-derivatives to accommodate the diverse sidechain library. Grey box: Retrosynthesis of the M-C adduct. Blue box: E/Z alkene switch to access both E and Z alpha isoprene units.

Prenyl Fragment breaks down into multiple pathways depending on the nature of the sidechain. Select *E* isomers can be obtained using commercially available prenyl, geranyl, and farnesyl halides or can be synthesized in 1-2 steps from commercially available alcohols.

The Prenyl Fragment can break down further to obtain all *Z* isomers, and all fully or partially saturated isomers with either E and Z alkenes will be obtained via further breakdown of the Prenyl Fragment into the Ketone Fragment and the *E/Z* Alkene Switch (shown in the blue box

in Figure 5.11). At this point, the stereochemistry of the alkene would be set using stereoselective alkene syntheses, such as Horner-Wadsworth-Emmons to access the E isomers and Still-Gennari to access the Z isomers. The phosphonate ester required to achieve either isomer would react with the Ketone fragment to achieve the desired Prenyl Fragment. Finally, the Ketone Fragment can break down further depending on the desired target. Many prenyl ketones are commercially available, and all fully saturated ketones can be synthesized in less than 10 steps.

5.4 Forward Synthesis

5.4.1. M-C Adduct

The micelle catalyzed Diels-Alder reactions to synthesize the M-C adduct **6** were investigated first (Figure 5.12). The reports by Singh and Ji (Singh, Raju et al. 1988, Ji, Zong et al. 2003) reported high yields and high purity in a shortened period of time compared to the route established by Rüttimann and Büchi. The use of hexadecyltrimethylammonium bromide (CTAB,

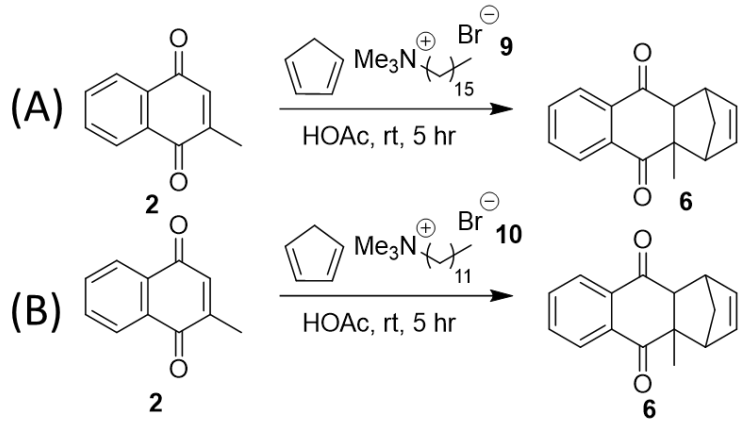

Figure 5.12. Methods towards the synthesis of the M-C adduct **6**. (A) Hexadecyltrimethylammonium bromide **9** micelles used as a catalyst using Ji and coworkers procedure. (B) Ji and coworkers estbalished procedure using dodecyltrimethylammonium bromide **10** (Ji, Zong et al. 2003)

9) was used by Singh and coworkers, and dodecyltrimethylammonium bromide (LTAB, **10**) was used by Ji and coworkers. Since the surfactants only differed by chain length, I used the first one to arrive with the higher yielding method first: Ji and coworkers protocol using CTAB as a

surfactant (Figure 5.12A). The Ji procedure used LTAB as their chosen surfactant (Figure 5.12B)(Ji, Zong et al. 2003). Using this route, only the first attempt yielded pure, white adduct **6** (Figure 5.15 in Section 5.4.1.3.) in 40% yield after recrystallization.

The first reaction performed yielded **6** as a chalky white solid (See Table 5.1, Entry 1 in Section 5.4.1.1). In each subsequent trial, I attempted to repeat the experiment to obtain the white solid as reported, but every trial after the first one was met with great difficulty. There were many factors that could have contributed to the poor results, such as the purification of the crude product, surfactant purity, and reaction conditions such as time and temperature. In the sections below, I have grouped similar factors together. The common thread between all these attempts is the inability to purify the crude M-C adduct via recrystallization, which was the most common method of purification.

5.4.1.1. Investigation of solvent and surfactant

After repeating Ji and coworkers' procedure multiple times (Table 5.1) using CTAB and LTAB with little to no success after recrystallization (Table 5.1 Entries 1-6), I switched to Singh and coworkers method. This method utilizes water as a solvent rather than glacial acetic acid. Beginning with CTAB, the reaction was monitored over the course of three days, and no product spot was observed (Figure 5.13, Table 5.1, Entry 2)(Singh, Raju et al. 1988). After three more days, the reaction showed an incomplete reaction by TLC. According to the procedure, the reaction is run at room temperature, however the definition of room temperature changes in different parts

of the world. Singh and coworkers are based in India and their definition of room temperature may be slightly higher. From this, I ran another trial at a slightly elevated temperature, 30-35°C.

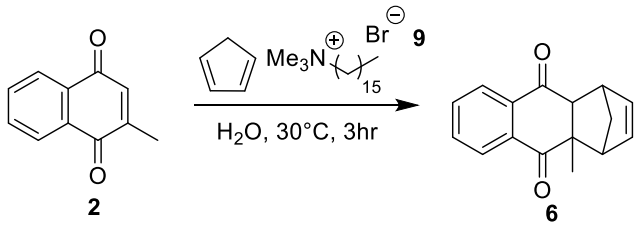

Figure 5.13. Synthesis of M-C adduct using hexadecyltrimethylammonium bromide as established by Singh and coworkers. (Singh, Raju et al. 1988)

Table 5.1. Synthetic trials of the synthesis of M-C adduct **6**.

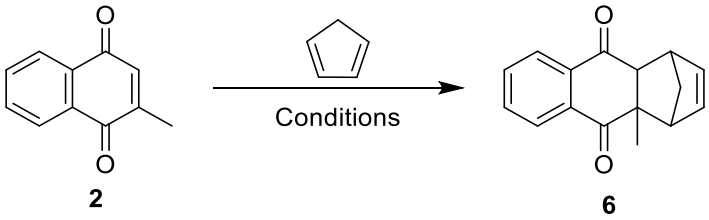

Entry	Reagents	Conditions	Yield of 6	Comment
1	CTAB (**9**) CPD (2.8 eq)	HOAc, rt, 2 days	40% After recrystallization	Recrystallization afforded the expected chalky, white solid.
2	CTAB (**9**) CPD (2 eq)	H_2O, rt, 3 hr	No rxn	NMR showed only starting material. Either time or solvent was insufficient.
3	CTAB (**9**) CPD (4 eq)	H_2O rt, 24 hr	No yields calculated	Longer reaction time produced some product. Product was lost during repeated attempted to recrystallize to look like Entry 1.
4	CTAB (**9**) CPD (4 eq)	HOAc, rt, 24 hr	No mass obtained	Recrystallization afforded a dark tan solid. Continued repeated attempts to optimize recrystallization
Comparison study between LTAB & CTAB				
Entry	**Reagents**	**Conditions**	**Yield of 6**	**Comment**
5	LTAB (**10**) CPD (2.8 eq)	HOAc, rt, 6 hr	No mass collected.	Produced a white solid. NMR confirmed it was product. Product lost in recrystallization.
6	CTAB (**9**) CPD (2.8 eq)	HOAc, rt, 7 days	No mass collected	Brown solid prior to recrystallization. Light tan product post recrystallization. Continued to suspect recrystallization was the primary issue

Temperature comparison study with LTAB				
7	LTAB (**10**) CPD (2.8 eq)	HOAc, rt, 48 hr	No rxn	Produced a yellow solid. Turned brown after recrystallization
8	LTAB (**10**) CPD (2.8 eq)	HOAc, **35°C**, 48 hr	39% after recrystallization	Brown solid prior to recrystallization. Light tan product post recrystallization

However, even with this change in temperature, the reaction yielded only starting material in the reported amount of time (3 hours) at 30°C. The reaction was allowed to continue for a total of 24 hours, and the temperature was increased to 35 °C (Table 5.1 Entry 3). After ~ 24 hours, no starting material was present on TLC, and the reaction yielded a light yellow solid. Upon recrystallization, the product turned brown, rather than white, indicating something went wrong with the recrystallization. Similar trials were performed with LTAB in glacial acetic acid at room temperature at 35°C (Table 5.1, Entries 7 and 8) and ended with similar results. When comparing the progress of the reactions run in glacial acetic acid versus water, the reactions run in glacial acetic acid seemed to promote the reaction at room temperature better. Despite a complete reaction by TLC, significant amounts of product was lost during recrystallization due to a suspected decomposition of the M-C adduct back to menadione and cyclopentadiene. Details regarding the inefficacy of recrystallization as a purification method can be found in Section 5.4.1.3.

5.4.1.2. Surfactants and Solvents

With the results of both Ji and Singh's procedure trials, the quality of the surfactant was now under consideration. The first use of CTAB (straight from the bottle) yielded pure, desired product, albeit in lower than reported yields. Both surfactants were purified and stored under an inert atmosphere in the freezer or in a desiccator. The newly purified surfactants did not seem to have any significant impact in improving the reaction overall. The collected products were still tan/brown solids after recrystallization.

In light of these observations, the micelle catalyzed procedures were put aside to explore the Rüttimann and Büchi procedure which utilized glacial acetic acid as a solvent without a surfactant (Figure 5.14). In the first trial performed, the starting materials were stirred in glacial acetic acid for 2 days to yield the M-C adduct **6** in 14% yield. From this, the presence of surfactants

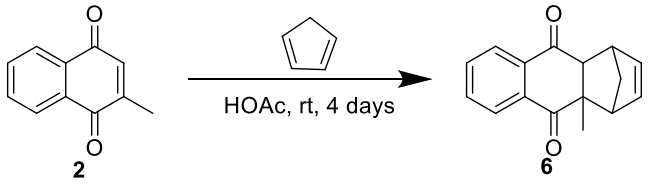

Figure 5.14. Synthesis of M-C adduct using Buchi & Ruttimann conditions (Büchi and Rüttimann 1986).

in the Diels-Alder reaction did seem to have a significant impact on the reaction. In later trials, LTAB was used as the default surfactant because it performed better than CTAB in a comparison study (See above: Table 5.1, Entries 5 and 6). The LTAB reaction showed complete conversion by TLC in 6 hours whereas the CTAB experiment took more than 7 days. In both studies, no mass was collected because a significant amount of product was lost during recrystallization that resulted in the tan/brown solid.

5.4.1.3. Purification methods

In all the above described trials, M-C adduct product was formed and confirmed by a crude NMR sample. Repeated attempts to recrystallize the crude M-C adduct to remove the unreacted menadione showed a colorimetric trend; the presence of menadione is evident in the color of the solid (Figure 5.15), where the increased concentration of unreacted menadione gradually changes the color of the solid from light tan to yellow-brown to yellow. Before recrystallization, product would start as a light tan and progressively become darker brown throughout the recrystallization. In addition, insoluble solids were present in the crude reaction mixture which led to the incorrect assumption that more solvent was necessary to dissolve the crude product. It was also suspected that prolonged time on the hot plate encouraged retro-Diels-Alder reactions to occur and undergo decomposition. Recrystallization of the crude material only produced the white solid in the very first attempt to synthesize the M-C adduct(Table 5.1, Entry 1).

Figure 5.15. Different colors of M-C products observed. Far left: Pure M-C adduct. Rest are contaminated with unreacted menadione.

The inconsistency of recrystallization as a purification method inspired a search for alternative purification methods, particularly using an aqueous work-up. Ongini and coworkers used an aqueous work-up that poured the reaction over a mixture of ice and water followed by a

liquid-liquid extraction (Ongini, Almirante et al. 2014). When this procedure was followed, an unexpected light yellow-white solid precipitated upon quenching over ice-water. Ongini and coworkers did not mention the precipitate in their patent. Before continuing with the extraction, I filtered off the precipitate and then continued the extraction with the filtrate. After rinsing with ice-cold water, the precipitate was a white solid, and it was found to be pure M-C adduct **6** by NMR. The product collected after liquid-liquid extraction was a light yellow solid, and it was found to be a mixture of M-C adduct and menadione which was consistent with Ongini and coworkers reported results. This modification led to 83% yield of pure M-C adduct, which was an improvement over Ongini's crude yield of 78%. At this point, this became the preferred purification method over removal of the acetic acid under reduced pressure and recrystallization.

5.4.1.4. Investigation into reaction time, temperature, and equivalents of cyclopentadiene

Other points of optimization occurred via manipulation of the reaction time, temperature, and equivalents of cyclopentadiene. Overall, increasing the reaction time showed favorable results to improve yield. This is in line with Büchi & Rüttimann's procedure that took 4 days. Increasing the temperature also showed favorable results. These reactions tended to occur quicker but resulted in darker brown solids upon recrystallization (These observations occurred prior to the use of the Ongini aqueous work-up described above). A table summarizing the conditions attempted can be found in the Supplemental Material in Table V.1 in Appendix V.

Throughout the trials described in sections above, the crude M-C adduct was saved. In an attempt to maximize resources, the crude M-C adduct was subjected to the Diels-Alder conditions using stoichiometric amounts of cyclopentadiene assuming the grams of crude M-C adduct used was pure menadione starting material. As the reaction progressed, the crude mixture showed 100% conversion by TLC after a few hours. These trials demonstrated that the crude adduct can be

recycled to generate more M-C adduct by taking advantage of LeChatelier's principle. These trials started an investigation into the optimization of the delivery method and equivalents of cyclopentadiene used in the Diels-Alder reaction. Using this information, a second equivalent of cyclopentadiene was added to the Rüttimann and Büchi conditions after the reaction had been running for approximately 48 hours. At 48 hours, TLC showed an incomplete reaction, and upon addition of the second dose of cyclopentadiene, the reaction stirred for another 24 hours (Figure 5.16). On TLC, there was noticeably more M-C adduct formed and the menadione spot had significantly diminished. After a total of two equivalents of cyclopentadiene were added to the reaction, this reaction produced an 83% yield after using Ongini's aqueous work-up. I anticipate the reaction time can be reduced further upon the addition of more equivalents of cyclopentadiene earlier during the reaction to shift equilibrium sooner.

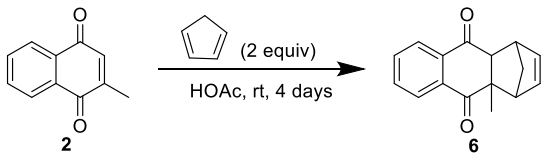

Figure 5.16. Synthesis of the M-C adduct using 2 equivalents of freshly distilled cyclopentadiene. Followed by Ongini aqueous workup, this reaction yielded 83% of pure M-C adduct.(Büchi and Rüttimann 1986, Rüttimann 1986, Ongini, Almirante et al. 2014)

5.4.2 Enolate Alkylation

The alkylated M-C adduct is prone to spontaneous retro-Diels-Alder; therefore, the alkylated adduct intermediate was immediately carried forward to the retro-Diels-Alder step to exert control over the rate of reaction. A summary of trials can be found in the Supplemental Materials found in Table V.2 in Appendix V. All the observations and conclusions for the determining the success of each set of conditions are based on TLC plates, visual observations of the reaction appearance, identifying the product in crude NMR samples, and NMR of preparatory TLC samples. In brief, a side reaction was occurring in the flask between the base and the alkyl

halide to produce an elimination product with the electrophile. As a result, each enolate alkylation reaction was ended before it could reach total conversion to establish "proof of concept". Each enolate alkylation was worked up accordingly and immediately carried over to the retro Diels-Alder step to control the decomposition of the alkylated adduct. If this project were to continue, the enolate alkylation step requires **significant optimization**.

Many reaction conditions were attempted to prevent the formation of the elimination side reaction (Table V.2 in Appendix V). Prevention of the side reaction was difficult and not achieved simply by varying the alkyl halide delivery method, such as diluted and added dropwise over 15-30 minutes, via syringe pump, and/or added slowly along the wall of the flask. After these trials showed the delivery method had little to no effect on preventing the side reaction, the base used in the enolate formation was taken under investigation. The typical enolate alkylation procedure of the M-C adduct follows similar conditions (Figure 5.17): the base (usually potassium t-butoxide,

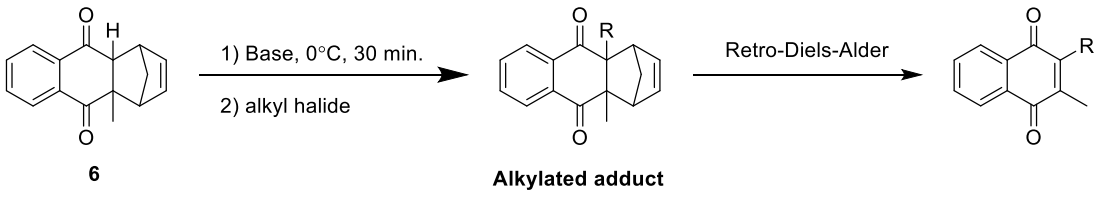

Figure 5.17. General three step sequence towards the alkylation of the M-C adduct.

KOtBu) is dissolved in THF at 0°C, and the M-C adduct **6** is added to the flask under an inert atmosphere. The color of the solution changes from colorless to dark, blood red (Figure V.1A in the Supplemental Material in Appendix V). The mixture stirs at 0°C for approximately 30 minutes. At this point, the alkyl halide is added dropwise or slowly along the side of the flask. The addition of the electrophile results in a distinct change in the color of the solution from dark red to a dark orange. After all the alkyl halide has been dispensed at 0°C, the reaction would stir for another hour at 0°C. When the alkylation reaction is complete, the solution is acidified to a pH of 1, causing

all the remaining red enolate to be protonated to form a yellow solution. The yellow color seemed to be indicative of the reformation of menadione and was confirmed by TLC.

Throughout the trials described in Table V.2 in Appendix V, three different bases were used to optimize the enolate alkylation reaction. The most common base used in the literature is KOtBu. In use, there is a significant amount of KOtBu that does not dissolve in THF at 0°C, and it sits on the bottom of the flask, often preventing the reaction from stirring effectively. This excess of solid base was initially thought to be the culprit for the elimination side reaction. The undissolved KOtBu reacts with the alkyl halide before it would have a chance to reach the enolate *in situ*.

Alternatives to KOtBu were then used to avoid the solubility issue. LDA was freshly prepared from distilled diisopropylethylamine and n-butyl lithium. LDA was effective at forming the enolate, as evident by the dark red color, but no alkylation reaction was observed on TLC after 2 hours. KHMDS was also investigated. Enolate formation with KHMDS produced a lighter orange color upon deprotonation, and the product appeared on TLC after 3 hours. The color of the reaction gradually became more orange as the alkylation reaction progressed (Figure V.2 in Appendix V). The reaction was stopped when the elimination product was observed on TLC.

After retro-Diels-Alder reactions in HOAc, both the KOtBu and KHMDS reaction produced ~11% MK-2 by NMR. This suggests KHMDS is comparable to KOtBu. Most of the protocols using KOtBu call for freshly prepared KOtBu from potassium metal and t-butyl alcohol. Even though the reaction is straightforward, handing potassium metal is extremely dangerous and should be avoided, if possible. This is especially significant if non-chemist researchers employ these reactions in their laboratories. KHMDS is sold as a solution as is easier to handle under anhydrous technique than potassium metal.

Overall, a strong base is required to form the M-C enolate. The color of the solution is indicative of the extent of enolate formation, and the color of the solution throughout the alkylation reaction gives rise to the progress of the alkylation reaction. The best method to deliver the alkyl halide is slowly over extended periods of time. In hindsight, more equivalents over a long period of time may have eventually led to complete conversion at the expense of the formation of the elimination product. In addition, it would have been interesting to observe how alternating the addition of base and alkyl halide would affect the reaction. Alternate addition of base and electrophile was successful in the protection amino acids, such as was used to protect 1-amino-1-cyclopropylcarboxylic acid with a Cbz protecting group (Appendix IV).

5.4.3 Retro-Diels-Alder Conditions

The enolate alkylation reaction described in the section above was worked up and immediately followed by the retro-Diels-Alder (RDA) reaction to remove the auxiliary cyclopentadiene group. Rüttimann and Büchi achieved complete RDA in toluene at reflux for 15 minutes in the dark for the synthesis of vitamin K_1 (Büchi and Rüttimann 1986, Rüttimann 1986). When this process was repeated for these truncated MK-derivatives, the RDA reaction proceeded quickly, but the product decomposed during the work up, which consisted of removing toluene under reduced pressure with a water bath set to 40-50°C. This suggests toluene was better suited for the longer chain, hydrophobic MK-derivatives, like vitamin K_1, whereas the high heat encouraged the decomposition of the truncated MK-derivatives.

Although the micellar catalysts did not significantly affect the formation of the M-C adduct, their presence did seem to influence the retro-Diels-Alder. The crude alkylated product was redissolved in HOAc, and LTAB **10** was added to the solution (Figure 5.18) (Ji, Zong et al.

2003). The reaction was heated to 90°C with a condenser under argon for 15-30 minutes depending on the conditions used in that respective trial.

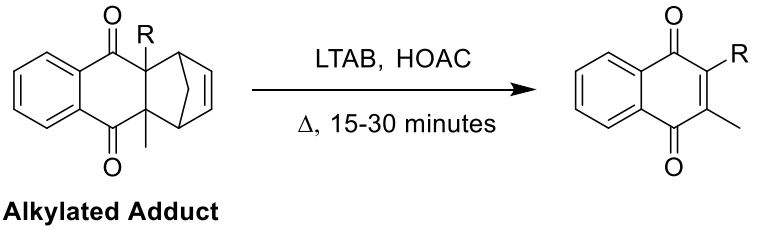

Figure 5.18. General conditions for the retro Diels-Alder reaction (Ji, Zong et al. 2003)

On TLC, the alkylated M-C adduct spot converged into a single spot which confirmed a successful retro-Diels-Alder reaction. Due to the precursor being carried forward crude, the TLC plate of the RDA reaction was messy, however it can be attributed to the incomplete alkylation reaction from the previous step. As described previously, an aqueous work up was the preferred method over removing the glacial acetic acid solvent under reduced pressure to prevent decomposition.

5.5. Conclusion

The Diels-Alder approach to synthesizing MK-derivatives has a long way to go before it can compete with the currently preferred Friedel-Crafts route. The formation of the M-C adducts did not occur as reported in the literature and adjustments had to be made to ensure a high purity product. The work-up method established by Ongini and coworkers is the most consistent method to isolate pure M-C adduct rather than recrystallizing based on my observations. The enolate alkylation reaction needs the most optimization. If I had more time, I would have liked to have tried using KHMDS again with geranyl bromide or citronellyl halide for the enolate alkylations. Finding the balance between basicity and electrophile delivery is going to be key to the success of this step. And lastly, the milder retro Diels-Alder conditions using glacial acetic acid and a surfactant are preferred over the harsh condition refluxing in toluene.

References

Braasch-Turi, M. and D. C. Crans (2020). "Synthesis of Naphthoquinone Derivatives: Menaquinones, Lipoquinones and Other Vitamin K Derivatives." Molecules **25**(19).

Brodie, A. F. (1961). Federation Proc. **20**: 995.

Brodie, A. F. (1963). "Isolation and photoinactivation of quinone coenzymes." Methods Enzymol. **6**: 295-308.

Büchi, G. and A. Rüttimann (1986). Process For The Manufacture of Quinone Derivatives. United States of America, Hoffmann-La Roche, Inc.

Coman, S. M., V. I. Parvulescu, S. Wuttke and E. Kemnitz (2010). "Synthesis of Vitamin K_1 and K_1-Chromanol by Friedel–Crafts Alkylation in Heterogeneous Catalysis." ChemCatChem **2**(1): 92-97.

Coppa, F., F. Fontana, F. Minisci, M. C. Nogueira and E. Vismara (1991). "Homolytic Alkylation of Naphthoquinone and Methyl-Naphthoquinone. Enthalpic, Steric, and Polar Effects." Tetrahedron **47**(35): 7347-7352.

Dunphy, P. J. and A. F. Brodie (1971). [233] The structure and function of quinones in respiratory metabolism. Methods Enzymol., Elsevier. **18:** 407-461.

Hamamura, K., T. Iwama, C. Seki and M. Monishi (1994). Preparation process of quinone deriovatives and the intermediate for the preparation thereof. **EP 0613877A1**.

Ishihara, M. and H. Sakagami (2007). "QSAR of Molecular Structure and Cytotoxic Activity of Vitamin K2 Derivatives with Concept of Absolute Hardness." Anticancer Res. **27**: 4059-4064.

Ji, Y.-F., Z.-M. Zong, X.-Y. Wei, T. Guang-Zhong, L. Xu and L.-T. He (2003). "Improved Synthesis of Vitamin K1." Synthetic Communications **33**(5): 763-772.

Katoh, T., H. Monma, J. Wakasugi, K. Narita and T. Katoh (2014). "Synthesis of beta-lapachone, a potential anticancer agent from the lapacho tree." Eur. J. Org. Chem. **2014**(32): 7099-7103.

Koehn, J. T., C. N. Beuning, B. J. Peters, S. K. Dellinger, C. Van Cleave, D. C. Crick and D. C. Crans (2019). "Investigating Substrate Analogues for Mycobacterial MenJ: Truncated and Partially Saturated Menaquinones." Biochemistry **58**(12): 1596-1615.

Koehn, J. T., D. C. Crick and D. C. Crans (2018). "Synthesis and Characterization of Partially and Fully Saturated Menaquinone Derivatives." ACS Omega **3**(11): 14889-14901.

Koehn, J. T., E. S. Magallanes, B. J. Peters, C. N. Beuning, A. A. Haase, M. J. Zhu, C. D. Rithner, D. C. Crick and D. C. Crans (2018). "A Synthetic Isoprenoid Lipoquinone, Menaquinone-2, Adopts a Folded Conformation in Solution and at a Model Membrane Interface." J. Org. Chem. **83**(1): 275-288.

Oberhauser, C., V. Harms, K. Seidel, B. Schroder, K. Ekramzadeh, S. Beutel, S. Winkler, L. Lauterbach, J. Dickschat and A. Kirchning (2018). "Exploiting the Synthetic Potential of Sesquiterpene Cyclases for Generating Unnatural Terpenoids." Angew. Chem. Int. Ed. **57**(36): 11802-11806.

Ongini, E., N. Almirante and L. Storoni (2014). Quinone based nitric oxide donating compounds for ophthalmic use.

Reetz, M. T., S. Huttenhain and F. Hubner (1981). "Lewis Acid Alkylation of Ketones Using SN1-Reactive Acetates." Syn. Commun. **11**(3): 217-222.

Rüttimann, A. (1986). "Recent Advances in the Synthesis of K-Vitamins." Chimia **40**(9): 290-306.

Simes, D. C., C. S. B. Viegas, N. Araujo and C. Marreiros (2020). "Vitamin K as a Diet Supplement with Impact in Human Health: Current Evidence in Age-Related Diseases." Nutrients **12**(1): 138.

Singh, V. K., B. N. S. Raju and P. T. Deota (1988). "Micellar Catalysts Π4S + Π2S Cycloaddition in Aqueous Media." Syn. Commun. **18**(6): 567-574.

Siu, J. C., J. B. Parry and S. Lin (2019). "Aminoxyl-Catalyzed Electrochemical Diazidation of Alkenes Mediated by a Metastable Charge-Transfer Complex." J. Am. Chem. Soc. **141**(7): 2825-2831.

Suhara, Y., A. Wada, Y. Tachibana, M. Watanabe, K. Nakamura, K. Nakagawa and T. Okano (2010). "Structure–activity relationships in the conversion of vitamin K analogues into menaquinone-4. Substrates essential to the synthesis of menaquinone-4 in cultured human cell lines." Bioorg. Med. Chem. **18**(9): 3116-3124.

Sukheja, P., P. Kumar, N. Mittal, S.-G. Li, E. Singleton, R. Russo, A. L. Perryman, R. Shrestha, D. Awasthi, S. Husain, P. Soteropoulos, R. Brukh, N. Connell, J. S. Freudlich and D. Alland (2017). "A Novel Small-Molecule Inhibitor of the Mycobacterium tuberculosis Demethylmenaquinone Methyltransferase MenG is Bactericidal to Both Growing and Nutritionally Deprived Persister Cells." mBio **8**(1): 1-15.

Teitelbaum, A., M. Scian, W. Nelson and A. Rettie (2015). "Efficient Syntheses of Vitamin K Chain-Shortened Acid Metabolites." Synthesis **47**(07): 944-948.

Upadhyay, A., F. L. Fontes, M. Gonzalez-Juarrero, M. R. McNeil, D. C. Crans, M. Jackson and D. C. Crick (2015). "Partial Saturation of Menaquinone in *Mycobacterium tuberculosis* : Function and Essentiality of a Novel Reductase, MenJ." ACS Cent. Sci. **1**(6): 292-302.

Wuttke, S., S. M. Coman, G. Scholz, H. Kirmse, A. Vimont, M. Daturi, S. L. M. Schroeder and E. Kemnitz (2008). "Novel Sol-Gel Synthesis of Acidic MgF2−x(OH)x Materials." Chem. Eur. J. **14**(36): 11488-11499.

Chapter 6:
Summary & Future Directions

6.1. Summary

The research in this dissertation demonstrates the utility of organic synthesis in solving biological problems. Although this dissertation is not written in the chronological order of the work that I have done, it is important to me to highlight that I learned the rigors of synthesis through my work on the versiquinazolines, and I was then able to apply it to the biological problems presented in the menaquinone project. I am going to use the skills I have gained in both fields to continue thinking about biological problems and understand the role each compound plays into the larger picture.

Chapter 2 is a review of the lipoquinone literature focusing on the properties, syntheses, and membrane location of lipoquinones and highlights the controversies within the field. The properties of ubiquinones, plastoquinones, and menaquinones often seem to be ignored or simply forgotten when interpreting the results. This has led to controversial claims about their location in the membrane and disagreements throughout the literature. The review highlights the inconsistency between the number of experimental and computational studies and their outcomes. More recent reports are computational studies which rely on databases for parameters. The review encourages more properties-focused experimental studies to validate the recent computational work to fill in the gaps and clarify the location of lipoquinones in the membrane.

Chapter 3 discusses the conformation and location of ubiquinone-2 in AOT reverse micelles and compares it to the results of an analogous study performed with menaquinone-2 by

the Crans group at Colorado State University. 1D 1H NMR and 2D NOESY and ROESY NMR spectroscopy studies were used to determine the conformation of UQ-2 in organic solvents. UQ-2 adopts a folded conformation in organic solvents, which is defined by an approximate 90°C angle between the headgroup and the sidechain. The study also showed the position of the end of the sidechain is sensitive to the polarity of the solvent. In polar solvents, such as DMSO and acetonitrile, UQ-2 adopts a folded, U-shaped conformation which described the end of the sidechain to be located directly above the headgroup. In nonpolar solvents, like pyridine and benzene, UQ-2 was found to adopt a folded-extended conformation or a more open U-shaped conformation which described the end of the sidechain to be far enough away from the headgroup that it is outside the range of the Overhauser Effect. In AOT reverse micelles, UQ-2 was found to adopt a U-shaped conformation as well. In addition, the headgroup protons and sidechain protons of UQ-2 were found to be within the NOE range of the polar headgroup protons of AOT which suggests it is located near the lipid-water interface. When comparing UQ-2 and MK-2, both lipoquinones adopt a folded conformation in organic solvents and AOT reverse micelles. UQ-2 is located closer to the lipid-water interface than MK-2, which is thought to be due to the increased polarity of the headgroup. Interestingly, the orientation of UQ-2 and MK-2 points the open end of the U-shape towards the nonpolar region of the AOT reverse micelle. As of right now, there is no concrete explanation, but we hypothesize the hydrophobicity of the truncated lipoquinones as a whole still tries to minimize surface area interactions with water.

Chapter 4 discussed a review of the literature regarding the synthesis of naphthoquinone derivatives. There are 5 main synthetic categories that have been reported to synthesize naphthoquinones derivatives: nucleophilic ring, sidechain extensions, metal-mediated/radical, electrophilic ring, and pericyclic reactions. The advantages and disadvantages of each method

were discussed, and a best representative of category was highlighted in the conclusion. When comparing each method, key features, such as number of steps, selectivity, and overall safety were considered. Safety was a specific feature to highlight since naphthoquinone derivatives are used in biological assays, and non-chemists are likely to be the ones synthesizing the derivatives for their experiments.

Chapter 5 explores the synthesis of truncated menaquinone derivatives using a Diels-Alder approach for a convergent synthesis. A diverse library of compounds could be possible using this regioselective and stereoretentive approach. Through the formation of a Diels-Alder adduct between commercially available menadione and cyclopentadiene, a regioselective enolate alkylation can be performed at the resultant sp^3 hybridized alpha carbon with an alpha proton. Diverse sidechains including E/Z isomers and partially saturated isoprene units are possible using stereoselective alkene syntheses, such as Horner-Wadsworth-Emmons and Still-Gennari. In practice, achieving the enolate alkylation of the Diels-Alder adduct was difficult to achieve. A prevalent, undesired elimination reaction was observed between the alkyl halide and the bulky base, KOtBu. Steps were taken to utilize alternative bases, but no significant strides were obtained until the very end of my time at Colorado State University. Due to the poor decision to not purify the alkyl halide prior to using it, the results of using KHMDS were inconclusive in the end.

The exploration of the total synthesis of two alkaloids, versiquinazoline A and versiquinazoline B is described in Appendix IV. Through retrosynthetic analysis, I designed a linear sequence to synthesize each alkaloid and potentially some derivatives. Starting with versiquinazoline B, the synthesis of 1-amino-1-cyclopropylcarboxylic acid was achieved through a Hofmann rearrangement using NaOCl and NaOH, which was then immediately protected with a benzyloxycarbonyl group. With this in hand, it could be coupled to Troc-protected tryptophan

methyl ester. Coupling 1-amino-1-cyclopropylcarboxylic acid to the indoline ring proved to be very difficult due to the incredibly sterically hindered system. Many attempts were made using a variety of peptide coupling agents, but none afforded the desired product. Success was finally achieved upon switching to Cbz-protected alanine, which contributed to the synthesis of versiquinazoline A. Upon successful coupling, attempts were made to rearomatize the indoline ring back to indole with some success using DDQ. At this point, the lab was shut down due to COVID-19, and the project was ended after the loss of Dr. Robert M. Williams. May he rest in peace. (I like to imagine him in chemistry heaven, hanging out with the "Chemistry Gods" and standing in front of an infinite chalkboard in deep discussion about total synthesis with his mentors, Dr. Robert B. Woodward and Dr. Yoshito Kishi, coming up with the most interesting transformations to make the most extravagant natural products.)

6.2. Future Directions

Currently, the only project moving forward is the menaquinone project (Chapter 5), but it is not necessarily moving forward with the Diels-Alder approach in mind. Skyler Markham and Kate Kostenkova are pursuing their own exploratory routes to synthesize MK-derivatives using cross coupling methods and revisiting the Friedel-Crafts approach. I am looking forward to the big picture results of the structure-activity relationship studies for the MK project.

If someone were to continue the Diels-Alder approach, I would recommend taking extreme care in maintaining an anhydrous environment. I am certain my systems were not anhydrous enough. I would also recommend trying to alternate the addition of base and electrophile to encourage the substitution reaction. This worked well during the Cbz protection of 1-amino-1-cyclopropylcarboxylic acid. I think KHMDS is a good base for this purpose, and it would be quite simple to control the amounts added in an alternating fashion under anhydrous conditions. I would

also explore synthesizing the DMK derivatives using the Diels-Alder adduct with cyclopentadiene. Also, purify everything. It's time consuming, but in the end the correct thing to do.

If someone were to pick up the synthesis of versiquinazolines, I would recommend identifying a more convergent and then divergent approach. There are many interesting places to functionalize on those ring systems that would be especially useful to derivatize in a structure-activity relationship study. My approach was perfectly linear, so even if it were successful, you would have to start all the way at step 3 to go from versiquinazoline B to versiquinazoline A. Starting with the synthesis of the 6-6-6 ring system would be a unique starting point to make the 5-5-6 ring system the divergence point.

Even though the menaquinone project is going into a new direction, I think the work the group is doing to understand the conformation and location of menaquinones and ubiquinones in the membrane is going to revolutionize how we think about the electron transport chain which will cascade into how we think about energy production in cells and life itself.

Appendix I:

Chapter 3: Supplemental Material

I A. NMR spectra for synthesized compounds

Fig. 3.S1. ^{1}H NMR (400 MHz) spectrum of 2,3,4-trimethoxy-6-methylbenzaldehyde (2) in $CDCl_3$

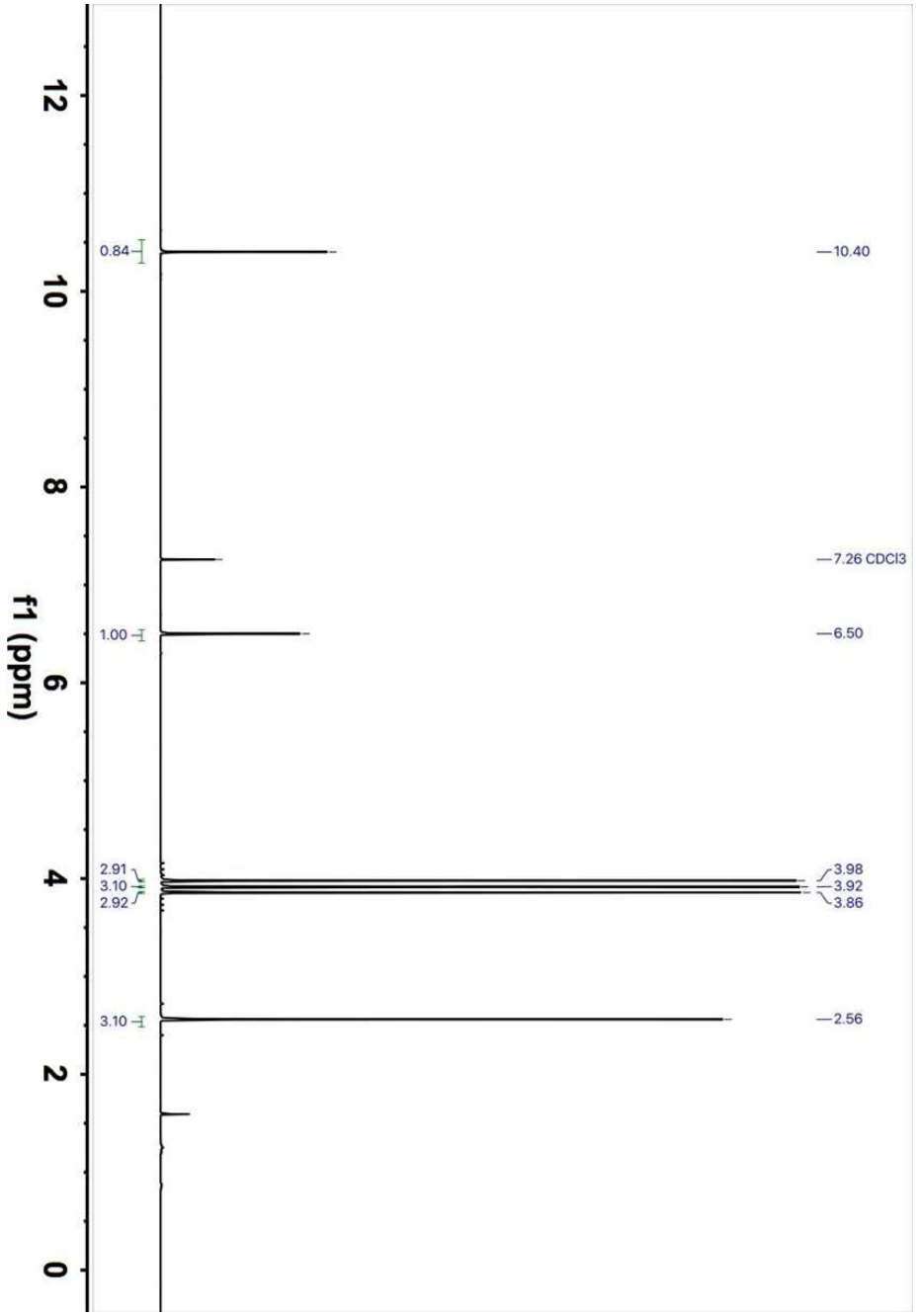

Fig. 3.S2. ^{13}C NMR (101 MHz) spectrum of 2,3,4-trimethoxy-6-methylbenzaldehyde (2) in $CDCl_3$

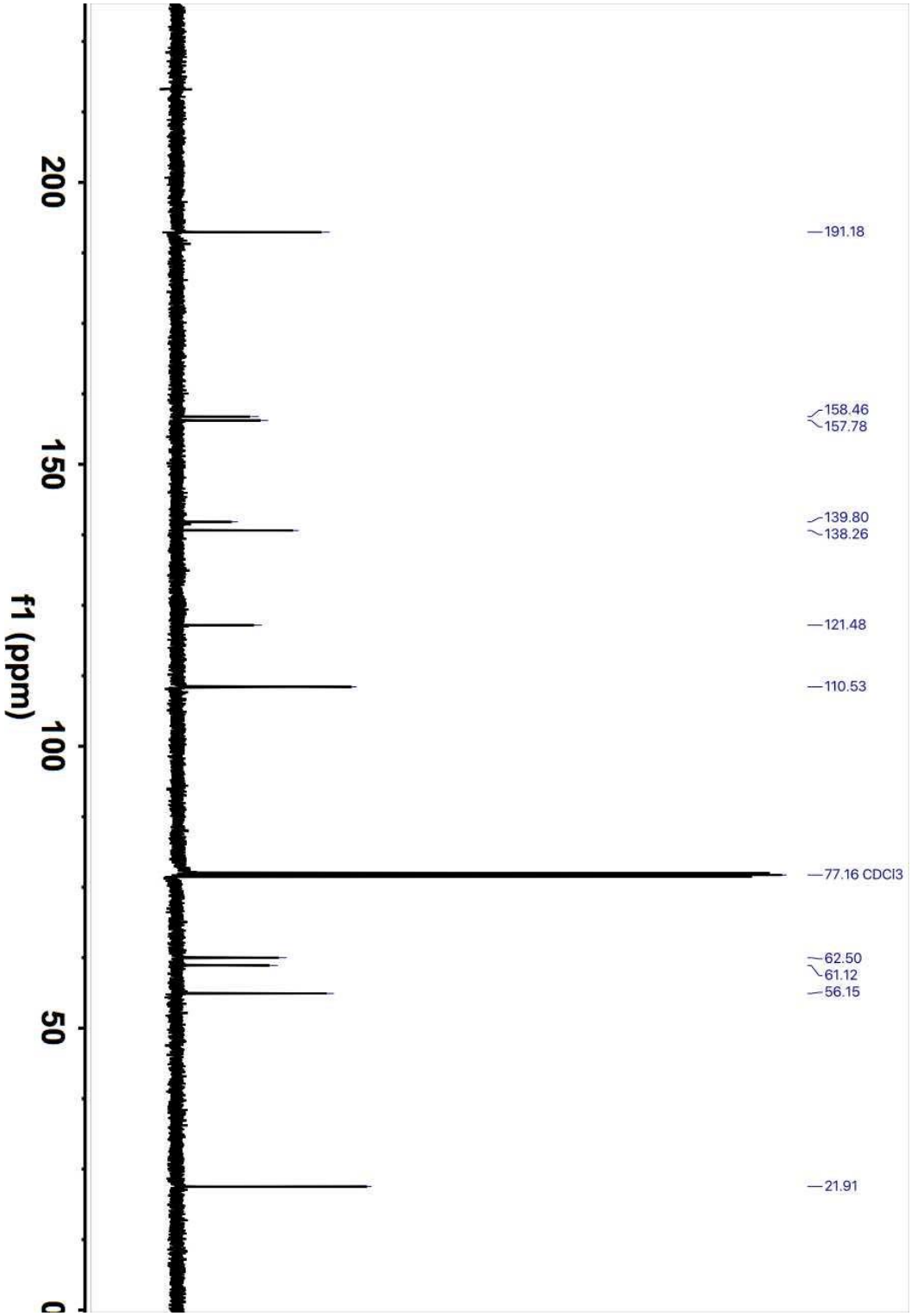

Fig. 3.S3. ^{1}H NMR (400 MHz) spectrum of 2,3,4-trimethoxy-6-methylphenol (3) in $CDCl_3$

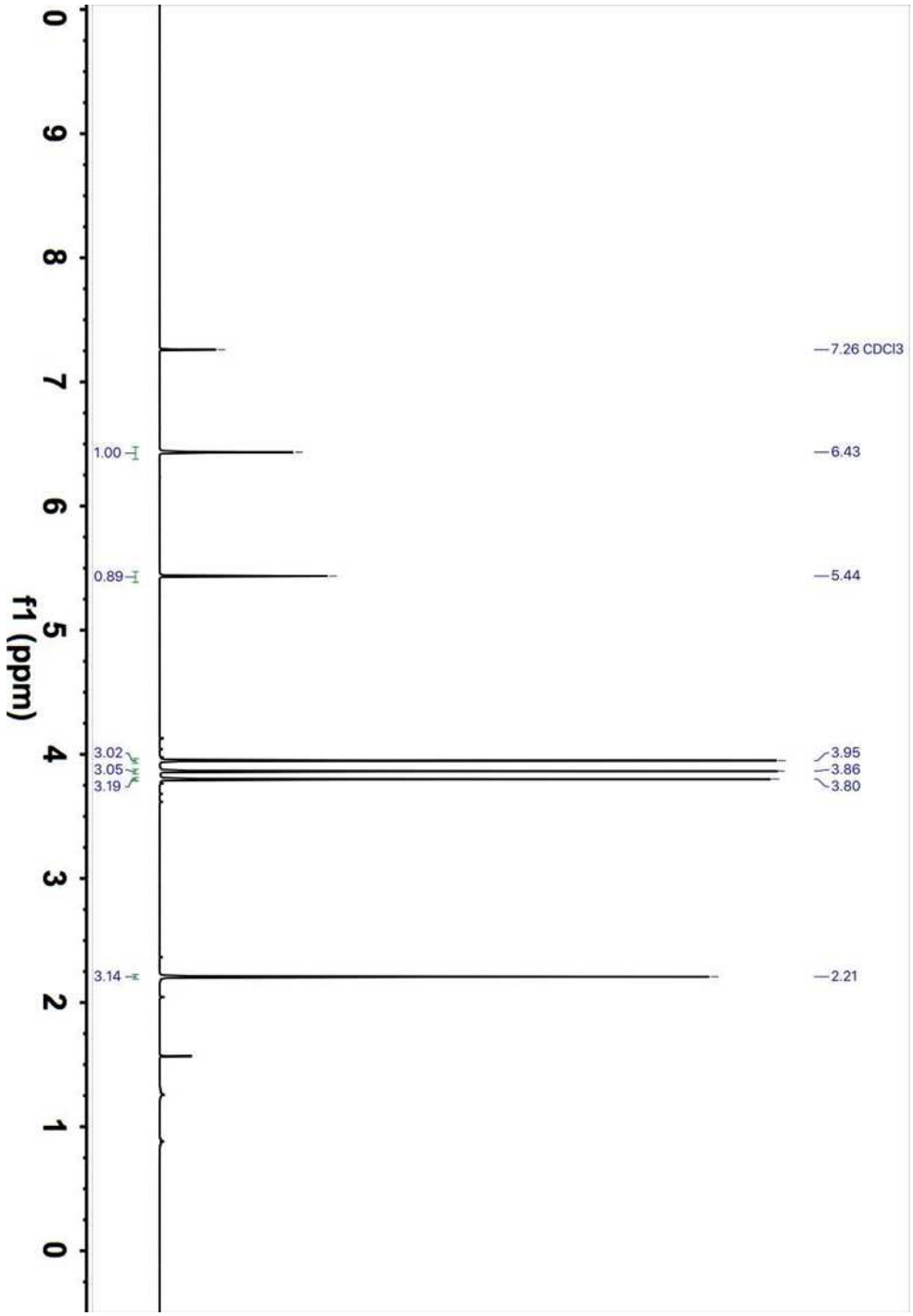

Fig. 3.S4. ^{13}C NMR (101 MHz) spectrum of 2,3,4-trimethoxy-6-methylphenol (3) in $CDCl_3$

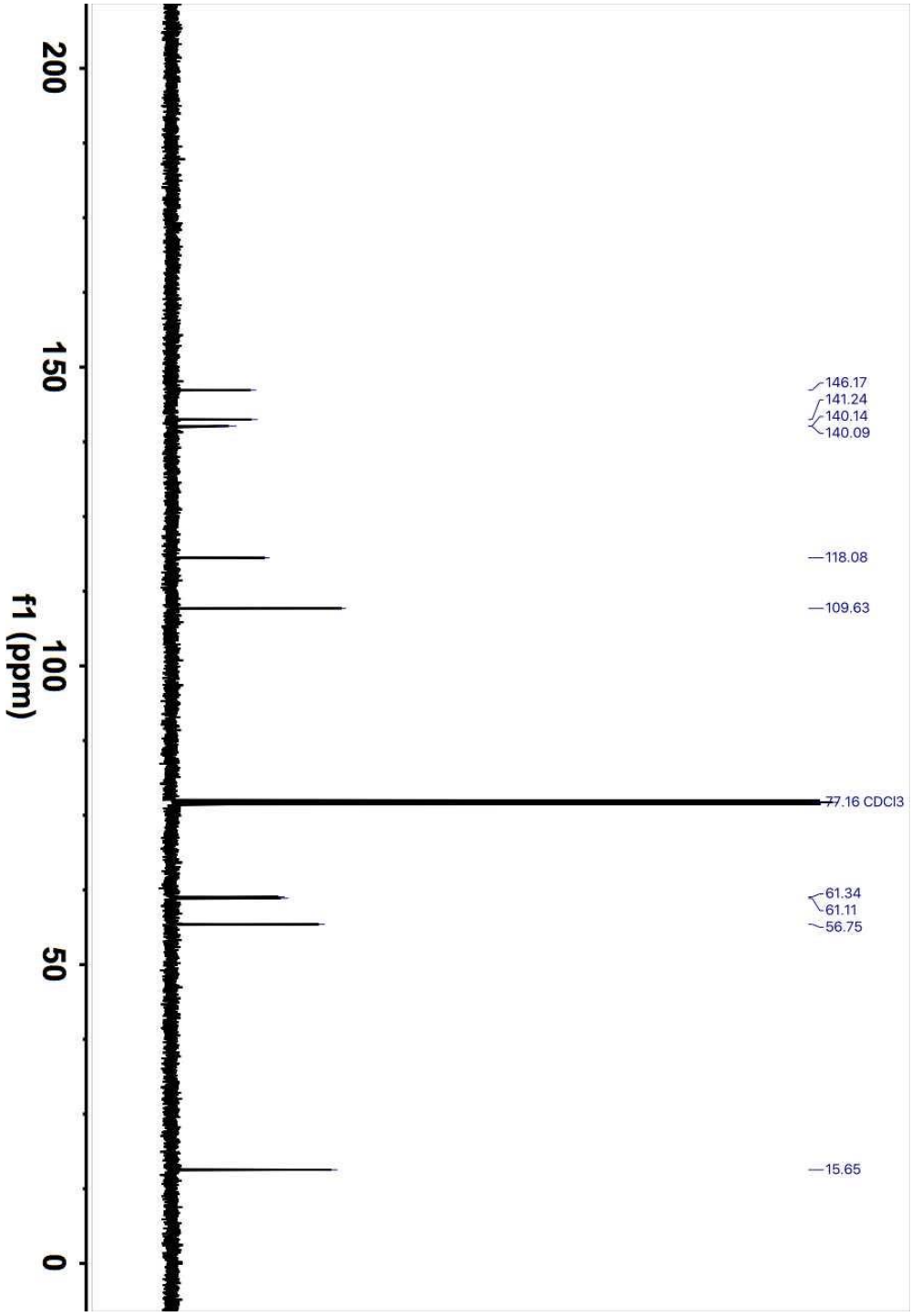

Fig. 3.S5. ^{1}H NMR (400 MHz) spectrum of geranyl 2,3,4-trimethoxy-6-methylphenyl ether (6) in $CDCl_3$

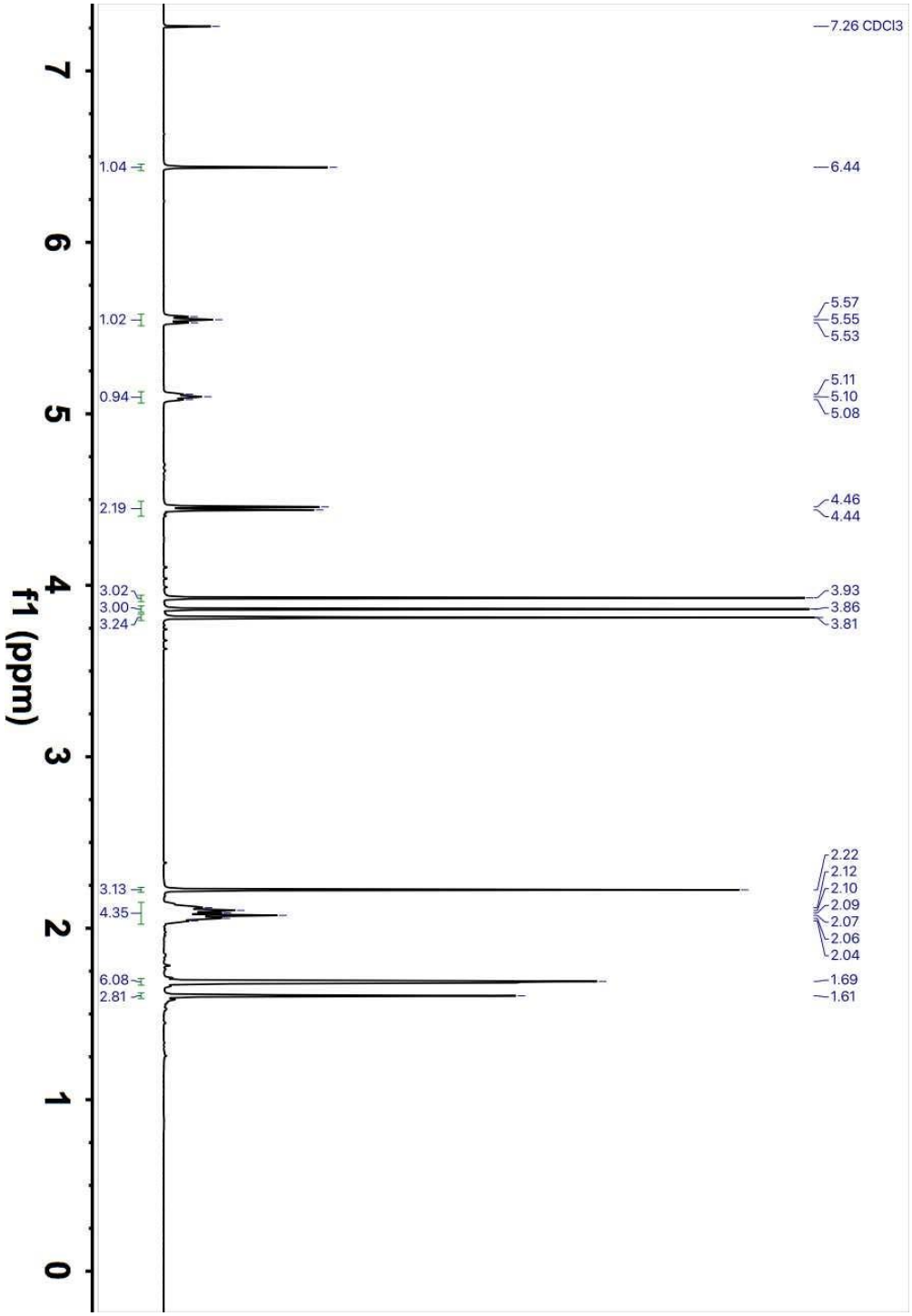

Fig. 3.S6. ^{13}C NMR (101 MHz) spectrum of geranyl 2,3,4-trimethoxy-6-methylphenyl ether (6) in $CDCl_3$

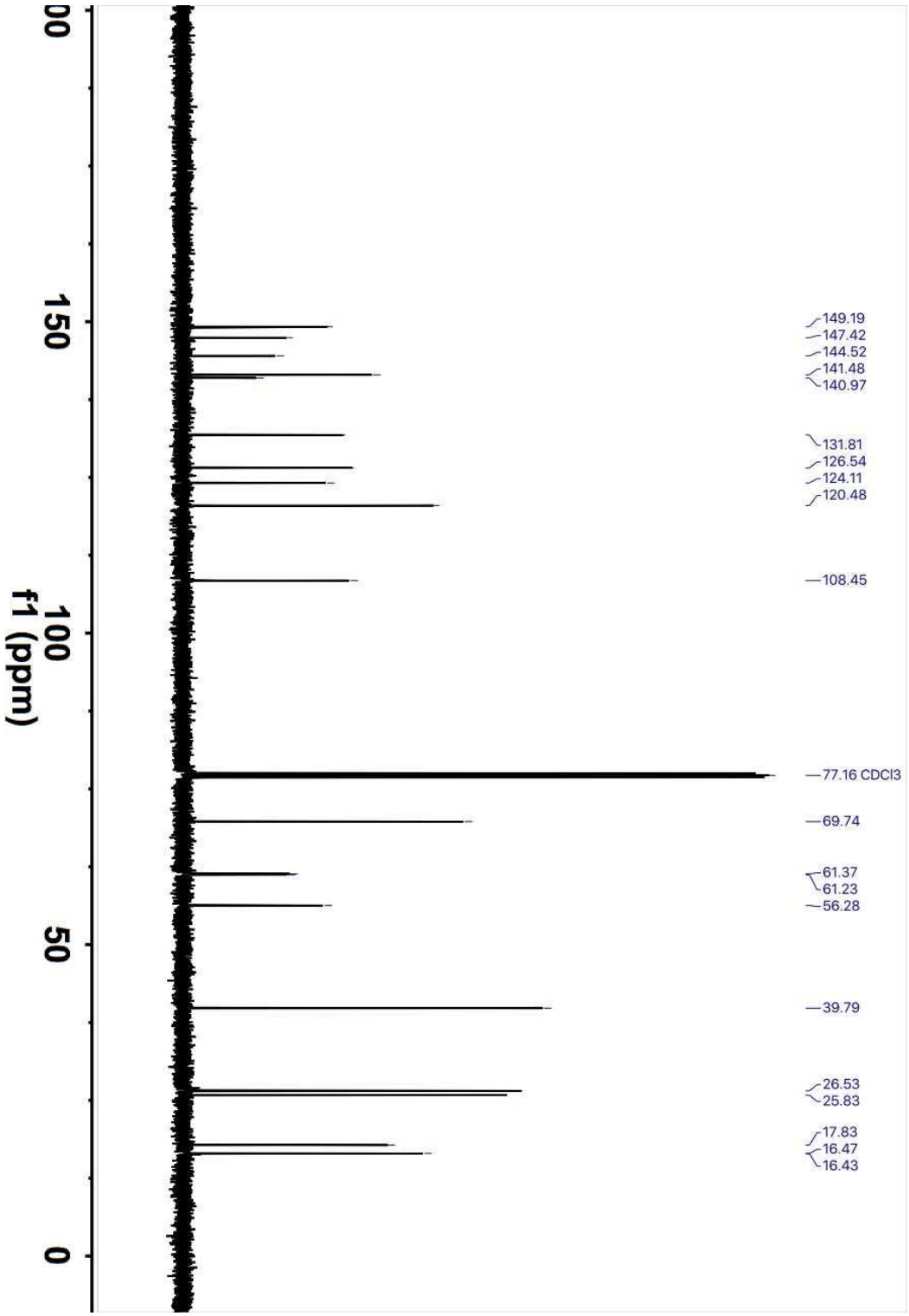

Fig. 3.S7. ^{1}H NMR (400 MHz) spectrum of 5-geranyl-2,3,4-trimethoxy-6-methyl-phenol (7) in $CDCl_3$

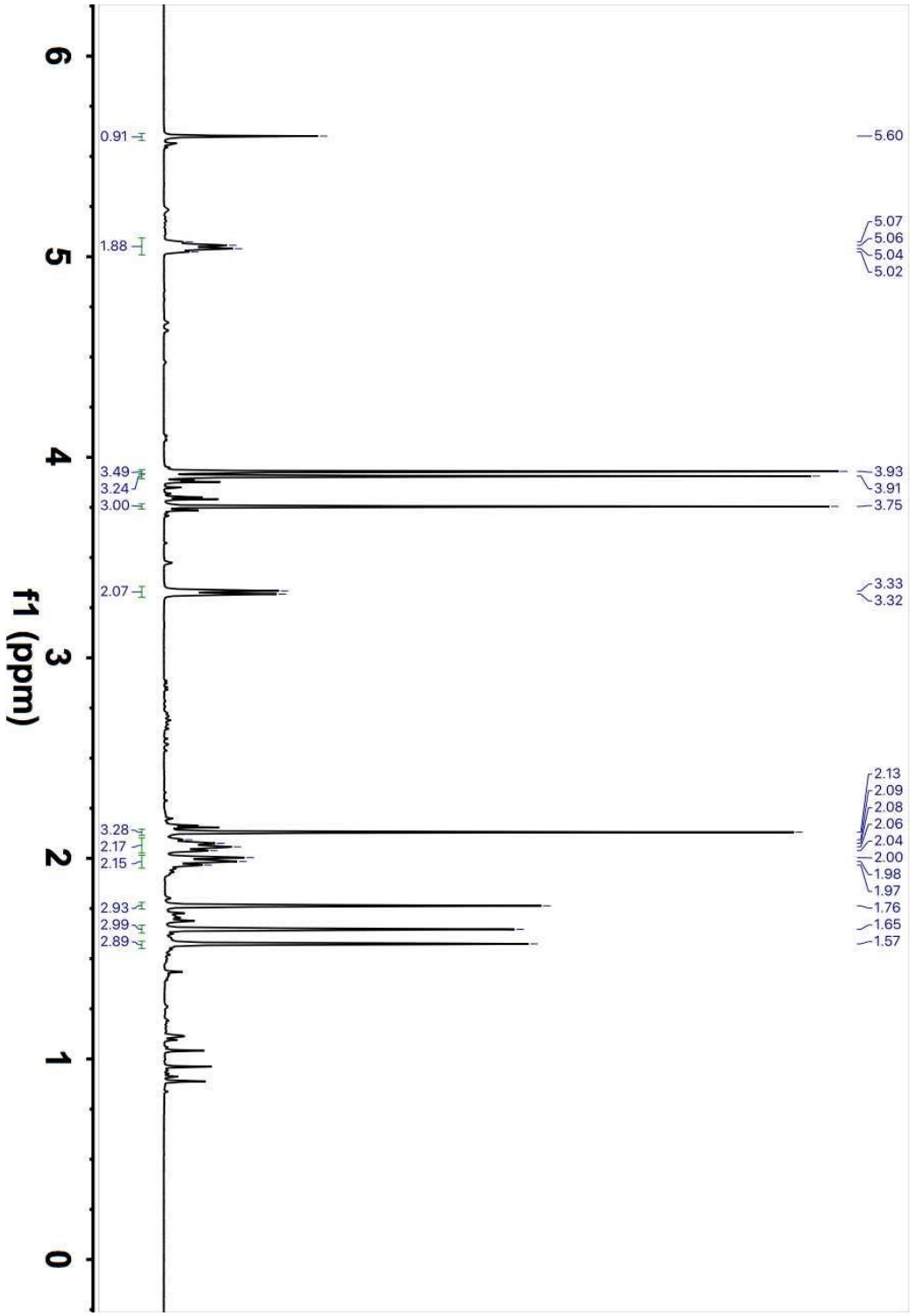

Fig. 3.S8. ^{13}C NMR (101 MHz) spectrum of 5-geranyl-2,3,4-trimethoxy-6-methyl-phenol (7) in $CDCl_3$

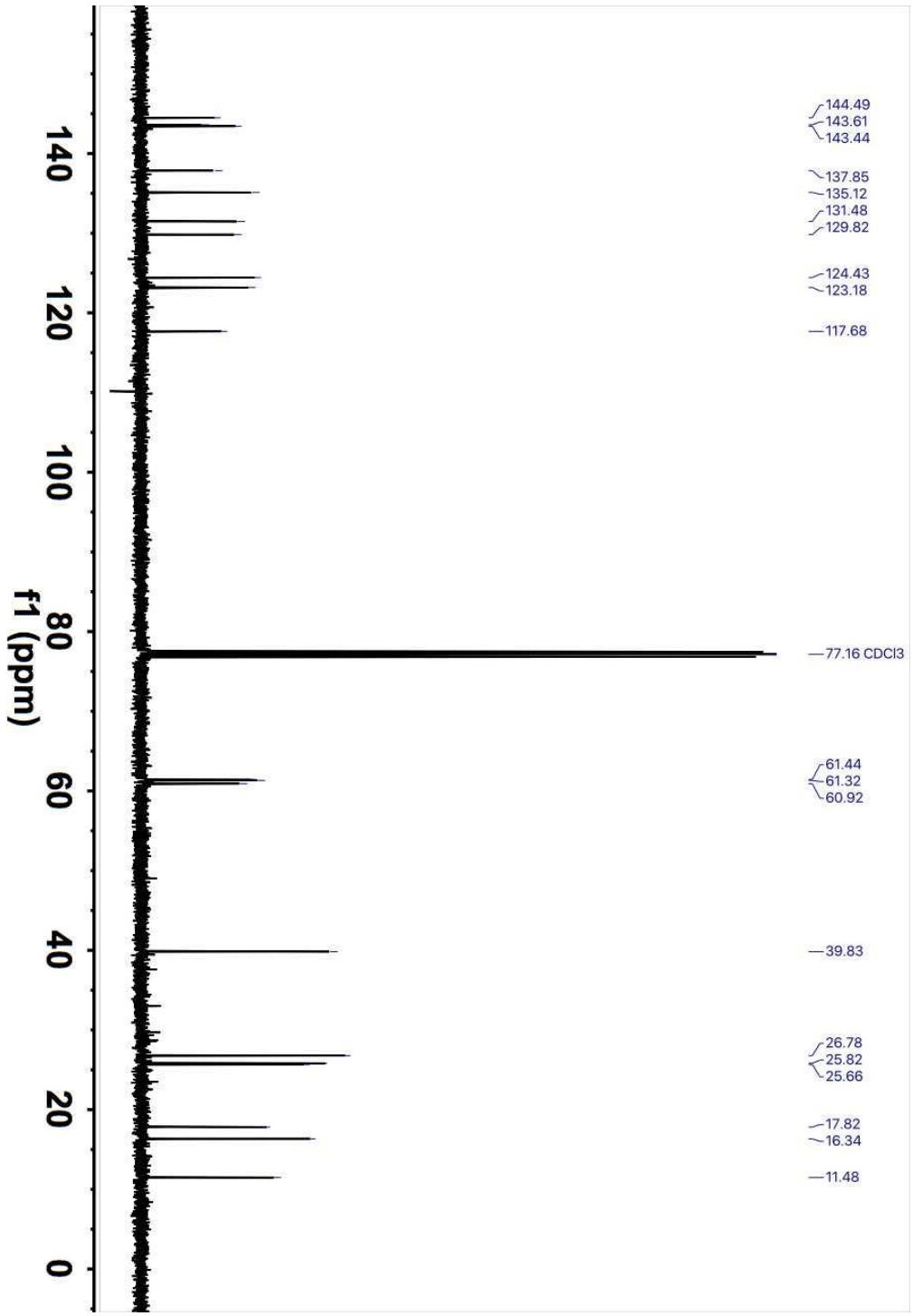

Fig. 3.S9. ^{1}H NMR (400 MHz) spectrum of ubiquinone-2 (8) in $CDCl_3$

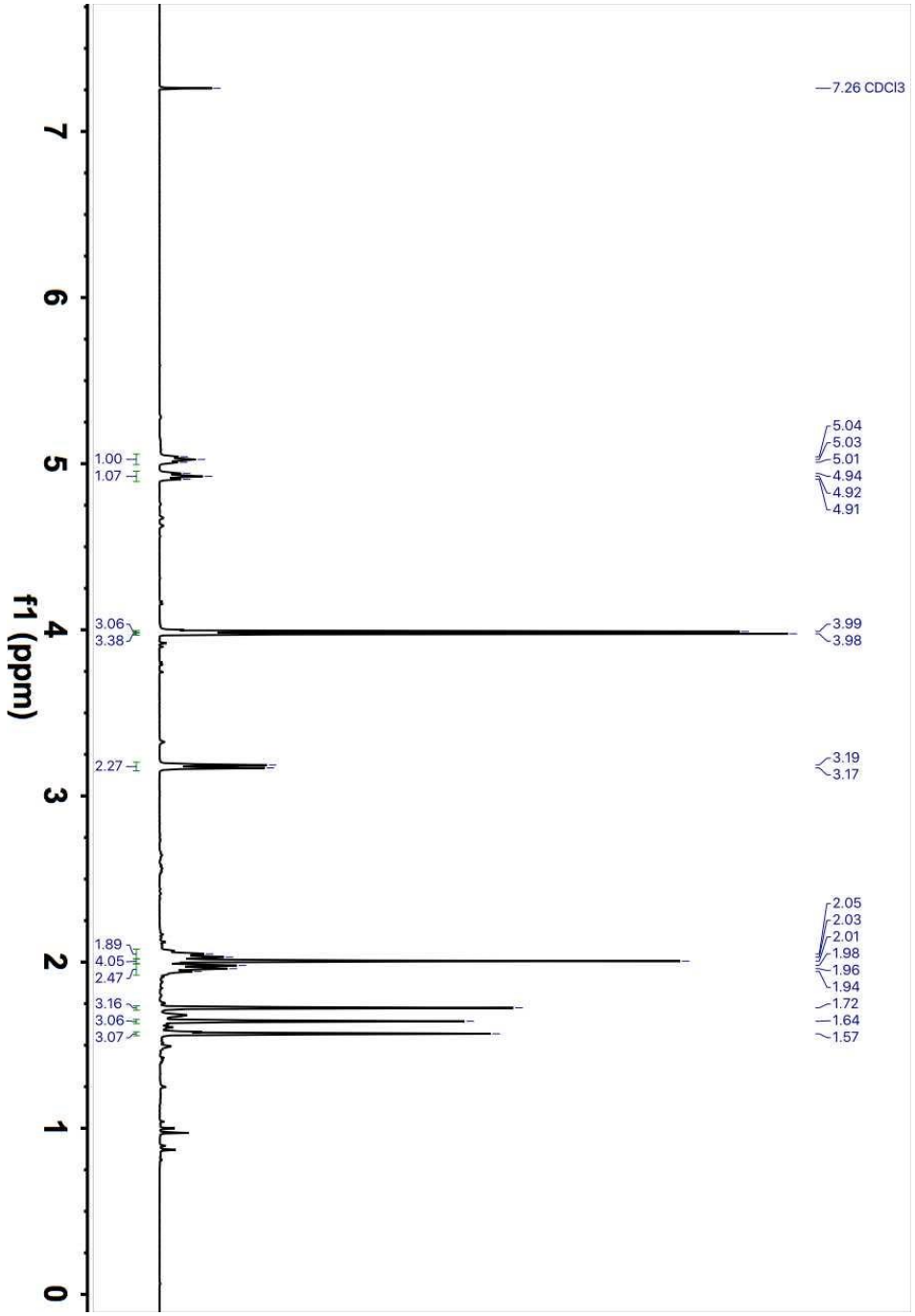

Fig. 3.S10. ^{13}C NMR (101 MHz) spectrum of ubiquinone-2 (8) in $CDCl_3$

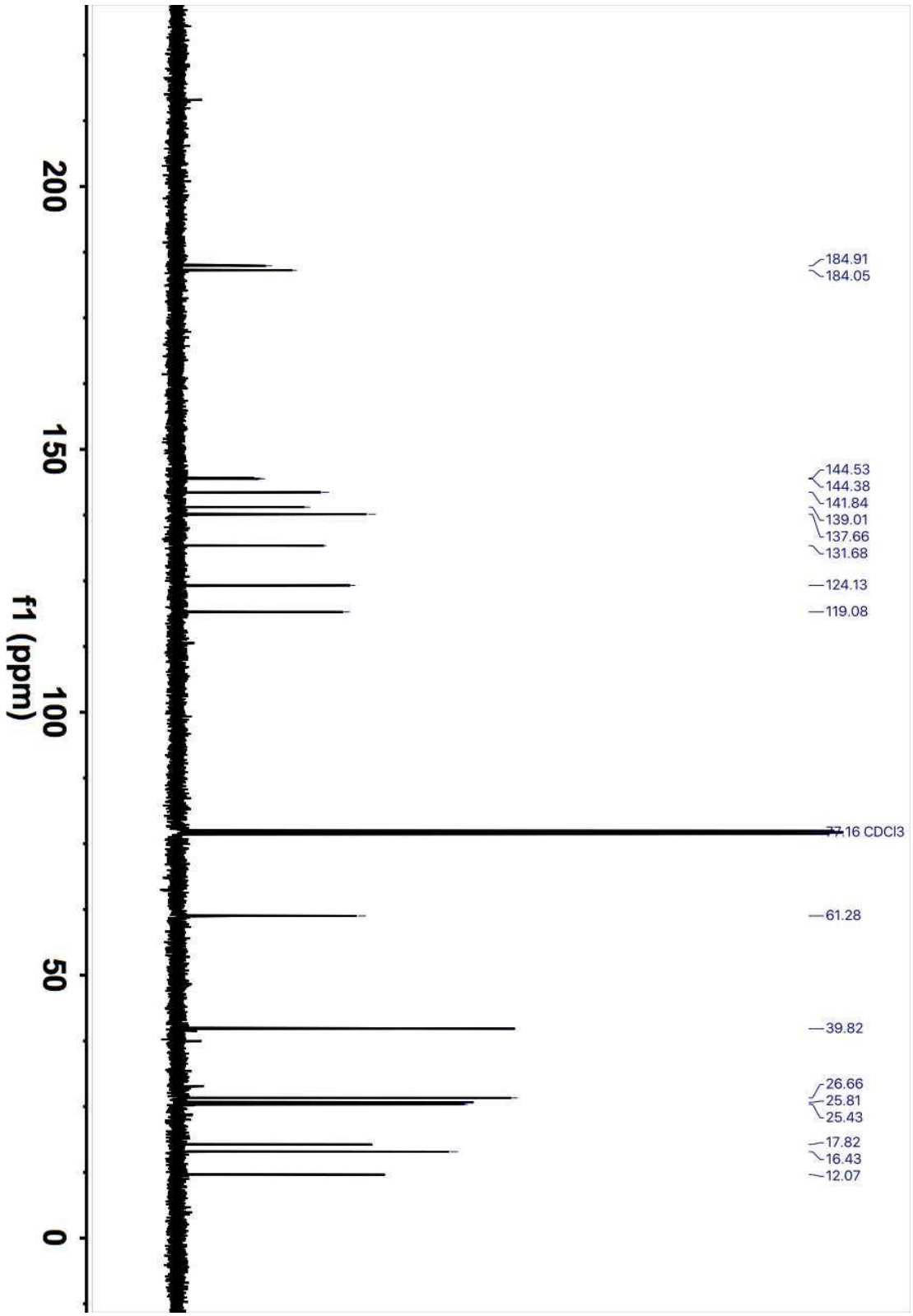

Fig. 3.S11. ^{1}H-^{1}H 2D gCOSY NMR (400 MHz) spectrum of ubiquinone-2 (8) in $CDCl_3$

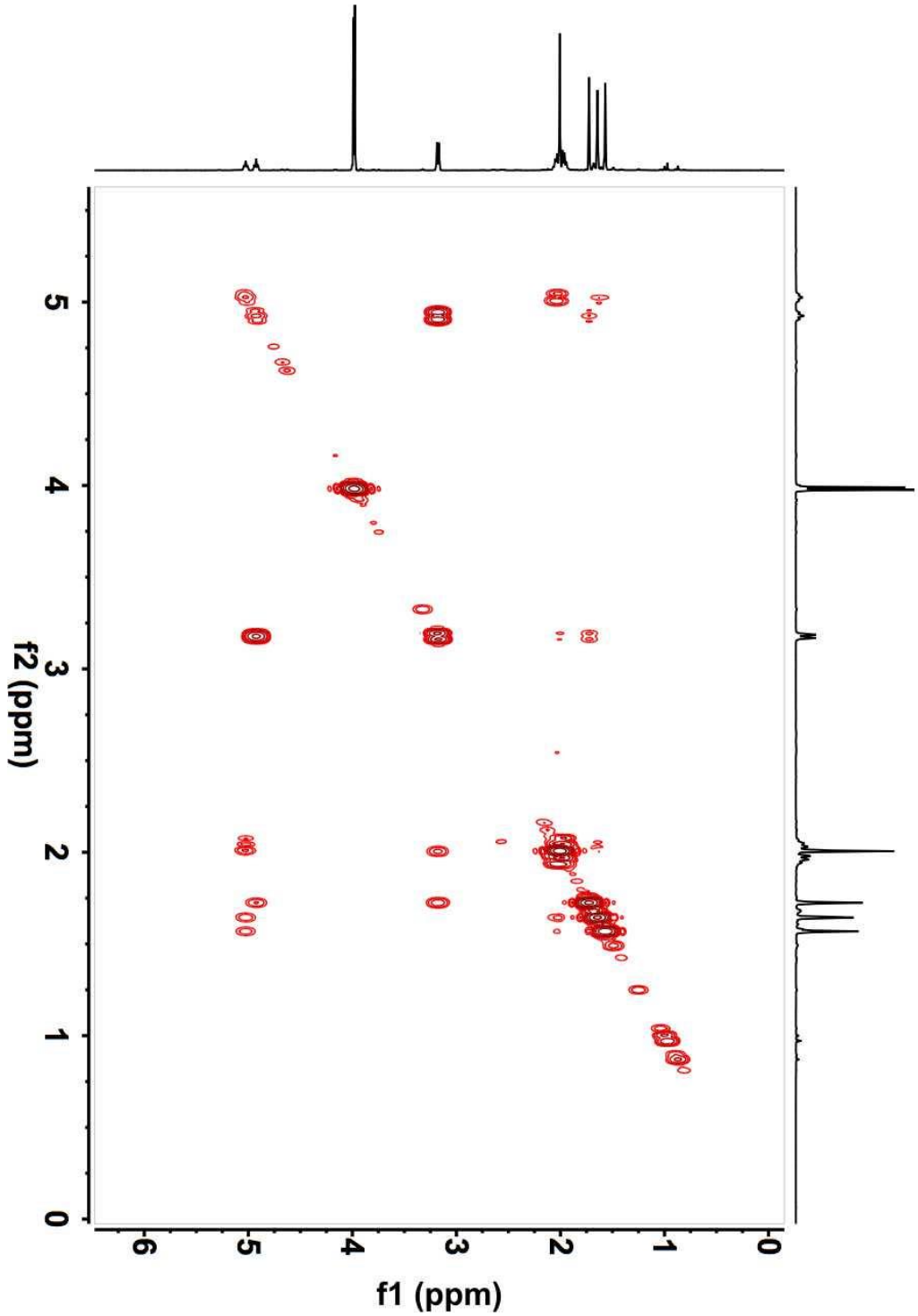

Fig. 3.S12. ^{1}H-^{13}C 2D HSQC NMR (400 MHz) spectrum of ubiquinone-2 (8) in $CDCl_3$

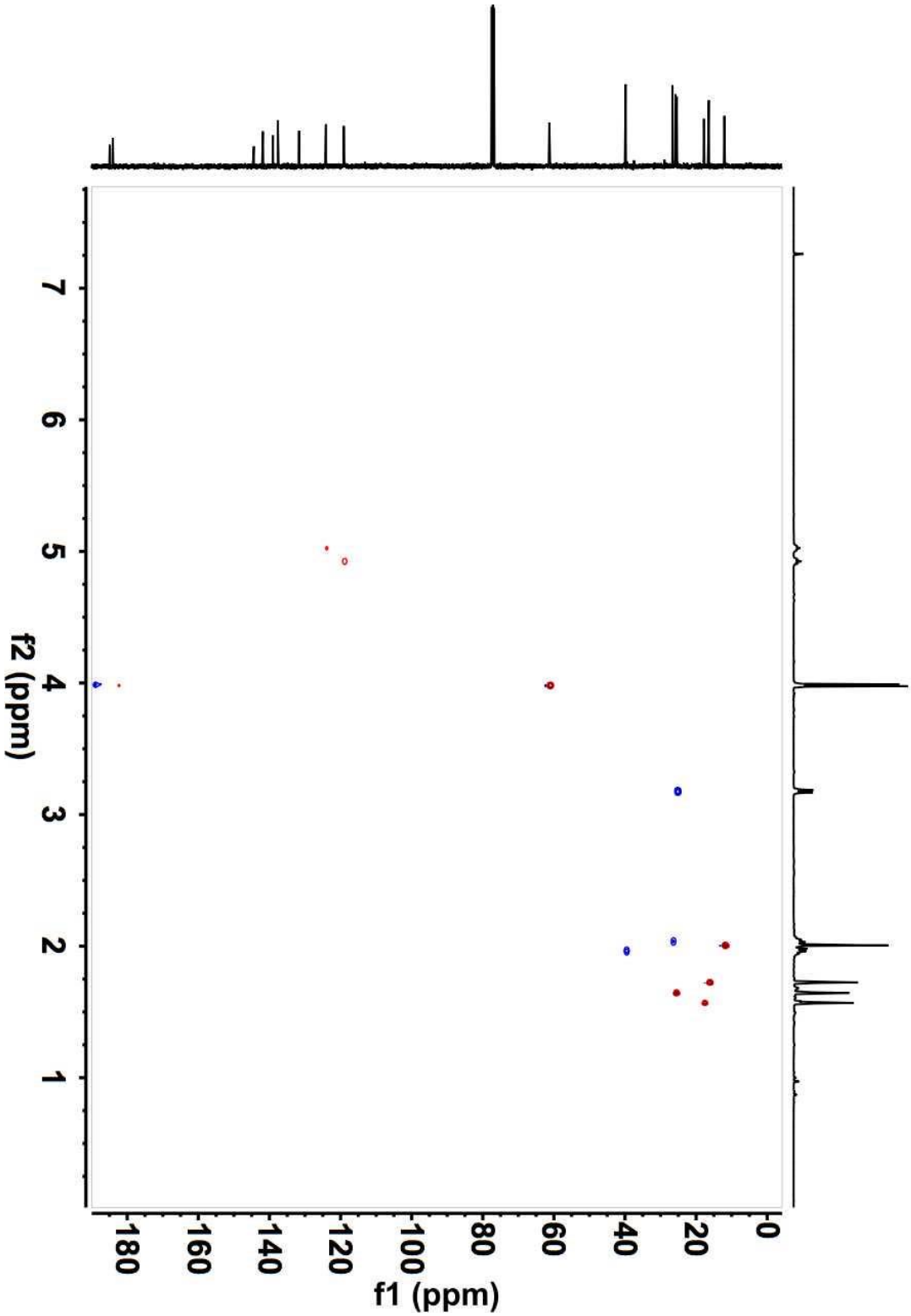

I B. NMR spectra for UQ-2

Fig. 3.S13. ^{1}H-^{1}H 2D ROESY NMR (400 MHz) spectrum of 20.0 mM UQ-2 at 25 °C in d_6-DMSO. A standard ROESYAD pulse sequence was used consisting of 256 transients with 16 scans in the f1 domain using a 400 ms mixing time and 2.0 sec. relaxation delay per t1 increment.

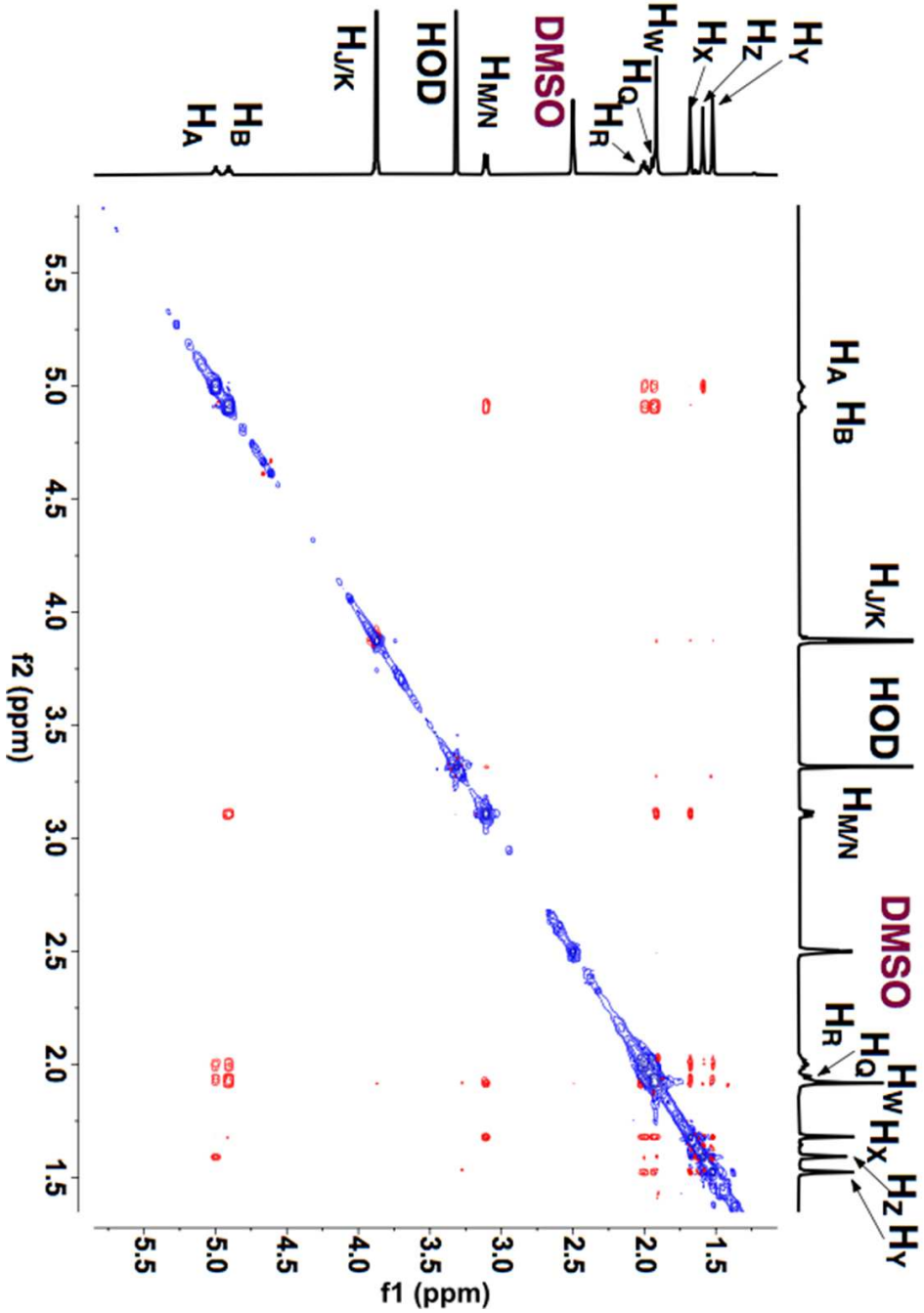

Fig. 3.S14. ^{1}H-^{1}H 2D gCOSY NMR (400 MHz) spectrum of 20.0 mM UQ-2 in d_6-DMSO at 25 °C. A standard gCOSY pulse sequence was used consisting of 200 t1 increments with 8 scans per t1 increment.

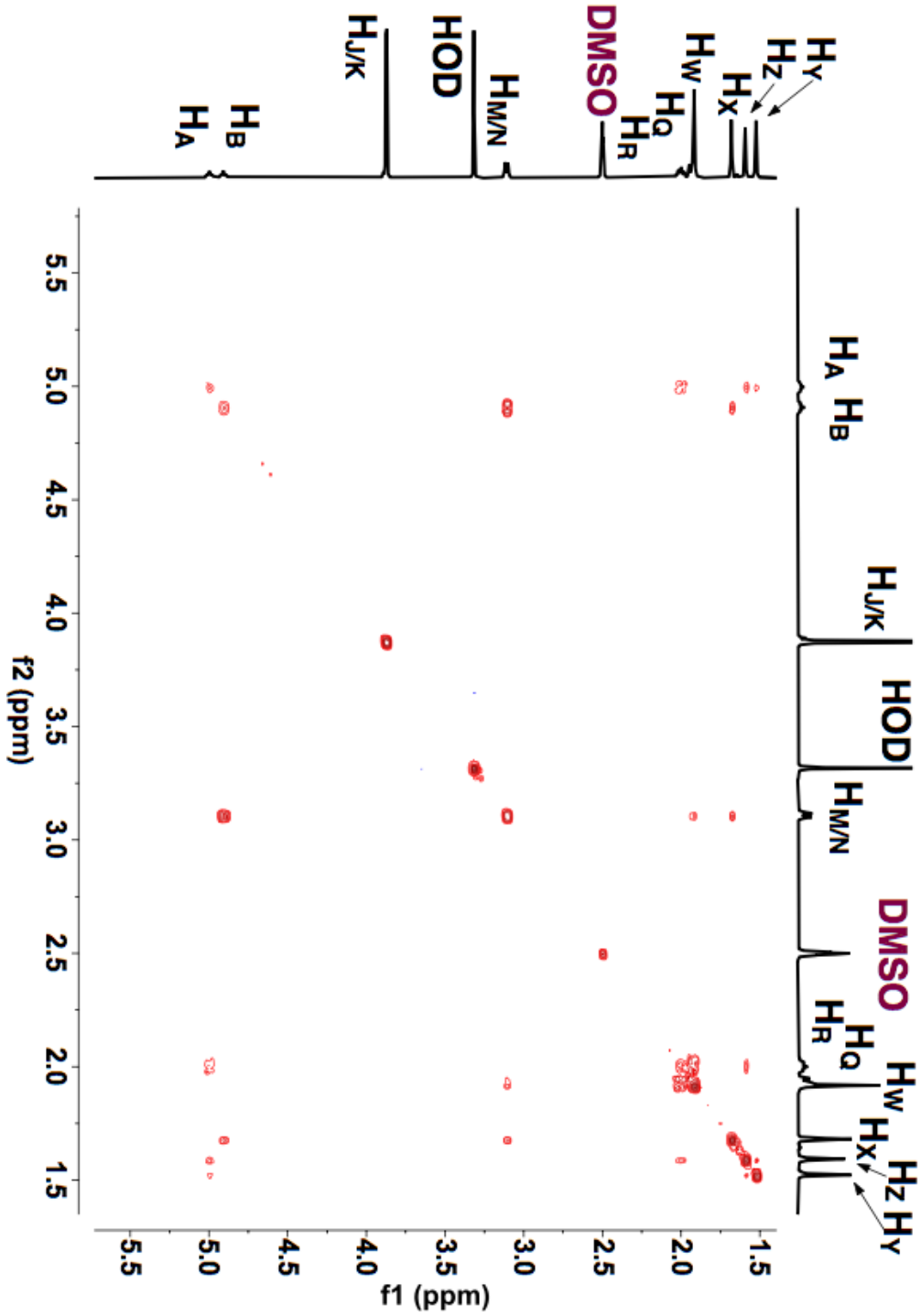

Fig. 3.S15. ^{1}H-^{1}H 2D gCOSY NMR (400 MHz) spectrum of 20.0 mM UQ-2 in d_3-acetonitrile at 25 °C. A standard gCOSY pulse sequence was used consisting of 200 t1 increments with 8 scans per t1 increment.

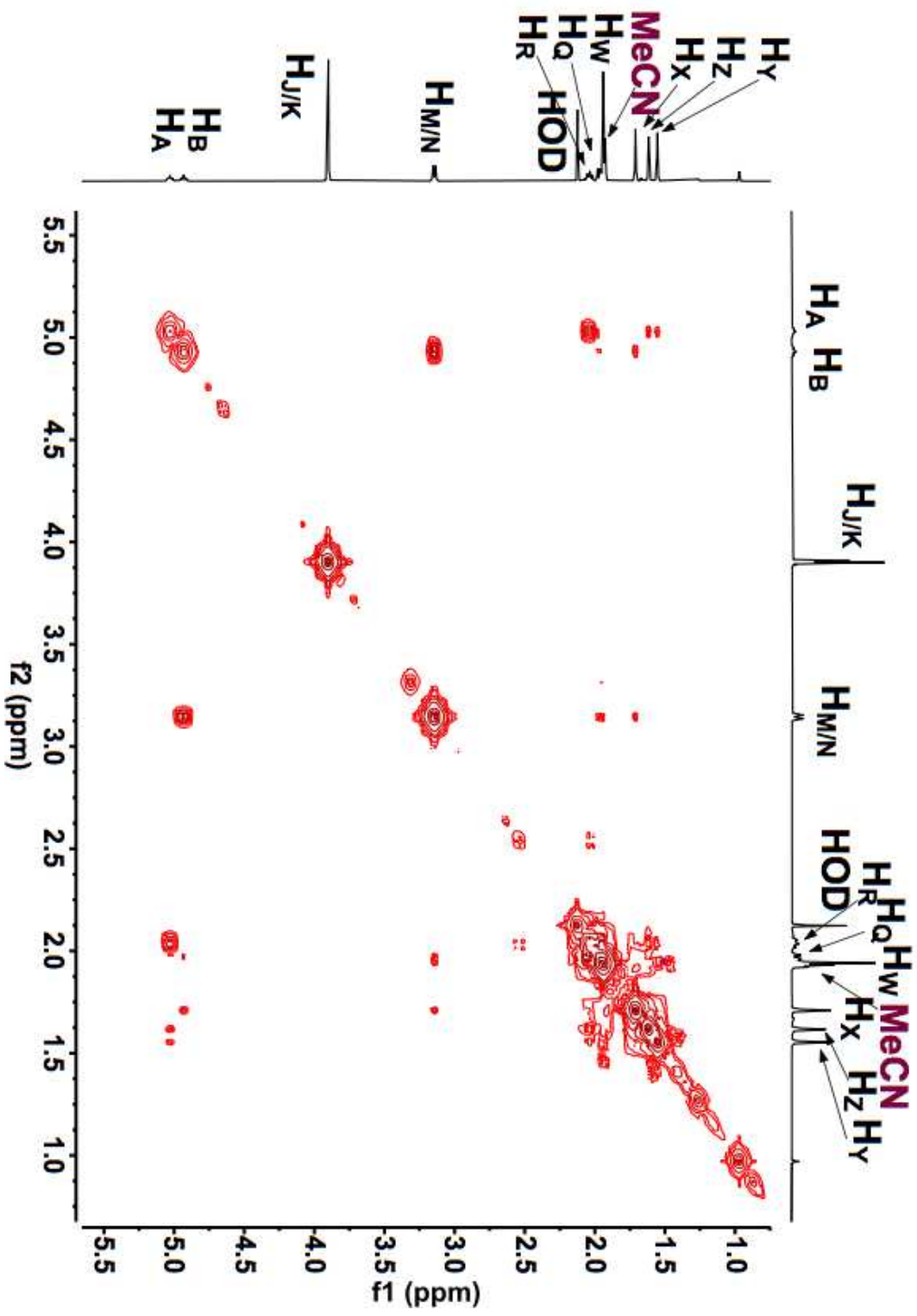

Fig. 3.S16. ^{1}H-^{1}H 2D NOESY NMR (400 MHz) spectrum of 20.0 mM UQ-2 at 25 °C in d_3-acetonitrile. A standard ROESYAD pulse sequence was used consisting of 256 transients with 16 scans in the f1 domain using a 400 ms mixing time and 2.0 sec. relaxation delay per t1 increment.

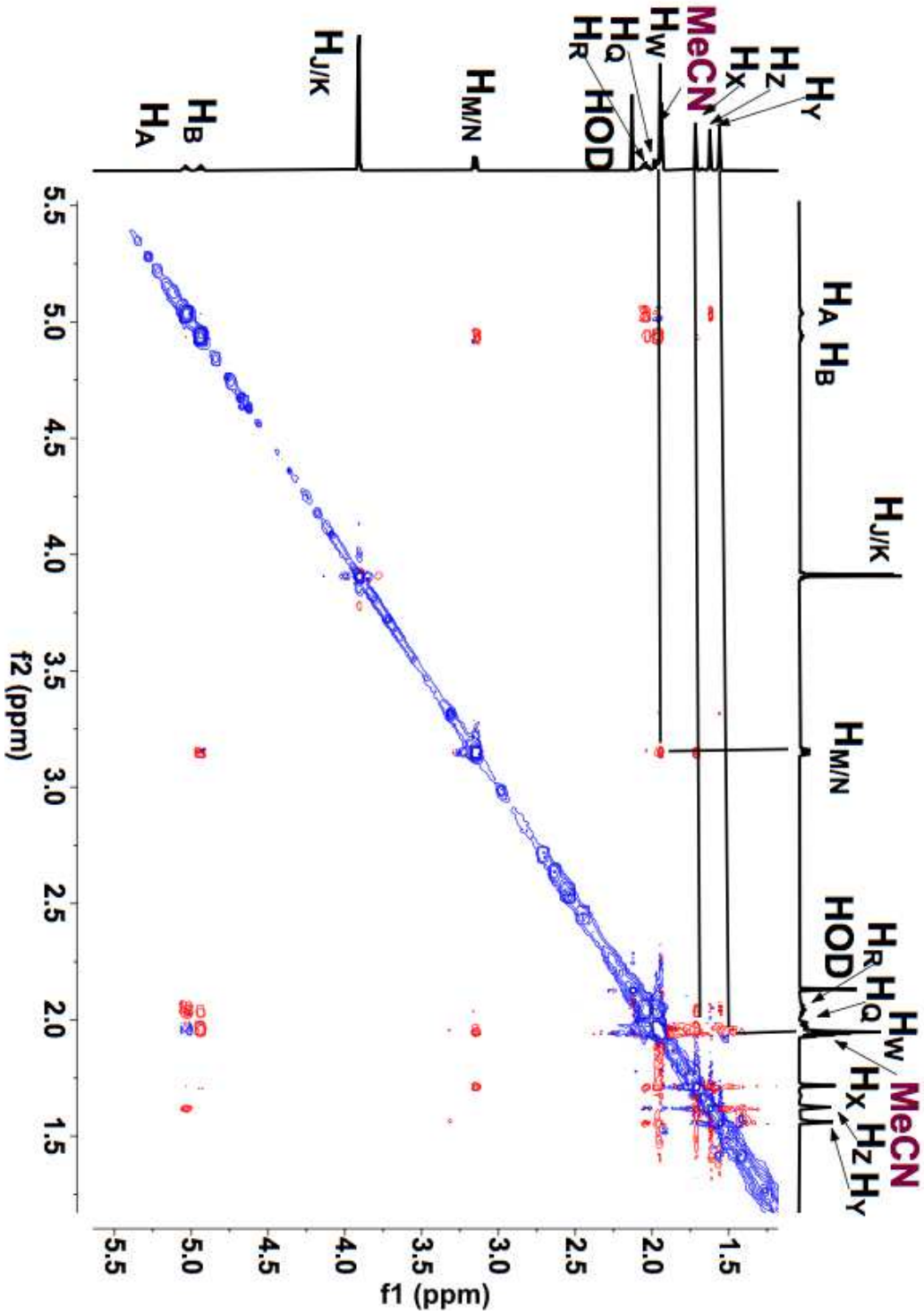

Fig. 3.S17. ^{1}H-^{1}H 2D ROESY NMR (400 MHz) spectrum of 20.0 mM UQ-2 at 25 °C in d_3-acetonitrile. A standard ROESYAD pulse sequence was used consisting of 256 transients with 16 scans in the f1 domain using a 400 ms mixing time and 2.0 sec. relaxation delay per t1 increment.

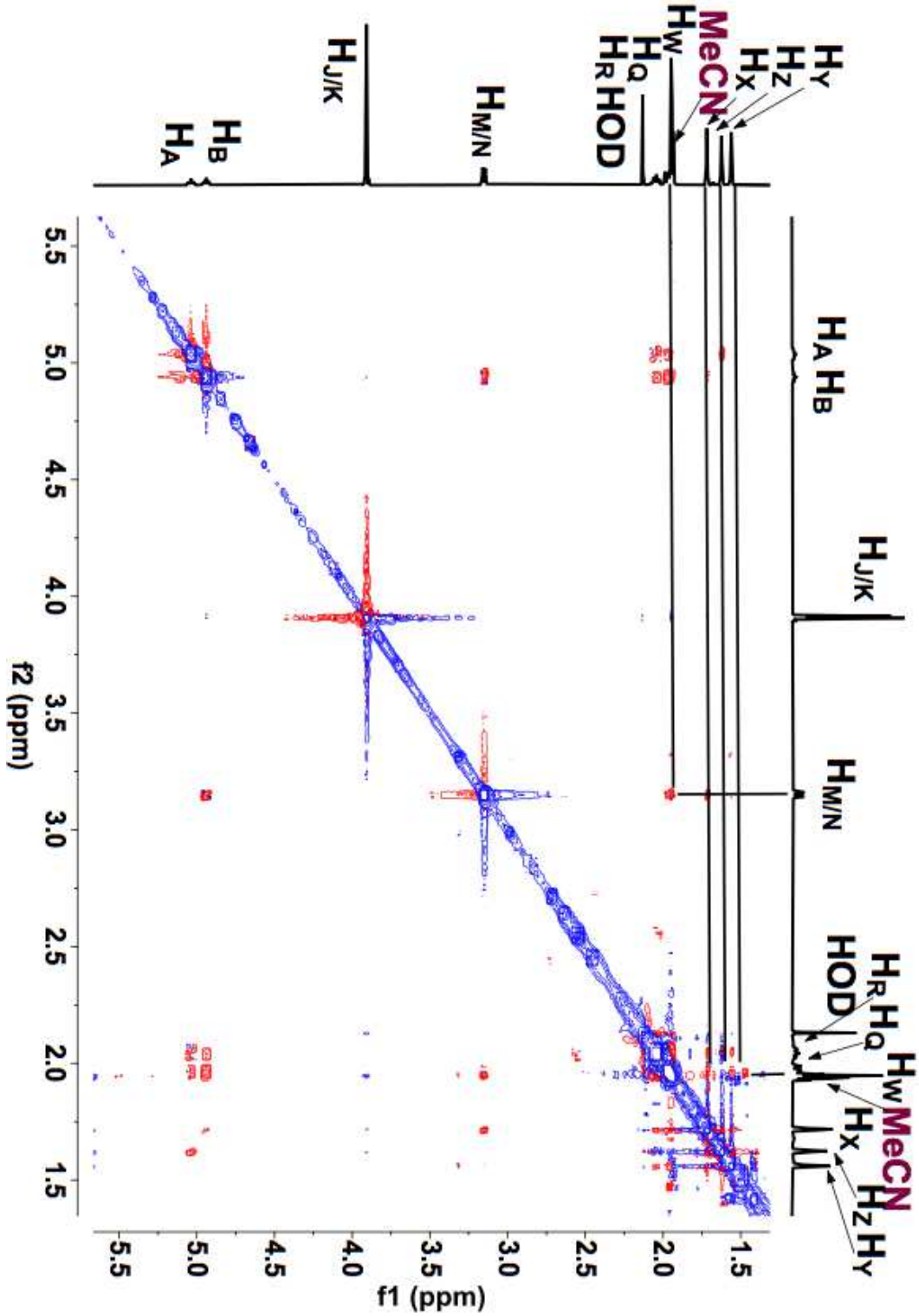

Fig. 3.S18. ^{1}H-^{1}H 2D gCOSY NMR (400 MHz) spectrum of 20.0 mM UQ-2 in C_6D_6 at 25 °C. A standard gCOSY pulse sequence was used consisting of 200 t1 increments with 8 scans per t1 increment.

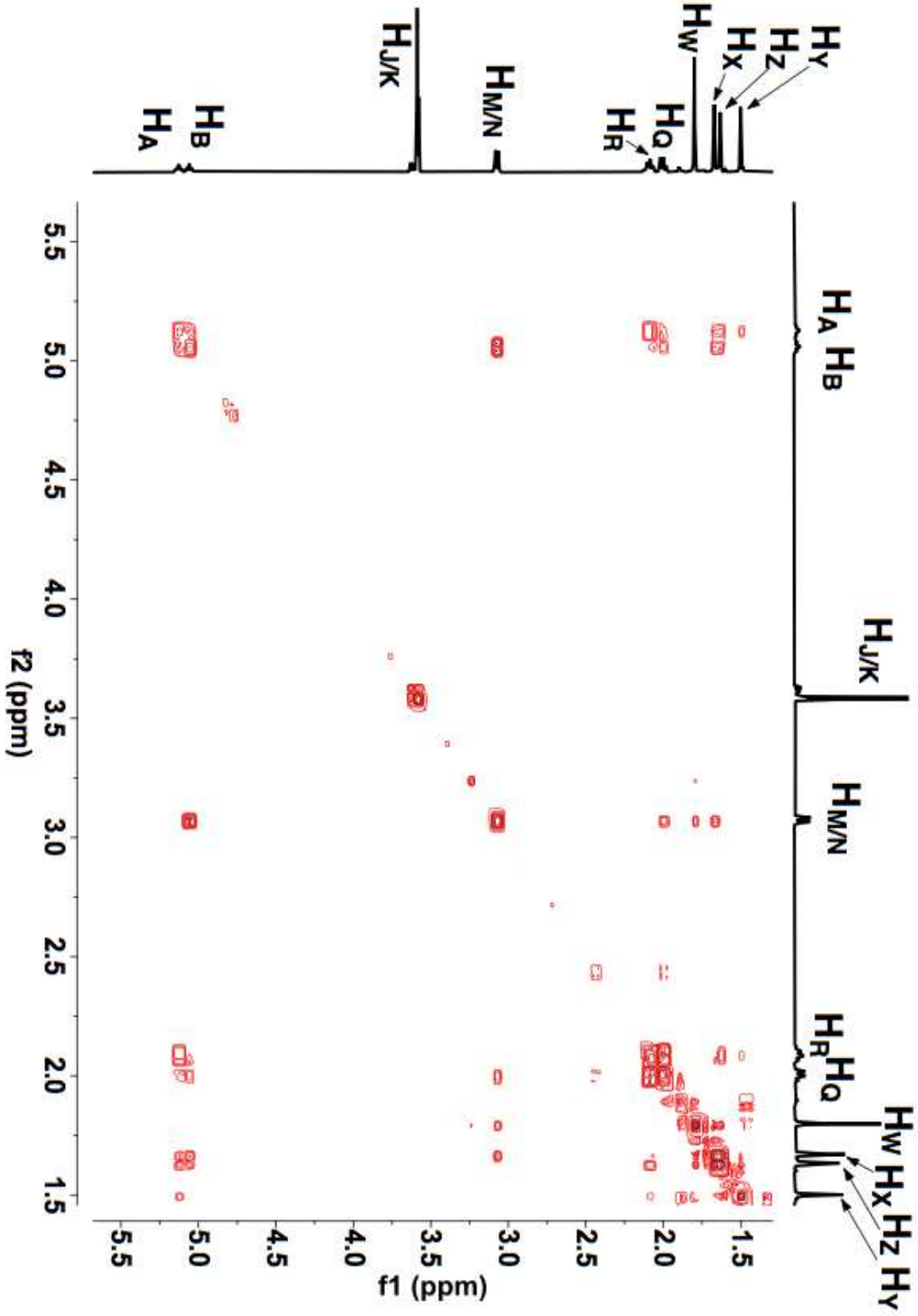

Figure 3.S19. (A) ^{1}H-^{1}H 2D Full NOESY and (B) ^{1}H-^{1}H 2D Partial NOESY NMR (400 MHz) spectra of 20 mM UQ-2 at 25 °C in C_6D_6. A standard NOESY pulse sequence was used consisting of 256 transients with 16 scans in the f1 domain using a 500 ms mixing time and 1.5 sec relaxation delay.

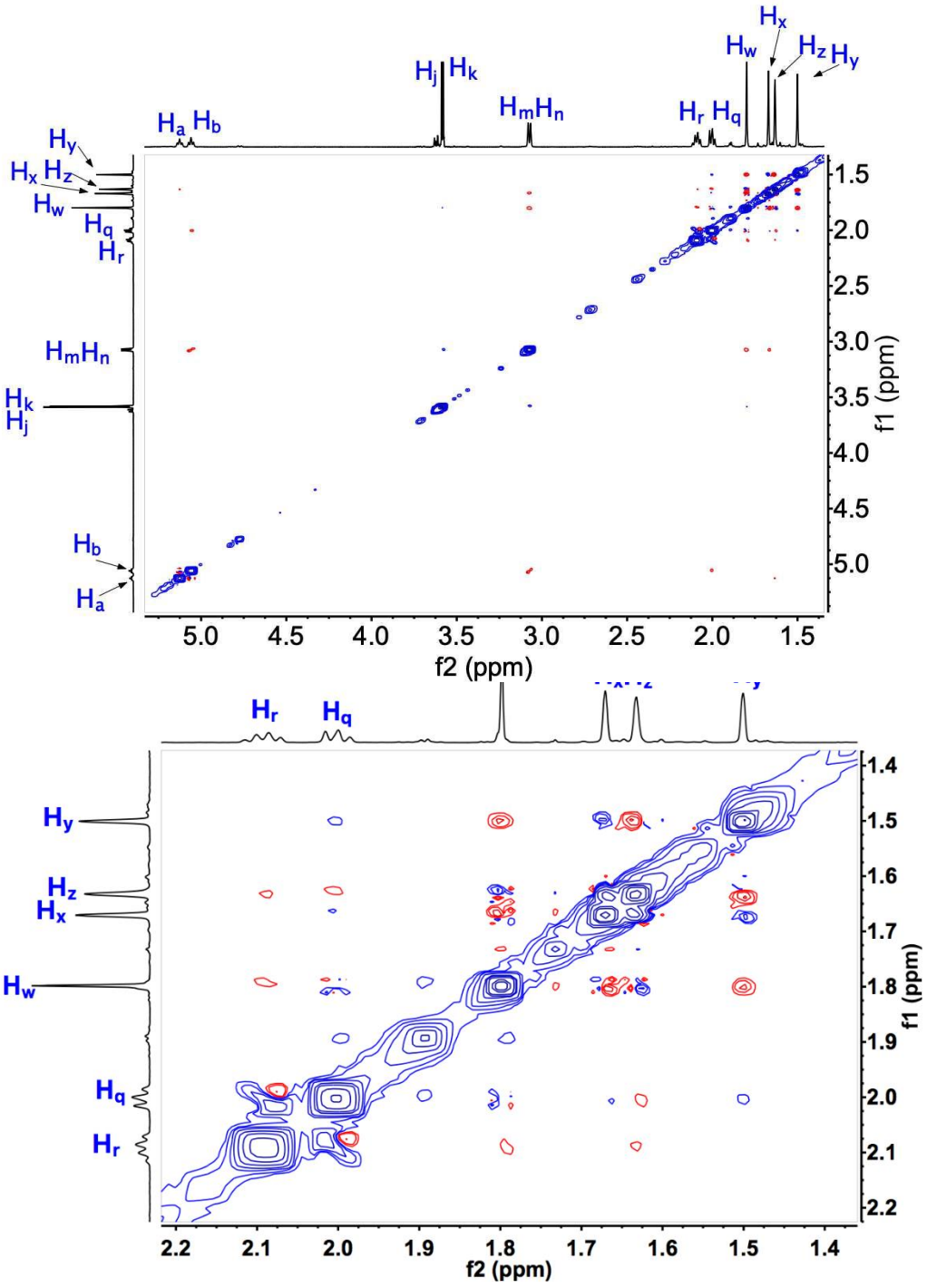

Fig. 3.S20. ^{1}H-^{1}H 2D ROESY NMR (400 MHz) spectrum of 20.0 mM UQ-2 at 25 °C in C_6D_6. A standard ROESYAD pulse sequence was used consisting of 256 transients with 16 scans in the f1 domain using a 400 ms mixing time and 2.0 sec. relaxation delay per t1 increment.

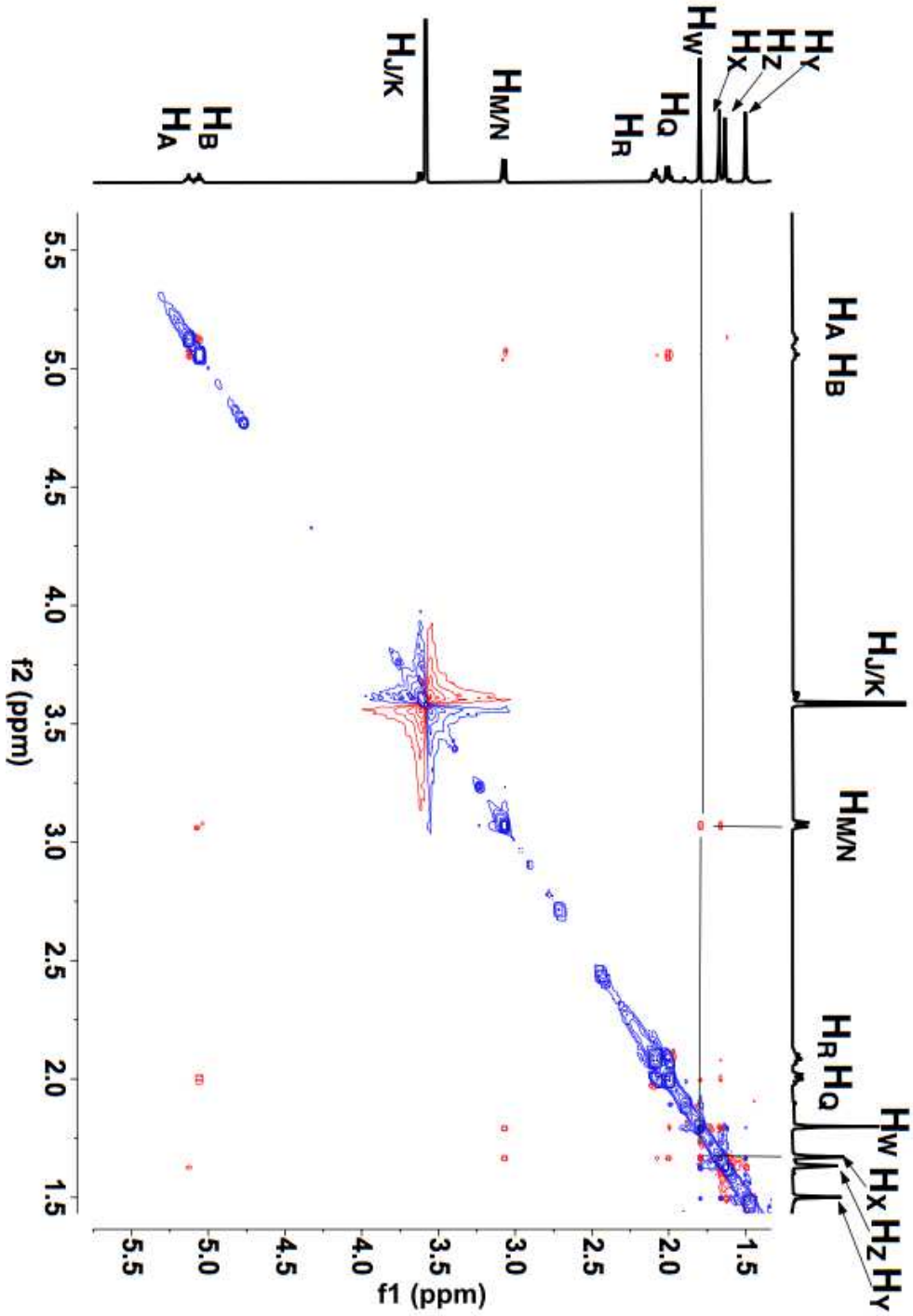

Fig. 3.S21. ^{1}H-^{1}H 2D gCOSY NMR (400 MHz) spectrum of 20.0 mM UQ-2 in d_5-pyridine at 25 °C. A standard gCOSY pulse sequence was used consisting of 200 t1 increments with 8 scans per t1 increment.

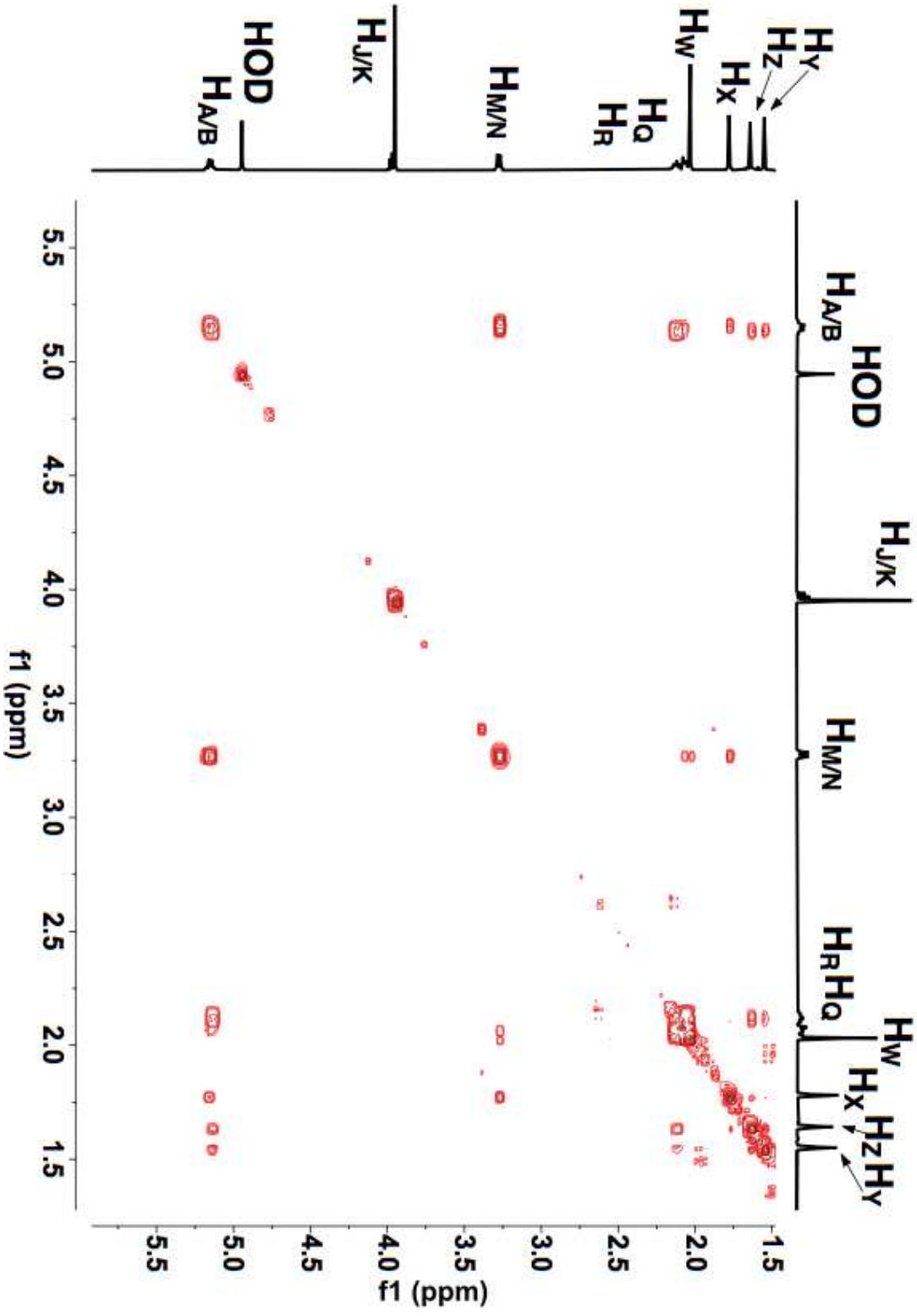

Figure 3.S22. (A) ^{1}H-^{1}H 2D Full NOESY and (B) ^{1}H-^{1}H 2D Partial NOESY NMR (400 MHz) spectra of 20 mM UQ-2 at 25 °C in d_5-pyridine. A standard NOESY pulse sequence was used consisting of 256 transients with 16 scans in the f1 domain using a 500 ms mixing time and 1.5 sec relaxation delay.

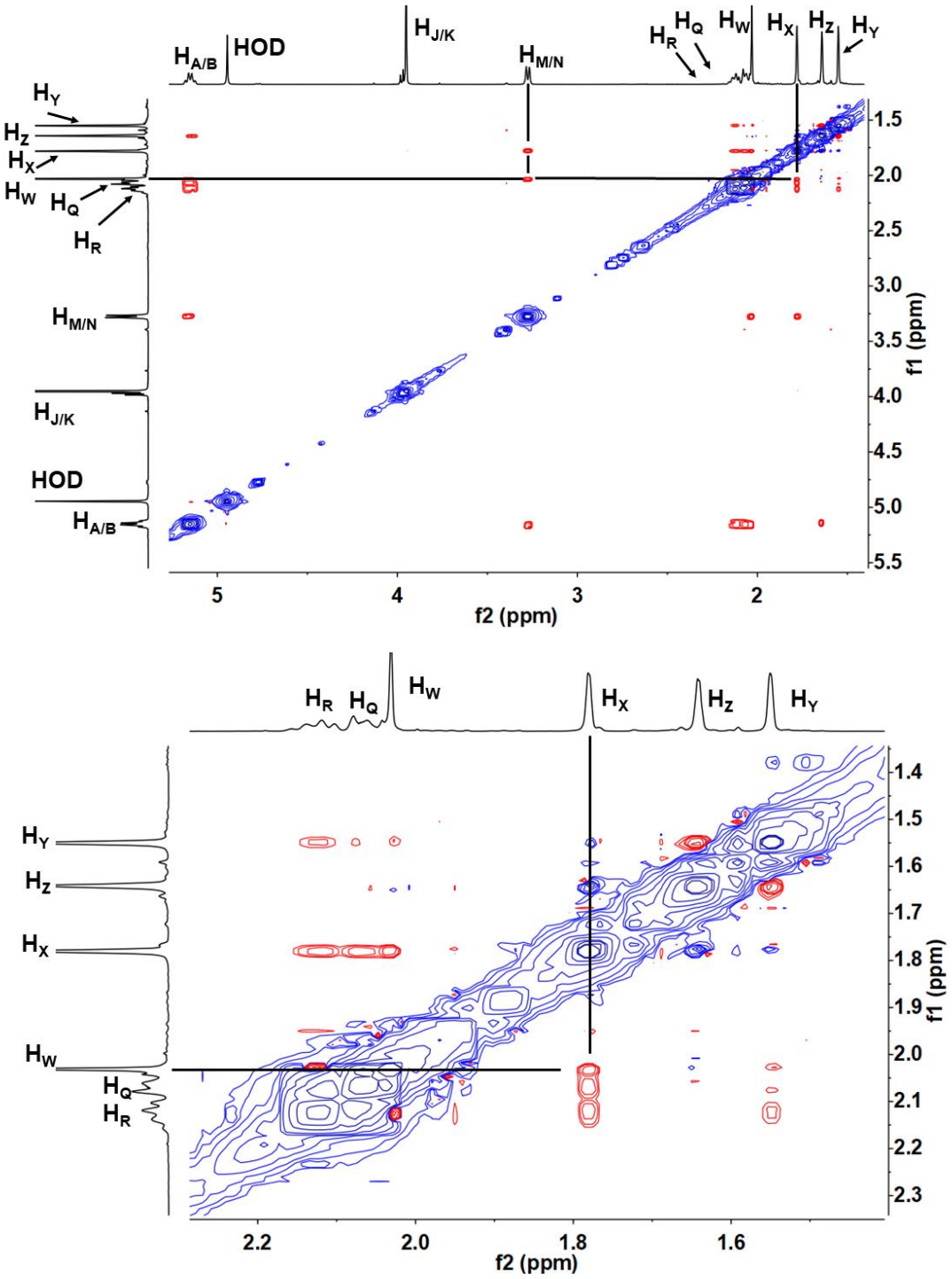

Fig. 3.S23. ^{1}H-^{1}H 2D ROESY NMR (400 MHz) spectrum of 20.0 mM UQ-2 at 25 °C in d_5-pyridine. A standard ROESYAD pulse sequence was used consisting of 256 transients with 16 scans in the f1 domain using a 400 ms mixing time and 2.0 sec. relaxation delay per t1 increment.

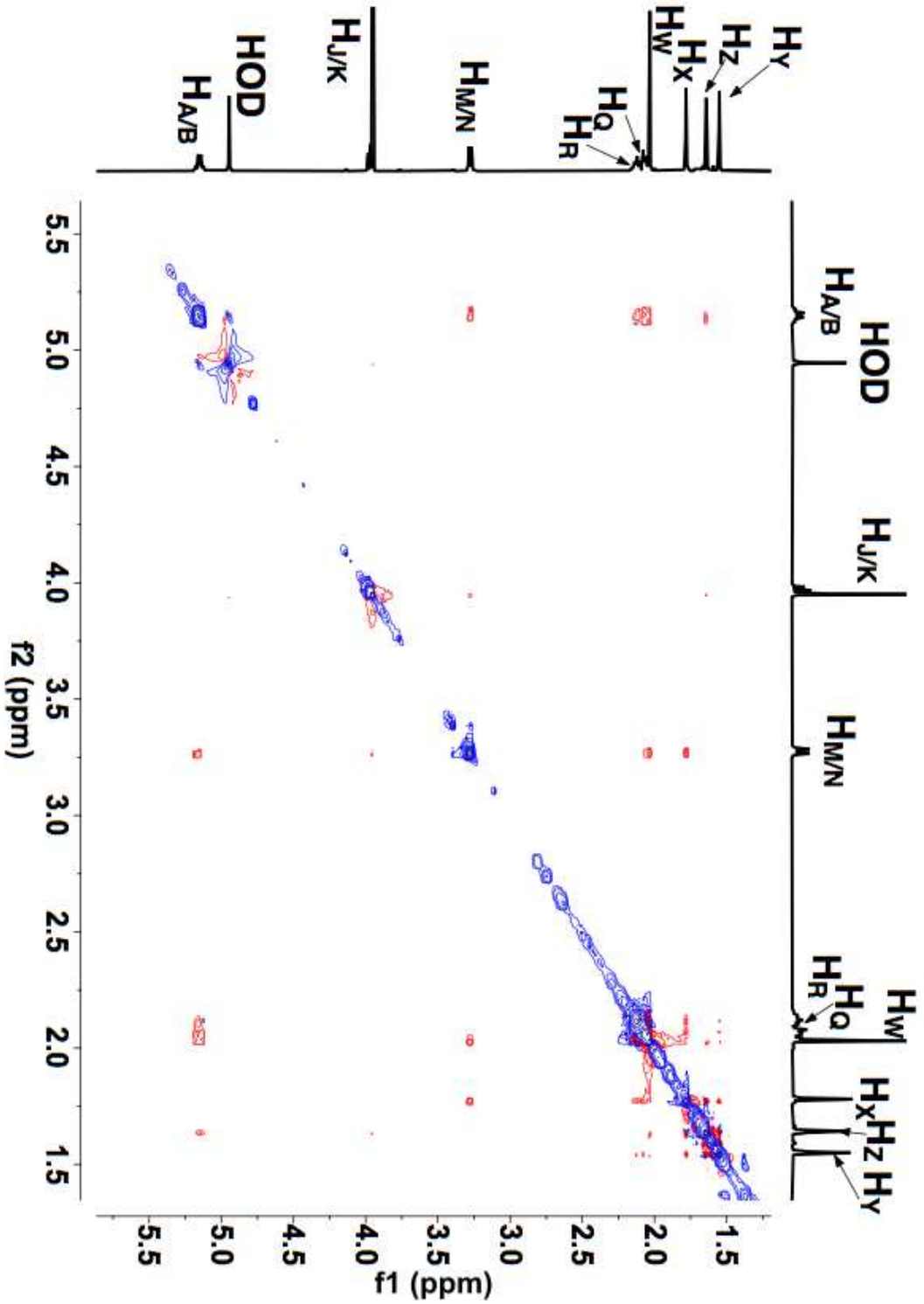

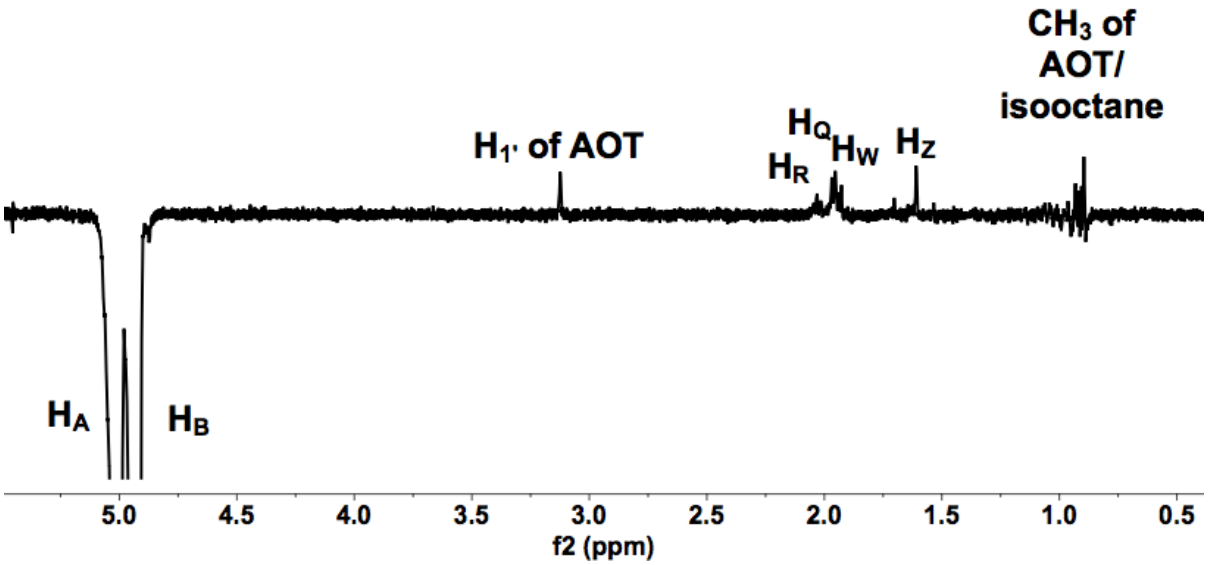

Fig. 3.S24. ^{1}H-^{1}H 1D NOESY in *w0* 12 reverse micelles with irradiated H_A and H_B protons (5.14 ppm, 80.871 Hz). A NOESY1D pulse sequence consisted of 128 transients in the f1 domain using a 200 ms mixing time and 2.0 sec relaxation delay.

IC. Molecular Mechanics: conformational analysis of UQ-2 and MK-2 and proton distances

To generate visual aids for UQ-2 conformations, Merck Molecular Force Field 94 (MMFF94) Molecular Mechanics gas phase simulations were conducted using ChemBio3D Ultra 12.0 at 25 °C. Conformations were generated using ChemBio3D Ultra 12.0 where UQ-2 structures were built and then desired bonds rotated to reflect the inter-atomic distances observed by NMR spectroscopy. Conformations were then energy minimized with a root mean square (RMS) gradient of 0.1 and 10 iterations to obtain proper bond lengths and angles to result in the conformations that agreed with our interpretation of the cross-peak observations in the ^{1}H-^{1}H 2D NOESY and ROESY NMR spectral data.

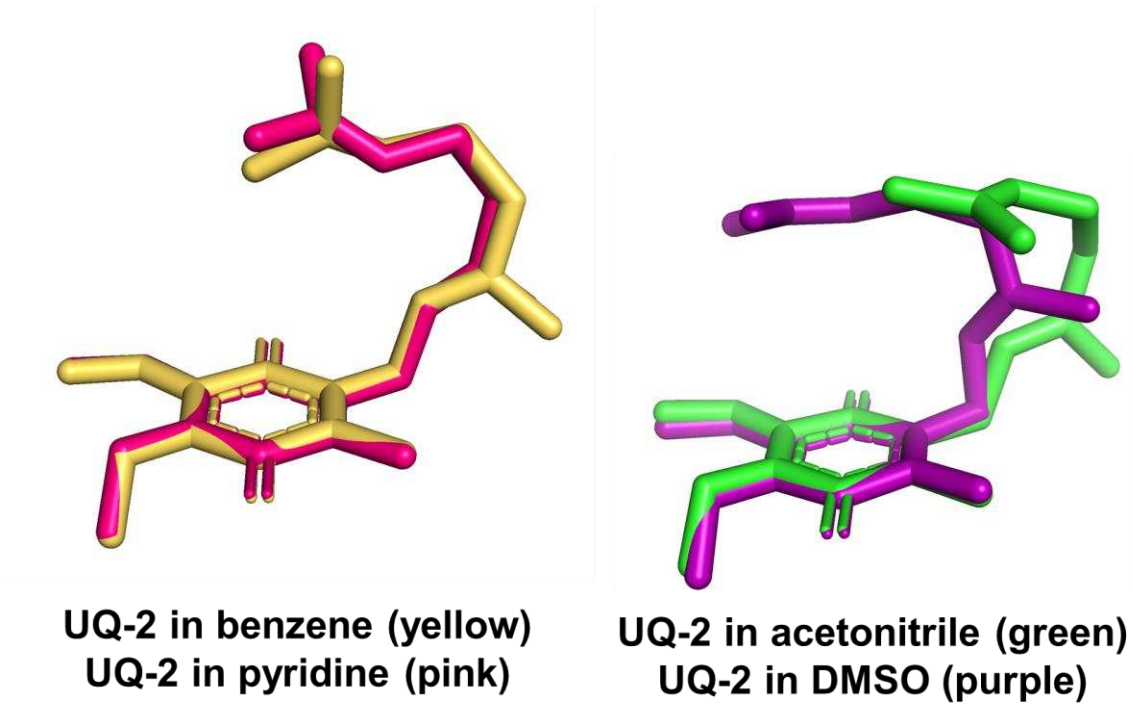

Fig. 3.S25 Comparison of superimposed 3D conformations of UQ-2 based on the 2D NMR data in d_3-acetonitrile / d_6-DMSO and d_6-benzene / d_5-pyridine. The images were generated using PyMOL molecular visualization system.

Table 3.S1. Comparison of interproton distances of UQ-2 and MK-2 in d_6-DMSO and d_5-pyridine.

Proton Pair	d_6-DMSO		d_5-pyridine	
	UQ-2	MK-2	UQ-2	MK-2
$H_W – H_M$	3.6 Å	3.7 Å	3.7 Å	3.5 Å
$H_W – H_N$	2.1 Å	2.2 Å	2.3 Å	2.0 Å
$H_W – H_X$	3.2 Å	2.5 Å	3.9 Å	2.7 Å
$H_W – H_Y$	3.1 Å	2.6 Å	8.1 Å	6.1 Å
$H_W – H_Z$	5.1 Å	4.8 Å	5.3 Å	7.0 Å
$H_W – H_A$	6.2 Å	6.5 Å	3.9 Å	7.1 Å
H_W - H_B	5.0 Å	4.1 Å	2.9 Å	4.7 Å
$H_W – H_R$	4.7 Å	5.9 Å	5.5 Å	6.6 Å
H_W - H_Q	5.9 Å	4.7 Å	5.0 Å	5.4 Å

Table 3.S2. Comparison of interproton distances of UQ-2 and MK-2 w_0 12 reverse micelles. The interproton distances for UQ-2 were measured from nearest proton to nearest proton (i.e., closest H_W proton to closest H_Y proton)

Proton Pair	UQ-2	MK-2
$H_W – H_M$	3.6 Å	3.7 Å
$H_W – H_N$	2.1 Å	2.2 Å
$H_W – H_X$	2.6 Å	2.7 Å
$H_W – H_Y$	4.6 Å	4.2 Å
$H_W – H_Z$	3.7 Å	4.0 Å
$H_W – H_A$	4.3 Å	5.6 Å
H_W - H_B	4.2 Å	4.1 Å
$H_W – H_R$	5.3 Å	5.6 Å
H_W - H_Q	4.9 Å	4.6 Å

1D. Langmuir Monolayers for UQ-2

Methods: Compression Modulus Analysis of Langmuir Monolayers

The compression moduli of normalized compression isotherms were calculated with equation 3.S1, where C_s^{-1} is the compression modulus, A is the normalized area per phospholipid ($Å^2$), and π is the surface pressure (mN/m).

$$C_s^{-1} = -A\left(\frac{d\pi}{dA}\right) \quad (3.S1)$$

Compression modulus calculations were performed in Origin 2021. The derivative of surface pressure was smoothed with a Savitsky-Golay function (2nd degree polynomial, 350 points per window) before being multiplied with negative area.

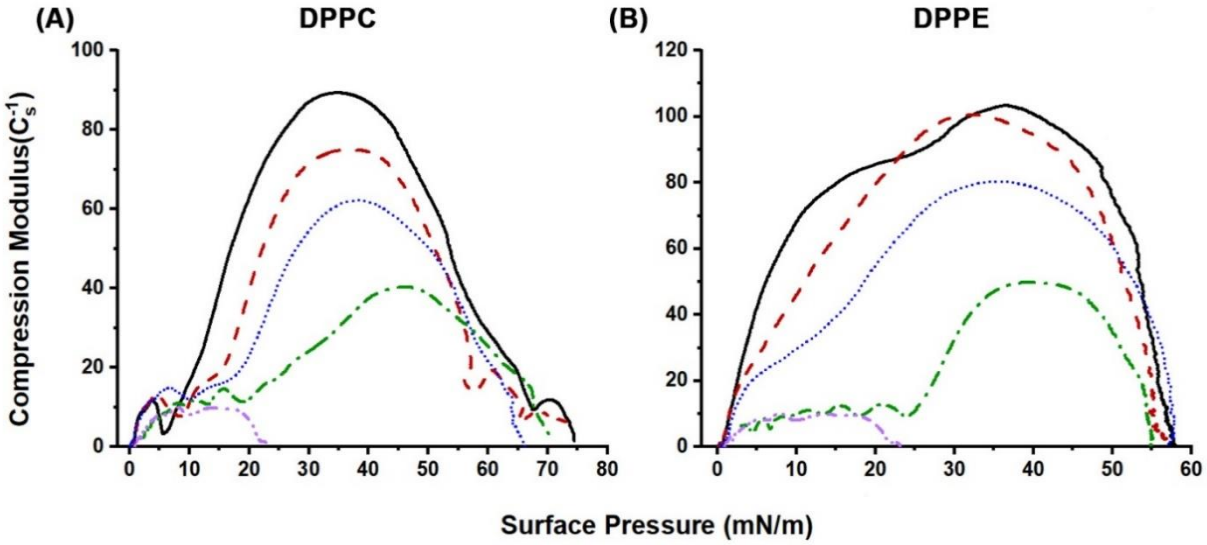

Figure 3.S26. The compression moduli of normalized UQ-2 mixed monolayers of (A) DPPC or (B) DPPE. Solid black curves represent lipid controls, red dashed curves represent 75:25 lipid:UQ-2 films, blue dotted curves represent 50:50 lipid:UQ-2 films, green dash-dot curves represent 25:75 lipid:UQ-2 films, and purple dash-dot-dot curves represent UQ-2 films.

Table 3.S3. Percent difference between the area of mixed DPPC:UQ-2 monolayers and the DPPC control. Positive numbers indicate an expansion of area while negative numbers suggest a condensation. The shaded rows indicate physiological surface pressure.

Surface Pressure (mN/m)	75:25 DPPC:UQ-2	50:50 DPPC:UQ-2	25:75 DPPC:UQ-2
5	10.9	26.6	92.9
10	19.5	49.2	111.9
15	14.0	39.0	91.0
20	8.6	28.0	66.8
25	6.8	21.6	48.4
30	6.2	19.0	36.5
35	5.6	17.4	27.7
40	5.5	16.6	22.3
35	4.5	15.4	18.5
50	4.0	15.0	15.7
55	4.6	13.5	14.1

Table 3.S4. Percent difference between the area of mixed DPPE:UQ-2 monolayers and the DPPE control. Positive numbers indicate an expansion of area while negative numbers suggest a condensation. The shaded rows indicate physiological surface pressure.

Surface Pressure (mN/m)	75:25 DPPE:UQ-2	50:50 DPPE:UQ-2	25:75 DPPE:UQ-2
5	14.9	39.0	208.3
10	11.9	31.5	145.8
15	10.2	25.9	104.9
20	9.4	22.0	71.5
25	9.4	20.3	44.1
30	9.5	19.3	29.1
35	9.9	19.0	25.0
40	10.1	18.5	22.5
35	9.8	17.5	20.6
50	8.7	16.7	16.9
55	7.0	16.6	5.4

Dynamic Light Scattering data for UQ-2

Table 3.S5. Dynamic Light Scattering measurements on UBQ-2 in 0.1 M AOT/isooctane RMs

Dynamic Light Scattering measurements on UQ-2 in 0.1 M AOT/isooctane RMs

w_0	N (probes)	N (Micelles)	N (probes) / N (Micelles)	(UBQ-2) r_h[a] (nm)	(UBQ-2) PDI	Blank r_h[a] (nm)	r_h[b] Literature (nm)	PDI Empty RM
20	1.07×10^{18}	8.20×10^{17}	1.30	4.2 (± 0.1)	0.60 (± 0.14)	4.5 (± 0.3)	4.4	0.38 (± 0.28)
12	6.34×10^{17}	2.09×10^{18}	0.30	3.7 (± 0.6)	0.14 (± 0.04)	3.72 (± 0.02)	3.7	0.19 (± 0.01)
4	2.00×10^{17}	8.31×10^{19}	0.02	2.3 (± 0.3)	0.16 (± 0.03)	2.0 (± 0.1)	2.5	0.31 (± 0.05)

[a] Radius measurements were taken from the volume distribution. [b] (Maitra 1984).

RM Sample Preparation for Dynamic Light Scattering (DLS) Studies.

RMs for DLS studies were prepared as described for the NMR spectroscopic studies except that distilled deionized (DDI) H_2O was used as the water pool instead of D_2O and the 0.50 M AOT was diluted with isooctane after the RM had formed to a final concentration of 0.1 M AOT.

DLS Measurements.

The hydrodynamic radius of the RMs was determined by DLS measurements performed on a Malvern Zetasizer Nano ZS instrument (Malvern Instruments, Malvern, UK). The DLS cuvette (1 cm X 1 cm, glass) was washed out three times with isooctane followed by three washes with the RM sample. Then, the cuvette was filled with 1 mL of the RM sample and closed with a Teflon cap. Each experiment was conducted at 25 °C and consisted of a 700 sec. sample equilibration period followed by 10 measurements consisting of 15 scans each (Peters, Groninger et al. 2016).(Peters, Groninger et al. 2016) Each sample was measured in triplicate and the radius and

pdi were recorded. The data were analyzed using Malvern Zetasizer Software Version 711 and compared to values reported in literature.(Maitra 1984)

DLS measurements of UBQ-2 containing AOT/isooctane RMs.

DLS measurements of UQ-2 containing AOT/isooctane RMs. DLS established the formation of RMs. Samples of UQ-2 RMs were prepared using 0.10 M AOT/isooctane and the results are shown in Table 3.S5. The average radius obtained from w_0 sizes 4, 12, and 20 compared favourably with those reported previously in the literature.(Maitra 1984), (Eicke and Rehak 1976), (Zulauf and Eicke 1979) These results were observed with RMs prepared with and without UQ-2. These results showed that RMs formed, and that the presence of UQ-2 did not significantly affect the size or stability of the RM.

References

Eicke, H. F. and J. Rehak (1976). "FORMATION OF WATER-OIL-MICROEMULSIONS." Helv. Chim. Acta 59(8): 2883-2891.

Maitra, A. (1984). "DETERMINATION OF SIZE PARAMETERS OF WATER AEROSOL OT OIL REVERSE MICELLES FROM THEIR NUCLEAR MAGNETIC-RESONANCE DATA." J. Phys. Chem. 88(21): 5122-5125.

Maitra, A. (1984). "Determination of size paramters of water-Areosol OT-oil reverse micelles from their nuclear magnetic resonance data." J. Phys. Chem. 88(21): 5122-5125.

Peters, B. J., A. S. Groninger, F. L. Fontes, D. C. Crick and D. C. Crans (2016). "Differences in Interactions of Benzoic Acid and Benzoate with Interfaces." Langmuir 92: 9451.

Peters, B. J., A. S. Groninger, F. L. Fontes, D. C. Crick and D. C. Crans (2016). "Differences in Interactions of Benzoic Acid and Benzoate with Interfaces." Langmuir 32(37): 9451-9459.

Zulauf, M. and H. F. Eicke (1979). "INVERTED MICELLES AND MICROEMULSIONS IN THE TERNARY-SYSTEM H2O-AEROSOL-OT-ISOOCTANE AS STUDIED BY PHOTON CORRELATION SPECTROSCOPY." J. Phys. Chem. 83(4): 480-486.

Appendix II:
Distribution of Work

Chapter 1

Opening remarks written by Margaret Braasch-Turi

Chapter 2

The author contributions are as follows: Margaret Braasch-Turi (M.B.T), Debbie C. Crans (D.C.C) and Jordan T. Koehn (J.T.K).

Conceptualization, D.C.C. and M.B.T.; writing—original draft preparation, M.B.T. and D.C.C.; writing—review and editing, M.B.T, D.C.C., and J.T.K. supervision, D.C.C.; project administration, D.C.C.; funding acquisition, D.C.C. All authors have read and agreed to the published version of the manuscript.

Chapter 3

The author contributions are as follows: Margaret Braasch-Turi (MB-T), Debbie C. Crans (DC (Crans)), Jordan T. Koehn (JK), Kate Kostenkova (KK), Dean Crick (DC (Crick)), Heide Murakami (HM), Cameron Van Cleave (CC), and Jacob Ives (JI).

Project conception JK; Project management DC (Crans); Experimental design JK, DC (Crans), CC; Experiments JK, JI, CC, KK, HM; Verification MB-T, JK, DC (Crans); Manuscript preparation MB-T, JK, DC (Crans); Editing MB-T, JK, DC (Crans), KK, CC, HM; Preparation of grant funding DC (Crans) and DC (Crick). All authors helped edit and have approved the submitted manuscript.

Chapter 4

The author contributions are as follows: Margaret Braasch-Turi (MB-T) and Debbie C. Crans (DCC).

The contributions to the work are as follows conceptualization, D.C.C. and M.B.-T.; methodology, M.B.-T. and D.C.C.; investigation, M.B.-T. and D.C.C.; writing—original draft preparation, M.B.-T.; writing—review and editing, M.B.-T. and D.C.C.; supervision, D.C.C.; project administration, D.C.C.; funding acquisition, D.C.C. All authors have read and agreed to the published version of the manuscript.

Chapter 5

All the syntheses and characterization described was performed by Margaret Braasch-Turi. This section was written by Margaret Braasch-Turi.

Chapter 6

Closing remarks and future directions. This section was written by Margaret Braasch-Turi

Appendix IV

All the syntheses and characterization described was performed by Margaret Braasch-Turi. This section was written by Margaret Braasch-Turi.

Appendix V

All the syntheses and characterization described was performed by Margaret Braasch-Turi. This section was written by Margaret Braasch-Turi.

Appendix III:
Permissions for Figures

Chapter 2

Figure 2.4

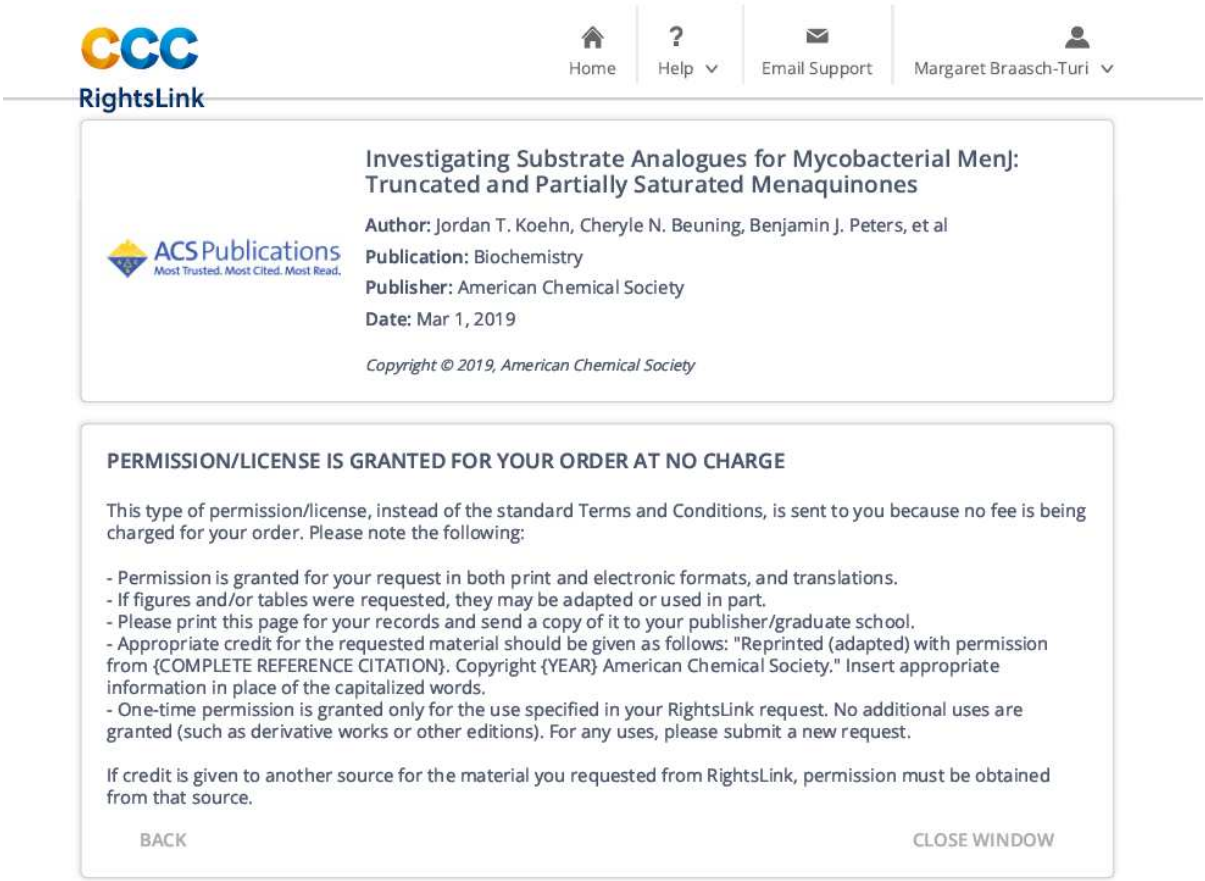

Figure 2.15

CCC Marketplace

This is a License Agreement between Margaret Braasch-Turi ("User") and Copyright Clearance Center, Inc. ("CCC") on behalf of the Rightsholder identified in the order details below. The license consists of the order details, the Marketplace Order General Terms and Conditions below, and any Rightsholder Terms and Conditions which are included below.
All payments must be made in full to CCC in accordance with the Marketplace Order General Terms and Conditions below.

Order Date	13-Oct-2022	Type of Use	Republish in a thesis/dissertation
Order License ID	1278977-1	Publisher	RSC Publishing
ISSN	2046-2069	Portion	Image/photo/illustration

LICENSED CONTENT

Publication Title	RSC advances	Publication Type	e-Journal
Article Title	Effects of lipid composition on membrane distribution and permeability of natural quinones	Start Page	16892
		End Page	16899
Date	01/01/2011	Issue	29
Language	English	Volume	9
Country	United Kingdom of Great Britain and Northern Ireland	URL	http://pubs.rsc.org/en/journals/journalss...
Rightsholder	Royal Society of Chemistry		

REQUEST DETAILS

Portion Type	Image/photo/illustration	Distribution	Worldwide
Number of Images / Photos / Illustrations	1	Translation	Original language of publication
Format (select all that apply)	Print, Electronic	Copies for the Disabled?	No
Who Will Republish the Content?	Academic institution	Minor Editing Privileges?	Yes
Duration of Use	Life of current edition	Incidental Promotional Use?	No
Lifetime Unit Quantity	Up to 499	Currency	USD
Rights Requested	Main product		

NEW WORK DETAILS

Title	Synthesis of Biologically Relevant Molecules	Institution Name	Colorado State University
		Expected Presentation Date	2022-10-28
Instructor Name	Margaret Braasch-Turi		

ADDITIONAL DETAILS

Order Reference Number	N/A	The Requesting Person/Organization to Appear on the License	Margaret Braasch-Turi

REUSE CONTENT DETAILS

Title, Description or Numeric Reference of the Portion(s)	Figure 2	Title of the Article/Chapter the Portion Is From	Effects of lipid composition on membrane distribution and permeability of natural quinones
Editor of Portion(s)	Teixeira, Murilo Hoias; Arantes, Guilherme Menegon	Author of Portion(s)	Teixeira, Murilo Hoias; Arantes, Guilherme Menegon
Volume of Serial or Monograph	9		
Page or Page Range of Portion	16892-16899	Issue, if Republishing an Article From a Serial	29
		Publication Date of Portion	2019-05-23

Chapter 3

The figures used in Chapter 3 were published in *Frontiers in Chemistry*, an open access journal. This journal is licensed through Creative Commons CC-BY, version 4.0.

Chapter 4

The figures used in Chapter 4 were published in *Molecules,* an open access MDPI journal. This journal is licensed through Creative Commons CC-BY, version 4.0.

Appendix IV
Progress toward the synthesis of versiquinazolines A and B

IV.0. Note about this chapter.

The work described towards the syntheses of versiquinazoline A and B was a very rocky road. Very little of what I tried was successful, with success being defined as a 75% yield or higher, particularly for the early steps of a linear synthesis. I performed each reaction myself (with some help from undergraduate students whom I was mentoring). I received very little feedback from my advisor and group members about the quality of my work. At the time, Bob was focused on the work being done for his company and was preoccupied by his cancer treatments. I do not blame my failures on Bob. All the decisions I made were my own. Looking back, I do wish I had received more feedback from Bob and from the group, but there is nothing I can do about that now. Through all this, I have learned to become an independent worker.

It should be noted that the experiments described here were pieced together to create the most coherent story. I pursue alternate routes for months, but I always made the decision to go "back to square one". The experimental methods described at the end of the chapter are of the reactions that I deemed successful. Everything else is summarized in tables of conditions. Not all these attempts will be described in the narrative. In the end, realizations of what I should have done came too late and I spun my wheels for too long. Although the work is not great, I think there is something to be said that I never stopped trying.

IV.1. Background Information: Isolation and Motivation.

Versiquinazolines A-K (Figure IV.1) are novel, polycyclic alkaloids isolated in 2016 from *Aspergillus versicolor* LZD-14-1 that was found within the *Pseudopterogorgia* species of coral in the South China Sea (Cheng, Lou et al. 2016). Out of the eleven novel, fumiquinazolines-type alkaloids, versiquinazolines A, B, G, and K exhibited significant inhibition (IC_{50}= <50 μM) against thioredoxin reductase (TrxR) (Cheng, Lou et al. 2016, Braasch-Turi 2018), an enzyme that is closely related to tumor metastasis and overexpressed in many different types of aggressive cancers, such as breast, thyroid, prostate, colorectal carcinoma, and malignant melanoma (Lincoln, Ali Emadi et al. 2003). The focus of this project was to synthesize versiquinazoline B (VQB) and versiquinazoline A (VQA) (Figure IV.1 in blue) because they both exhibited low IC_{50} values

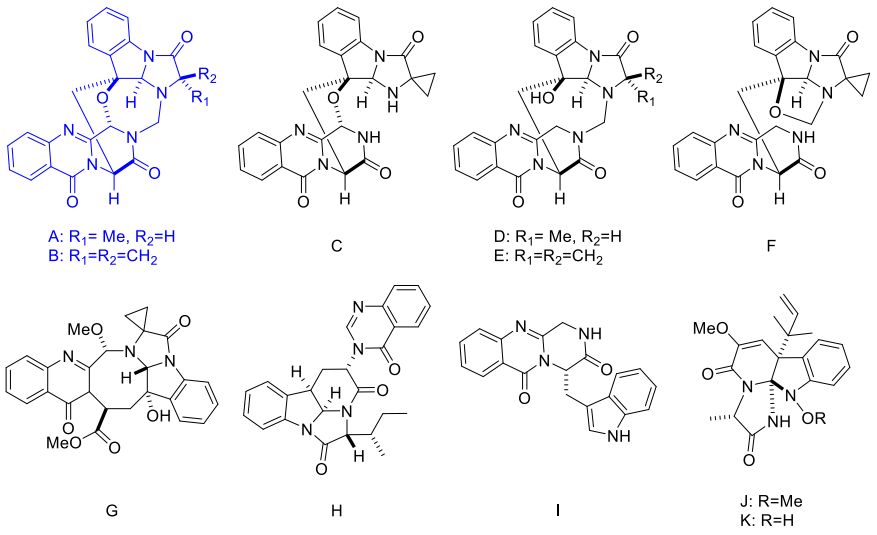

Figure IV.1. Structures of eleven novel natural products, versiquinazolines A-K. Versiquinazolines A and B are highlighted in blue.

against TrxR. The derivatives share nearly identical scaffolds, only differing in the amino acid comprising the 5-5-6 ring system: alanine for A and 1-aminocyclopropylcarbocylic acid (ACC) for B. Of the two derivatives, synthesizing versiquinazoline B was the primary focus.

As previously mentioned, VQA and VQB are part of the fumiquinazoline structural family (Figure IV.2). Most molecules share the pyrazinoquinazolinedione (6-6-6) and imidazoindolone

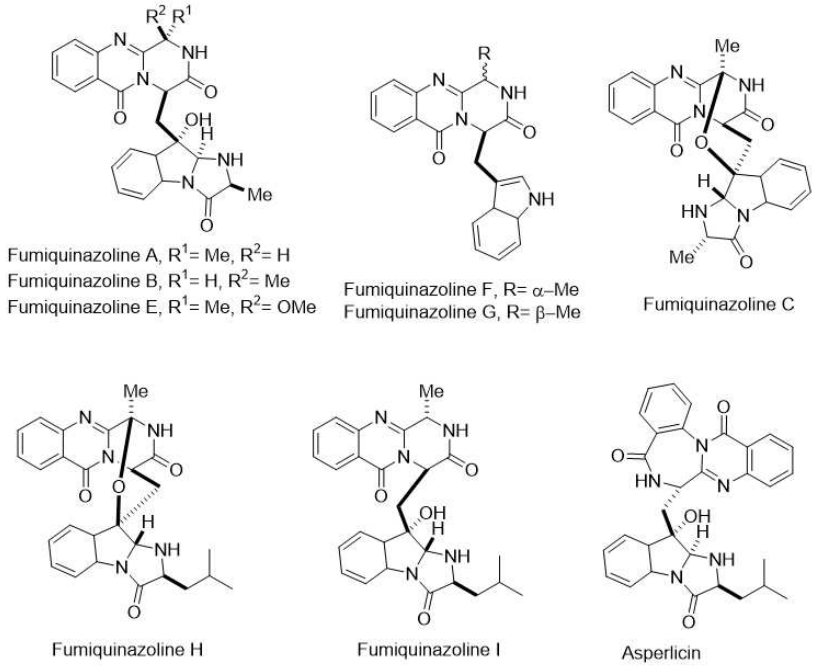

Figure IV.2. Fumiquinazoline family of compounds synthesized by Snider and coworkers (Takahashi, Matsushita et al. 1995, He and Snider 1997, He, Foxman et al. 1998, Snider and Zeng 2000, Snider and Zeng 2002).

(5-5-6) ring systems (Figure IV.3). Barry Snider and coworkers spearheaded the total synthesis of many members of this family by synthesizing fumiquinazoline G, the simplest molecule in the family. The remaining members of the family, fumiquinazolines A-C, E, H, I, and asperlicin (Figure IV.2), were synthesized soon after (He and Snider 1997, He, Foxman et al. 1998, Snider and Zeng 2000, Snider and Zeng 2002). The retrosynthetic analysis of each compound breaks down to common starting materials that mimic the proposed biosynthesis of these compounds: anthranilic acid, tryptophan, and one or two other proteinogenic amino acids (Ames, Liu et al. 2010, Ames and Walsh 2010, Ames, Haynes et al. 2011). Versiquinazolines are comprised of both the 5-5-6 and 6-6-6 ring systems that are connected in two additional positions: 1) a C16-C3 ether connection which is shared with many fumiquinazolines, and 2) N-N diamine bridge which is a

novel connection (Figure IV.3). Another major difference between the versiquinazolines and fumiquinazolines is the relative stereochemical assignments between the C16 alcohol and the C17 hydrogen of the 5-5-6 ring system. The fumiquinazolines feature a *syn* relationship, and the versiquinazolines were found to have an *anti*-relationship.

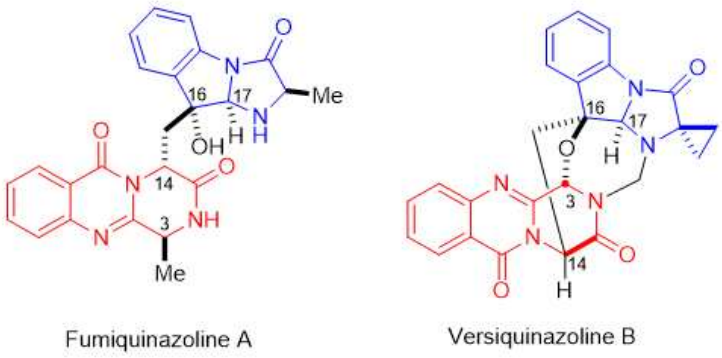

Figure IV.3. Anti vs syn relationship between C16 alcohol and C17 hydrogen. Pyrazinoquinazolinedione (6-6-6) shown in red. Imidazoindolone (5-5-6) shown in blue.

The versiquinazoline family of natural products serves as a novel starting point to synthesize new drugs that target TrxR to treat cancer. Total synthesis of versiquinazoline A and B will provide a route to the material needed to conduct biological studies due to their low bioavailability within the *Pseudopterogorgia* sp. This interesting scaffold has already caught the attention of chemists and pharmacologists to add more diversity to the scaffold of drug compounds from nature. With the compounds in hand, studies can be performed to evaluate the effectiveness against TrxR and other cancer targets as an anti-cancer drug, confirm the structure to compare to the isolated spectroscopic studies, and be used to investigate the biosynthetic pathway of these molecules such that they can be biosynthesized for mass production by bacteria. Structural confirmation is important to be able to understand the 3D conformation of the molecule within the enzyme active sites and how it is biosynthesized within the organism. The fumiquinazolines family of compounds feature a *syn*-relationship between the C16 alcohol and C17 hydrogen, whereas the

versiquinazoline family were assigned an *anti*-relationship at these two positions (Figure IV.3). This subtle but significant difference between the two families could be a result of variations in the biosynthetic pathway or incorrect spectroscopic assignment.

IV.2.Previous Work—Established Syntheses of Fumiquinazoline Natural Products.

Snider established a synthetic route to form the complex ring systems featured in the fumiquinazoline-type natural products. Formation of the 6-6-6 ring system was accomplished in the total synthesis of fumiquinazoline G using carbodiimide and acyl chloride coupling strategies. The peptide portion of D-tryptophan was coupled to anthranilic acid and an alanine derivative (He and Snider 1997). The synthesis of the 5-5-6 ring system was first achieved during the total synthesis of asperlicin, a distant member of the fumiquinazolines (Figure IV.2). The C2-C3 double bond of indole **2** (Figure IV.4) was reduced using borane/THF and then the indole nitrogen was coupled to N-Cbz-L-Leu using dicyclohexylcarbodiimide (DCC). The ring was oxidized back to

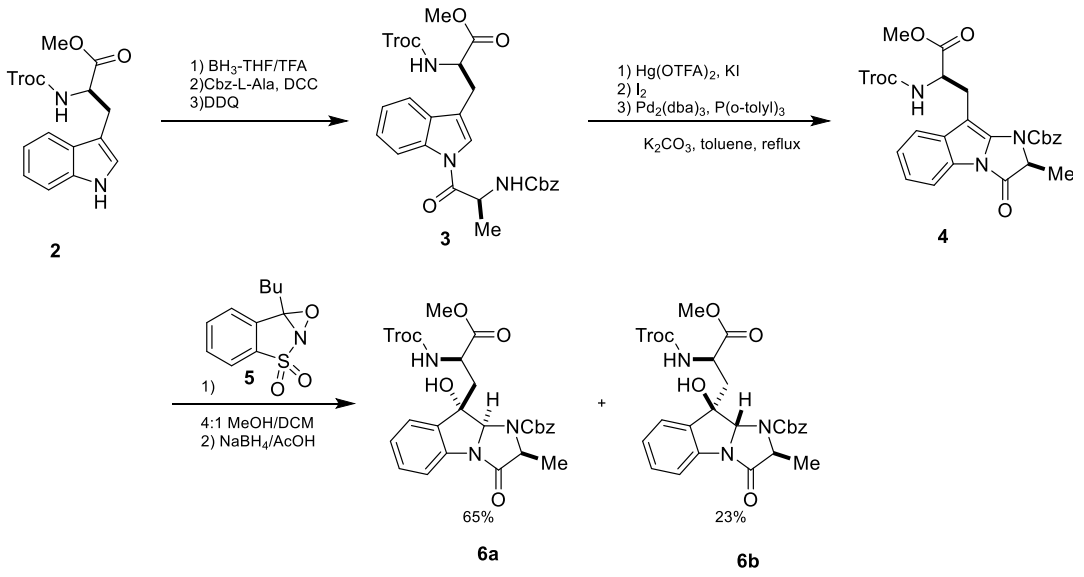

Figure IV.4. Synthesis of the 5-5-6 ring system towards asperlicin (He, Foxman et al. 1998).

indole, **3**, with 2,3-dichloro-5,6-dicyano-1,4-benzoquinone (DDQ). Iodination of the C2 carbon allowed Buchwald amination to occur with the carboxybenzyl carbamate (Cbz) protected nitrogen

of leucine, **4**. Epoxidation with Davis oxaziridine **5** and reductive ring opening formed a mixture of diastereomers, **6a** and **6b**, favoring the *S* diastereomer (He, Foxman et al. 1998, Snider and Zeng 2002). Alternatively, dimethyldioxirane was used to achieve the corresponding *R* diastereomer for fumiquinazolines A, B, and I (Snider and Zeng 2000).

Moving forward, the synthesis of the 6-6-6 ring system is common across all the fumiquinazoline-type compounds. Fumiquinazoline C is the most structurally similar to VQA and VQB (Snider and Zeng 2002); therefore it served as synthetic inspiration. Continuing from the synthesis of the 5-5-6 ring system described above, the construction of the 6-6-6 ring begins with demethylation of the methyl ether in **7** with $NaBH_4$. Cyclization of the resulting in an alcohol (not shown) to lactone **13** was achieved in the presence of SiO_2 (Figure IV.5). Building off the tryptophan α-amine, deprotection of the 2,2,2-trichloroethyl carbamate (Troc) group allowed anthranilic acid to couple using 1-ethyl-3-(3-dimethylaminopropyl)carbodiimide (EDCI). Anthranilic acid is then coupled to N-Fmoc-Se-phenyl-selenocysteine **14** to form lactone **15**. Under intriguing Mazurikiewicz-Ganesan cyclization conditions, the fused 6-6-6 ring system was achieved to form cyclic intermediate **16**. Piperidine was used to deprotect the fluorenylmethyloxycarbamate (Fmoc) group and achieve the intermediate **17**. Lactone opening by the free amine and cyclization was achieved at reflux in acetonitrile, **18** (Snider and Zeng 2000,

Snider and Zeng 2002). The formation of the C16-C3 ether connection was built into these early steps of the synthesis through the installation of N-Fmoc-Se-phenyl-selenocysteine **14** to form a

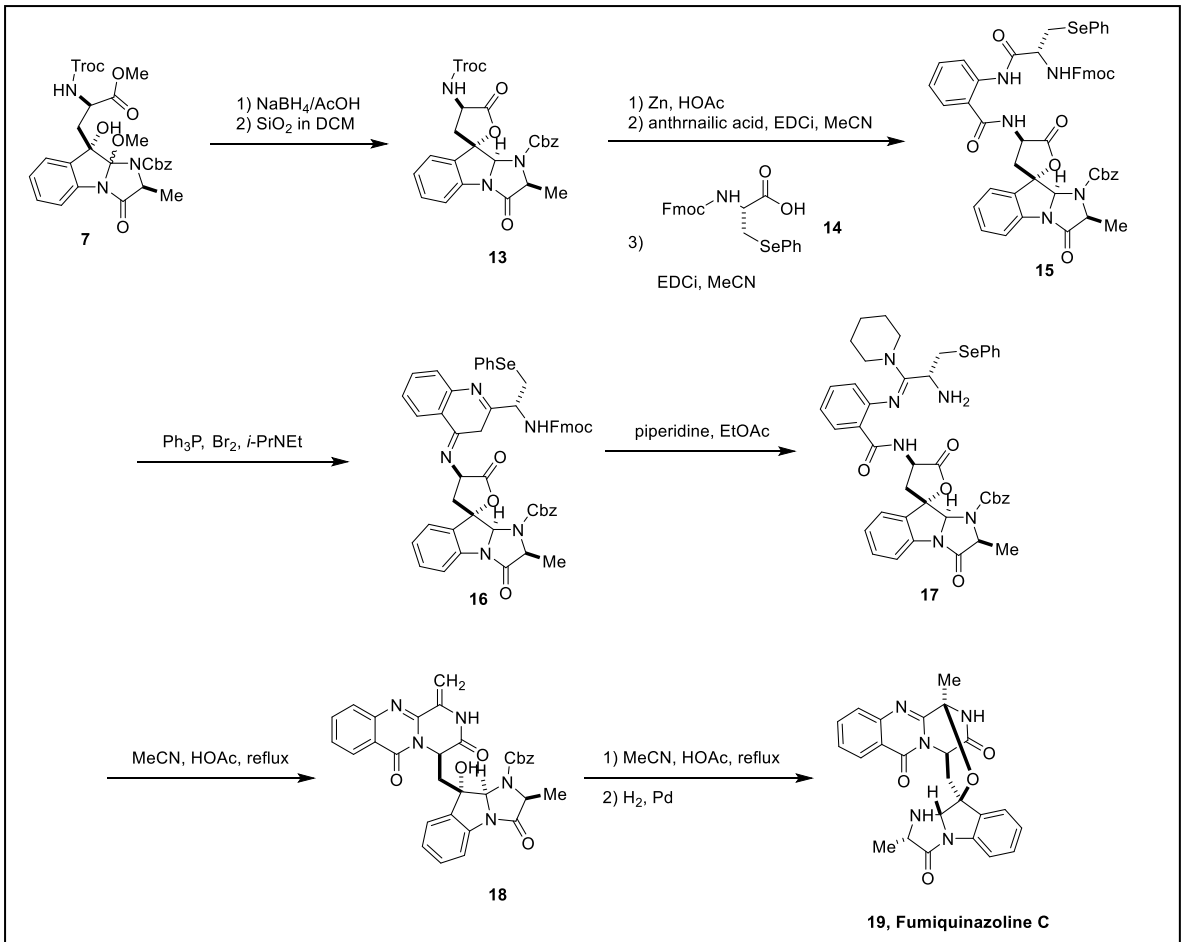

Figure IV.5. Synthesis of the 6-6-6 ring system towards Fumiquinazoline C (Snider and Zeng 2002).

dehydroalanine moiety. Using acidic conditions, the phenylselenide moiety was eliminated to form **18** and then the dehydroalanine double bond was activated receive the C16 alcohol as a nucleophile to form the ether, thus restoring the methyl group stereoselectively at that position. Hydrogenation deprotection of the Cbz group completed the synthesis of fumiquinazoline **C**, **19** (Snider and Zeng 2002).

IV.3. Retrosynthetic Analysis of versiquinazoline A and B

Versiquinazolines A and B are structurally similar to fumiquinazoline C (Figure IV.6). All three compounds contain the ether connection between C16 and C3. Fumiquinazoline C and versiquinazoline A both contain alanine in the 5-5-6 ring system, whereas versiquinazoline B

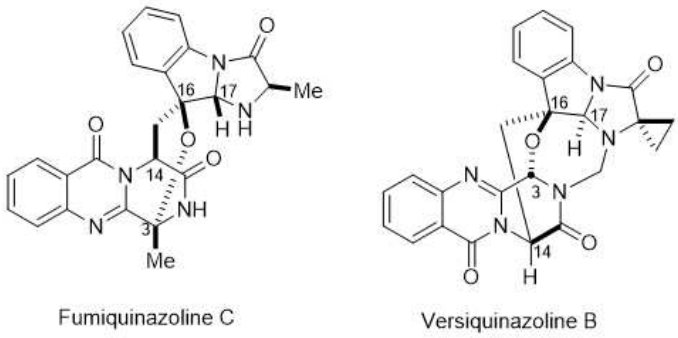

Figure IV.6. Comparison of versiquinazoline B and fumiquinazoline C.

contains nonproteinogenic 1-amino-1-cyclopropane-1-carboxylic acid. In addition, the versiquinazoline derivatives contain a third connecting point between ring systems: methanediamine bridge connecting the secondary amines on each ring system. Snider's work provided excellent groundwork and inspiration for the retrosynthetic analysis of the complex ring systems. Snider's retrosynthesis and the retrosynthesis for versiquinazolines A and B fragment the compound into similar intermediates that break down into commercially available materials: L-tryptophan methyl ester hydrochloride, anthranilic acid, glycine, and ethyl 2-cyanoacetate (Figure IV.7).

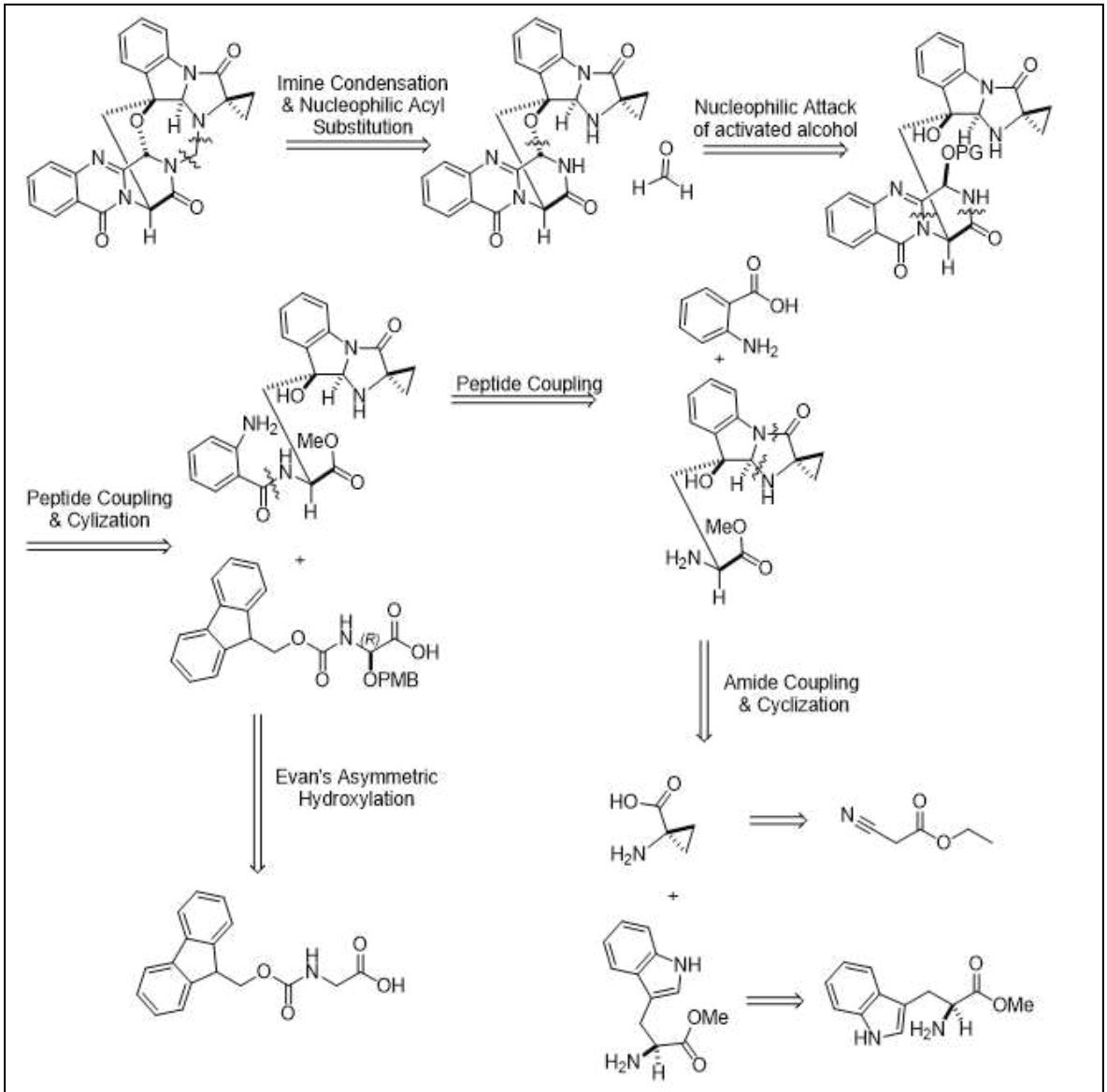

Figure IV.7. Retrosynthetic analysis of versiquinazoline A and B.

The retrosynthetic analysis of versiquinazoline A and B gives rise to a mostly linear sequence (Figure IV.7). The methanediamine bridge is projected to form with imine condensation and nucleophilic acyl substitution of formaldehyde onto one of the secondary amines on each ring system (Coyle and Bryant 1983, Solomon, Hua et al. 2009, Davidovich, Aksenova et al. 2015). Snider achieved the ether connection by installing a dehydroalanine via a series of elimination and activation steps starting with N-Fmoc-Se-phenyl-selenocysteine to receive a hydroxy group as a

nucleophile to stereoselectively install the methyl group. Since VQA and VQB do not have this moiety, an activated hydroxy leaving group will be installed at that position to ultimately function as a leaving group for nucleophilic attack. α-Halo amino acids were considered, but the reactivity of that center was deemed too high, leading to the consideration of α-hydroxy amino acids instead. A protected alcohol should remain unscathed until deprotection and transformation into a proper leaving group. Formation of the 6-6-6 ring system will be formed with sequential amide coupling of anthranilic acid and the protected α-hydroxy amino acid. The formation of the 5-5-6 ring system would be synthesized in a similar fashion to Snider's established work, but the need for iodination and Buchwald amination will be replaced with nucleophilic substitution at C17.

One key difference between the fumiquinazolines and the versiquinazolines is the configuration of the C16 and C17 alcohol and hydrogen. The fumiquinazolines have *syn* conformations whereas versiquinazoline B has an *anti*-configuration (Figure IV.6). The relative stereochemistry of the C16 alcohol is proposed to occur via Sharpless asymmetric dihydroxylation using AD-mix β to install *syn* diols above the plane of the double bond.(Kolb, Van Nieuwenhze et al. 1994) Inversion of the resulting secondary alcohol is proposed to occur with Mitsunobu conditions. Deacylation and mesylation of the inverted carbon center primes the ring closure, resulting in *anti*-conformation. The synthesis of ACC is adapted from known methods in three steps (Il'yasov and Galust'yan 1995).

IV.4. Progress Towards Versiquinazoline B

IV.4.1 Synthesis of non-proteinogenic amino acid, 1-amino-1-cyclopropane-1-carboxylic acid (ACC).

To begin the synthesis of VQB, a reliable route to the commercially expensive 1-amino-1-cyclopropane-1-carboxylic acid (ACC) was required. Multiple routes were considered before the present route was adapted from known methods in three steps (Figure IV.8) (Il'yasov and

Galust'yan 1995). Following the work established by Il'yasov and Galust'yan, ethyl 2-cyanoacetate **42** underwent intramolecular enolate alkylation with 1,2-dibromoethane to form the

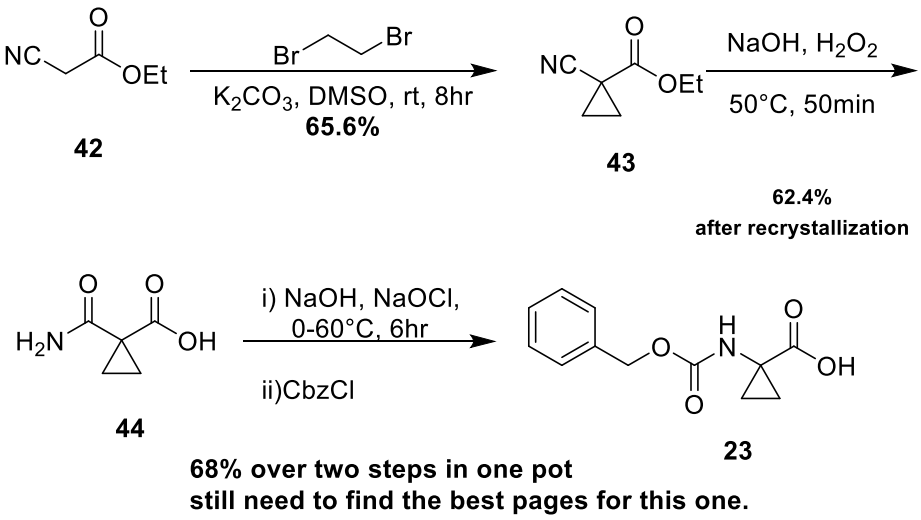

Figure IV.8. Synthesis of N-Cbz-1-amino-1-cyclopropane-1-carboxylic acid (Cbz-ACC) in yield 67.9% over three steps.

cyclopropane ring **43** in 65.6% yield. Oxidation with hydrogen peroxide in basic conditions afforded 1-carboxycyclopropane-1-carboxamide **44** in 62.4% yield. To transform the newly formed amide into a free amine, the literature source used traditional Hofmann rearrangement conditions of NaOH and Br_2. This reaction, however, was reported to be very low, with a 28% yield (Il'yasov and Galust'yan 1995). In addition, the hazards associated with using Br_2 were strongly taken into consideration; therefore, different Hofmann rearrangement conditions were investigated. The Hofmann rearrangement to direct carbamate protection of the amine could be achieved using iodobenzene diacetate and either benzyl or allyl alcohol (Satoh, Akiba et al. 2009). These transformations, however, were unsuccessful. Finally, conditions using household bleach and NaOH were found (Bauer, Kleemiss et al. 1998). This reaction proved to be successful, however isolating the zwitterionic product proved troublesome. Instead of isolating ACC, the amine was immediately protected with Cbz in a tandem, one pot reaction (Ueda, Yamaguchi et al. 2014). Purification of the product occurred via acid/base extraction producing N-Cbz-ACC **5** in

yield 67.9% over three steps. NMR of this reaction shows product and benzyl alcohol byproduct from unreacted Cbz. Although this reported yield is a result of a slightly impure mixture, it is an improvement over the original literature conditions yielding <28%.

IV.4.2 Progress Towards the 5-5-6 Ring System

According to the retrosynthetic analysis, the 5-5-6 ring system is comprised of the indole ring of tryptophan and the formation of a new ring from ACC or Ala to synthesize VQB and VQA, respectively. Since the versiquinazolines are closely related to the fumiquinazolines, Snider's conditions were used to begin the synthesis. Starting with tryptophan methyl ester hydrochloride **20** (Figure IV.9), Troc protection to make **21** proceeded in 93% yield in accordance with the literature. The reduction of the indole C2-C3 double bond with BH_3·THF in trifluoroacetic acid to produce the reduced species, [R]-Troc-Trp-OMe **22,** in quantitative yields. Reducing the C2-C3 double bond controls the reactivity of the ring by shifting the nucleophilicity from the C3 position to the resulting indoline nitrogen, setting the stage for peptide coupling reaction. Cbz-Ala was used to synthesize fumiquinazoline A and B using DCC as a coupling agent (Snider and Zeng 2000). This precedent was unsuccessful in coupling **22** to Cbz-ACC.

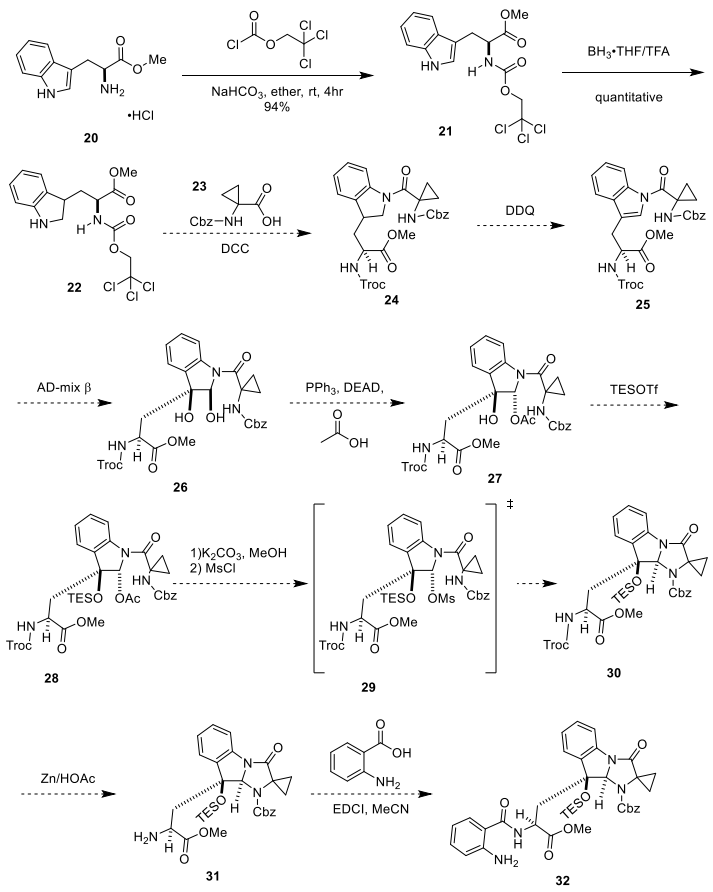

Figure IV.9. Proposed synthesis to form VQB. This route remained unfruitful due to the incompatible steric hinderances of the cyclopropyl ring of ACC and indoline.

IV.4.2.1 Peptide Coupling Conditions to Couple ACC

Alternative methods to couple **22** to Cbz-ACC were investigated to synthesize **24**. Many coupling methods have found success in transforming the carboxylic acids into a more reactive ester. Snider and coworkers reported the use of *p*-nitrophenol (PNP) esters as an alternate route to coupling (Snider and Zeng 2002). Attempts to synthesize the PNP activated ester of Cbz-ACC in the presence of EDC and DIPEA were not successful and yielded only starting material. These conditions were attempted once more but with DMAP as an additive. This too yielded only starting material.

Inspired by the DCC coupling of **22** and Cbz-Ala towards Snider and coworker's synthesis of fumiquinazoline C, other traditional coupling methods were investigated; however, the use of

DCC, EDC, and CDI only yielded starting material (Table IV.1, Entries 1-4). With the repeated failures of traditional and usually dependable carbodiimide coupling agents, I decided to use acid chloride coupling partners instead. Cbz-ACC was converted to the corresponding acid chloride (Cbz-ACC-Cl) using oxalyl chloride and DMF in quantitative yields. Trials to couple Cbz-ACC-Cl to **22** with pyridine were unsuccessful (Table IV.1, Entry 5). This was initially thought to be due to inadequate anhydrous conditions, but the reaction was still unsuccessful after anhydrous conditions were met.

Table IV.1: Attempted coupling conditions

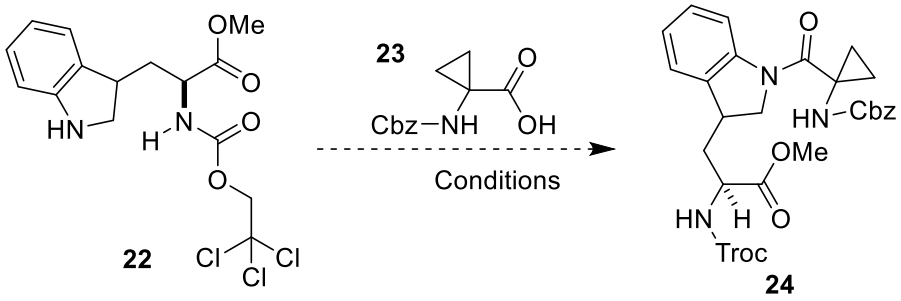

Entry	Reagents	Conditions	Results	Comment	Reference
1	**22** (1.1 eq), DCC (1 eq), Cbz-ACC (1 eq)	DCM, rt, o/n	No reaction Recovered starting material	-	(Snider and Zeng 2002)
2	**22** (1.1 eq), DCC (1 eq), Cbz-ACC (1 eq)	DMAP (10%), DCM, rt, o/n,		NMR showed mostly DCU	
3	**22** (1.1 eq), EDC (1 eq), Cbz-ACC (1 eq)	DIPEA (0.25 eq) DCM, rt, 5 hr		-	
4	**22** (1 eq), CDI (1.2 eq), Cbz-ACC (1.08 eq)	DMF, rt, o/n		-	(Bang-Anderson, Larsen et al. 2007)
5	**22** (1.5 eq), Cbz-ACC-Cl (1 eq), DMF	DCM, pyridine (10 eq), rt, o/n		No reaction	(Dunne 2018)

Since traditional coupling methods were not producing the correct, if any, transformations, other factors must be interfering with the coupling. There are three factors that could be interfering

with the success of this coupling: (1) incomplete reduction of the indole C2-C3 bond, (2) undesired oxidation of indoline back to indole, and (3) the combined steric influences of the cyclopropyl ring and indoline nitrogen. The reduction of the indole ring consistently showed complete conversion via TLC. Although the reduction was quantitative, the product was found to rearomatize and oxidize the C2-C3 bond within a matter of days. This was evident by the color of the foamy solid. To prevent oxidation, freshly prepared **22** was used for these coupling reactions. Lastly, the steric hinderance of ACC in combination with the size of the indoline ring are indisputable hinderances in amide coupling reactions.

With this in mind, amide coupling reactions of bulky carboxylic acids and/or large secondary amines were investigated. One literature source showed the coupling of α-methylalanine coupling to pyrrolidine nitrogen of proline *t*-butyl ester using bromotripyrrolidinophosphonium hexafluorophosphate (PyBroP), a derivative of benzotriazol-1-yl-oxytripyrrolidinophosphonium hexafluorophosphate (PyBOP) coupling agent (Frerot, Coste et al. 1991). The geminal dimethyl groups on α-methylalanine occupy more space than the methylenes of the cyclopropyl ring on ACC, however the cyclopropyl group is more rigid. The ability of the methyl groups to freely rotate additionally obscures the carbonyl carbon from the nucleophilic species. The pyrrolidine ring of proline is much smaller than the indoline, however the reaction center is similar. According to the literature, the coupling of N-Cbz-α-methylalanine to proline *t*-butyl ester was achieved in 95% yield using PyBroP, diisopropylethylamine (DIPEA) in dichloromethane (DCM) at room temperature in one hour. Despite the similarities between the reported substrates and this system, this too proved to be unsuccessful when the reaction yielded only starting material. This confirmed the direct peptide coupling of Cbz-ACC to the indoline nitrogen was not going to be achieved. Alternative routes of installation were then investigated.

IV.4.2.2 Alternate Routes Towards Coupling ACC

Many other methods were investigated in pursuit of coupling conditions that were eventually unsuccessful. A series of direct N-coupling were attempted using strong bases (NaH, nBuLi, NaHDMS) with acetyl chloride as a model system (Table IV.2). Acetyl chloride was successfully installed using NaHMDS, but Cbz-ACC was still difficult to install. The formation of product was speculated via NMR of prep TLC samples, but never fully confirmed (Table IV.2). Anyway, this route was quickly abandoned due to the strong bases' interactions with the Troc protecting group and competition between N-acylation and Pictet-Spengler reactions. These conditions are summarized in Table IV.2.

Table IV.2: Direct N-Acylation conditions.

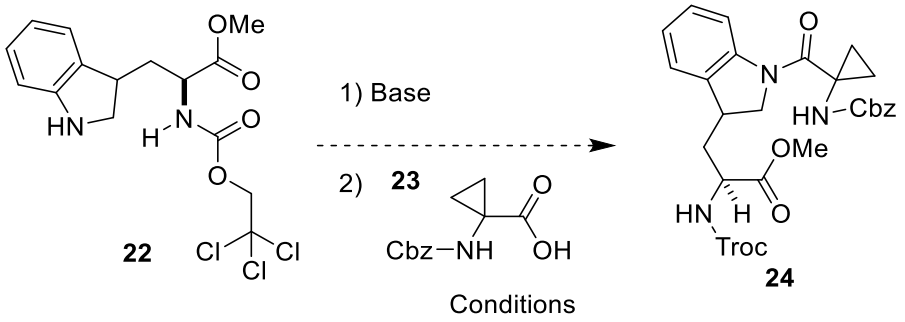

Reagent	Base	Conditions	Results	Comment
22 (1 eq), Acetyl chloride (1-1.5 eq)	NaH (60% dispersion in mineral oil)	DMF, 0°C, 5 hr	No reaction	Undesired side reactions
	nBuLi (2 eq, 1.6M in hexanes)	THF, -78°C, 3 hr	N-Ac pdt formed	Verified by NMR. Proof of concept reaction. No mass obtained.
	NaHMDS (1.05-2 eq, 1M in THF)	THF, -78°C, 6 hr	93% N-Ac pdt	Crude yield
22 (1 eq), Cbz-ACC-Cl (1.08 eq)	NaHMDS (1.05 eq, 1M in THF)	THF, -78°C, 6 hr	**24,** 39%	Crude yield. Product formation speculated by NMR

In addition, I had the opportunity to consult with Dr. Nobuyoshi Yasuda, a consultant for Cetya Therapeutics (one of Bob's start-up companies) and former Senior Principal Investigator at Merck. He suggested several more modern coupling strategies using activated esters that have been gaining popularity in industry. Each recommendation was taken into consideration, but they ultimately were unsuccessful. These conditions are summarized in Table IV.3.

Table IV.3: Coupling condition recommendations by Dr. Nobuyoshi Yasuda

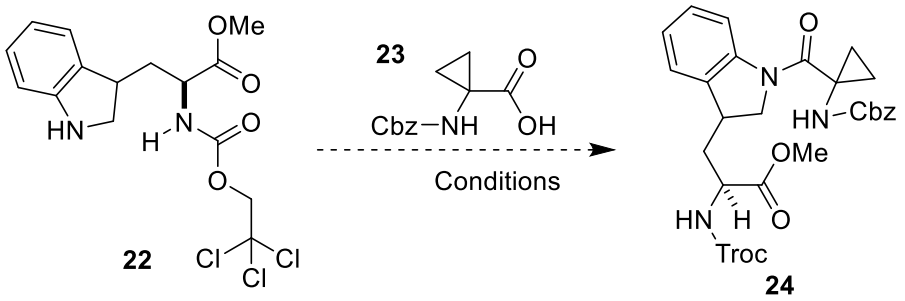

Reagent	Conditions	Results	Reference
22 (1 eq), Ghosez's Reagent (1.43 eq) Cbz-ACC (1.18 eq)	$NaHCO_3$ (10.25 eq) DCM, rt, o/n	No reaction	(Elbatrawi, Kang et al. 2018)
22 (1 eq), TCFH (1.1 eq) Cbz-ACC (1 eq)	NMI (3.5 eq), MeCN, rt, o/n	Recovered starting material	(Beutner, Young et al. 2018)
	NMI (3.5 eq), MeCN, -78°C, o/n	Recovered starting material	

In another privileged consultation, I had the opportunity to discuss my research with Dr. Tohru Fukuyama. He looked at my target molecule and said "Whoa, that's a difficult endgame". He recommended protecting the stereochemistry of tryptophan via an acetonide and using Boc as a protecting group. This would allow for more robust attempts to direct N-acylation, which was my current pursuit at the time. Although several transformations through this sequence were successful, the acetonide was ultimately never formed. This route was abandoned in favor of the

work established by Snider and coworkers, which led back to "Square One". The details regarding these reactions have been omitted from this dissertation because they do not contribute to the overall story.

IV.4.2.3 Investigation of Constructing ACC After Peptide Coupling

After going through traditional to more modern peptide coupling strategies, carboxylic acid derivative activations, and direct N-acylations, it was clear the peptide coupling between **22** and Cbz-ACC was not going to be feasible. An alternative route to install ACC on the indole N was hypothesized via post-coupling transformations. Since ethyl 2-cyanoacetate is a precursor to Cbz-ACC, it seemed like a good candidate to install the backbone of ACC to the indoline N of **22** (Figure IV.10)**.** If this were to work with **22**, then the remaining functional groups of ACC could be installed using the same reaction sequence used to synthesize Cbz-ACC. The primary concern

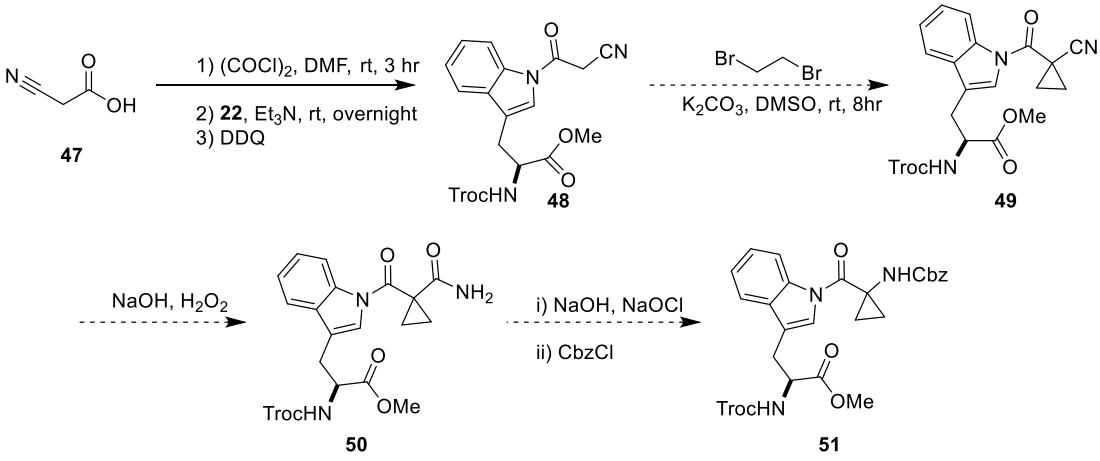

Figure IV.10. Proposed installation of ACC via 2-cyanoacetic acid.

for pursuing this proposed sequence is the risk of racemizing the α- carbon of the tryptophan moiety. In pursuit of this route, 2-cyanoacetic acid **47** was transformed into the corresponding acid chloride in the presence of oxalyl chloride and DMF in DCM at 0°C (Figure IV.10). To the same pot, indoline **22** was added slowly at 0°C followed by dropwise addition of Et_3N. The coupled

product **48** was formed as a mixture of diastereomers in 35.61% yield. Even with this product in hand, the risk of racemization at the α- carbon of the tryptophan moiety was deemed too high, and the synthesis of versiquinazoline B was abandoned in favor of synthesizing only versiquinazoline A.

IV.4.2.4 Decision to Focus on Versiquinazoline A

After careful consideration of the above trials, I decided to abandon the total synthesis of versiquinazoline B in favor of versiquinazoline A. This decision was supported by the repeated attempts to couple the sterically hindered Cbz-ACC to the indoline nitrogen of **22** and support from the reported couplings of R-**22** to Cbz-Ala by Snider and coworkers (Snider and Zeng 2000). Cbz-Ala is the other amino acid that comprises the 5-5-6 ring system of versiquinazoline A. If given the opportunity to work on this project again, I would investigate utilizing a biomimetic approach towards installing the cyclopropane ring. ACC is produced biosynthetically through the cyclization of methionine towards the production of ethylene, which plays a critical role in hormone regulation in plants (Polko and Kieber 2019).

IV.5 Progress Towards Versiquinazoline A.

IV.5.1 Coupling of Cbz-Ala

Snider and coworkers coupled Troc-D-Trp-OMe **2** to Cbz-Ala in a three step sequence (Figure IV.11) towards the synthesis of fumiquinazolines A, B, C, E, H and I (Snider and Zeng 2000, Snider and Zeng 2002). First, the indole ring of Troc-Trp-OMe **2** was reduced using BH_3·THF to form R-**22** (not pictured). After purification by column chromatography, the indoline nitrogen was coupled to Cbz-Ala with DCC which was used without further purification in the

subsequent step. Re-aromatization of the indole ring **3** was achieved with DDQ yielding 78% over three steps.

Figure IV.11: Three step sequences to couple Cbz-Ala to Troc-D-Trp-OMe (2).(Snider and Zeng 2000)

This sequence was replicated using Troc-L-Trp-OMe (**20**) towards the synthesis of the 5-5-6 ring system of versiquinazoline A. Starting with Troc-L-Trp-OMe, reduction of the indole C2-C3 double bond was achieved using BH_3·THF to form indoline **22** as described previously (Figure IV.12). DCC was used to couple Cbz-Ala to the indoline nitrogen forming the indoline N-coupled product (**52**). The reaction mixture was filtered through a pad of celite to remove dicyclohexylurea (DCU) from the reaction mixture, and then the crude product was carried over to the next step

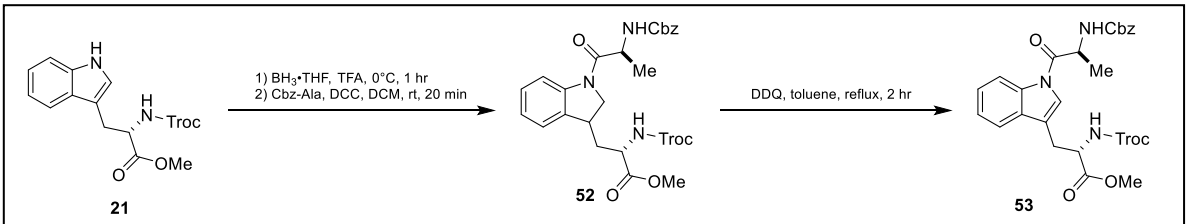

Figure IV.12: Synthesis of N-acylated product **53.**

without further purification. The aromatic system of the indole ring was restored using DDQ in toluene at reflux for 2 hours, as described by Snider and coworkers. The resulting crude oil was purified via column chromatography to produce 0.04g of the desired oxidizes N-coupled product (**53**). Although Snider and coworkers reported high yields over three steps, initial attempts to repeat their procedure yielded less than 3% yield over three steps(Snider and Zeng 2000). The

unreacted **52** was collected and resubjected to DDQ oxidation. The combined totals of both trials yielded 5% over three steps.

The low yield was attributed to impure reagents off the shelf and suspected decomposition in toluene at reflux. To improve upon the observed yield, steps were taken to purify and preserve the reagents. DDQ was easily recrystallized from chloroform and stored under argon at a reduced temperature. DCC, on the other hand, was more difficult to purify. DCU is insoluble in most organic solvents, so it was difficult to determine the purity of the reagent. The solid DCU byproduct is generally considered favorable because it can be filtered out during the workup. The purification of DCC was difficult (recrystallization, distillation, and dissolution and filtration) as each attempt produced more undesired DCU. Filtering DCU from the reaction mixture is not particularly simple. Storing the reaction mixture at low temperatures and repeated filtrations are necessary to remove DCU, and even then, it is not fully removed.

When considering how to move forward, coupling agents with water soluble byproducts were attractive alternatives to DCC to couple Cbz-Ala to **22**. First, HATU was used through the recommendations and reported successes of its use within in the Williams' lab. Freshly prepared **22** was dissolved in DMF, Cbz-Ala was added, and the reaction was cooled to 0°C. DIPEA, HATU, and HOBt were added and the reaction was stirred and allowed to warm up room temperature overnight (Figure IV.13A) (Perez-Balado, Rodriguez-Grana et al. 2009, El-Faham and Albericio 2011). Column of the resulting crude mixture produced a white solid **53**, and NMR revealed a 1:6 ratio of product to unreacted Cbz-Ala. The reaction yielded 11.6% by 1H NMR.

Although successful by NMR, its initial yield was deemed to be too low to continue pursuing HATU as a viable coupling agent.

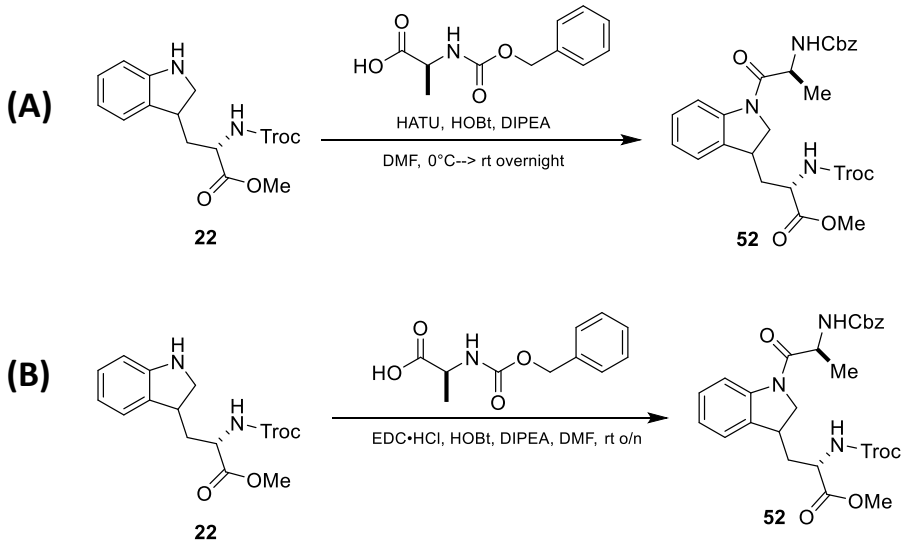

Figure IV.13: Synthesis of reduced indole N-acylated product **52. (A)** HATU conditions. (B) EDC conditions

Next, EDC was utilized. The reaction between Cbz-Ala and **22** in the presence of EDC produced a crude yield of 73.57% (Figure IV.13B) (Sheehan, Cruickshank et al. 1961). ^{1}H NMR of the crude sample showed a 1.6:1 of product to Cbz-Ala ratio. The next trial used EDC and HOBt, and it yielded 77.88% crude yield, but showed a 1:4.6 product to Cbz-Ala ratio in the ^{1}H NMR. This variability in the results led to this route being abandoned in favor of the pre-established success of using DCC.

In hindsight, EDC had marginal success based on NMR yields. It produced the highest product-to-starting material ratio of all the attempted conditions and showed potential for optimization. If this project were to be picked up again, this is a set of conditions would be revisited.

Upon circling back to using DCC as a coupling agent, it was necessary to make changes to the procedure to mediate the effects of DCU-contaminated DCC. In the initial attempts, 0.905

equivalents of DCC and Cbz-Ala were used to 1 equivalent of **22** (Figure IV.14). The amount of DCC and Cbz-Ala was increased to 0.95 equivalents to counteract the presence of DCU in the DCC, and additional steps were taken to remove DCU produced during the reaction.

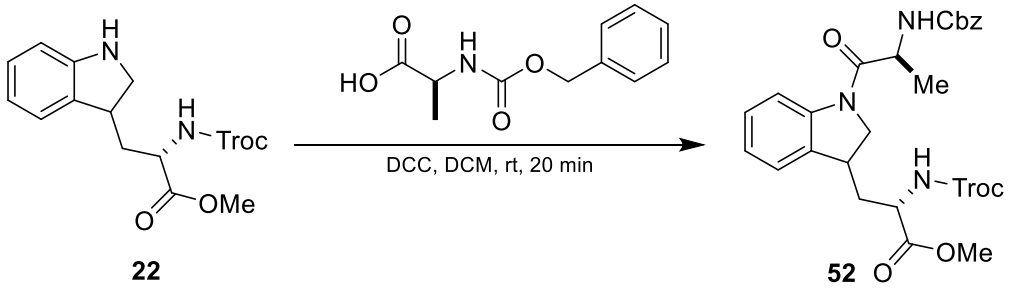

Figure IV.14: Synthesis of reduced indole N-acylated product **52** via improved DCC conditions (Snider and Zeng 2000)**.**

Ester **22** was prepared fresh as previously described and dissolved in DCM. Cbz-Ala and DCM were added, and the resulting mixture was stirred at room temperature for 20 minutes. The reaction started as a light tan color and progressed to an opaque peachy orange. After the reaction was complete by TLC, the reaction mixture was immediately filtered through a pad of celite and the solvent was removed to reveal a powdery white solid. NMR of the crude products showed a significant amount of DCU still present in the product, evident in the white powder. The crude product was redissolved in a minimal amount of ethyl acetate and placed in the freezer overnight. The following day it was removed from the freezer and filtered a second time through a pad of celite while still cold, and the solvent was removed. NMR of the product showed trace amounts of DCU remained in the product. The product was a diastereomeric mixture of **52.** A mixture of diastereomers at this point was inconsequential because the stereocenters would be removed upon re-aromatization of the indole ring. It was a white, foamy solid and it was produced in 59% yield.

IV.5.2 Oxidation of the indoline ring to indole towards VQA.

With some coupled product in hand, I was finally able to move on to the re-aromatization reaction of the indole ring. Snider and workers used DDQ refluxed in toluene to produce the 5-5-6 ring system for fumiquinazoline A (Figure IV.11). In Section IV.5.1, this sequence was repeated and yielded less than 3% over three steps. The crude NMR showed trace amounts of product, starting material, and decomposed starting material. The high temperature reflux was most likely the cause for decomposition, so alternative DDQ oxidation conditions were investigated at lower temperatures (Figure IV.15).

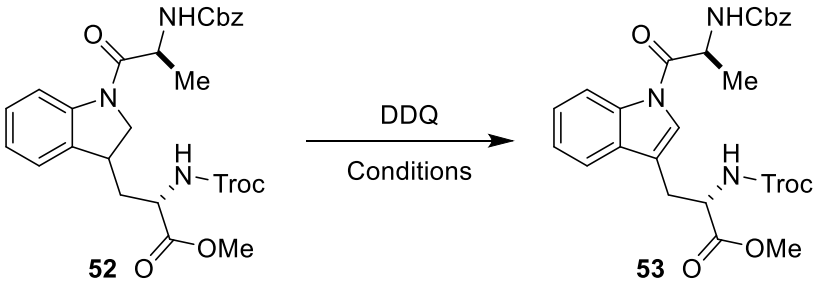

Figure IV.15: Oxidation of **52** in the presence of DDQ to synthesize the oxidized coupled product **53.**

It was unclear why Snider and coworkers utilized toluene as a solvent when much of the DDQ oxidation literature utilizes DCM as a solvent. The first set of conditions tried was 1.05 equivalents of DDQ in DCM at 0°C for 20 minutes (Table IV.4, Entry 1)(Baran, Guerrero et al. 2003). This procedure led to the recovery of starting material. From one extreme to the next, this reaction must have been too cold to elicit the reaction. Using the same equivalents, the next attempt was refluxed for 24 hours (Table IV.4 Entry 2). After three hours, the formation of the product was evident by TLC. After refluxing for nearly 20 hours, there was no change on the TLC from the previous evening. A second equivalent of DDQ was added and refluxed for an additional 24 hours. NMR of the crude material showed the formation of **53** in 28% (mostly pure) yield. From this, it seemed more equivalents of DDQ would be required earlier on in the reflux to encourage

complete conversion. Snider and coworker's method added DDQ in two portions (2/3 the amount and the remaining 1/3) over the course of 2 hours (Snider and Zeng 2000). With this in mind, perhaps adding the equivalents of DDQ in small portions throughout the refluxing period would increase the yield. Two equivalents of DDQ in DCM seemed to be the best set of conditions to move forward from this point.

Table IV.4: Summary of oxidation conditions used to synthesize **53**.

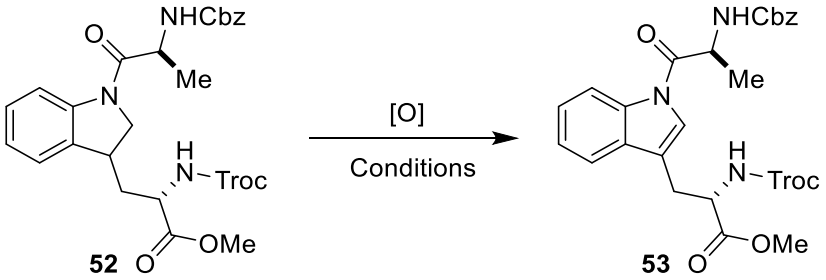

Entry	[O] Reagent	Conditions	Results	Comment
1	DDQ (1.05eq)	DCM, 0°C, 20 min	No reaction	
2	DDQ (2 eq)	DCM, reflux, 48 hr	**53**, 28%	Crude yield
3	DDQ (2 eq)	DCM, reflux, o/n	**53,** 45%	Over 3 steps
4	Chloranil (2 eq)	DCM, rt 24 hr	No reaction	
5	MnO_2 (10 eq)	DCM, rt 24 hr	No reaction	

Other oxidation methods were considered but were quickly eliminated from the list of viable conditions. Chloranil (Entry 4) was used with the same conditions as DDQ. This reaction yielded only starting material after refluxing for 3 days. Manganese (II) oxide (Entry 5) was also considered, but yielded only starting material (Aoyama, Sonoda et al. 1998).

Using these conditions, the entire three step sequence to synthesize **53** was repeated beginning with Troc-L-Trp-OMe (**21**) (Figure IV.16). Troc-L-Trp-OMe (**21**) was reduced in the presence of BH_3·THF and TFA at 0°C for 1 hour to form [R]-Troc-L-Trp-OMe (**22**) as a diastereomeric mixture is quantitative yields (Snider and Zeng 2000). The resulting foamy white-to-tan solid was carried forward without further purification to prevent the indoline ring from oxidizing back to indole. Using Snider and coworkers coupling conditions, **22** was coupled to Cbz-

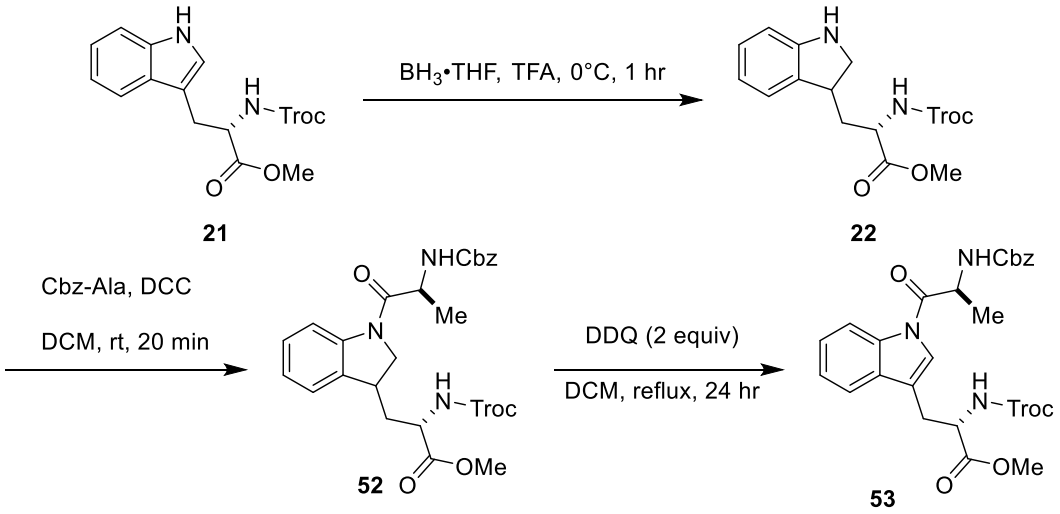

Figure IV.16: Three step sequence of the conversion of Troc-L-Trp-OMe (**21**) to [O]-coupled product (**53**) to synthesize the 5-5-6 ring system towards the total synthesis of versiquinazoline A.

Ala using DCC at 0°C for 20 minutes (Snider and Zeng 2000) to form [R]-coupled product **52.** Using the modified work-up, the resulting crude solid was carried forward to the DDQ oxidation step without further purification. Using the conditions in Entry 3 of Table IV.4, the [O]-coupled product **53** was formed in 45% yield over three steps.

IV.6. Conclusion

This successful sequence prompted a series of optimization reactions to finetune the three step sequence to obtain high yields in high purity to provide a strong foundation for the rest of my proposed synthesis of versiquinazoline A. The optimization reactions of the three step sequence were put on hold due to my advisor, Dr. Williams, shutting down the lab on March 5, 2020, in

accordance with Colorado State University's COVID-19 Public Health directives. During the COVID-19 lockdowns, plans to stereoselectively install an alcohol on C16 of versiquinazoline A via Sharpless dihydroxylation using AD mix-β were being investigated. On May 13, 2020, Dr. Robert M. Williams passed away after a 2 year battle with prostate cancer.

Upon receiving the news of Bob's death, I was at a crossroads with my project. Under my new advisor, Dr. Debbie C. Crans, I could continue to work on my total synthesis, or I could switch to a new project. After long and hard considerations of my future, I made the incredibly difficult decision to switch projects. This project was not an easy path. Taking on this project alone was one of the most difficult things I have ever done. Even though none of this work resulted in a publication, I am proud of the work I did, all the problems I learned to solve, and the technical and critical thinking skills I learned along the way. If I could start all over again knowing what I know now, I would slow down and really think about how I should spend my time. I spun my wheels for so long thinking that I was the problem when reactions did not work. It took me too long to be able to trust myself as a chemist and truly think about the properties of these compounds. If I had done so, I would have spent less time trying to correct myself and spent more time trying new and different reactions.

In hindsight, my approach to synthesizing versiquinazoline A and B was not conducive to a divergent synthesis. The proposed synthesis was entirely linear. Looking back, I would have tried to approach the synthesis convergently and divergently, synthesizing each ring system separately and then connect them together.

References

. "Cancer Statistics." Retrieved August 25, 2018, from https://www.cancer.gov/about-cancer/understanding/statistics.

Ames, B., S. Haynes, X. Gao, B. Evans, N. Kelleher, Y. Tang and C. Walsh (2011). "Complexity Generation in Fungal Peptidyl Alkaloid Biosynthesis: Oxidation of Fumiquinazoline A to the Heptacyclis Hemiaminal Fuimiquinazoline C by the Flavoenzyme Af12070 from Aspergillus Fumigatus." Biochem. **50**: 8756-8769.

Ames, B., X. Liu and C. Walsh (2010). "Enzymatic Processing of Fumiquinazolines F: A Tandem Oxidative-Acylation Strategy for the Generation of Multicyclic Scaffolds in Fungal Indole Alkaloid Biosynthesis." Biochem. **49**: 8564-8576.

Ames, B. and C. Walsh (2010). "Anthranilite-Activiating Modules from Fungal Nonribosomal Peptide Assembly Lines." Biochem. **49**: 3351-3365.

Aoyama, T., N. Sonoda, M. Yamauchi, K. Toriyama, M. Anzai, A. Ando and T. Shioiri (1998). "Chemical manganese dioxide (CMD), an efficient activated manganese dioxide. application to oxidation of benzylic and allylic alcohols." Synlett **1998**(1): 35-36.

Bang-Anderson, B., K. Larsen and N. Mork (2007). Novel 2,3-Dihydroindole Compounds. **WO2007/019867 A1**.

Baran, P. S., C. A. Guerrero and E. J. Corey (2003). "Short, Enantioselective Total Synthesis of Okaramine N." J. Am. Chem. Soc. **125**(19): 5628-5629.

Bauer, F., W. Kleemiss and M. Feld (1998). Process for the Preparation of Aminoacetic Acids with a Tertiary Hydrocarbon Radical in the α-Position, or Their Nitriles. **5831119**.

Beutner, G. L., I. S. Young, M. L. Davies, H. Matthew R, H. Park, J. M. Stevens and Q. Ye (2018). "TCFH-NMI: Direct Access to N-Acyl Imidazoliums for Challenging Amide Bond Formations." Org. Lett. **20**(14): 4218-4222.

Braasch-Turi, M. (2018). Question Regarding the journal article "Versiquinazolines A-K, Fumiquinazoline-type Alkaloids from the Gorgonian0Derived Fungus Aspergillus versicolor LZD-14-1". D. W. Lin.

Cheng, Z., L. Lou, X. Liu, P. Proksch, S. Yin and W. Lin (2016). "Versiquinazoline A-K, Fumiquinazoline-Type Alkaloids from the Gorgonnian-Derived Fungus Aspergillus Versicolor LZD-14-1." J. Nat. Prod **79**: 2941-2952.

Coyle, J. and L. Bryant (1983). "Synthesis of Diazaheterocycles with a Bridgehead Nitrogen by Photocyclisation of N-Substituted Acyclic Imides." J. Chem. Soc. Perkin Trans. 1: 2857-2865.

Davidovich, P., V. Aksenova, V. Petrova, D. Tentler, D. Orlova, V. Smirnov II, V. Gurzhy II, A. Okorokov, A. Garabadzhui and G. Melino (2015). "Discovery of Novel Istatin-Based P53 Inducers." ACS. Med. Chem. Lett. **6**(8): 856-860.

Dunne, C. (2018). Procedure for Acyl Chloride Amide Coupling. M. Braasch-Turi.

El-Faham, A. and F. Albericio (2011). "Peptide Coupling Reagents, More than a Letter Soup." Chem. Rev. **111**(11): 6557-6602.

Elbatrawi, Y. M., C. W. Kang and J. R. D. Valle (2018). "Total Synthesis of L-156, 373 and an oxoPiz Analogue via a Submonomer Approach." Org. Lett. **20**(9): 2707-2710.

Frerot, E., J. Coste, A. Pantaloni, M. Dufour and P. Jouin (1991). "PyBOP and PyBrOP: Two Reagents for the Difficult Coupling of the a,a-Dialkyl Amino Acid, Aib." Tetrahedron **47**(2): 259-270.

He, F., B. Foxman and B. Snider (1998). "Total Synthesis of (-)-Asperlicin and (-)-Asperlicin C." J. Am. Chem. Soc. **120**(25): 6417-6418.

He, F. and B. Snider (1997). "Total Synthesis of (+)-Fumiquinazoline G and (+)-Dehydrofumiquinazoline G." SynLett **1997**: 483-484.

Il'yasov, E. and G. Galust'yan (1995). " Synthesis of 1-Aminocyclopropane-1-Carboxylic Acid." Chem. Nat. Compd. **31**(6): 719-720.

Kolb, H., M. Van Nieuwenhze and K. Sharpless (1994). "Catalytic Asymmetric Dihydroxylation." Chem. Rev. **94**(8): 2483-2547.

Lincoln, D., E. Ali Emadi, K. Tonissen and F. Clarke (2003). "The thioredoxin-thioredoxin reductase system: over-expression in human cancer." Anticancer Res. **23**(3B): 2425-2433.

Perez-Balado, C., P. Rodriguez-Grana and A. R. d. Lera (2009). "Stereocontrolled and Versatile Total Synthesis of Bispyrrolidinoindoline Diketopiperazine Alkaloids: Strcutrual Revision of the Fungal Isolate (+)-Asperdimin." Chem. Eur. J. **15**(38): 9928-9937.

Polko, J. K. and J. J. Kieber (2019). "1-Aminocyclopropane-1-Carboxylic Acid and Its Emerging Role as Ethylene-Independent Growth Regulator." Front. Plant Sci. **10**: 1602.

Satoh, N., T. Akiba, S. Yokoshima and Y. Fukuyama (2009). " A Practical Synthesis of (−)-Oseltamivir." Tetrahedron **65**(16): 3239-3245.

Sheehan, J., P. Cruickshank and G. Boshart (1961). "Notes- A Convenient Synthesis of Water-Soluble Carbodiimides." J. Org. Chem. **26**(7): 2525-2528.

Snider, B. and H. Zeng (2000). "Total Synthesis of (-)-Fumiquinazolines A, B, and I." Org. Lett. **2**(25): 4103-4106.

Snider, B. and H. Zeng (2002). "Total Synthesis of (-)-Fumiquinazoline C, E, and H." Org. Lett. **4**(7): 1087-1090.

Solomon, V., C. Hua and H. Lee (2009). "Hybrid Pharmacophore Design and Synthesis of Istatin-Benzothiazole Analogs for Their Anti-Breast Cancer Activity." Bioorg. Med. Chem. **17**: 7585-7592.

Takahashi, C., T. Matsushita, M. Doi, K. Minoura, T. Shingu, Y. Kumeda and A. Numata (1995). "Fumiquinazolines A-G, Novel Metabolites of a Fungus Separated from a Pseudolabrus Marine Fish." J. Chem. Soc. Perkin Trans. 1: 2345-2353.

Ueda, H., M. Yamaguchi, H. Kameya, K. Sugimoto and H. Tokuyama (2014). " Autotandem Catalysis: Synthesis of Pyrroles by Gold-Catalyzed Cascade Reaction." Org. Lett. **16**: 4948-4951.

IV.7. Experimental Section

IV.7.1. General Materials and Methods

All reactions were conducted under argon atmosphere unless otherwise noted. All reagents were used as purchased unless otherwise noted. Solvents were dried by passing through an alumina drying column (Solv-Tek Inc.) under argon pressure (DCM, THF, Diethyl Ether).

IV.7.2. Towards the Preparation of N-Cbz-ACC

IV.7.2.1. Ethyl 1-cyanocyclopropane-1-carboxylate (Il'yasov and Galust'yan 1995) (43):

To a 250 mL round bottom flask was added ethyl 2-cyanoacetate (5.32mL, 50.73mmol), 1,2-dibromoethane (6.7mL, 77.4mmol), and DMSO (40mL) and cooled to 10°C. After sufficiently cooled, potassium carbonate (19.97g, 144.5 mmol) was added to the flask. The reaction was allowed to warm to ambient room temperature and stirred under argon for 8hr. Cold water (100mL) was added to the reaction, and then was extracted with ether (5 x 50mL). Additional water (~25mL) was added to dissolve unreacted potassium carbonate. The combined organic layers were dried over anhydrous Na_2SO_4, and then the solvent was removed under reduced pressure at ambient temperature. The product was dried under reduced pressure overnight, which yielded a colorless oil (4.6286g, 65.57%).^{1}H NMR (400 MHz, $CDCl_3$) δ: 4.26 (qd, J=4 Hz, 8 Hz, 2H), 1.68 (td, J=4 Hz, 2H), 1.62 (td, J=4 Hz, 2H), 1.33 (td, J=4 Hz, 8 Hz, 3H).

1H NMR

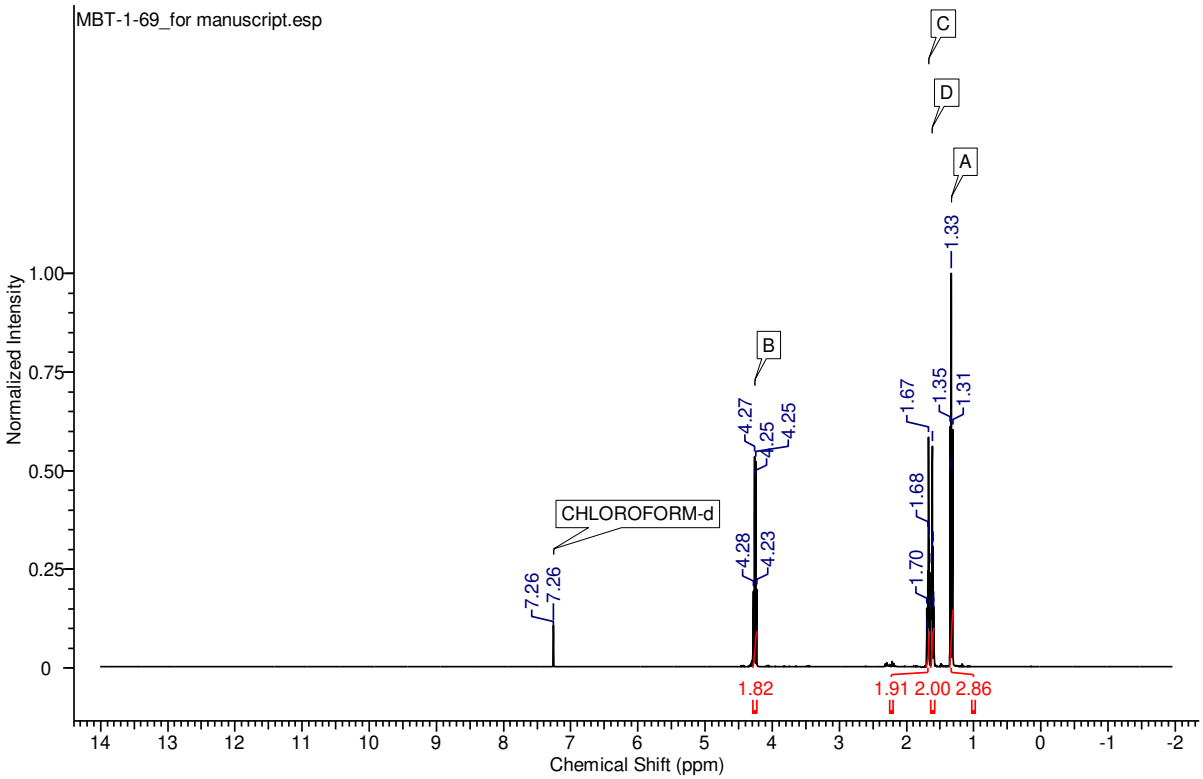

IV.7.2.2. 1-Carboxycyclopropane-1-carboxamide (Il'yasov and Galust'yan 1995) (44):

To a 1L round bottoms flask was added **43** (9.5653g, 68.74 mmol), NaOH (7.11g, 177.75 mmol), and DI H_2O (36mL). The solution was stirred at 50°C for 30 minutes. The reaction was cooled to ambient room temperature. While stirring, 30% hydrogen peroxide (23.8mL) was added very slowly along the walls of the flask. The reaction was again heated to 50°C for 20 minutes. The reaction was allowed to cool to room temperature and further cooled in an ice bath, and then it was acidified to a pH of 2 with 1:1 con. HCl: glacial acetic acid on the ice bath. The resulting solid was filtered and rinsed with ice cold DI H_2O. The resulting white powder was recrystallized in DI H_2O resulting in a white crystalline solid. The slid was collected and dried under reduced pressure overnight, which produced 5.54g, a 62.4% yield. ^{1}H NMR (400 MHz, D_2O) δ: 1.64 (q, J=4 Hz), 1.56 (q, J=4 Hz).

1H NMR

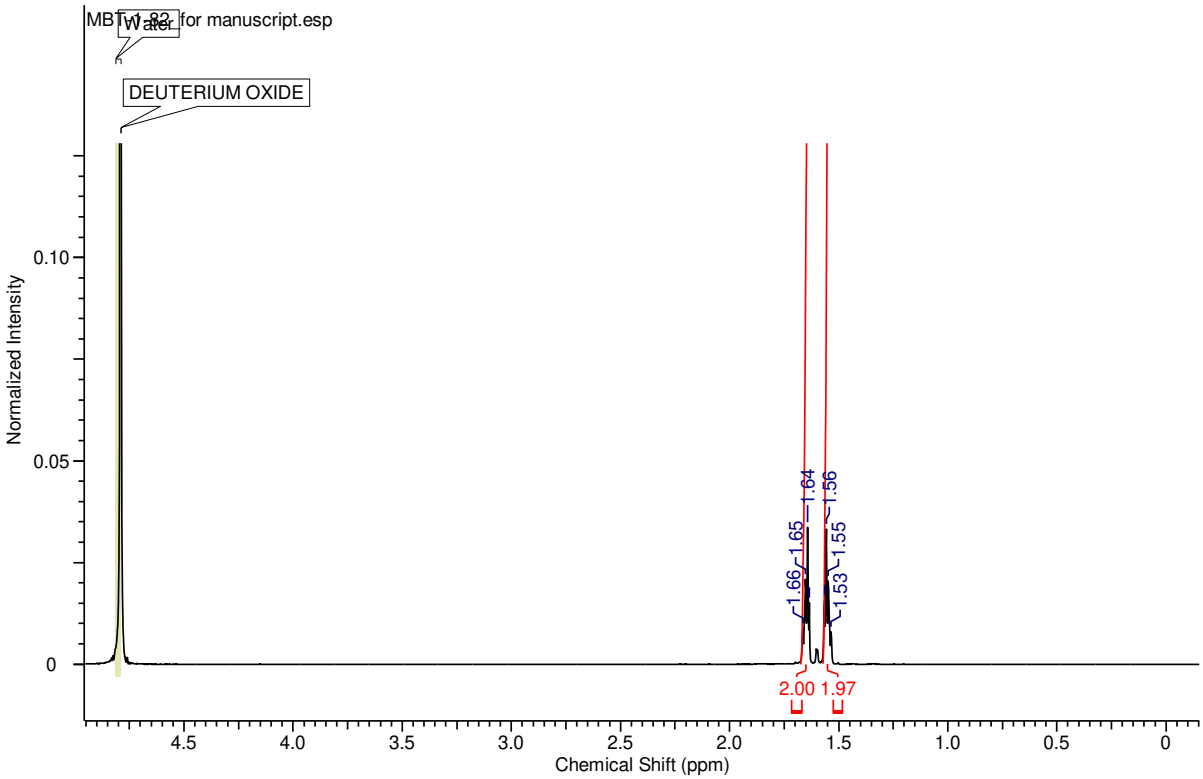

IV.7.2.3. N-Carbobenzyloxy-1-aminocyclopropane-1-carboxylic acid (Bauer, Kleemiss et al. 1998, Ueda, Yamaguchi et al. 2014) (N-Cbz-ACC, 23):

To a 100mL round bottom flask cooled to 0°C, **44** (0.9989g, 7.736 mmol) was dissolved in 10% NaOH (3.2mL) under an inert atmosphere. The remaining 10% NaOH (6.08mL) solution was added. Household bleach (6% NaOCl, 10mL) was added slowly while on an ice bath. The reaction was stirred for 3 hr while maintaining a reaction temperature of ≤ 10°C under an inert atmosphere. The reaction was then heated to 60°C with a condenser for 3 hr. The reaction was then allowed to cool to room temperature and acidified to a pH of 7 with HCl. The resulting solution was cooled to 0°C, then 2M NaOH (7.6mL) was added to the flask. CbzCl (0.31mL) and 2M NaOH (0.62mL) were alternatingly added to the flask a total of 5 times each over 1 hr at 0°C (CbzCl, NaOH, CbzCl, NaOH, CbzCl, NaOH, CbzCl, NaOH, CbzCl, NaOH), then the reaction was stirred at room temperature overnight. The resulting solution was extracted with ether

(3x25mL). The aqueous solution was acidified to a pH of 1 in an ice bath. The acidified solution was extracted with ethyl acetate (4x 25mL). The combined ethyl acetate organic layers were dried over anhydrous Na_2SO_4, and the solvent was removed under reduced pressure. The resulting solid was dried under reduced pressure overnight, which yielded a white solid (1.2373g, 67.9%)^{1}H NMR (400 MHz, MeOD) δ: 7.35 (m, 5H), 5.09 (s, 2H), 1.48 (br s/q, 2H), 1.13 (br q, 2H).

1H NMR

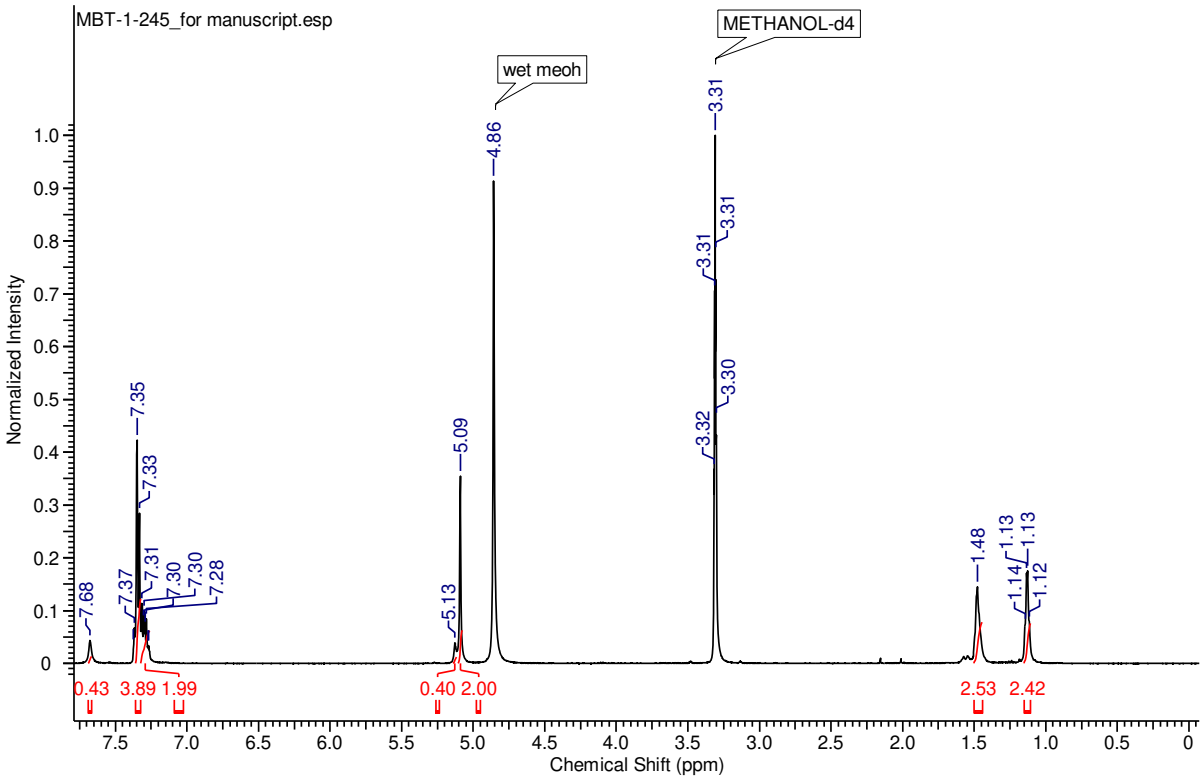

IV.7.3. Preparation of the 5-5-6 Ring System

IV.7.3.1. N-((2,2,2-Trichloroethoxy)carbonyl)-S-tryptophan methyl ester (Snider and Zeng 2000) (Troc-Trp-OMe, 21):

To a 250mL round bottom flask was added ether (40mL), 10% $NaHCO_3$ (40mL), and $NaHCO_3$ (3.3242g, 39.5705 mmol) and cooled to 0°C. Tryptophan methyl ester hydrochloride **20** (9.9984g, 39.254 mmol) was added in small amounts over 10 minutes. The reaction flask was

cooled to 0°C, and a solution of 2,2,2-trichloroethoxycarbonyl chloride (5.40mL, 39.228 mmol dissolved in 40mL ether) was added dropwise over 1 hour. The reaction was allowed to warm to room temperature and stir for 4 hours. The biphasic reaction was allowed to separate into layers, and the organic layer was removed. The aqueous layer was extracted with ether (2x50mL). The combined organic layers were washed with brine (80mL) and dried over anhydrous Na_2SO_4. The Solvent was removed under reduced pressure and dried overnight under reduced pressure. The crude pink oil was purified via column chromatography (1:20 pdt:silica, dry load product with DCM and rinse with hexanes 3 times, elute with 2:1 ethyl acetate/hexanes), which yielded a foamy white/beige solid (14.48g, 93.8%). I ^{1}H NMR (400 MHz, $CDCl_3$) δ: 8.06 (br s, 1H), 7.55 (d, J= 8 Hz, 1H), 7.36 (d, J=8Hz, 1H), 7.20 (td, J=2 Hz, 8 Hz 1), 7.12 (td, J= 2 Hz, 8Hz, 1H), 7.02 (d, J=4 Hz, 1H), 5.55 (br d, J= 8 Hz, 1H), 4.80 (d, J=12 Hz, 1H), 4.75 (dt, J= 4 Hz, 8Hz, 1), 3.70 (s, 3H), 3.35 (d, J=4 Hz, 2H).

1H NMR

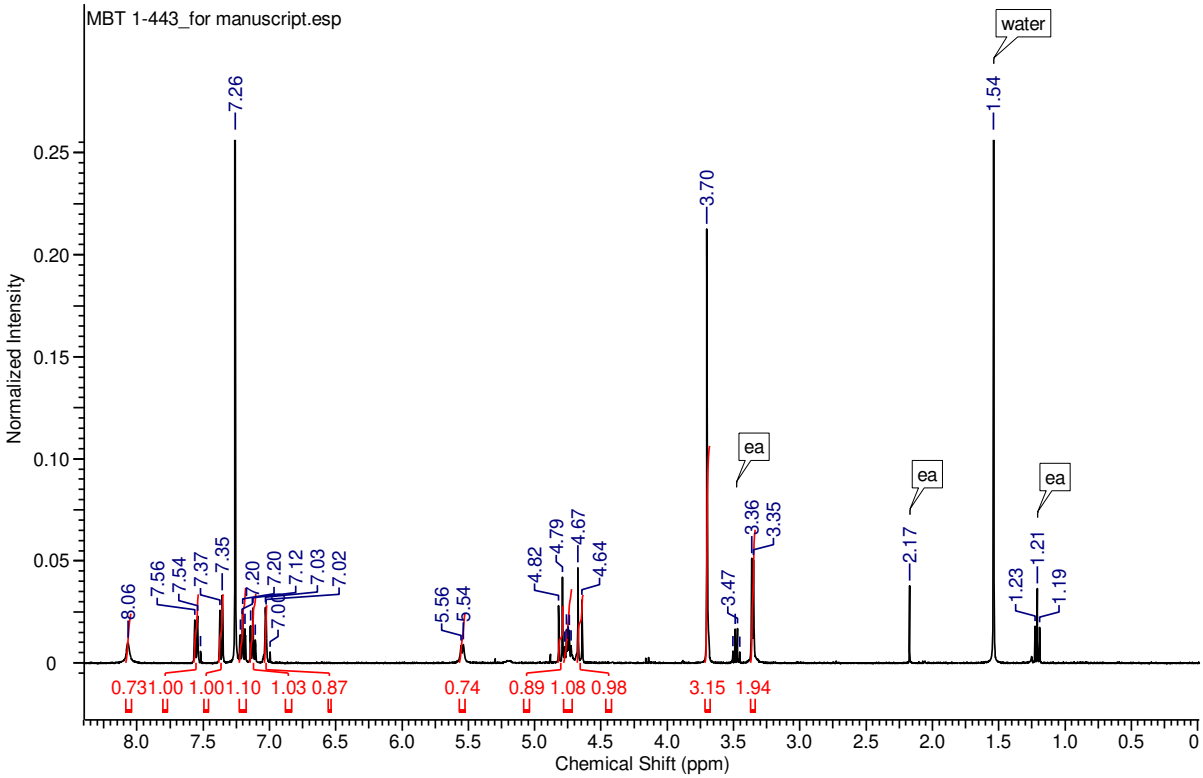

IV.7.3.2. Methyl (2S)-3-(indolin-3-yl)-2-(((2,2,2-trichloroethoxy)carbonyl)amino)propanoate (Snider and Zeng 2000) ([R]-Troc-Trp-OMe, 22):

To flame dried 100mL round bottom flask was added **21** (3.01g, 7.6463 mmol) and trifluoroacetic acid (15mL) under an inert atmosphere. The flask was cooled to 0°C and 1M BH_3·THF (18mL, 18 mmol) was added slowly (~ 1mL/min). The reaction was stirred at 0°C for 1 hour and concentrated under reduced pressure. The residue was dissolved in ethyl acetate (50mL) which was washed with saturated $NaCHO_3$ (3 x 50mL), brine (50mL), and dried over anhydrous Na_2SO_4. The solvent was removed under reduced pressure and dried overnight under reduced pressure. The resulting product was a white foamy solid (2.82g, 93.2%). The diastereomeric mixture was used without further purification. ^{1}H NMR (400 MHz, $CDCl_3$) δ: 7.06 (d, J= 4 Hz, 1H), 7.05 (d, J=4 Hz, 1H), 6.72 (t, J=8 Hz, 1H), 6.66 (t, J=8 Hz, 1H), 5.80/5.69 (br d, J=8 Hz, 1H), 4.67-4.83 (m, 2H), 4.49 (m, 1H), 3.76 (s, 3H), 3.72 (t, 2H), 3.30-3.39 (m, 2), 2.11 (m, 2).

1H NMR

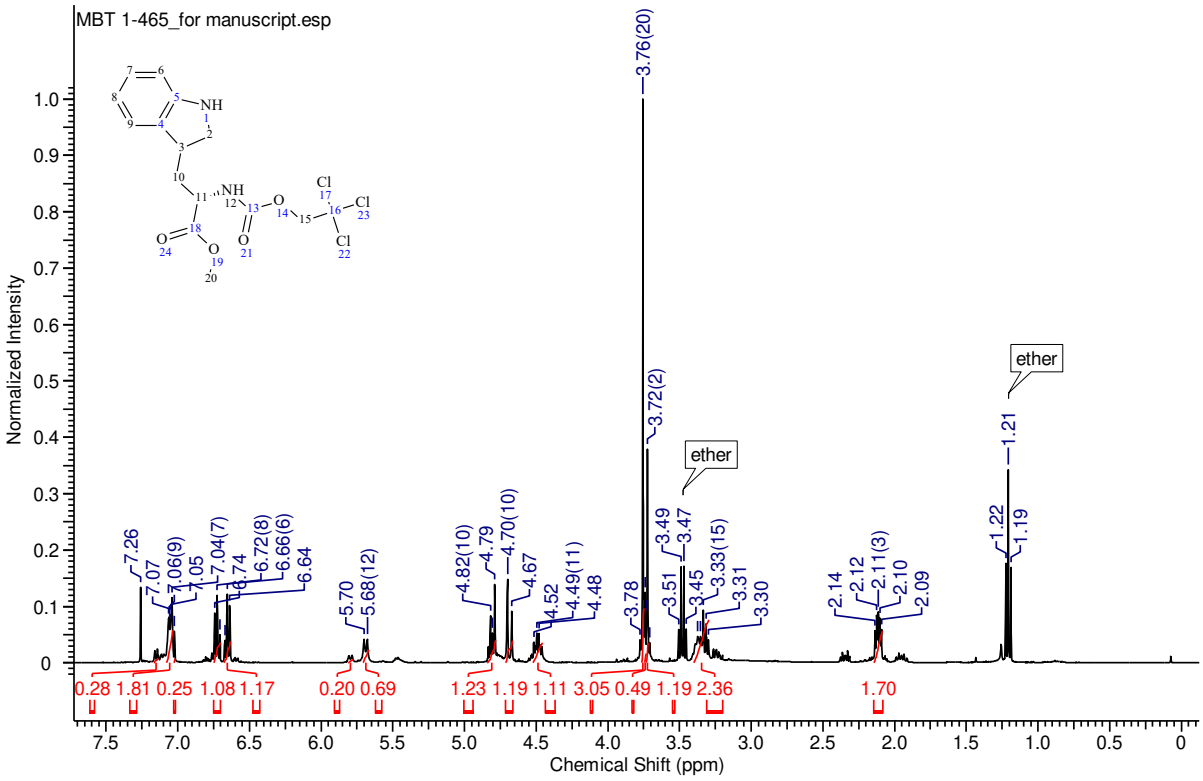

IV.7.3.3. Methyl 1-(2-cyanoacetyl)-N$^{\alpha}$-((2,2,2-trichloroethoxy)carbonyl)-L-tryptophonate (Zhou, Wang et al. 2016) (48):

To a flame-dried 25mL round bottom flask was added a suspension of 2-cyanoacetic acid (0.2880g, 3.3858 mmol, 1.3 equiv) in DCM (10 mL) under an inert atmosphere. The flask was cooled to 0°C and oxalyl chloride (0.27 mL, 1.2 equiv)) was added. Three drops of DMF were added, and the reaction stirred at 0°C for five hours. During the chlorination reaction, **[R]-Troc-Trp-OMe 22** (1 equiv) was freshly prepared using the method described above in quantitative yield. The resulting product was dissolved in DCM (10 mL) and to the 2-cyanoacetyl chloride reaction along the sides of the flask with an additional rinse of DCM (10 mL). Et_3N (0.90mL) was added dropwise to the pot, and allowed to stir overnight, gradually warming to room temperature. The solvent was removed via rotary evaporation to produce a dark orange-brown solid. The precipitate was collected via vacuum filtration and rinsed with methanol (50 mL). Oily product

went through to the filtrate. The filtrate was collected, and the solvent was removed. The resulting solid was collected via vacuum filtration and washed with methanol (50mL). All solid collected via vacuum filtration was collected and dried under reduced pressure overnight. The crude solid was purified via column chromatography (10% ethyl acetate, 90% DCM, 1:20 pdt:silica, dry load product with DCM). The diastereomeric product was a white foamy solid (0.4156, 35.61%). ^{1}H NMR (400 MHz, $CDCl_3$) δ: 8.14-8.17 (m, 2H), 7.09-7.17 (m, 3H), 5.72 (d, J= 8.5 Hz, 1H), 5.67 (d, J-8.5Hz, 1H), 4.78-4.85 (dd, 4H), 4.70 (d, 1H), 4.67 (d, 1H), 4.49-4.54 (q, 2H), 4.23-4.33 (dt, 2H) 3.82 (s, 3H), 3.65 (m, 4H), 2.13 (t, 2H). ^{13}C NMR (101 MHz, d6-DMSO) δ: 172.12, 172.09, 161.45, 161.40, 154.65, 154.57, 141.92, 141.85, 134.75, 134.28, 127.97, 127.80, 124.64, 124.15, 115.92, 96.04, 95.98, 73.58, 53.69, 52.14, 36.29, 27.03

1H NMR

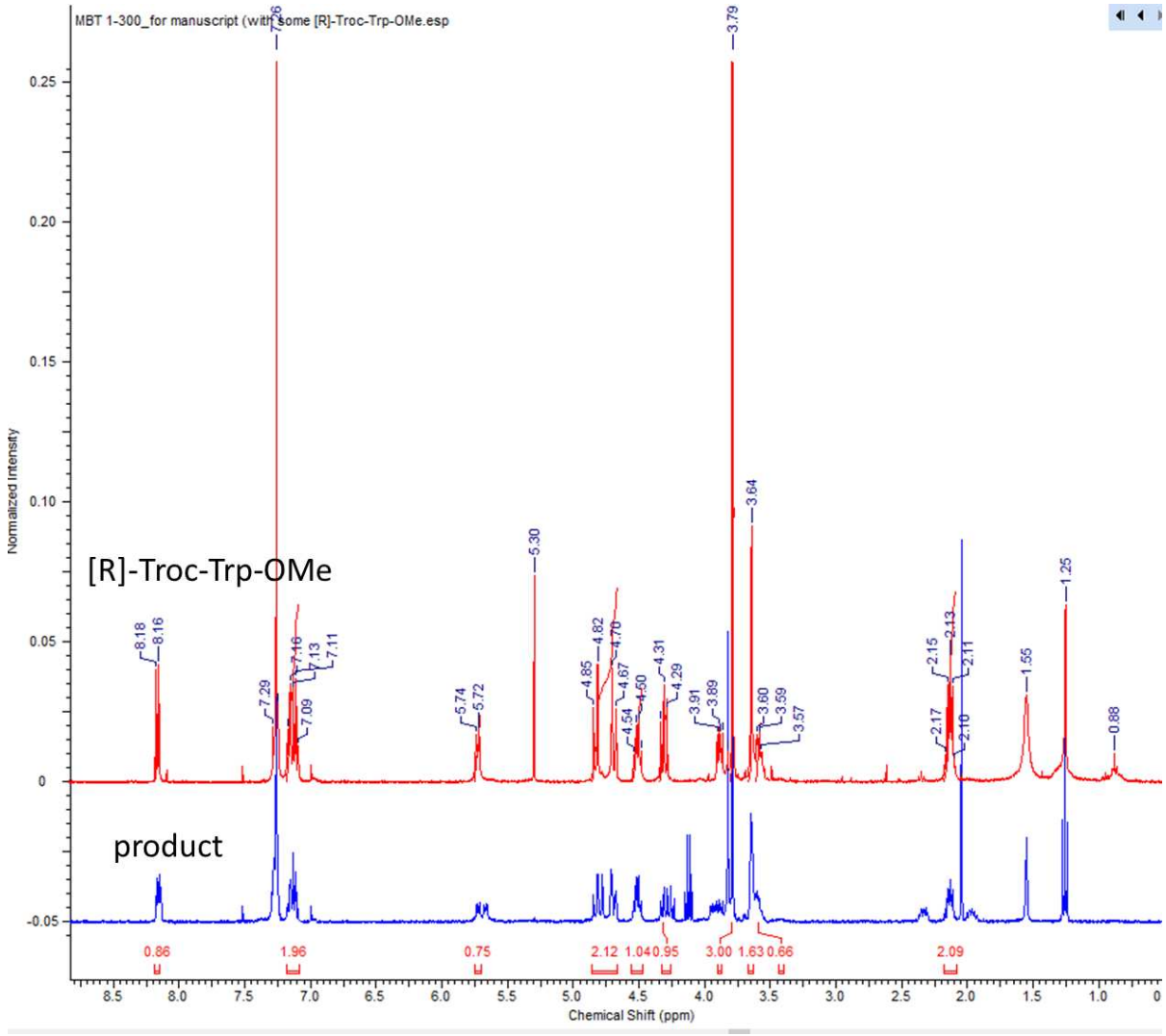
MBT 1-300_for manuscript (with some [R]-Troc-Trp-OMe.esp
[R]-Troc-Trp-OMe
product
Normalized Intensity
Chemical Shift (ppm)
0.86
1.96
0.75
2.12
1.04
0.95
3.00
1.63
0.66
2.09

13C NMR

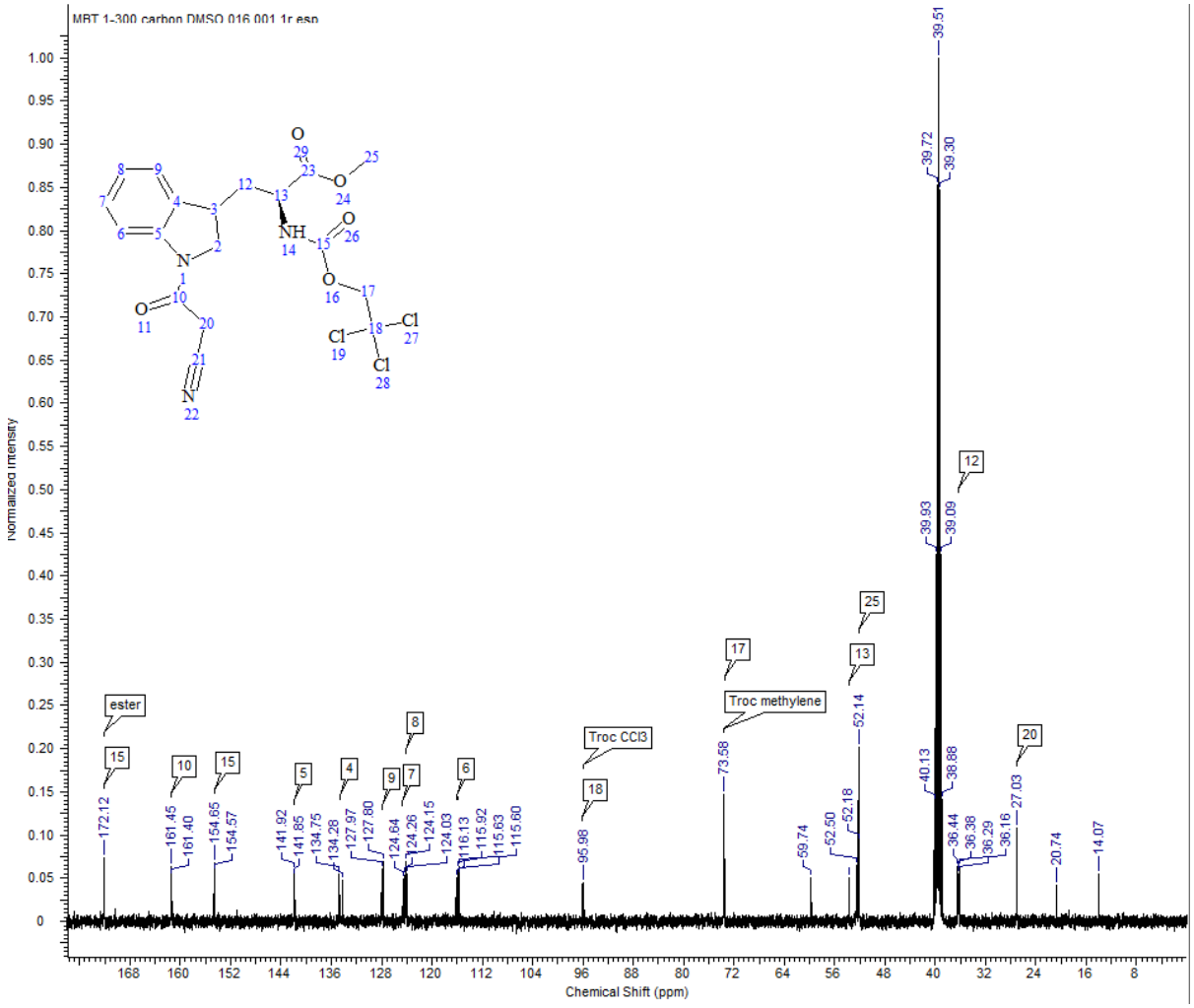
Normalized Intensity
Chemical Shift (ppm)
ester
Troc CCl3
Troc methylene
172.12
161.45
161.40
154.65
154.57
141.92
141.85
134.75
134.28
127.97
127.80
124.64
124.26
124.15
124.03
116.13
115.92
115.63
115.60
95.98
73.68
59.74
52.50
52.18
52.14
40.13
39.93
39.72
39.51
39.30
39.09
38.88
36.44
36.38
36.29
36.16
27.03
20.74
14.07

IV.7.3.4. Methyl (2S)-3-(1-(((benzyloxy)carbonyl)-L-alanyl)indolin-3-yl)-2-(((2,2,2-trichloro-ethoxy)carbonyl)amino)propanoate (52):

HATU Conditions (Perez-Balado, Rodriguez-Grana et al. 2009): To a flame-dried 50mL round bottom flask , freshly prepared **22**(0.4928g, 1.25 mmol) was dissolved in DMF (25 mL). Cbz-Ala (0.8725g, 3.9 mmol) was added and the mixture was cooled to 0°C. DIPEA (0.80 mL, 4.5mmol) recrystallized HATU (1.4615g, 3.84 mmol), and HOBt (0.5484g, 4.05mmol) was added, and the mixture was stirred at room temperature overnight. The reaction was diluted with 10% LiCl (50 mL) and DI H_2O (50 mL). The biphasic solution was extracted with ethyl acetate (4 x 50 mL). The organic layer was collected and washed with 10% LiCl (5 x 50 mL) and brine (50 mL). The organic layer was dried with anhydrous Na_2SO_4. The solvent was removed under reduced pressure and dried overnight under reduced pressure. The resulting product was an off-white solid. The crude product was purified via column chromatography (50:50 ethyl acetate to hexanes, 1:20 pdt :silica gel ratio, dry loaded with hexanes) to produce a foamy, white solid, 0.610g, 81.5% yield. The NMR revealed the isolated product was a 1:6 mixture or product to Cbz-Ala. ^{1}H NMR (400 MHz, $CDCl_3$) δ: 8.18 (d, 1H), 7.35 (m 30H—Cbz-Ala included), 7.23 (d, 1H), 7.17 (d, 1H), 7.09 (q of d, 1H), 5.30 (d, 4H), 5.16 (d, 2H), 5.13 (d, 10H—Cbz-Ala), 4.87-4.63 (m, 2H), 4.43 (t, 3H), 3.77 (s, 3H), 1.47 (d, 19H)

1H NMR

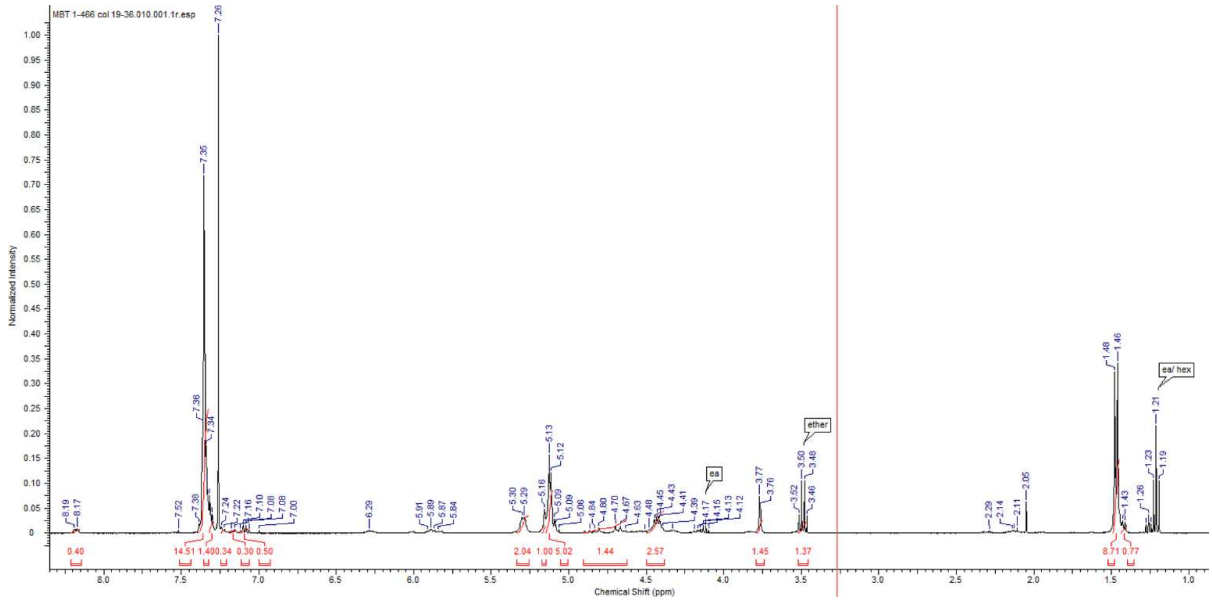

EDC Conditions (Perez-Balado, Rodriguez-Grana et al. 2009): To a flame-dried 50mL round bottom flask, freshly prepared **22**(0.5045g, 1.3 mmol) was dissolved in DMF (13 mL). Cbz-Ala (0.0.2901, 1.3 mmol) was added, and the mixture was cooled to 0°C. Recrystallized EDC (1.4615g, 3.84 mmol), DIPEA (0.57mL) and recrystallized HOBt (0.2183g , 1.6 mmol) was added, and the mixture was stirred at room temperature overnight. The reaction was diluted with 10% LiCl (25 mL) and DI H_2O (25 mL). The biphasic solution was extracted with ethyl acetate (5 x 25 mL). The organic layer was collected and washed with 10% LiCl (5 x 25 mL) and brine (25 mL). The organic layer was dried with anhydrous Na_2SO_4. The solvent was removed under reduced pressure and dried overnight under reduced pressure. The resulting product was a brown foamy solid. The crude product was purified via column chromatography (50:50 ethyl acetate to hexanes, 1:20 pdt :silica gel ratio, dry loaded with hexanes) to produce a foamy, white solid, 0.610g, 81.5% yield. The NMR revealed the isolated product was a 1.6:1 mixture of product to Troc-Trp-OMe. ^{1}H NMR (400 MHz, $CDCl_3$) δ: 8.18 (d, 1H), 7.35 (m 30H—Cbz-Ala included), 7.23 (d, 1H), 7.17 (d, 1H),

7.09 (q of d, 1H), 5.30 (d, 4H), 5.16 (d, 2H), 5.13 (d, 10H—Cbz-Ala), 4.87-4.63 (m, 2H), 4.43 (t, 3H), 3.77 (s, 3H), 1.47 (d, 19H)

1H Crude NMR

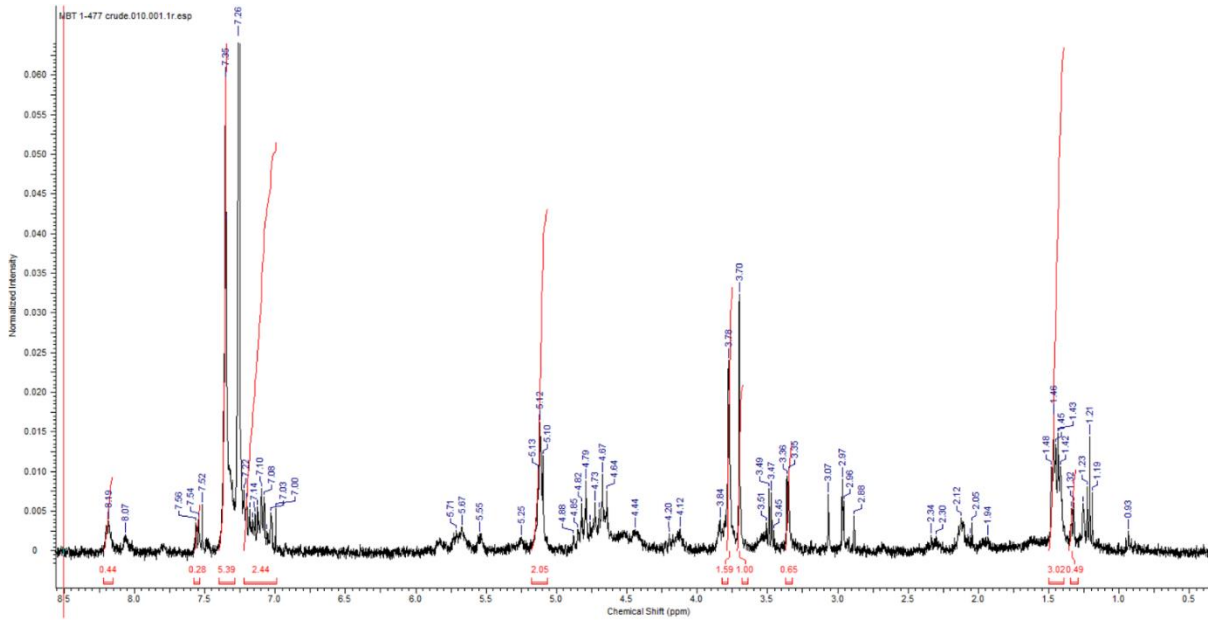

DCC Conditions (Snider and Zeng 2000): To a flame-dried 100mL round bottom flask was added Cbz-Ala (1.5101g, 6.765 mmol) was dissolved in DCM (20 mL). DCC (1.4119g, 6.843 mmol) was added. The solution was stirred for 5 minutes. Freshly prepared **22** was dissolved in DCM (5mL) and added to the reaction mixture. The flask containing **22** was rinsed with additional DCM (7mL) and added to the reaction mixture. The resulting mixture was stirred at room temperature for 20 minutes. Upon completion via TLC, the reaction was filtered through a pad of celite and rinsed with a minimal amount of cold DCM. The solvent was removed under reduced pressure to reveal an off-white solid. The crude product was dissolved in a minimal amount of ethyl acetate and placed in a freezer overnight (~ 12 hr). The resulting white precipitate was removed via cold filtration through a pad of celite. The solvent was removed to yield a foamy, white solid (2.4039g, 59% yield) as a diastereomeric mixture of coupled products, **52.** ^{1}H NMR

(400 MHz, $CDCl_3$) δ: 8.20 (d, 1H), 7.40-7.30 (m, 7H), 7.22-7.16 (m, 2H), 7.09 (q, 1H) 7.03 (t, 1H), 5.65 (br s, 1H), 5.12 (br s, 2H), 4.88-4.41 (m, 6H), 3.78 (s, 3H), 1.46 (d, 2H), 1.42 (d, 2H).

1H Crude NMR

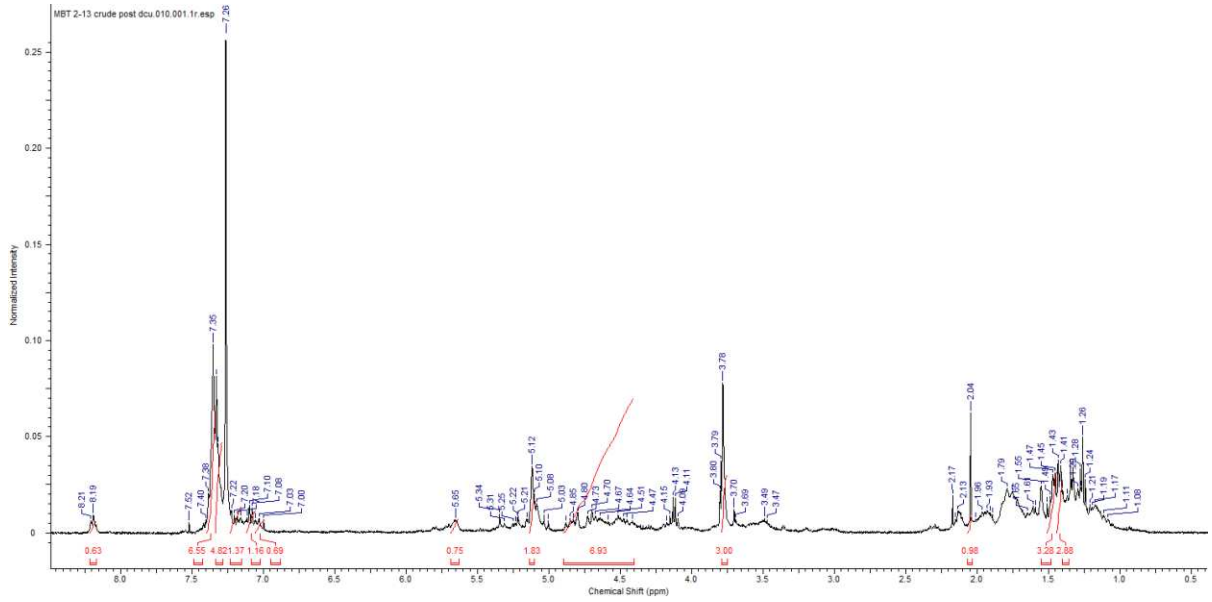

IV.7.3.5. Methyl 1-(((benzyloxy)carbonyl)-L-alanyl)-Na-((2,2,2-trichloroethoxy)carbonyl)-L-trypto-phanate (Snider and Zeng 2000)(53):

Snider & Coworkers Replicated Conditions- Full Three Step Sequence (Snider and Zeng 2000): To a flame-dried 50mL round bottom flask was added Troc-Trp-OMe **21** (0.979g, 2.5 mmol) was reduced following the above procedure to synthesize **22** and carried forward without column purification. To another flame-dried 50mL round bottom flask, Cbz-Ala (0.5027g, 2.25 mmol) was dissolved in DCM (6mL) under an inert atmosphere. DCC (0.5342, 2.6 mmol) was added after all the Cbz-Ala was dissolved. The resulting white suspension was stirred at room temperature for 5 minutes. A solution of **22** in DCM (5 mL) and added to the white suspension, resulting in an opaque, yellow mixture. The reaction stirred at room temperature for 20 minutes, then was filtered through a pad of Celite and rinsed once with cold DCM. The solvent was removed

from the crude product via rotary evaporator in a flame-dried 100mL round bottom flask to produce a foamy, yellow solid (**52**) in 1.948g in 143% crude yield.

The resulting product **52** was dissolved in toluene (7.5 mL). DDQ (0.4035g, 1.777m mmol) was added, and the flask was fitted with a reflux condenser and refluxed for 1 hour. After 1 hour, a second amount of DDQ (0.2162g, 0.9524 mmol) and refluxed for another hour. The reaction was cooled to room temperature and filtered through a pad of celite. The filtrate was washed with saturated sodium bicarbonate (2 x 50mL), brine, and dried with Na_2SO_4. The solvent was removed under reduced pressure (azeotrope with methanol) and dried overnight under reduced pressure. The resulting product was a brown foamy solid. The crude product was purified via column chromatography (50:1 DCM/ethyl acetate, 1:20 pdt:silica) to produce a brown foamy solid, 0.04g, 2.966% yield over three steps. ^{1}H NMR (400 MHz, $CDCl_3$) δ: 8.40 (d, 1H), 7.51-7.50 (d, 1H), 7.43 (s, 1H), 7.35-7.26 (m, 7H), 6.06-6.00 (dd, 2H), 5.13 (q, 1H) 5.10 (d, 2H), 4.77 (d, 2H), 4.64 (d, 1H), 3.69 (s, 3H), 3.32-3.27 (dd, 1H), 3.20-3.15 (dd, 1H), 1.51 (d, 3H). ^{13}C NMR (101 MHz, $CDCl_3$) δ: 171.32, 171.32, 170.80, 155.55, 153.91, 136.01, 135.78, 130.21, 128.32, 127.98, 127.85, 125.62, 124.04,122.47, 118.86, 117.78, 116.68, 95.19, 74.38, 60.22, 53.93, 52.48, 49.31, 27.49, 20.82, 19.13

1H NMR

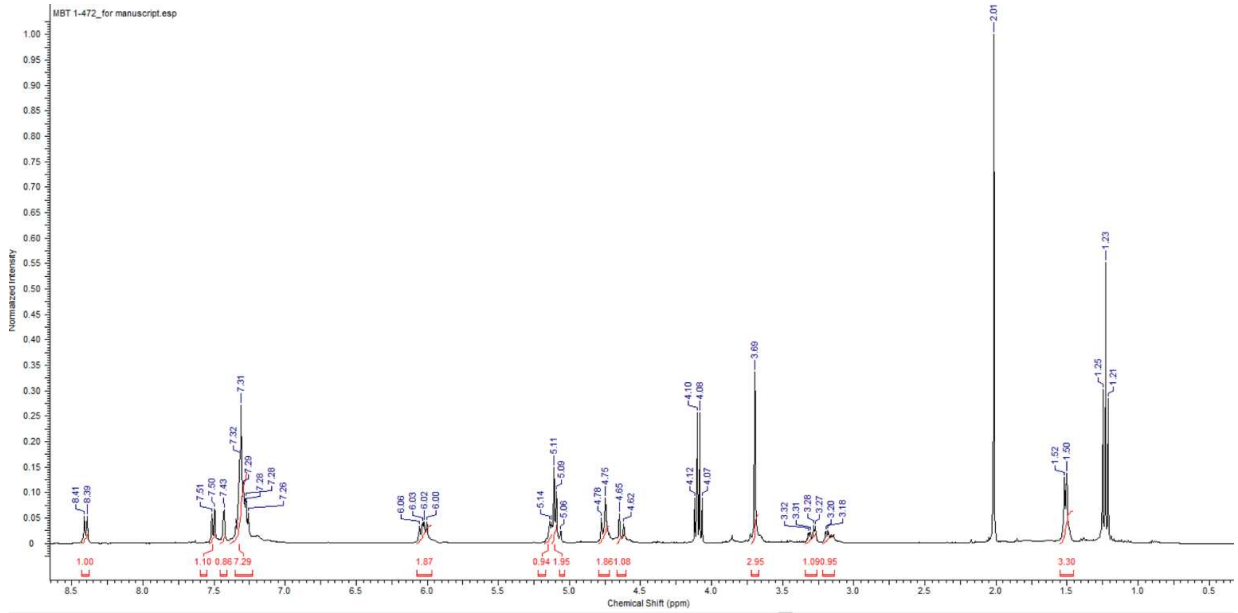

13C NMR

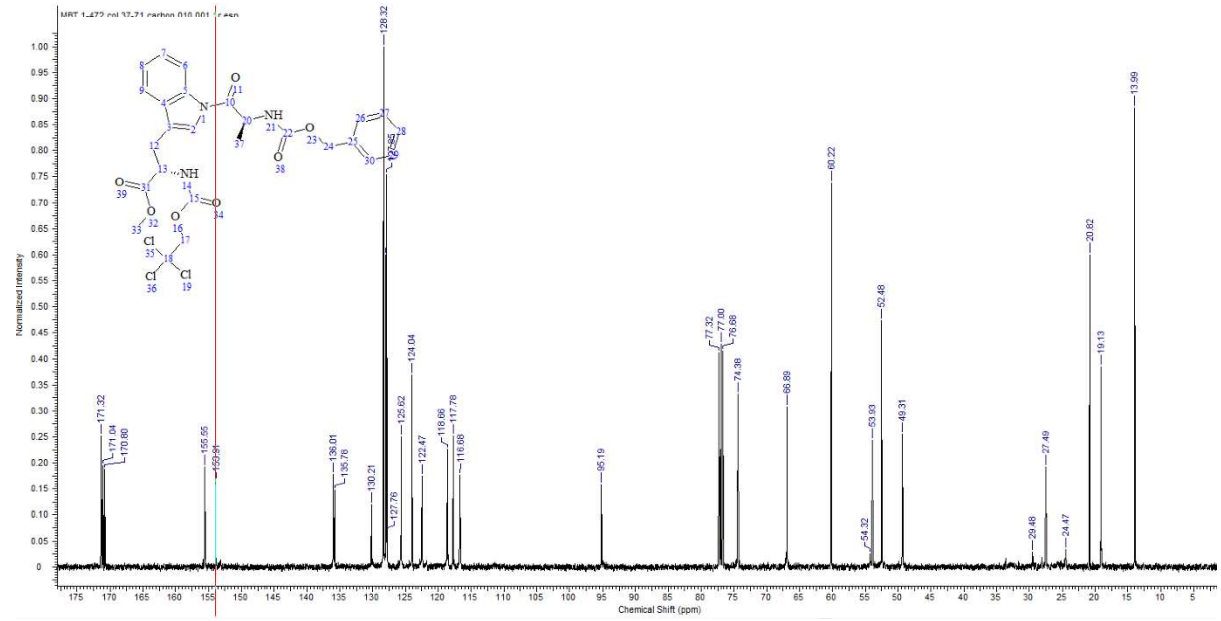

HSQC

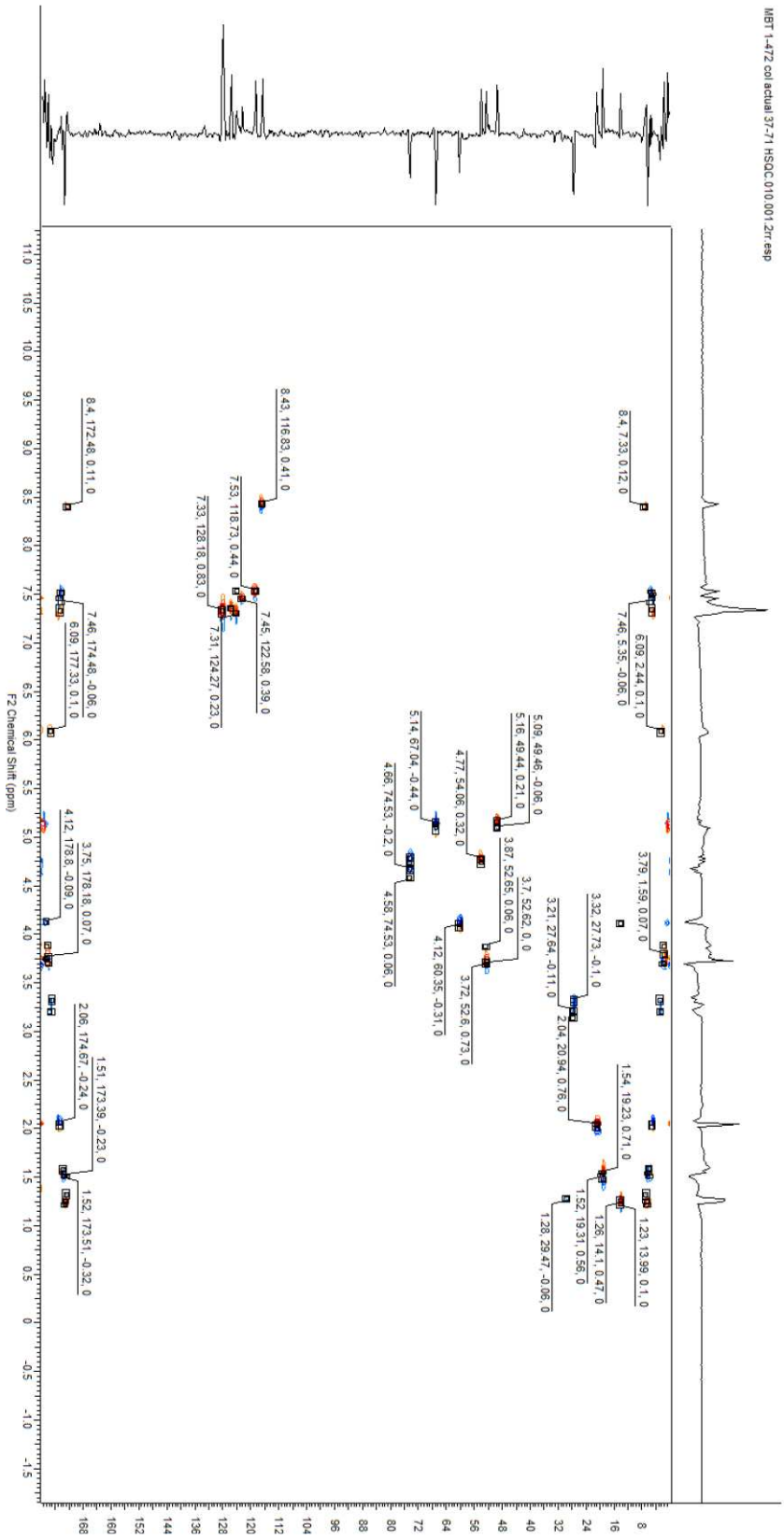
MBT 1-472 col actual 37-71 HSQC 010 001 2rr esp
F2 Chemical Shift (ppm)

DDQ Oxidation of 52→53: To a flame-dried 2-neck 15mL round bottom flask was added **52** (0.4939g, 0.82 mmol) in DCM (8 mL) under an inert atmosphere. Recrystallized DDQ (0.2515g, 1.12 mmol) was added to the solution resulting in a dark black-red mixture. The flask was fitted with a reflux condenser and refluxed for 24 hours under argon. DCM was added as needed through the other neck to replenish the solvent level throughout the reflux duration. After 24 hours, a second equivalent of DDQ (0.2018g, 0.889 mmol) was added. The reaction was brought to a reflux again for an additional 24 hours. After cooling to room temperature, the mixture was filtered through a pad of celite and rinsed with DCM. The filtrate was diluted with ethyl acetate (100 mL) and washed with 10% sodium bicarbonate (3 x 200mL). The emulsion that results upon extraction was remediated by added DI H_2O (2 x 200mL) and brine (100mL) until two clear layers were identified. The organic layer was dried with $MgSO_4$, and the solvent was removed under reduced pressure. The resulting crude product was a dark brown foam (0.14g, 28.4% crude). ^{1}H NMR (400 MHz, $CDCl_3$) δ: 8.43 (d, 1H), 7.53 (d, 1H), 7.40-7.32 (m, 10H), 5.68 (q, 2H), 5.13 (d, 2H), 5.12 (br d, 2H), 4.83-4.79 (t, 2H), 4.68 (d, 2H), 3.73 (s, 3H), 3.30 (qd, 4H), 1.54 (d, 4H)

1H NMR

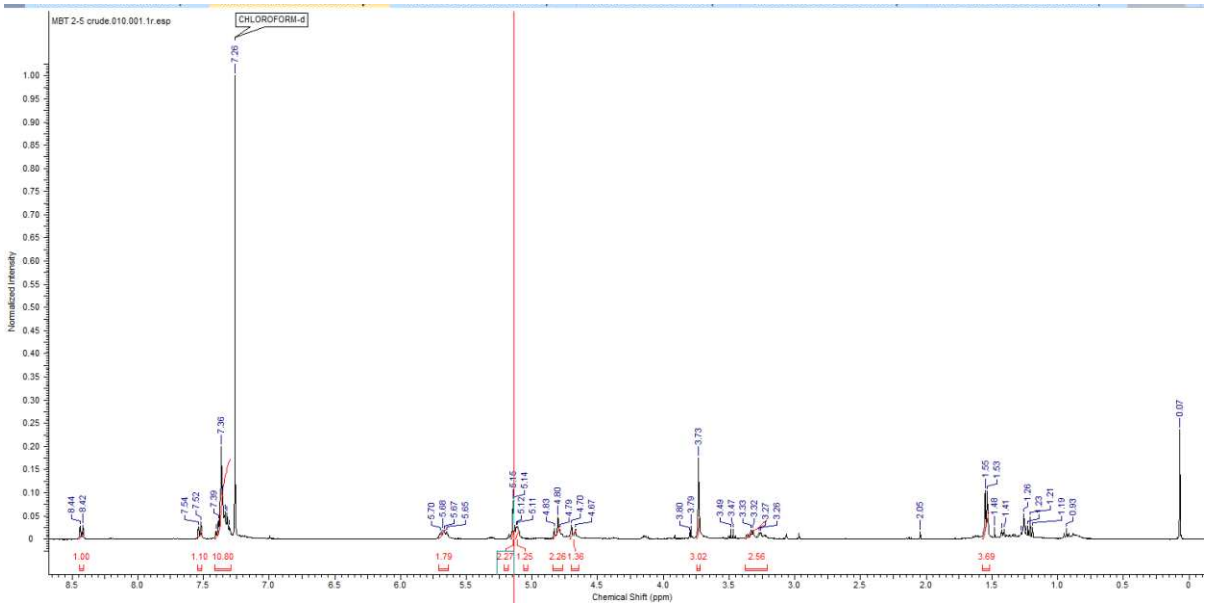
MBT 2-5 crude.010.001.1r.esp
CHLOROFORM-d
Normalized Intensity
Chemical Shift (ppm)

References

Bauer, F., W. Kleemiss and M. Feld (1998). Process for the Preparation of Aminoacetic Acids with a Tertiary Hydrocarbon Radical in the α-Position, or Their Nitriles. **5831119**.

Il'yasov, E. and G. Galust'yan (1995). " Synthesis of 1-Aminocyclopropane-1-Carboxylic Acid." Chem. Nat. Compd. **31**(6): 719-720.

Perez-Balado, C., P. Rodriguez-Grana and A. R. d. Lera (2009). "Stereocontrolled and Versatile Total Synthesis of Bispyrrolidinoindoline Diketopiperazine Alkaloids: Strcutrual Revision of the Fungal Isolate (+)-Asperdimin." Chem. Eur. J. **15**(38): 9928-9937.

Snider, B. and H. Zeng (2000). "Total Synthesis of (-)-Fumiquinazolines A, B, and I." Org. Lett. **2**(25): 4103-4106.

Ueda, H., M. Yamaguchi, H. Kameya, K. Sugimoto and H. Tokuyama (2014). " Autotandem Catalysis: Synthesis of Pyrroles by Gold-Catalyzed Cascade Reaction." Org. Lett. **16**: 4948-4951.

Zhou, T., Y. Wang, B. Li and B. Wang (2016). "Rh(III)-Catalyzed Carbocyclization of 3-(Indolin-1-Yl)-3-Oxopropanenitriles with Alkynes and Alkenes through C–H Activation." Org. Lett. **18**(19): 5066-5059.

Appendix V
Chapter 5: Supplemental Material

V.1. Tables of Reaction Conditions

Table V.1. Effect of multiple doses of cyclopentadiene in the synthesis of M-C adduct **6**.

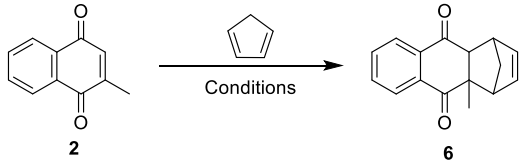

Entry	Reagents	Conditions	Yield of 6	Comment
1	CTAB (**9**) CPD (5.6 eq)	HOAc, **35°C**, 72 hr	62% Crude after recrystallization	Ran for 2 days, reupped CPD with a 2nd dose. Product was recrystallized. Light tan solid
2	LTAB (**10**) CPD (5.6 eq)	HOAc, **35°C**, 72 hr	58% Crude after recrystallization	Ran for 2 days, reupped CPD with a 2nd dose. Product was recrystallized. Light tan solid
3	LTAB (**10**) CPD (5.6 eq)	HOAc, **35°C**, 48 hr	58% Crude after recrystallization	At this point, I was fed up with the inconsistencies of recrystallization. Continued to produce crude product.
4	CPD (1.5 eq)	HOAc, rt, 2 days	14%	Ongini Patent Aqueous work-up. Reaction was poured over ice-water. White precipitate formed. NMR confirmed it was CLEAN product.
5	CPD (4.5 eq, 3 doses)	HOAc, rt, 4 days	83%	Dosed with additional CPD, after 48 hrs, then at 72 hr. Improved Ongini purity and yield

Table V.2 Summary of enolate alkylation (Part A) and retro-Diels-Alder trials (Part B).

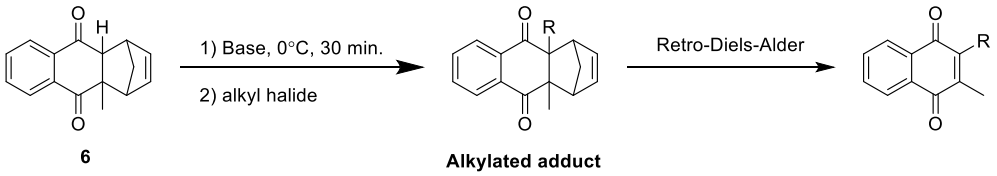

6 **Alkylated adduct**

Entry	Reagents	Conditions	Yield after Retro-Diels Alder	Comment
1A	**6,** KOtBu (5.25 eq) (Stir for 30 min at 0°C)	Citronellyl iodide(1.15 eq, dropwise over 30 min), THF, 0°C, 3 hr	16% over 2 steps	Enolate alkylation incomplete after 3 hours. Quenched and moved on Yield after column chromatography. NMR showed product.
1B	LTAB	HOAc, 90°C, 15 min		
2A	**6,** KOtBu (5.25 eq) (Stir for 30 min at 0°C)	Citronellyl iodide(1.15 eq, dropwise over 30 min), THF, 0°C, 6 hr	16% over 2 steps	Enolate alkylation incomplete after 6 hours. Rxn dosed a 2nd time with citronellyl iodide (total of 2.3 eq). No change after 1 hour. Yield after column chromatography. NMR showed product. Elimination side rxn prevalent. Started to think too much base.
2B	LTAB	HOAc, 90°C, 15 min		
3A	**6,** KOtBu (1 eq) (stir for 30 min at 0°C)	Citronellyl iodide(1.15 eq, dropwise over 30 min), THF, 0°C, 6 hr	43% extrapolated from preparatory TLC	Too much Toluene used during extraction in enolate alkylation work up suspected to be part of the problem. Probably great for vitamin K1, but not for this truncated derivative.
3B	LTAB	HOAc, 90°C, 15 min		
4A	**6,** LDA (1.2 eq) (stir for 30 min at -78°C)	Citronellyl iodide(1.15 eq, dropwise over 30 min), THF, -78°C, 2 hr Added 0.10mL of acetyl chloride	No mass collected.	Switched to LDA for irreversible enolate alkylation: Enolate Alkylation: solution was noticeably orange rather than red. Incomplete deprotonation of M-C adduct? When citI was added, no change on TLC after 2 hours Noticeable change in appearance up addition of acetyl chloride. New spot on TLC. Did not continue to RDA.
5A	**6,** KOtBu (5.25 eq) (stir for 30 min at 0°C)	Citronellyl bromide(1.15 eq, dropwise over 30 min), THF, 0°C-rt, 24 hr	No mass collected. Proof of concepts	Cit Br side pdt forming around 5 hr. let run over night to see what would happen. After 24 hr, pdt spots larger, M-C adduct smaller, and side pdt is darker.
5B	LTAB	HOAc, 90°C, 15 min		
6A	**6,** KOtBu (4:1 tBuOH:toluene) (2 eq) (stir for 5 min at 0°C)	Citronellyl bromide(1.15 eq, dropwise over 15 min), THF, 0°C- rt, 24 hr	No mass obtained	Ran it like Rüttimann & Büchi. Lost product during RDA step. Seemed to decompose in toluene at reflux in 15 min. At this point, starting to suspect how soluble KOtBu is in THF at 0°C. Lots of solid is present in the flask when M-C adduct is added.
6B		Toluene, reflux, 15 min		

7A	**6,** KOtBu (1.5 eq) (stir for 30 min at 0°C)	Allyl bromide (1.6 eq, added slowly to the side of the flask), THF, 0°C, 2 hr	No mass collected	Repeat of Ongini patent. Extraction with ether and AQ work-up. Crude NMR showed alkylated adduct
7B		Toluene, 120°C, 5 hr		Proof of concept.
8A	**6,** KOtBu (1.5 eq) (stir for 30 min at 0°C)	citronellyl bromide (1.6 eq, added slowly to the side of the flask), THF, 0°C-rt, 24 hr	No mass collected	Added alkyl halide too quickly.
8B		Toluene, 120°C, 5 hr		Pdt present on TLC Too aggressive. Revery back to HOAC at 90°C for 15 min.
9A	**6,** KOtBu (1.5 eq) (stir for 30 min at 0°C)	geranyl bromide (1.6 eq, added dropwise over 15 min, impure from the bottle), THF, 0°C, 3 hr		Used impure geranyl bromide to see what would happen. Yes, I should have purified it. NMR supports presence of M-C alkylated product, M-C, and geranyl bromide
9B	LTAB	HOAc, 90°C, 15 min		
10A	**6,** KOtBu (1.5 eq) (stir for 30 min at 0°C)	geranyl acetate (1.6 eq, added dropwise over 15 min, impure from the bottle), THF, 0°C, 3 hr	11.26% after column	Used geranyl acetate. I read that it is a better LG. more a SN1 than Sn2. After 1 hr, no rxn, so Added a 2nd dose of Geranyl bromide neat from the bottle. b/c that one did work before. Started to see alkylated pdt spots.
10B	LTAB	HOAc, 90°C, 15 min		Proof of concept
11A	**6, *KHMDS*** (1.5 eq) (stir for 30 min at 0°C)	geranyl acetate (1.6 eq, added dropwise over 15 min, impure from the bottle), THF, 0°C, 3 hr	11% by NMR	Used geranyl acetate. I read that it is a better LG. more a SN1 than SN2. After 1 hr, no rxn, so Added a 2nd dose of Geranyl bromide neat from the bottle. b/c that one did work before. Started to see alkylated pdt spots.
11B	LTAB	HOAc, 90°C, 15 min		KHMDS appeared to work better than KOtBu by TLC

V.2. Enolate Alkylation Reaction Images

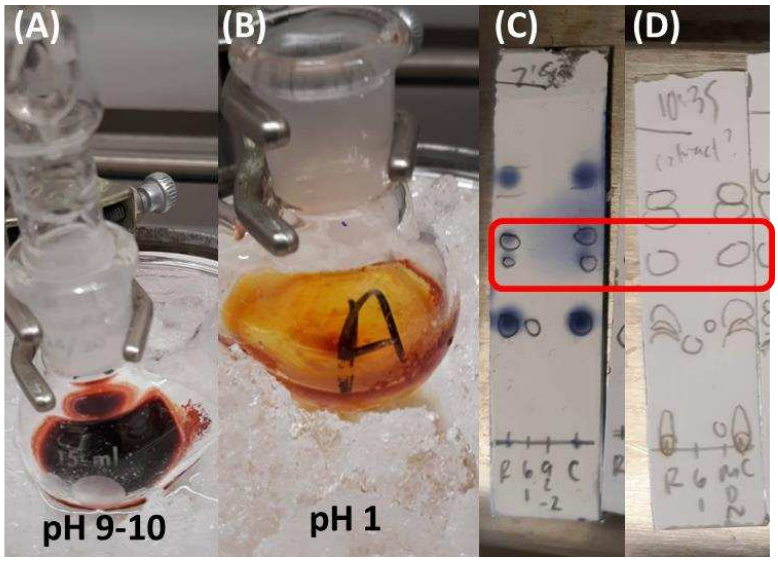

Figure V.1. Pictures of the enolate alkylation steps. (A) Dark red color of the M-C enolate (B) transition from red to yellow during acidic work up of the alkylation. TLC plates depicting the (C) formation of the alkylated adduct and (D) the convergence of the two spots upon retro-Diels-Alder conditions.

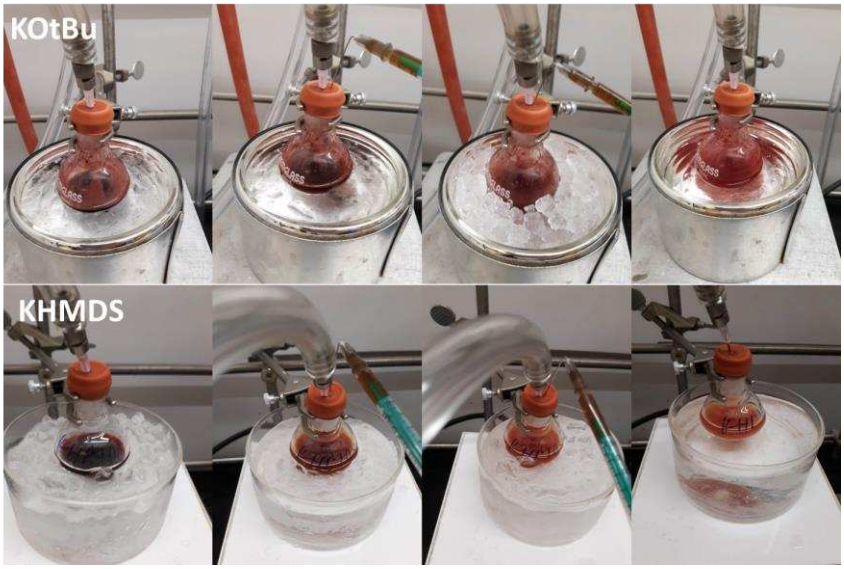

Figure V.2. Comparison of the KOtBu reaction (top) to the KHMDS reaction (bottom). Pictures is the portion-wise addition of neat, impure geranyl bromide (brown solution in syringe). As the alkylation progressed, the KHDMS reaction became progressively lighter in color, suggesting a more complete alkylation reaction.

V.3. Experimental Section

V.3.1. General Materials and Methods

All reactions were carried out under argon atmosphere unless otherwise noted. Dicyclopentadiene was distilled before each use and stored under argon over dry ice and acetone before use. Dodecyltrimethylammonium bromide, hexadecyltrimethylammonium bromide, and triphenylphosphine were recrystallized before use. Each was stored under argon in the freezer. All the other reagents were used as purchased unless otherwise noted. Solvents were dried by passing through an alumina drying column (Solv-Tek Inc.) under argon pressure (DCM, THF, Diethyl Ether).

V.3.2. Syntheses & NMR

V.3.2.1. 4a-Methyl-1,4,4a,9a-tetrahydro-1,4-methanoanthracene-9,10-dione (M-C Adduct, 6)(Ongini, Almirante et al. 2014)

To a 250mL round bottom flask was added menadione (4.4076g, 25.60 mmol) and dissolved in glacial acetic acid (64 mL) under inert atmosphere. Freshly distilled cyclopentadiene (5mL) was added under an inert atmosphere. The resulting bright yellow solution was stirred at room temperature for 4 days. After stirring for ~ 48 hours, a second equivalent of cyclopentadiene (5 mL) was added to the now darker yellow/orange solution. After 4 days, the reaction was poured over an ice/water mixture (~200mL) and allowed to sit for 2-3 hours. The resulting heterogenous mixture was vacuum filtered to collect the precipitate (keeping the filtrate. Work up continued below). The resulting off-white-light yellow crystalline solid dried under reduced pressure overnight (5.0586g, 82.93%).^{1}H NMR (400 MHz, $CDCl_3$) δ: 8.04 (m, 2H), 7.71-7.69 (dd, 2H), 6.11-6.10 (dd, 1H), 5.92-5.91 (1H), 3.35 (s, 1H), 3.22 (s, 1H), 3.06 (s,1H), 1.77 (d, 1H), 1.56 (s, 3H). ^{13}C NMR (101 MHz, $CDCl_3$) δ: 201.29, 198.04, 138.37, 135.43, 135.37, 134.98, 134.15, 133.90, 127.18, 126.63, 58.17, 54.16, 53.68, 49.62, 46.56, 26.86,

The filtrate was extracted with ethyl acetate (2 x 200 mL) and the combined organic layers were washed with saturated sodium bicarbonate (2 x 200 mL), DI H_2O (2 x 200mL), and brine (2 x 200mL). The combined organic layers were then dried with $MgSO_4$. The solvent was removed under reduced pressure to reveal a brown solid (0.9680g). ^{1}H NMR analysis showed the a 1:12 ratio of menadione: M-C adduct, which accounted for the brown color. This shows that more M-C adduct could be isolated via column chromatography if desired.

^{1}H NMR

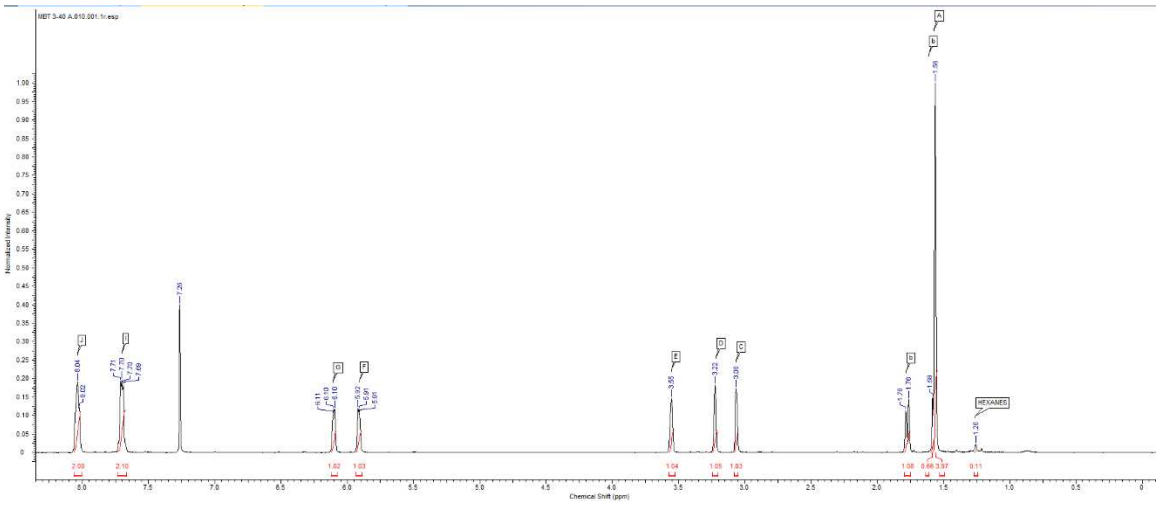

^{13}C

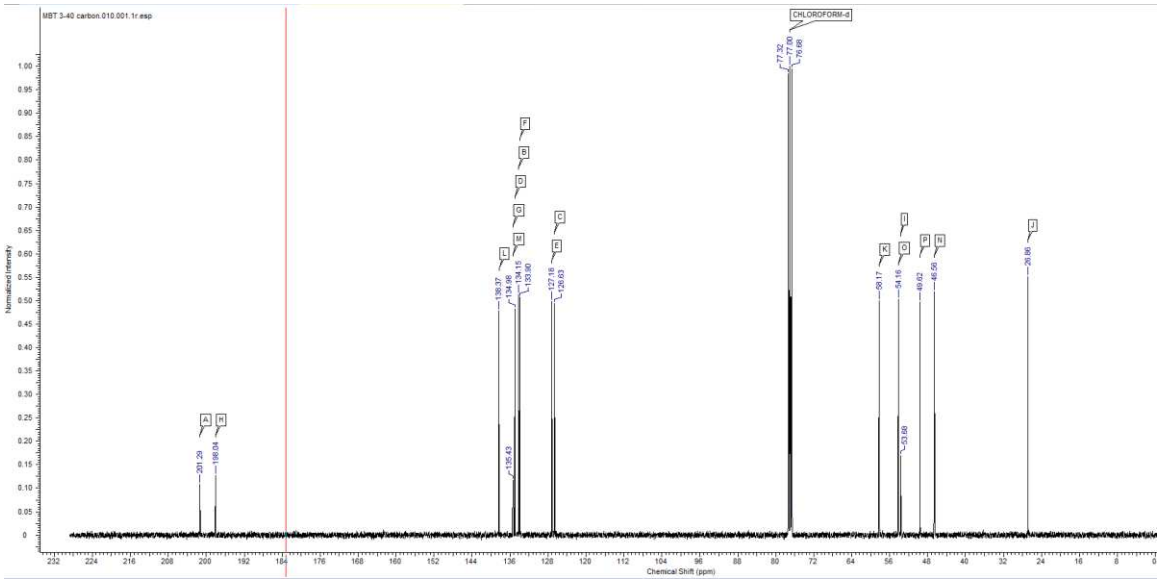

V.3.2.2. Syntheses of Sidechain Derivatives

Citronellyl iodide (Koehn, Crick et al. 2018): To a 250 mL round bottoms flask was added β-citronellol (6.6mL) and dry DCM (60mL) and was purged with argon for 5 minutes, then dry Et_3N (6.7mL) was added. The solution was cooled to 0°C. Mesyl chloride (3.2mL) was added dropwise over a period of 5 minutes. The solution was stirred under an inert atmosphere for 90 minutes. The reaction was quenched with saturated sodium bicarbonate (60 mL) at 0°C. The different phases were separated, and the aqueous layer was extracted with ether (3 x 60mL). The combined organic layers were washed with saturated sodium bicarbonate (2 x 30mL) and brine (2 x 30mL), and then dried with anhydrous Na_2SO_4. The solvent was removed under reduced pressure to reveal an orange oil.

The crude product was immediately carried forward to the second reaction. Under an inert atmosphere, the crude oil was dissolved in dry acetone (60 mL). NaI (9.6893g, 64.6410mmol) was added and the flask was fitted with a reflux condenser under an inert atmosphere. Before refluxing, the apparatus was purged with Ar for 5 minutes. The reaction was refluxed for 3 hours. The reaction was cooled to room temperature and then diluted with ice-cold DI H_2O (60 mL) and ether (30mL). The phases were separated, and the aqueous layer was extracted with ether (3 x 30mL). The combined organic layers were washed with saturated sodium bicarbonate (2 x 30mL) and brine (2 x 30mL), and then dried with anhydrous Na_2SO_4. The solvent was removed under reduced pressure to produce a yellow oil. The crude oil was purified using column chromatography (1:20 product: silica gel, 10:1 pentane: ethyl acetate). The product resulted in a loose colorless oil (6.6807g, 81.61%). ^{1}H NMR (400 MHz, $CDCl_3$) δ: 5.09 (qd, 1H), 3.20 (m, 2H), 1.95 (m, 2H), 1.88 (m, 1H), 1.69 (s, 3H), 1.65 (m, 1H), 1.61 (s, 3H), 1.56 (m, 1H) 1.39-1.30 (m, 1H), 1.22-1.13 (m, 1H), 0.89 (d, 3H)

1H NMR:

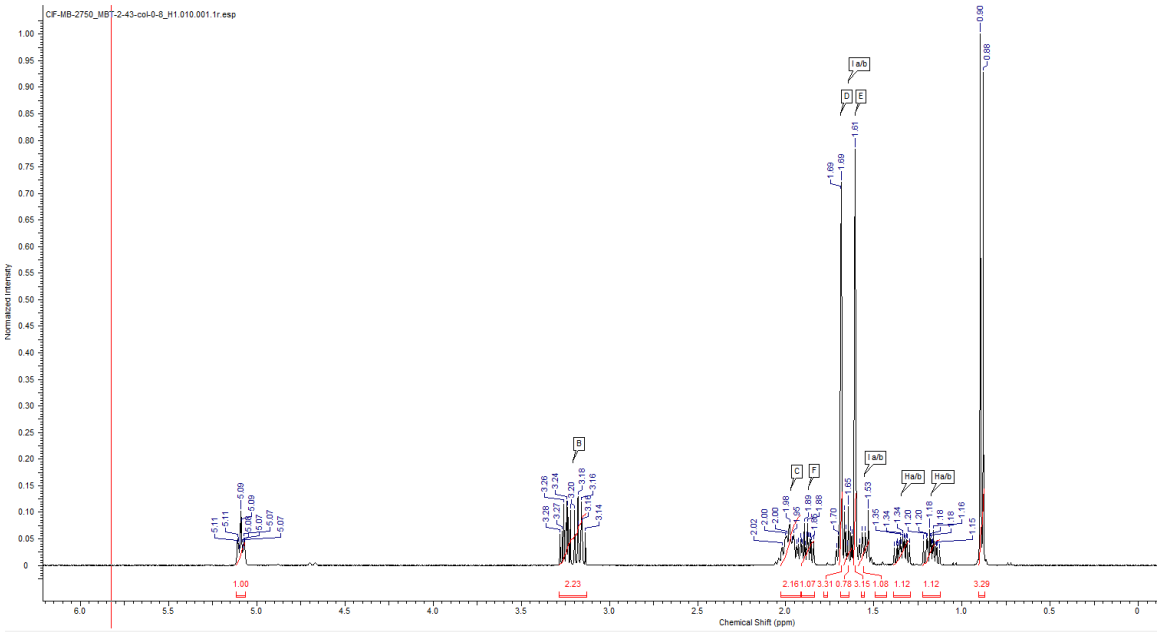

Citronellyl bromide (Siu, Parry et al. 2019): To a 100mL round bottom flask was added β-citronellol (1.5mL), CBr_4 (3.0352g, 9.1524mmol) and dry DCM (33mL), and the solution was cooled to 0°C. Recrystallized PPh_3 (2.5914g, 9.8799 mmol) was dissolved in DCM (9mL) and added to the reaction slowly at 0°C. The reaction stirred at 0°C for 2 hours. The reaction was quenched at the cold temperature with DI H2O (38mL), and the phases were separated. The aqueous layer was extracted with DCM (3 x 40mL) and the combined organic layers were dried with Na2SO4. The solvent was removed under reduced pressure to reveal a white solid (triphenylphosphine oxide). The solid was suspended in hexanes and filtered. The solid was rinsed thoroughly with hexanes. The filtrate was then rotovapped to reveal a colorless oil. The crude oil was purified via column chromatography (1:20 pdt: silica gel ratio and eluted with 100% hexanes). The product was isolated as a colorless oil (1.243g, 72.57%). ^{1}H NMR (400 MHz, $CDCl_3$) δ: 5.09 (qd, 1H), 3.49-3.39 (m, 2H), 1.98 (m, 2H), 1.88 (m, 1H), 1.69 (s, 3H), 1.65 (m, 1H), 1.61 (s, 3H), 1.56 (m, 1H) 1.39-1.30 (m, 1H), 1.22-1.15 (m, 1H), 0.90 (d, 3H)

1H NMR

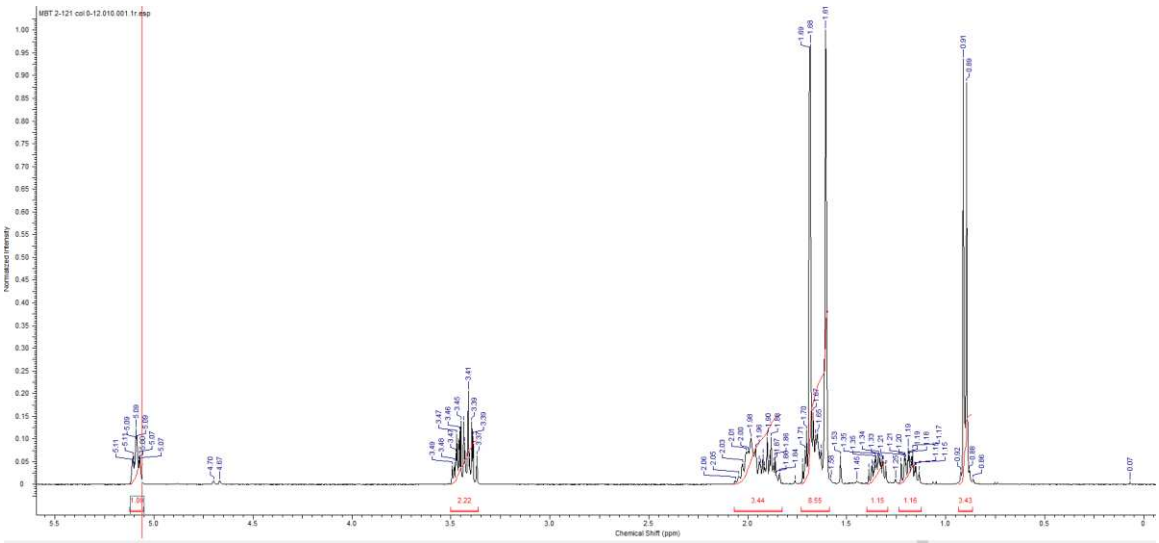

Geranyl acetate (Oberhauser, Harms et al. 2018): To a 100mL round bottom flask was added geraniol (4.445g, 5.0 mL, 28.8169 mmol), K2CO3 (5.7246 g, 41.4211 mmol), DMAP (0.0354g, 0.2829 mmol), and ethyl acetate (38 mL). Acetic anhydride (4.2mL, 4.536g, 44.4314 mmol) was added slowly. The resulting solution was stirred at room temperature for 1 hour. The solid was filtered off and the filtrate was quenched with saturated sodium bicarbonate (60mL) and stirred for 10 minutes. The organic phase was separated and dried with MgSO4. The solvent was removed to reveal a colorless oil. The crude product was purified via column chromatography (1:20 ratio of pdt : silica gel and eluted with 5% ethyl acetate: 95% hexanes) to produce a colorless oil (3.3691g, 60.23%). ^{1}H NMR (400 MHz, $CDCl_3$) δ: 5.34 (t, 1H), 5.08 (t, 1H), 4.59 (d, 2H), 2.09 (t, 2H), 2.06 (s, 3H), 1.70 (s, 3H), 1.69 (s, 3H), 160 (s, 3H)

1H NMR:

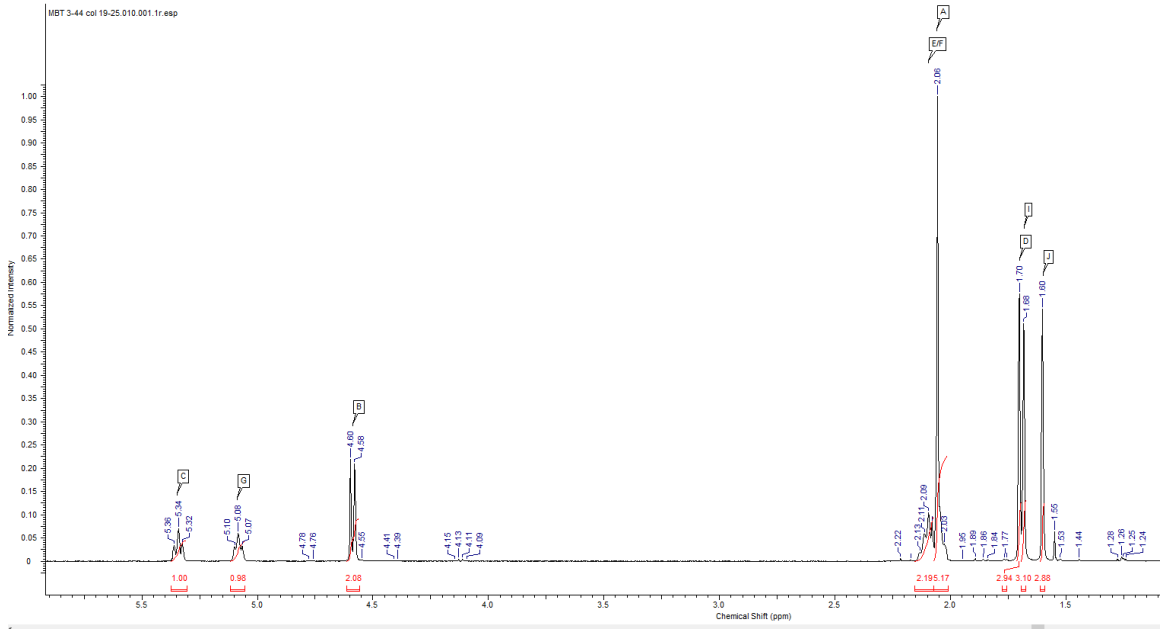

V.3.2.3. Enolate Alkylation Conditions- Full Three Step Sequence

Synthesis of MK-2(I-H^2) 21 using KOtBu: To a 2-neck 25mL round bottom flask was added freshly prepared KOtBu (0.5000g, 4.4559 mmol) in THF (4 mL). The solution was cooled to -3°C. M-C (0.2016g, 0.8421 mmol) was added, and rinsed in with THF (~1mL). The resulting dark red solution was stirred under an inert atmosphere for 30 minutes. Citronellyl iodide (0.17mL in 1mL THF) was added dropwise to the reaction over 30 minutes. The resulting reaction was stirred for 24 hours, allowing it to warm to room temperature. After 24 hours, a second equivalent of citronellyl iodide was added at 0°C dropwise for over 30 minutes and allowed to stir at 0°C for an additional 4 hours. The reaction was quenched with 2N HCl until a pH of ~1, resulting in a bright yellow solution. The solution was rotovapped to remove THF from the mixture, and the aqueous solution was extracted with toluene (2 x 10mL). The combined organic layers were washed with water (20mL), brine (20mL), and dried with Na2SO4. The solvent was removed under reduced pressure to form a crude, brown oil. The product was carried forward to the retro Diels-Alder reaction without further purification.

The crude oil was dissolved in HOAc (1.2mL) . LTAB (0.0082g) was added. The reaction was outfitted with a reflux condenser and put in an oil bath heated to 90°C for 60 minutes while monitoring with TLC (15 minutes was sufficient). The reaction was cooled to room temperature and the concentrated under reduced pressure. The crude product was purified via column chromatography (1:20 ratio of pdt : silica gel and eluted with 5%ether: 95% hexanes) to produce a yellow/orange oil (0.0427g, 16.26% over three steps). ^{1}H NMR (400 MHz, $CDCl_3$) δ: 8.08 (dd, 2H), 7.69 (dd, 2H), 5.10 (t, 1H), 2.19 (s, 3H), 1.68 (s, 3H), 1.61 (s, 3H), 1.42 (s, 2H), 1.00 (d, 3H)

1H NMR

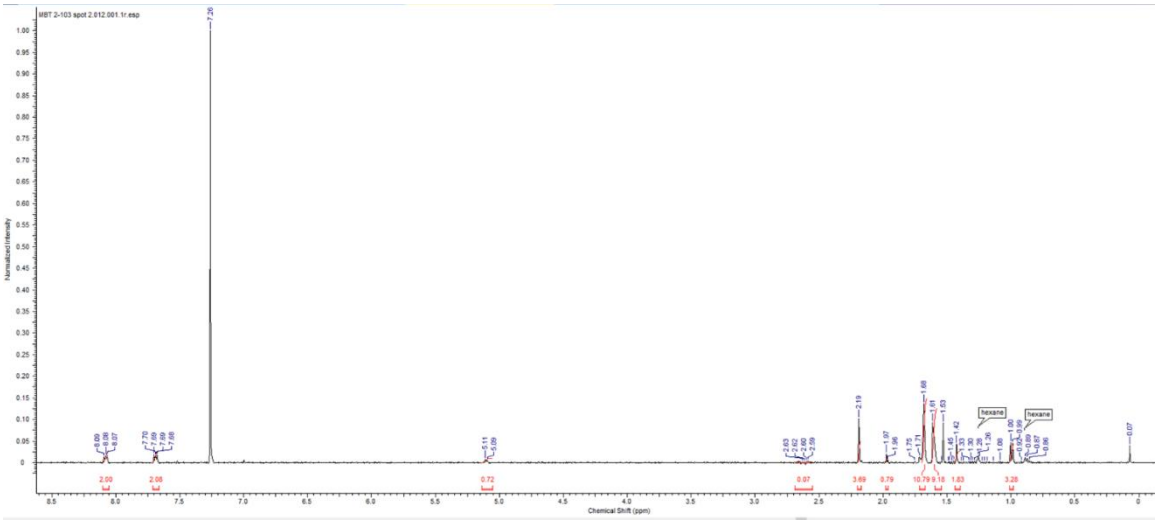

Synthesis of MK-2 1 using KOtBu: To a 50mL round bottom flask was added M-C adduct (0.4986g) in THF (9 ml). The reaction was cooled to 0°C. KOtBu(0.3553g) was added resulting in a dark red solution. The reaction was stirred at 0°C for 30 minutes. At this point, geranyl acetate (0.72mL dissolved in 7.5mL THF) was added to the reaction, but ultimately led nowhere. So, after 40 minutes of stirring at 0°C, neat geranyl bromide (impure, 0.67mL) was added dropwise over 30 minutes at 0°C. A second equivalent of geranyl bromide was added and allowed to stir for another hour. The reaction was quenched with DI H2O (10mL) and acidified using 1N HCl to a pH of 2. The resulting yellow solution was extracted with ether (3 x 25mL) and the combined

organic layers were washed with H2O, brine, and dried with Na2SO4. The solvent was removed and the crude product was carried forward without further purification.

The crude oil was dissolved in HOAc (3 mL) . LTAB (0.0211g) was added. The reaction was outfitted with a reflux condenser and put in an oil bath heated to 90°C for 60 minutes while monitoring with TLC (15 minutes was sufficient). The reaction was cooled to room temperature and diluted with H2O (25mL). The aqueous solution was extracted with ether (3 x 25mL), washed with water, and brined, and dried with Na2SO4. The solvent was removed under reduced pressure and purified via column chromatography (1:75 ratio of pdt:silica gel, eluted with 5% ethyl acetate: hexanes). The product was a yellow oil (0.2252g, 11.6% by NMR) that co-eluted with unreacted geranyl acetate. ^{1}H NMR (400 MHz, $CDCl_3$) δ: 8.08 (dd, 2H), 7.69 (dd, 2H), 5.03 (q, 1H), 3.37 (d, 1H), 2.06 (s, 3H), 1.76 (s, 3H), 1.70 (s, 3H), and 1.68 (s, 3H), 1.60 s(3H), 1.56 (d, 2H)

1H NMR:

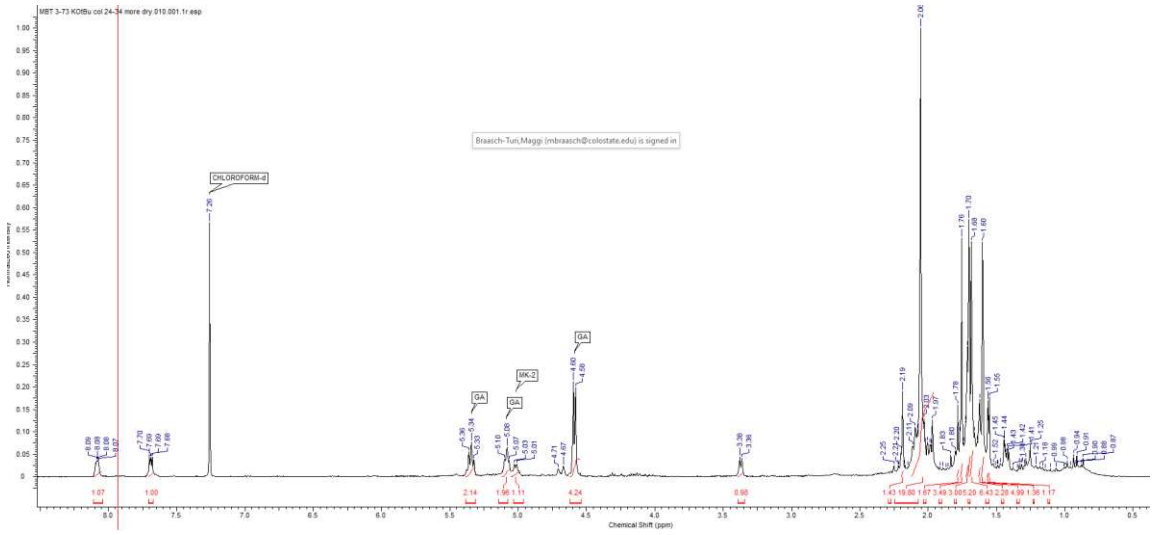

Synthesis of MK-2using KHMDS: To a 50mL round bottom flask was added M-C adduct (0.4980g) in THF (9 ml). The reaction was cooled to 0°C. KHMDS (0.5M in toluene, 6.3mL) was added resulting in a dark red solution. The reaction was stirred at 0°C for 30 minutes. At this point, geranyl acetate (0.72mL dissolved in 7.5mL THF) was added to the reaction, but ultimately led nowhere. So, after 40 minutes of stirring at 0°C, neat geranyl bromide (impure, 0.67mL) was added dropwise over 30 minutes at 0°C. A second equivalent of geranyl bromide was added and allowed to stir for another hour. The reaction was quenched with DI H2O (10mL) and acidified using 1N HCl to a pH of 2. The resulting yellow solution was extracted with ether (3 x 25mL) and the combined organic layers were washed with H2O, brine, and dried with Na2SO4. The solvent was removed and the crude product was carried forward without further purification.

The crude oil was dissolved in HOAc (3 mL) . LTAB (0.0210g) was added. The reaction was outfitted with a reflux condenser and put in an oil bath heated to 90°C for 60 minutes while monitoring with TLC (15 minutes was sufficient). The reaction was cooled to room temperature and diluted with H2O (25mL). The aqueous solution was extracted with ether (3 x 25mL), washed

with water, and brined, and dried with Na2SO4. The solvent was removed under reduced pressure and purified via column chromatography (1:100 ratio of pdt:silica gel, eluted with 5% ethyl acetate: hexanes). The product was a yellow oil (0.2252g, 11.6% by NMR) that co-eluted with unreacted geranyl acetate. ^{1}H NMR (400 MHz, $CDCl_3$) δ: 8.08 (dd, 2H), 7.69 (dd, 2H), 5.03 (q, 1H), 3.37 (d, 1H), 2.06 (s, 3H), 1.76 (s, 3H), 1.70 (s, 3H), and 1.68 (s, 3H), 1.60 s(3H), 1.56 (d, 2H)

1H NMR:

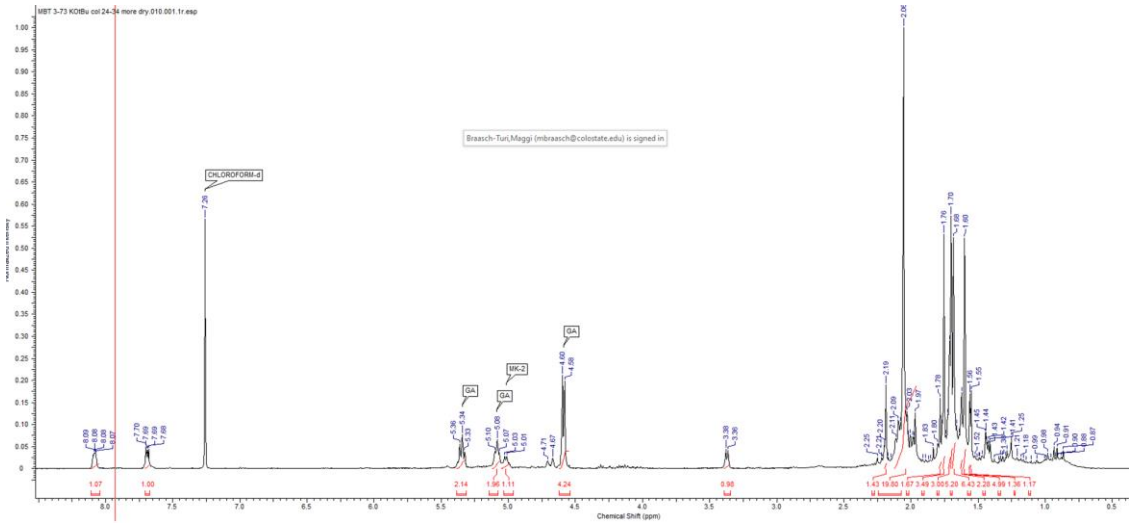

References

Koehn, J. T., D. C. Crick and D. C. Crans (2018). "Synthesis and Characterization of Partially and Fully Saturated Menaquinone Derivatives." ACS Omega **3**(11): 14889-14901.

Oberhauser, C., V. Harms, K. Seidel, B. Schroder, K. Ekramzadeh, S. Beutel, S. Winkler, L. Lauterbach, J. Dickschat and A. Kirchning (2018). "Exploiting the Synthetic Potential of Sesquiterpene Cyclases for Generating Unnatural Terpenoids." Angew. Chem. Int. Ed. **57**(36): 11802-11806.

Ongini, E., N. Almirante and L. Storoni (2014). Quinone based nitric oxide donating compounds for ophthalmic use.

Siu, J. C., J. B. Parry and S. Lin (2019). "Aminoxyl-Catalyzed Electrochemical Diazidation of Alkenes Mediated by a Metastable Charge-Transfer Complex." J. Am. Chem. Soc. **141**(7): 2825-2831.

List of Abbreviations

From all Chapters and Appendices.

ACC	1-aminocyclopropylcarboxylic acid
Ala	alanine
AOT	bis(2-ethylhexyl)sulfosuccinate sodium
AOT RMs	bis(2-ethylhexyl)sulfosuccinate sodium reverse micelles
ATP	adenosine triphosphate
BIHY	birch hydrogenolysis
CAN	ceric ammonium nitrate
CDI	1,1'-carbonyldiimidazole
CG	coarse grain
CL	cardiolipin
COSY	correlation spectroscopy
COVID-19	corona virus disease 2019
CV	cyclic voltammetry
DCC	N,N'-dicyclohexylcarbodiimide
DCM	dichloromethane

DCU	dicyclohexylurea
DDI	distilled deionized
DDQ	2,3-dichloro-5,6-dycyano-1,4-benzoquinone
DHPC	diheptanoylphosphatidylcholine
DIBAL-H	diisobutylaluminim hydride
DIPEA	diisopropylethylamine
DLPC	dilinoleoylphosphatidylcholine
DLPE	dilauroylphosphoethanolamine
DMAP	dimethylaminopyridine
DMF	dimethylformamide
DMPC	dimyristoylphosphatidylcholine
DMSO	dimethyl sulfoxide
DPPC	dipalmitoylphosphatidylcholine
DPPE	1,2-dipalmitoyl-sn-glycero-3-phosphorylethanolamine
EDCI	1-ethyl-3-(3-dimethylaminopropyl)carbodiimide
EPC	egg phosphatidylcholine
ESI	electrospray ionization
Et_3N	triethylamine

ETC	electron transport chain
ETS	electron transport system
HATU	1-[bis(dimethylamino)methylene]-1h-1,2,3-triazolo[4,5-b]pyridinium 3-oxide hexafluoro-phosphate
HMDS	hexamethyldisilazide
HOBt	hydroxybenzotriazole
HPLC	high performance liquid chromatography
HRMS	high resolution mass spectrometry
IC50	inhibition concentration
MD	molecular dynamics
MeCN	acetonitrile
MK	menaquinone
MMFF	Merck molecular force fields
MPD	2-methyl-2,4-pentanediol
NaH	sodium hydride
NaHMDS	sodium hexamethyldisilazide
NBDHA	6-(N-(7-nitrobenz-2-oxa-1,3-diazol-4-yl)amino)hexanoic acid
nBuLi	n-butyl lithium
NMI	N-methylimidazole

NMR	nuclear magnetic resonance
NOE	nuclear Overhauser effect
NOESY	nuclear Overhauser effect spectroscopy
o/n	overnight
PCC	pyridinium chlorochromate
PDB	Protein Data Bank
PNP	para-nitrophenol
POPC	palmitoyloleoylphosphatidylcholine
PQ	plastoquinone
PyBOP	benzotriazol-1-yl-oxytripyrrolidinophosphonium hexafluorophosphate
PyBrOP	bromotripyrrolidinophosphonium hexafluorophosphate
RM	reverse micelle
ROESY	rotating frame Overhauser enhancement spectroscopy
rt	room temperature
SN2	substitution nucleophilic bimolecular
TBSCl	tert-butyldimethylsilyl chloride
TCFH	N,N,N′,N′-tetramethylchloroformamidinium hexafluorophosphate
THF	tetrahydrofuran

TLC	thin layer chromatography
TMSCl	chlorotrimethylsilane
Trp	tryptophan
UA	united atom
UQ	ubiquinone
UV	ultraviolet
VQA	versiquinazoline A
VQB	versiquinazoline B
XRD	x-ray diffraction